AGU ADVANCING EARTH AND SPACE SCIENCE

Reviews of Geophysics

COMMISSIONED MANUSCRIPT
10.1029/2022RG000789

Secular Evolution of Continents and the Earth System

Peter A. Cawood[1], Priyadarshi Chowdhury[1,2], Jacob A. Mulder[3], Chris J. Hawkesworth[4], Fabio A. Capitanio[1], Prasanna M. Gunawardana[1], and Oliver Nebel[1]

[1]School of Earth, Atmosphere & Environment, Monash University, Melbourne, VIC, Australia, [2]School of Earth & Planetary Sciences, National Institute of Science Education and Research, HBNI, Bhubaneswar, India, [3]Department of Earth Sciences, The University of Adelaide, Adelaide, SA, Australia, [4]School of Earth Sciences, University of Bristol, Bristol, UK

Key Points:

- Long-term record of Earth evolution preserved in continental lithosphere
- Three main tectonic modes operated through Earth history: stagnant lid, squishy lid and rigid, active lid (plate tectonics)
- Stabilization of cratons at end of Archean marks transition to plate tectonics with supercontinent cycle controlling subsequent changes

Supporting Information:

Supporting Information may be found in the online version of this article.

Correspondence to:

P. A. Cawood,
peter.cawood@monash.edu

Citation:

Cawood, P. A., Chowdhury, P., Mulder, J. A., Hawkesworth, C. J., Capitanio, F. A., Gunawardana, P. M., & Nebel, O. (2022). Secular evolution of continents and the Earth system. *Reviews of Geophysics*, *60*, e2022RG000789. https://doi.org/10.1029/2022RG000789

Received 6 JUL 2022
Accepted 18 NOV 2022

Author Contributions:

Conceptualization: Peter A. Cawood, Chris J. Hawkesworth
Formal analysis: Jacob A. Mulder
Funding acquisition: Peter A. Cawood
Investigation: Peter A. Cawood, Priyadarshi Chowdhury, Jacob A. Mulder, Chris J. Hawkesworth, Fabio A. Capitanio, Oliver Nebel
Project Administration: Peter A. Cawood
Supervision: Peter A. Cawood
Writing – original draft: Peter A. Cawood
Writing – review & editing: Priyadarshi Chowdhury, Jacob A. Mulder, Chris

Abstract

Understanding of secular evolution of the Earth system is based largely on the rock and mineral archive preserved in the continental lithosphere. Based on the frequency and range of accessible data preserved in this record, we divide the secular evolution into seven phases: (a) "*Proto-Earth*" (ca. 4.57–4.45 Ga); (b) "*Primordial Earth*" (ca. 4.45–3.80 Ga); (c) "*Primitive Earth*" (ca. 3.8–3.2 Ga); (d) "Juvenile *Earth*" (ca. 3.2–2.5 Ga); (e) "*Youthful Earth*" (ca. 2.5–1.8 Ga); (f) "*Middle Earth*" (ca. 1.8–0.8 Ga); and (g) "*Contemporary Earth*" (since ca. 0.8 Ga). Integrating this record with knowledge of secular cooling of the mantle and lithospheric rheology constrains the changes in the tectonic modes that operated through Earth history. Initial accretion and the Moon forming impact during the Proto-Earth phase likely resulted in a magma ocean. The solidification of this magma ocean produced the Primordial Earth lithosphere, which preserves evidence for intra-lithospheric reworking of a rigid lid, but which also likely experienced partial recycling through mantle overturn and meteorite impacts. Evidence for craton formation and stabilization from ca. 3.8 to 2.5 Ga, during the Primitive and Juvenile Earth phases, likely reflects some degree of coupling between the convecting mantle and a lithosphere initially weak enough to favor an internally deformable, squishy-lid behavior, which led to a transition to more rigid, plate like, behavior by the end of the early Earth phases. The Youthful to Contemporary phases of Earth, all occurred within a plate tectonic framework with changes between phases linked to lithospheric behavior and the supercontinent cycle.

Plain Language Summary

The record of Earth evolution is preserved in the continental rock archive, but is incomplete and our knowledge of it decreases with increasing age and depth of preservation. Based on secular cooling of the mantle and associated changing lithospheric properties, we recognize three dominant tectonic modes that have operated on Earth; stagnant lid, squishy lid, and plate tectonics. After solidification of the Earth's initial magma ocean (>4.45 Ga), the lithosphere was likely dominated by mafic crust that existed until ca. 3.8 Ga. The tectonic mode that operated at this time involved either no lithosphere-mantle coupling (cf., stagnant lid), or coupling between non-rigid lithosphere and convecting mantle (cf., squishy lid). The latter mode likely operated through most of the Archean (ca. 3.8–2.5 Ga), and was associated with the formation of the stable interior of continents, called cratons. The stabilization of these cratons in the latter half of the Archean (ca. 3.2–2.5 Ga) is associated with the development of rigid lithosphere and the transition to a plate tectonic mode that continues to the present day. Further changes, likely in response to the supercontinent cycle, lead to subdivisions of the Earth system between ca. 1.8 and 0.8 Ga.

1. Introduction

Our planet is unique in the solar system in having a bimodal distribution of crustal types (continental and oceanic), the presence of liquid water at its surface, an oxygenated atmosphere, and a prolific and diverse biosphere. The evolving yet linked nature of these elements, across the range of spatial and temporal scales that operate on the planet, indicates complex and dynamic cycling between the solid (lithosphere, mantle, and core) and surficial (oceans, atmosphere, and biosphere) reservoirs. This linked evolution occurs in response to heat dissipation from the planet's interior, modulated by input of solar energy to the surficial reservoirs. During its very early history the Earth lacked these crustal and surficial features and, after initial accretion from the solar nebula, likely consisted of a magma ocean (e.g., Elkins-Tanton, 2012). Cooling, density settling, and crystallization resulted in rapid differentiation of the Earth, perhaps over a few tens of millions of years, and included formation of core, mantle, proto-crust, and atmosphere (Figure 1; Elkins-Tanton, 2008, 2012). Establishing the cascading succession of

J. Hawkesworth, Fabio A. Capitanio, Prasanna M. Gunawardana, Oliver Nebel

events, their links, and processes responsible for the change from this initial condition to the present day are key questions in the Earth Sciences (e.g., National Academies of Sciences, Engineering, and Medicine, 2020).

The continental crust serves as a record of change and is the long-term archive of our planet's evolution (Cawood et al., 2013; C. J. Hawkesworth et al., 2017). Unambiguously unraveling this record has been hindered by the incomplete nature of the continental rock record, which increases with increasing age, potential selective biasing of the record by the processes of its preservation, and the application of proxies for determining processes from the records, and thus open to varying degrees of interpretation. The aim of this paper is to review the first-order characteristics of the continents, outline secular changes in the continental record, especially during its early history, and speculate on tectonic modes that controlled their evolution. These changes detail that continental evolution resulted in a multifaceted and pulsed record, and the tectonic drivers are a response to the evolving thermal state of the mantle (cf., Holmes, 1931). In particular, changes in the rock- and mineral archive linked with secular changes in mantle temperature and its impact on lithospheric rheology indicate distinct changes at and after ca. 3.8 Ga that we relate to a change from a probable stagnant lid to internally deformable, squishy-lid behavior, and then by ca. 2.5 Ga a further transition to global-scale plate tectonics (e.g., Cawood et al., 2018; Mulder et al., 2021).

2. Key Terms and Definitions

The crust and the semi-rigid, non-convecting upper mantle defines the *lithosphere*, the mechanically strong outer layer of the Earth (Barrell, 1914; R. Daly, 1940). The lithosphere of the contemporary Earth is divisible into a series of rigid *tectonic plates*, the boundaries of which are marked by focused, generally narrow, zones of deformation (Kreemer et al., 2014). The plates are in motion with respect to each other and with the underlying convecting mantle (asthenosphere), and the plate boundaries form a continuous, linked system (Figure 2). The thickness of the lithosphere varies from <10 km at mid-ocean ridges to ~200 km or greater under cratons (e.g., Artemieva, 2009). Heat transport in the lithosphere is mostly conductive, and the base marks a rheological boundary with the convecting mantle (Sleep, 2005), and thus, the lithosphere-asthenosphere boundary represents the change from conductive, rheologically strong, to convecting, rheologically weak, and upper mantle (cf., Artemieva, 2009). The lithosphere-asthenosphere boundary is generally taken as an isotherm at ~1350°C (Herzberg et al., 2010) but is hard to delineate because deformation at the boundary is aseismic and it does not correspond to a marked change in composition or temperature (Priestley et al., 2018). In addition, different proxies are used to define the boundary (e.g., petrologic, geochemical, thermal, seismic velocity, seismic anisotropy, and electrical conductivity, Eaton et al., 2009), resulting in a number of definitions (seismic, electrical, and elastic lithosphere), the depths of which may vary (Figure 3).

The crust constitutes <0.5% of the mass of the Earth, yet its origin is fundamental to understanding the evolution of the planet. It ranges from no more than a few kilometers thick under mid-oceanic ridges to ~80 km under the Himalayas. The boundary between the crust and the underlying mantle, the *Mohorovičić discontinuity (Moho)*, is marked by a jump in the velocity of seismic primary waves (P-waves), reflecting an increase in the density (and changing composition) across the boundary (Mohorovičić, 1910). Seismic reflection profiles and data from xenoliths suggest a transitional, layered structure for the crust-mantle boundary, notably in off-craton zones, consisting of interlayered mafic and ultramafic rocks, with the mapped Moho corresponding to the base of this transition zone (Hale & Thompson, 1982; Mooney & Brocher, 1987; O'Reilly & Griffin, 2013). In addition to the seismic Moho, the boundary between crust and mantle has been based on mineralogy and rock composition, and electrical properties (Q. Wang et al., 2013). The petrologic Moho lies at the boundary of lower crustal felsic and mafic rocks containing feldspar, and their metamorphic equivalents (e.g., granulites), with underlying olivine dominated (peridotite) upper mantle (Mengel & Kern, 1992). The depth of the Moho at any place may vary slightly depending on the criteria (petrologic vs. seismic) used. Furthermore, like the continental crust, the development of the Moho reflects a complex multistage process (e.g., Grad et al., 2009; Jagoutz & Behn, 2013).

The crust is divisible into oceanic and continental types characterized by contrasting chemical and mechanical properties resulting in a bimodal hypsometry (Figure 4). On the contemporary Earth, *continental crust* is largely exposed across the continents of Africa, Antarctica, Asia, Australia, Europe, North America, and South America, and includes the bulk of the emerged crust as well as the submerged continental shelves, together constituting ~40% (~210 × 10^6 km^2) of the planet's surface area (Figure 2) but 70% of the total volume of oceanic and continental crust (~7,182 × 10^6 km^3). Continental crust has an average thickness of ~35–40 km but ranges from

10.1029/2022RG000789

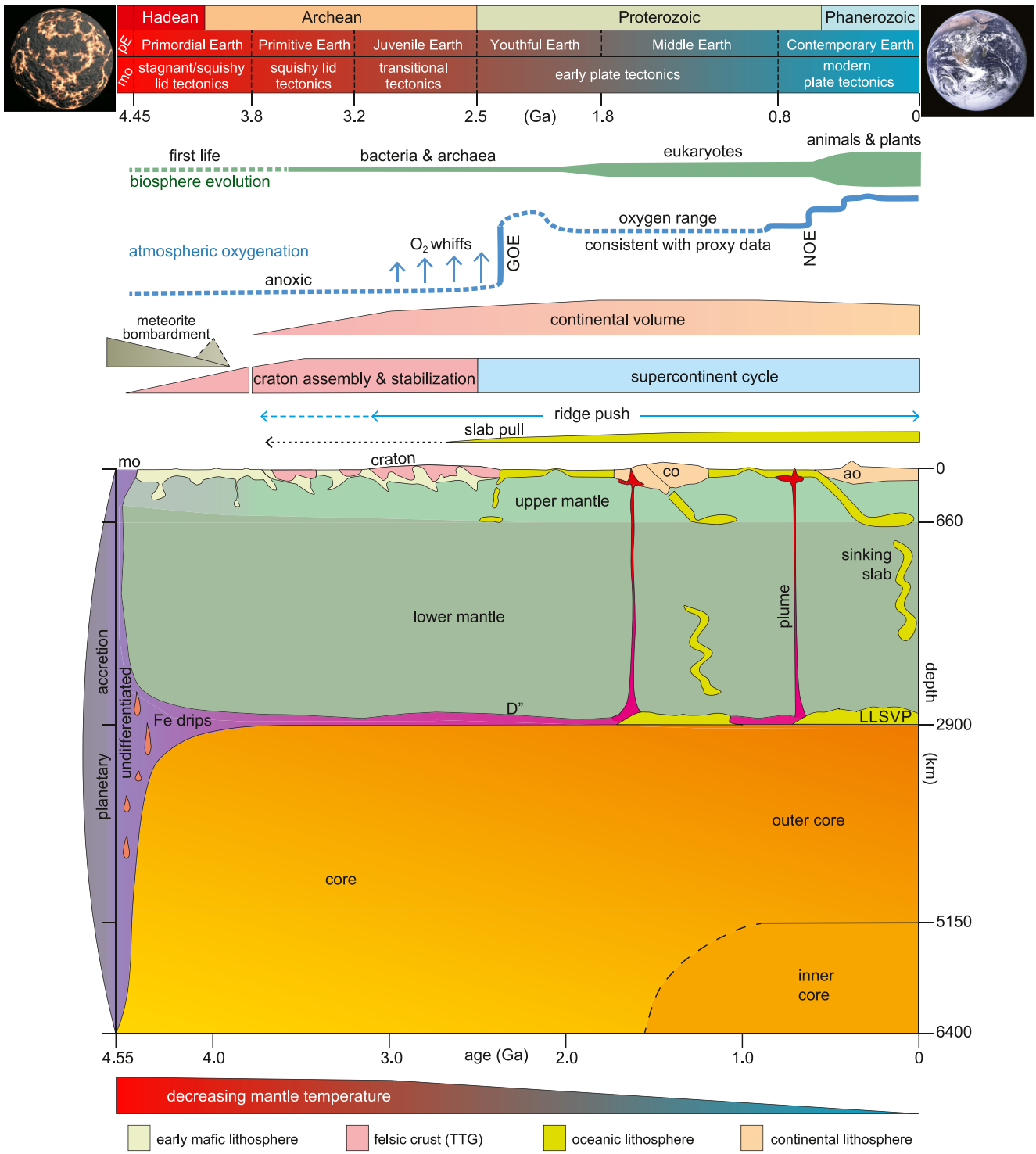

Figure 1. Schematic secular evolution of Earth since initial accretion from the solar nebula and intense early meteorite bombardment to today, highlighting changes in internal structure of the solid Earth, relative to decreasing mantle temperature, and changes in continental volume, tectonic mode, atmosphere composition, and biosphere evolution. Sources include: Cawood (2020), Cawood and Hawkesworth (2019), Hamblin and Christiansen (2004), Herzberg et al. (2010), Knoll and Nowak (2017), and Lyons et al. (2014). Major divisions of the Earth into various internal and surficial layers date from around the time of its accretion, apart from the inner core, which based on estimates from experimental measurement of electrical resistivity of iron only formed at ca. 1 Ga (Y. Zhang et al., 2020), but see also Biggin et al. (2015) and Ohta et al. (2016) for alternative ages of inner core formation. Timing of differentiation into upper and lower mantle is not well constrained and shown at ca. 3.8 Ga on figure. See discussion through the text for references on the timing of changes and duration of events (including phases I–VII) through the Earth system. Abbreviations: ao, accretionary orogen; co, collisional orogen; GOE, great oxidation event; LLSVP, large low-shear velocity provinces; NOE, Neoproterozoic oxidation event; pE, Proto-Earth; mo, magma ocean.

10.1029/2022RG000789

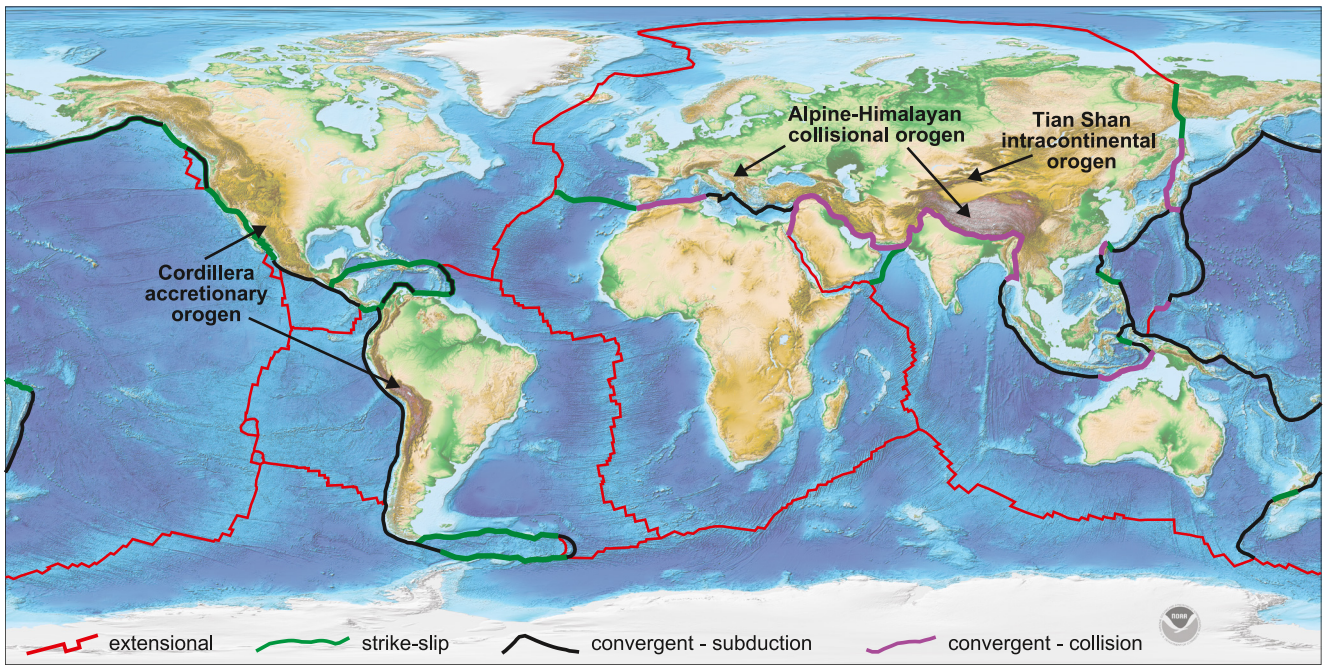

Figure 2. Present day global topography, plate boundaries and modern orogen types (Alpine-Himalayan collisional orogen, Cordillera accretionary orogen and Tien Shan intracontinental orogen). Global relief model based on National Oceanic and Atmospheric Administration (NOAA) ETOPO1 1 Arc-Minute Global Relief Model (Amante & Eakins, 2009).

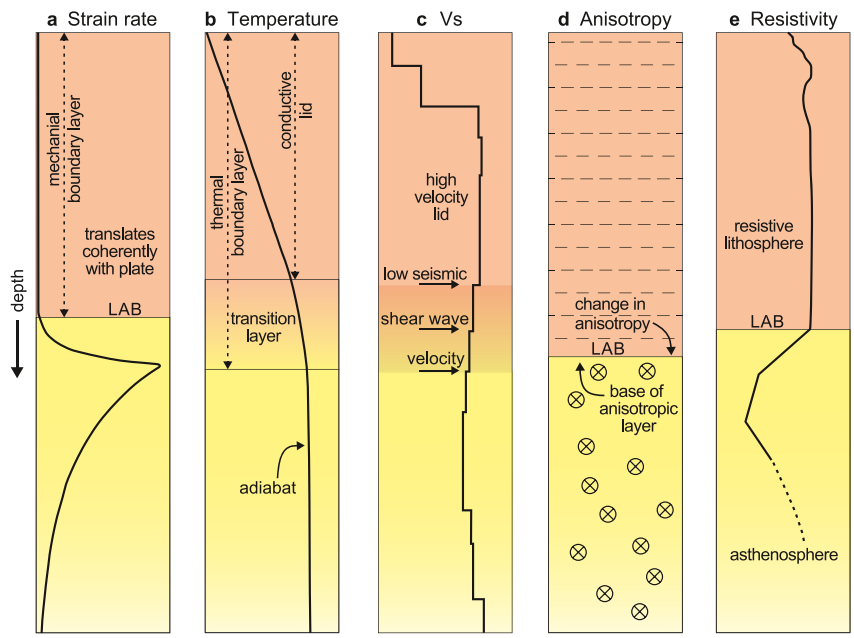

Figure 3. Diagram, adapted from Eaton et al. (2009), showing the lithosphere-boundary based on a range of criteria (a–e). Based on strain rate, the lithosphere is defined as a mechanical boundary layer, with the start of the asthenosphere representing a zone of decoupling and marked by increasing strain rate. The lithosphere as a thermal boundary layer (TBL) is divisible into a conductive lid and a transition layer, and is a region where temperature deviates from the adiabat. The lithosphere-asthenosphere boundary defined by seismic velocity (*Vs*) is taken as a region of decreasing velocity below a high-velocity lid. The position and velocity change corresponding to the base of the lid is dependent of velocity contrasts related to lithologies either side of the boundary and may vary spatially. The lithosphere-asthenosphere boundary may also correspond with extinction of, or change in direction of, seismic anisotropy. The electrical boundary marks a reduction in electrical resistivity.

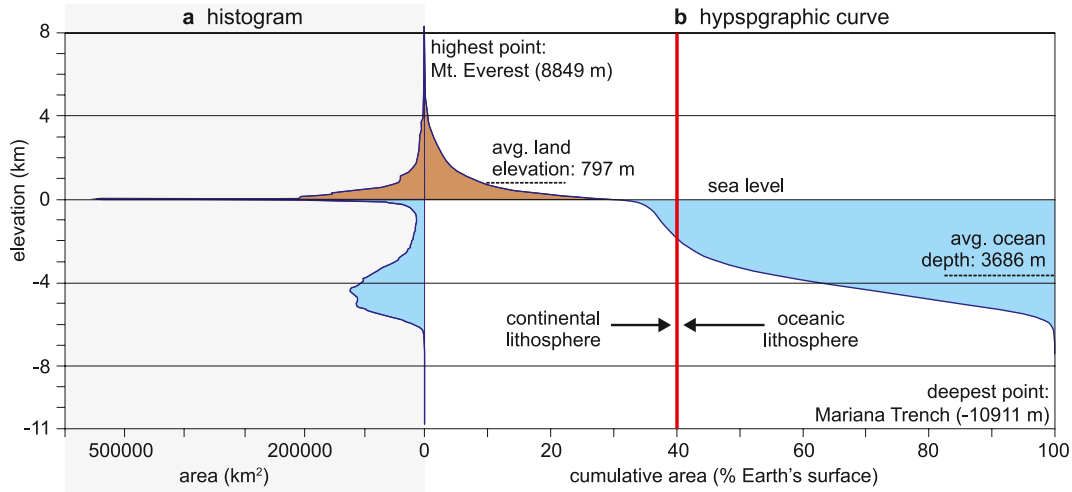

Figure 4. Histogram (a) and hypsographic curve (b, also termed hypsometric) of Earth's present day surface based on ETOPO1 global relief model (Amante & Eakins, 2009). Earth's surface is characterized by a bimodal elevation reflecting the contrasting physio-chemical properties of continental and oceanic lithosphere.

<20 km under hyperextended continental margins to >80 km under continent-continent collision zones such as the Himalayas in Tibet (Mooney, 2003; Priestley et al., 2008; Y. Huang et al., 2013). Owing to such thick crust, continents (including their submerged shelf areas) almost inevitably rest at higher elevation relative to the surrounding seafloor. *Oceanic crust* is relatively thin, being generally 6–7 km but it can range to as great as ~40 km at oceanic plateaus (Furumoto et al., 1976; Kerr, 2003) and zero at structurally modified sites at oceanic core complexes (e.g., Blackman et al., 2002; MacLeod et al., 2009). Compositionally, oceanic crust has a mafic composition (rich in FeO-MgO but poor in SiO_2) as compared to the andesitic composition of the bulk continental crust (rich in SiO_2, Al_2O_3 but depleted in FeO-MgO; see Section 3.1 for more discussion). The archaic terms sima and sial, meaning layers rick in silica and magnesium and silica and aluminum respectively, were applied to oceanic and continental crust, although continental crust also consists of a sialic upper layer and a simatic lower part (Jackson, 1997).

Notably, the distinction between continental and oceanic crust, whether in terms of thickness or composition, is a characteristic feature of the modern Earth and may have persisted over the last 2.5 billion years (cf., Cawood & Hawkesworth, 2019; Cawood et al., 2013). Prior to this time, the distinction between these two crustal types is less clear. It has been inferred that the >2.5 Ga-old oceanic-type crust was likely thicker (>20 km; e.g., Herzberg et al., 2010) than its modern counterpart, whereas the coeval continental-type crust may have been more mafic than its modern bulk composition (e.g., C. Hawkesworth & Jaupart, 2021; Dhuime et al., 2015; K. Chen et al., 2020; Tang et al., 2016). Therefore, in the context of pre-2.5 Ga Earth, it is necessary to agree on definitions of the oceanic and continental crust.

3. Continental Lithospheric Architecture

3.1. Crustal Structure, Composition, and Thermal Regime

The internal structure and composition of the continental crust and its relationship to underlying lithospheric mantle reveal a complex spatial and temporal record due to a protracted history of formation and reworking. The structure of the crust at any particular point in time records the cumulative history of multiple magmatic, deformational, metamorphic and sedimentary events. The heterogeneous internal structure of the crust revealed from mapping across a range of exposed crustal levels, xenolith data and geophysical studies are homogenized into crustal models divisible into two to three layers. These layers consist of an upper crust of felsic composition containing low-metamorphic grade igneous and sedimentary rocks transitioning into middle and/or lower crust of increasing metamorphic grade and more mafic composition (Figure 5; e.g., Rudnick & Fountain, 1995; Rudnick & Gao, 2003; Y. Huang et al., 2013; but Hacker et al. (2015) in their two layer model argue for a felsic lower crust). Differences between these two- and three-layer models relate to differences in the inferred distribution

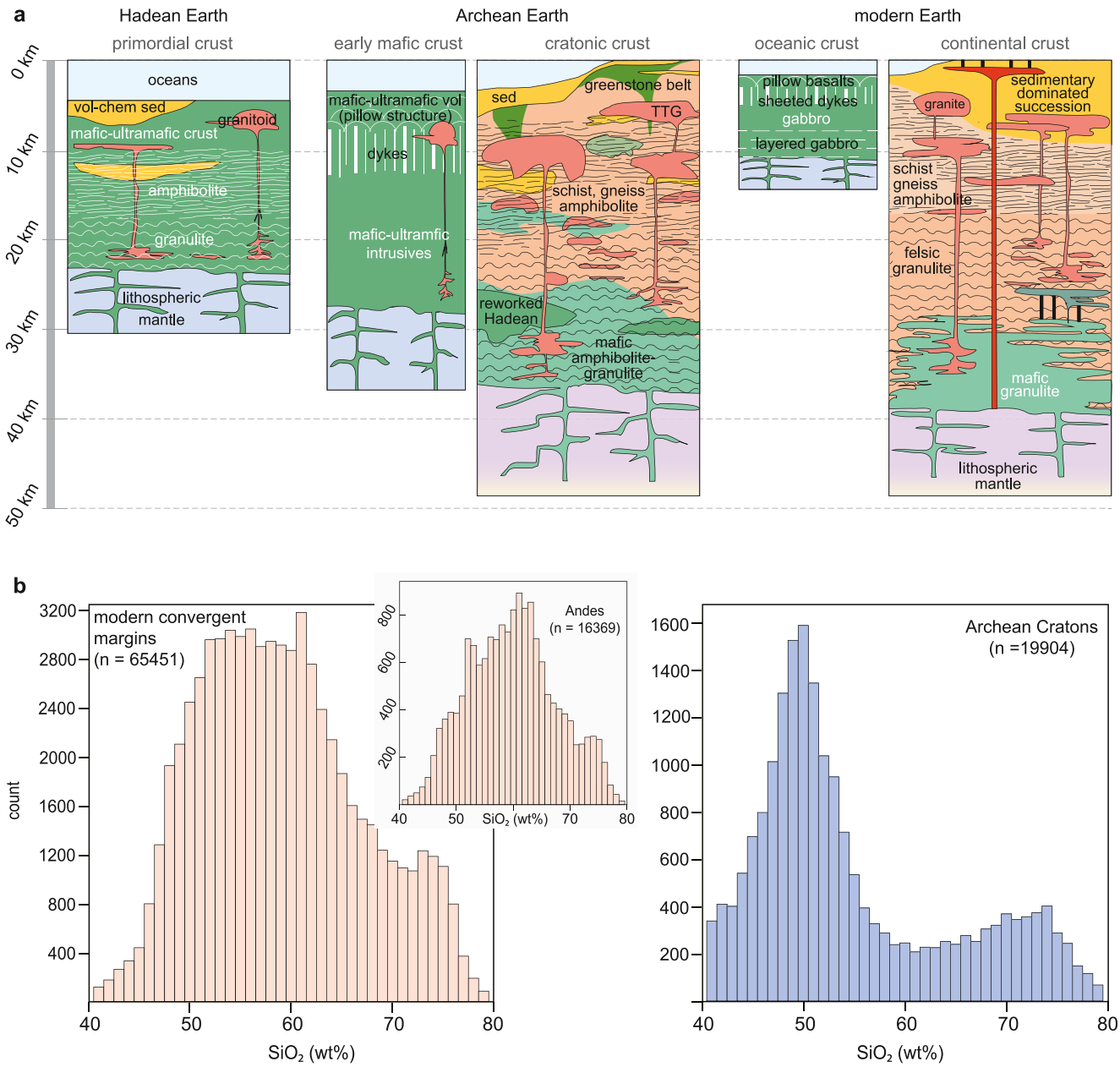

Figure 5. (a) Schematic sections of Hadean, Archean and modern continental-type crust, along with sections of early mafic crust and modern oceanic crust. Hadean and Archean sections for primordial and cratonic crust adapted from Kamber et al. (2005) and modern crust from C. J. Hawkesworth and Kemp (2006), the latter based on an internal three layer structure. (b) Whole rock SiO_2 distributions of igneous rocks from modern convergent margins and Archean cratons. Data sources are from GEOROC (http://georoc.mpch-mainz.gwdg.de/georoc/) and Gard et al. (2019), respectively.

of silica, and the resultant concentrations of heat producing elements (U, Th, and K), in the crust and heat flow input from the mantle, as well as the inferred processes for generating the continental crust's bulk composition (e.g., delamination vs. relamination). The inferred bulk composition of modern continental crust is similar to andesite with minor and trace element values typical of subduction-related magmas, arguing for continental growth at convergent plate margins (Davidson & Arculus, 2006; Hacker et al., 2011; Rudnick & Gao, 2003; S. R. Taylor, 1967). The overall andesitic composition of the continental crust necessitates a multistage formation process involving initial extraction of mafic magmas from the mantle and their differentiation by fractional crystallization or re-melting, followed by the return of the cumulate or residue to the mantle and/or relamination of previously formed crust (e.g., Davidson & Arculus, 2006; Hacker et al., 2011; but see also Castro et al. (2013), for direct formation of andesitic crust by melting of subducted rock mélanges). Furthermore, the preserved record

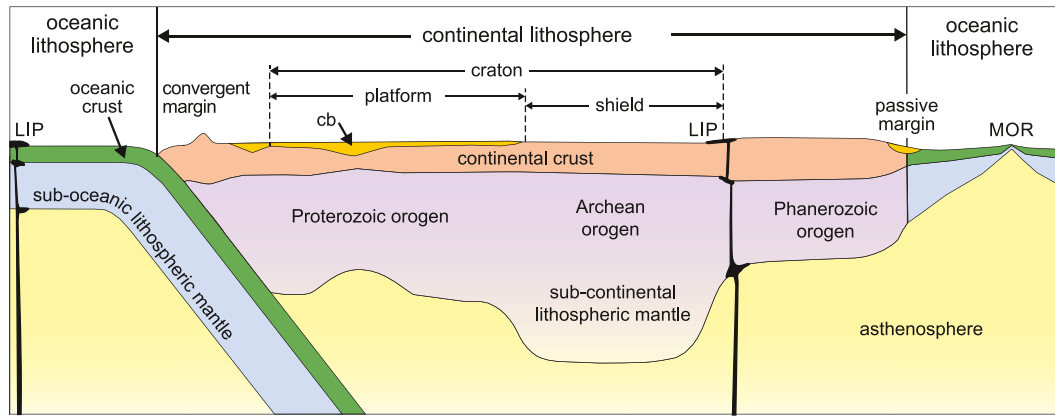

Figure 6. Idealized cross section of continental lithosphere displaying different overall thickness characteristics of Archean, Proterozoic and Phanerozoic crust and lithospheric mantle. Lithosphere beneath Archean regions is of the order of 200–250 km thick and oceanic lithosphere is up to 100 km. Abbreviation: cb, cratonic basin; LIP, large igneous province; MOR, mid-ocean ridge.

of the continental crust suggests fundamental changes in composition (and structure) in the late Archean (e.g., Figure 5).

Compilations of elemental abundances and ratios from sedimentary and igneous rocks suggest a change in the composition of at least the upper crust in the late Archean (C. B. Keller & Schoene, 2012; S. R. Taylor & McLennan, 1985). Tang et al. (2016) subsequently documented high Ni/Co and Cr/Zr ratios in Archean shales and glacial diamictites compared to younger sedimentary rocks. These ratios correlate with MgO contents in igneous rocks, suggesting the upper crust sampled by sedimentary rocks had MgO contents of ∼15% at 3.2 Ga and that this value had dropped to values similar to modern upper continental crust of ∼4% by 2.6 Ga. Similarly, compiled Cr/U in terrigenous sedimentary rocks suggest derivation from predominantly mafic crust prior to ca. 3 Ga, followed by a transition to crust of andesitic composition in post-Archean rocks (Smit & Mezger, 2017). The links between the composition of the bulk crust and the upper crust sampled by sediments remain a matter of debate (C. J. Hawkesworth et al., 2020).

In addition to the general increase in silica content of the continental crust through time, statistical geochemistry has revealed secular compositional changes within felsic and mafic continental igneous rocks (e.g., B. Keller & Schoene, 2018; C. B. Keller & Schoene, 2012; Johnson et al., 2019; Moyen & Laurent, 2018). Felsic igneous rocks show a decrease in Na_2O/K_2O, Sr and Eu/Eu* through time, which are interpreted to reflect a secular change in the physical conditions of felsic magmatism. Whereas secular changes in the composition of mafic igneous rocks, including an increase in La/Yb, a secular decrease in compatible element contents, and an increase in incompatible element contents are interpreted to reflect a decrease in the degrees of mantle melting through time in response to declining mantle temperatures.

The continental crust has a 100-fold enrichment of heat producing elements (U, Th, and K) over the mantle (Rudnick & Gao, 2003) such that although the crust only constitutes ∼0.5% of the Earth's mass, it contributes one-third of the radiogenic heat (Y. Huang et al., 2013). The surface heat flux of the present-day continental crust varies from place to place depending on the age of the terranes. It is generally low in Archean cratons, of the order of 30–40 mW m^{-2}, and as high as 60–80 mW m^{-2} in Proterozoic and younger crust (Jaupart et al., 2016). These values correspond to both decreasing lithospheric thickness from cratons to Phanerozoic orogens (e.g., Figure 6) and to the changing bulk composition of the continental crust (Figure 5). Integrating surface heat flow data from Archean cratons with *P-T* estimates from lithospheric mantle xenoliths, C. Hawkesworth and Jaupart (2021) calculated bulk crustal heat production values. These indicate that ∼70% of Archean continental crust, in the areas where heat flow data were available, had a relatively mafic composition (cf., Figure 5) and bulk crust MgO values of up to 10% compared to ∼5% for post-Archean crust. For comparison, the proportion of mafic crust in the present-day bulk continental crust is estimated by Rudnick and Gao (2014) at ∼43%, and is concentrated in the lower crust.

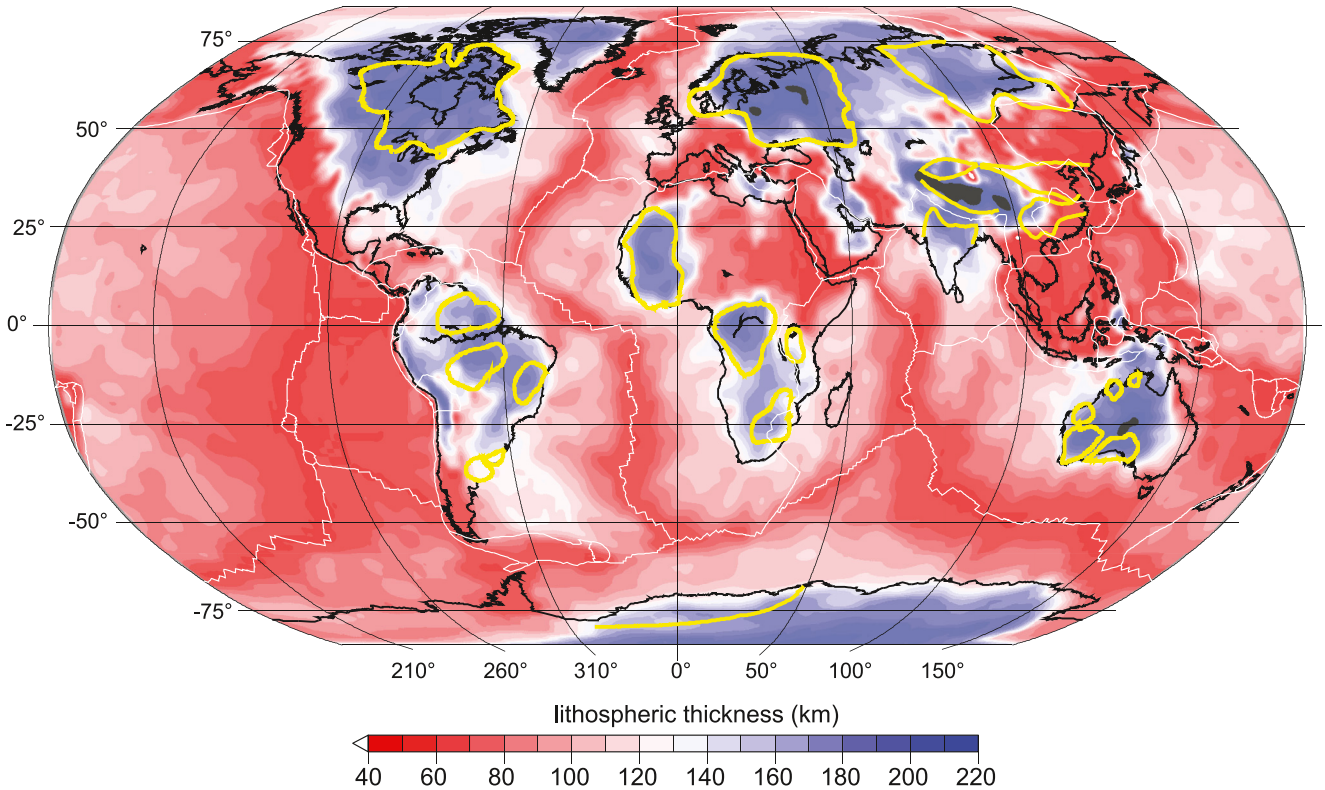

Figure 7. Global lithospheric thickness model (from Priestley et al. (2018)) derived from the $V_S(T)$ relationship and the upper mantle tomographic V_{Sv} model CAM2016Vsv. The yellow contour denotes the geologically mapped boundary of the shields at the surface (from Goodwin (1996)).

3.2. Continental Lithospheric Mantle

The lithospheric mantle contains melt-depleted peridotite. Extracting melt from peridotite results in an increase in MgO content and decreasing density and water content relative to undepleted asthenospheric peridotite (Pearson et al., 2021, and references therein). Together with cooling of the lithospheric mantle, the compositional changes induced by melt loss result in a more viscous and buoyant character relative to the underlying convecting mantle and account for the long-term stability of continental lithosphere (Jordan, 1978, 1988; Lee et al., 2011).

The thickness of continental lithospheric mantle varies from as little as a few 10s of km under hyper-extended continental margins to some 200 km or greater under some Precambrian cratons (Figure 7; Cooper et al., 2017; Priestley et al., 2018). The combination of tectonic and magmatic processes results in the thickness of crust and lithospheric mantle evolving over time, which on the contemporary Earth occurs close to active plate boundaries. The ratio between the thickness of continental crust and lithospheric mantle varies with overall age, and degree of depletion, of the lithosphere and tectonic setting (cf., Dewey, 1982). Modern convergent plate margins have a relatively large ratio of crust to lithospheric mantle thickness approaching 1, whereas stable Archean cratons can have ratios as small as 0.1 (Cooper et al., 2017; Pasyanos et al., 2014).

4. Continental Lithosphere Types: Orogens, Cratons, Basins, and LIPs

The preserved crustal record of the continental lithosphere is divisible into orogens (including cratons), basins, and large igneous provinces (LIPs) (Figure 6). The lithotectonic units and tectonothermal events of these continental lithospheric elements have differing but linked spatial and temporal histories. Orogens are the key building block of continents; they shape much of the rock record and what is preserved. Their history of sedimentation, magmatism, deformation and metamorphism provide the main record of continental formation, reworking, and stabilization. Cratons are orogens that have remained stable for long periods after their formation and are generally considered to be at least mid-Proterozoic in age or older (e.g., Pearson et al., 2021; Şengör et al., 2021). LIPs consist predominantly of mafic igneous rock sourced from upwelling and melting of mantle underlying the

lithosphere. Sedimentary basins form a cover on the other continental lithospheric components and are made up of clastic detritus derived from pre-existing elements, along with chemical sediments and biogenic accumulations. Basin deposits and LIPS are variously incorporated into orogens during tectonothermal events.

4.1. Orogens

Orogens contain a variably deformed and metamorphosed assemblage of sedimentary and igneous rocks. Orogens are segments of continental lithosphere that are generated and evolve through one or more cycles of sedimentation, subsidence, and igneous activity. The records of orogens are punctuated by tectonothermal events (orogenies), involving deformation, metamorphism, sedimentation, and further igneous activity that lead to thickening and stabilization of the lithosphere (Cawood et al., 2009; van Hinsbergen et al., 2021). Orogens may remain active over prolonged periods of time ranging from 10s to 100s of millions of years, with their duration thought to decrease with the age of Earth, perhaps in relation to mantle cooling (Chowdhury, Chakraborty, et al., 2021). Such long-lived orogens may have either experienced a single, continuous tectonothermal event (e.g., Napier Complex; Clark et al., 2018) or multiple tectonothermal events separated by periods of quiescence, each spanning over few 10s of millions of years (e.g., Central Indian Tectonic Zone; Bhowmik & Chakraborty, 2017). Short-lived orogenesis is known to have occurred on Earth (e.g., Dewey, 2005) and is on the order of millions to tens of millions of years. Cratons are those orogens that have been undeformed and stable for long periods of time (e.g., Figure 6; Holmes, 1965).

Orogen evolution involves the development of initial sites of subsidence, generally associated with lithospheric extension and/or thermal subsidence that act as a focus for later compression and basin inversion, lithospheric thickening and stabilization (Cawood et al., 2009). Based on the nature of the lithosphere involved (continental vs. oceanic) orogens can be grouped into three endmember types (Figure 8): collisional, accretionary, and intracontinental (Cawood et al., 2009). Collisional orogens form through collision of buoyant continental lithospheric fragments, whereas accretionary orogens form at the boundary between buoyant continental and dense oceanic lithosphere, and intracontinental orogens form within a pre-existing segment of buoyant lithosphere. The Alpine-Himalayan, Cordillera, and Tian Shan, respectively, are modern actualistic examples of these three orogen types (Figure 2). Subsidence associated with initiation of an orogenic cycle is driven by lithospheric extension with associated near surface rift basin sedimentation, faulting and magmatism and lower lithosphere ductile necking, which may progress to ultimate breakup and separation of lithosphere and resultant thermal subsidence leading to passive continental margin formation. Convergence between lithospheric segments with resultant coupling can result in periodic thickening and tectonothermal activity forming accretionary and collisional orogens, depending on whether one of the lithospheres is sufficiently thin and dense to be recycled into the mantle, or whether both lithospheres are buoyant, and convergence is terminated. Subsidence associated with intracontinental orogens occurs through thermal and/or rheological weakening (Sandiford et al., 2001) with subsequent crustal thickening and stabilization taking place away from active lithospheric margins but generally associated with far-field stresses (Cawood et al., 2009; Raimondo et al., 2014). The circum-Pacific Gondwanide and Terra Australis orogens are examples of accretionary orogens (Cawood, 2005), whereas the Variscan, Appalachian-Caledonian, Grenville and Trans-Hudson orogens formed through continent-continent collision (Dewey & Bird, 1970; Hoffman, 1988; Rivers, 2009; Weller et al., 2021; Wilson, 1966), and the Alice Springs and Petermann orogens of Central Australia and the Kwangsian (or Wuyi-Yunkai) orogen in South China (Li et al., 2010; Shu et al., 2015; Xu et al., 2016) formed in intra-continental settings (Raimondo et al., 2014). Although the role and extent of modern-style plate tectonics on the Precambrian Earth is disputed, classification into collisional, accretionary, and intracontinental, based on site of orogenesis with respect to lithosphere type, remains applicable irrespective of the ultimate geodynamic regime and tectonic driver (i.e., it can also be applied to non-plate tectonic regimes). In addition, the ultra-hot to hot Precambrian orogens (Chardon et al., 2009; Chowdhury et al., 2017; Perchuk et al., 2018) that are characterized by delamination, broad and flat zones of distributed deformation, melting, and ultra-high temperature metamorphism, form through convergence between thin blocks of continental lithosphere. These are different from modern collisional orogens and rather mimic the thermomechanical architecture of accretionary orogens. Their numerical simulations, which were undertaken at mantle temperatures hotter than today, resulted in an initial thickened collisional orogen that evolves into a long-lived hot broad accretionary-like orogen underlain by partially molten asthenosphere through delamination and peel-back tectonics (cf., Chowdhury et al., 2020).

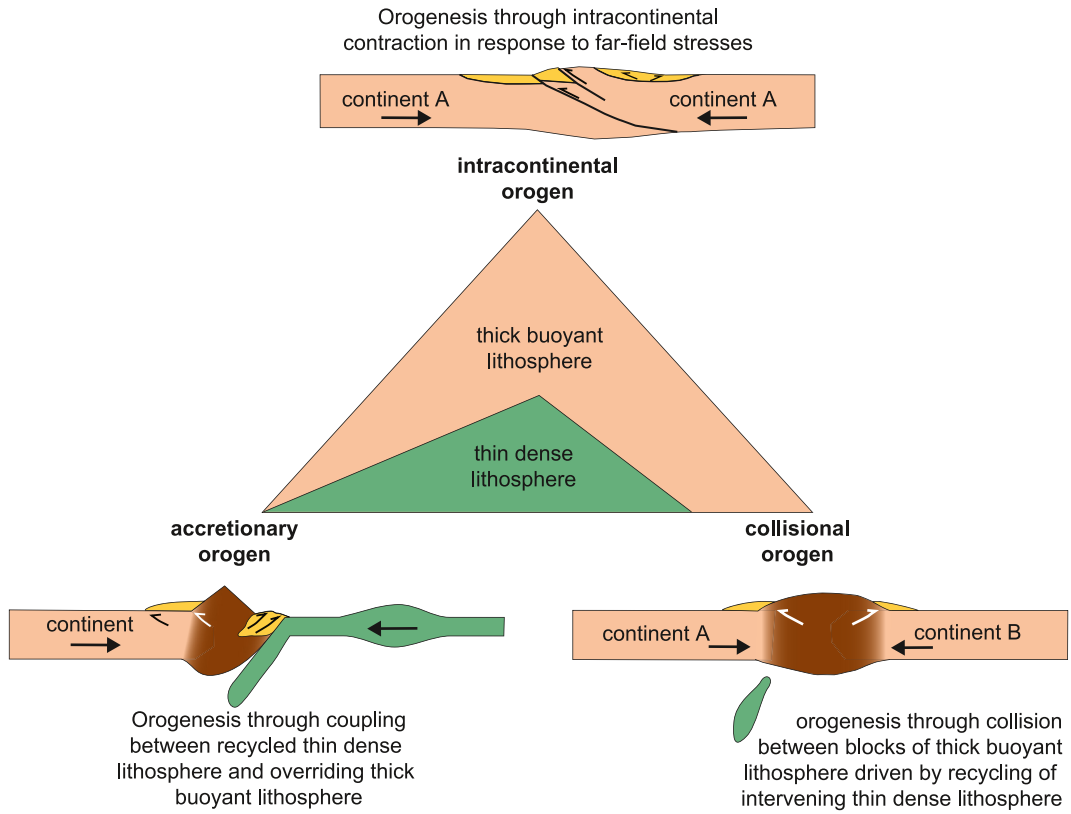

Figure 8. Orogen types. Orogen classification into accretionary, collisional and intracontinental based on nature of lithosphere (thick and buoyant or thin and dense). Collisional orogen is stabilized through collision between blocks of thick buoyant lithosphere. In an accretionary orogen, orogenesis is the result of coupling between thin dense lithosphere being recycled into the mantle and thick buoyant lithosphere. In an intracontinental orogen, orogenesis occurs within thick buoyant lithosphere in response to compression driven by far-field stresses.

Younger orogens inherit features from spatially overlapping older belts, in part by reworking of older rock assemblages, which commonly form a basement for the carapace of unconformably overlying syn-orogenic rock units. Accretionary and collisional orogens are sites for new crustal generation as well as for crustal reworking (Cawood et al., 2013; C. Hawkesworth et al., 2010). Accretionary orogens and the convergent stages of collisional orogens can result in the generation of continental crust. For accretionary orogens, this is generally invoked to involve fluxing of fluid and sediment derived from recycled dense oceanic lithosphere driving melting in the mantle and magmatism in the overlying lithosphere (Marschall & Schumacher, 2012). For recent collisional orogens, heat input to the lithosphere, perhaps facilitated by an increase in the rate of convergence or slab break-off, drives melting of the lower crust (D. C. Zhu et al., 2022a), whereas during the Earth's early history, high mantle potential temperatures would likely lead to decompression melting during inferred delamination and lithospheric peel-back in the zone of convergence (Chowdhury et al., 2020; Perchuk et al., 2018). The termination of convergence in collisional orogens results in continental growth and reworking through the assembly of largely preexisting lithosphere. As such, collisional orogens lie in the interior of continental lithosphere at the time of formation (Figure 2). On our constant radius Earth, the termination of convergence with the formation of collisional orogens appears to be compensated by, and coincident with, the development of convergence (and initiation of peripheral accretionary orogens) outboard, and at the margins, of the assembled continental lithosphere (Cawood & Buchan, 2007; Cawood et al., 2016, 2021; Murphy & Nance, 1991).

4.2. Cratons

The term "*kratogen*" was introduced by Kober (1921) to refer to strong crust that could resist buckling. It was shortened to "*kraton*," and the concept was further developed by Stille (1936), and then anglicized to "*craton*" by Kay (1944, 1951), and applied to areas of stable crust bounded by mountain belts (*geosynclines*). The meaning

of the term has continued to evolve with increasing knowledge of the continental lithosphere, especially of the cratonic roots, but also on whether the emphasis is top down (sedimentary successions accumulating on the craton) or bottom up (character of the underlying lithospheric mantle). The former focuses on long-term stability and overlying basins (e.g., Sloss, 1988a), whereas the latter is often concerned with thickness and composition of the lower crust and lithospheric mantle, and the boundary layer with the asthenosphere (e.g., Cooper & Conrad, 2009; Pearson et al., 2021; Priestley et al., 2018).

Cratons originally included both oceanic and continental crust that were separated by "*orthogeosynclines*" (i.e., orogens). The inclusion of oceanic crust was based on the belief that oceans were long-lived and stable. However, with the realization that oceanic crust is young and ephemeral, the term is now restricted to the stable interiors of continents (Sloss, 1988a) bounded by younger orogens. Cratons in the lithostratigraphic sense are strong stable surfaces that have generally maintained positions at or near sea-level for long periods of time, as evidenced by unconformably overlying sub-horizontal sedimentary sequences as old as late Archean and early Paleoproterozoic (e.g., Fairbridge & Finkl, 1980; Hickman, 2012; Occhipinti et al., 2017). Geophysical and geochemical data demonstrate that cratonic lithosphere is thick, generally in the range 170–250 km, with Archean cratons characterized by low heat flow relative to Proterozoic and Phanerozoic lithosphere (Artemieva, 2009; Lee et al., 2011). The cratonic lithospheric mantle is composed of dehydrated, melt-depleted peridotite (e.g., Griffin et al., 2009; Pearson et al., 1995), resulting in it being intrinsically buoyant and strong, which counteracts the destabilizing effect of its cold thermal state (Lee et al., 2011). Although characteristically thick, some cratons have a lithospheric thickness of less than 100 km (e.g., North China and Wyoming) attributed to subsequent removal of the thick root by thermal and chemical processes (S. Gao et al., 2002; Snyder et al., 2017). Furthermore, the Slave craton in Canada shows evidence, from the petrology of mantle xenoliths in kimberlites and geophysical data, for thinning in the Mesoproterozoic to <80 km and subsequent thickening to ∼200 km by the end of the Proterozoic. This deconstruction and reconstruction of the Slave lithosphere has been related to mantle upwelling of the Mackenzie LIP (J. Liu et al., 2021).

Cratons are divisible into shields, containing exposed crystalline igneous and metamorphic rocks, and platforms, which are overlain by flat lying to weakly deformed sedimentary successions (Figure 6; Holmes, 1965), with the latter divisible into two end-member successions of platform and cratonic basins (see below). Up to ∼60% of the present day continental lithosphere can be classified as cratons, depending on the definition used (e.g., Pearson et al., 2021). Some have argued that cratons may be continuing to form today. McKenzie and Priestley (2008) have highlighted that modern-day tectonically active regions such as the Tibet and Iran plateaus have lithosphere up to 260 km thick (Figure 7), although the lithospheric thickness in Tibet is variable and less under parts of northern and eastern Tibet (X. Zhang et al., 2014; Z. Zhang et al., 2010). Their formation and preservation requires stabilization of the lithosphere against convective instability and, like their Precambrian counterparts, this likely involves a reduction in mantle density through depletion by melt removal, which in combination with compression results in thickening of both the crust and lithospheric mantle (McKenzie & Priestley, 2016; Priestley et al., 2020). It has not been established that these inferred, recently formed, cratons contain low-Fe mantle lithosphere, a feature of Archean cratons (cf., Griffin et al., 2009; Pearson et al., 2021), and hence whether such regions are ultimately preserved can only be assessed with the passage of time. However, they provide potential insight into the processes of generating thick stable lithosphere.

The maximum thickness of the chemically defined continental lithosphere based on xenolith data is ∼200 km, whereas the maximum thickness based on thermal structure, as inferred from geophysical data, may be deeper (∼250 km) and include a transition zone between rigid lithosphere and convecting mantle (Cooper & Conrad, 2009). The thick roots of cratons are likely to increase coupling with the convecting asthenospheric mantle and potentially limit maximum lithospheric thickness (Conrad & Lithgow-Bertelloni, 2006; Cooper & Conrad, 2009). The thermal boundary layer at the base of the lithosphere will absorb some of the shear deformation resulting from coupling with the convecting mantle and the thickness of this layer decreases with increasing thickness of the cratonic root (rigid chemical boundary layer). Furthermore, Cooper and Conrad (2009) argue that vigorous convection in the hotter mantle of the early Earth promoted the generation of thick cratons because the convective stresses were smaller.

Relatively abrupt decreases in thickness at the margins of cratons mark major boundaries in the continental lithosphere. These are likely zones of stress localization (Yoshida & Yoshizawa, 2021) and may constitute zones of

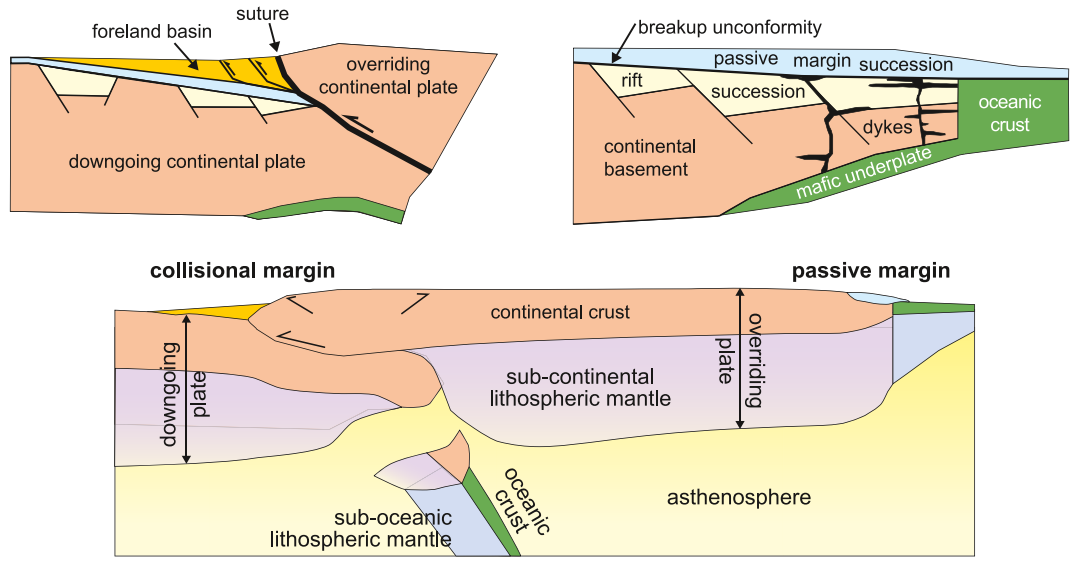

Figure 9. Schematic cross-sections of principal basin types. At a passive continental margin the transition from rift to thermal subsidence phases is marked by the break-up unconformity and the onset of sea-floor spreading. In a collisional setting, loading and subsidence of buoyant lithosphere being overridden leads to development of a foreland basin.

focused magmatic activity, fluid movement, and resultant large-scale mineralization (Groves & Santosh, 2020; Hoggard et al., 2020).

4.3. Basins

Subsidence of continental lithosphere is driven by lithospheric extension, thermal subsidence, and lithospheric loading. A carapace of sedimentary rocks extending from the continental interior to the margin often blankets continental crust. These sedimentary units are divisible into platform successions and cratonic basins, the latter also referred to as intracratonic basins (Figure 6). The platform succession consists of little deformed, unconformity bound, sequences that onlap onto the continent and extend into, and are reworked within, adjoining orogens (Bally, 1989; Sloss, 1963, 1988b), as well as extending onto modern continental margins. They provide a record of extension and thermal subsidence along the continental margin, associated with stretching and breakup of lithosphere, as well as eustatic events (Figure 9). Basins positioned inboard of contemporaneous accretionary and collisional orogens are termed foreland basins and inferred to form through lithospheric loading from the adjoining orogen (Figure 9; Beaumont, 1981; DeCelles & Giles, 1996). Foreland basin deposits can become variably incorporated into the orogen as the deformational front advances inboard toward the foreland. The oldest preserved large-scale passive margin and foreland basins recognized in the geological record are of the order of 3 Ga and their formation requires lateral motion of lithosphere through extension and compression, respectively (Bhattacharjee et al., 2021; Bradley, 2008; Camiré & Burg, 1993; Catuneanu, 2001; De, 2021; Hofmann et al., 2001; Mueller et al., 2005). The occurrence of large-scale, focused regions of lithospheric extension must be compensated by zones of concurrent compression, and vice versa (cf., B. Huang et al., 2022; Cawood et al., 2018). Thus, it is perhaps not surprising that passive margins and foreland basins both appear at similar times in the geological archive.

Cratonic basins are large, isolated, long-lived, slowly subsiding subcircular to equant basins filled with shallow marine to terrestrial sedimentary rocks (M. C. Daly et al., 2018). They unconformably overlie thick cratonic lithosphere (e.g., Figure 6) and generally lack evidence for extension, with subsidence related to cooling (McKenzie & Priestley, 2016; Sleep, 2018a).

4.4. Large Igneous Provinces

LIPs include extrusive phases and their feeder systems of dykes, sills, layered intrusions and crustal underplates. They are produced by large volume (>10^5 million km^3), dominantly mafic and ultramafic magmatic events that

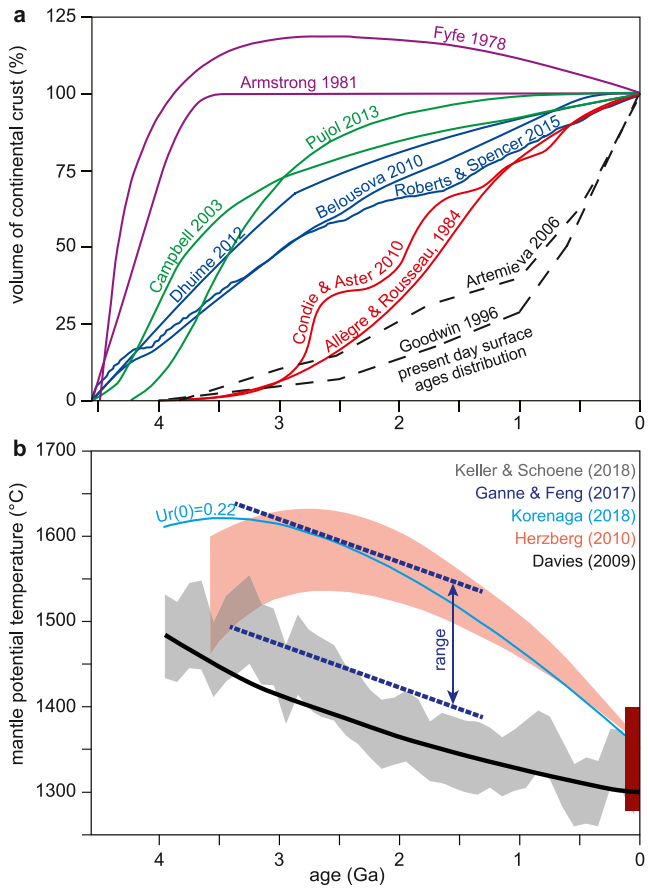

Figure 10. (a) Selected crustal growth models compared to the age distribution of presently preserved crust from Goodwin (1996). Models are determined relative to the present volume of the continental crust. Some curves are based on present day distributions and do not account for the current paucity of the early rock record due to possible selective preservation and recycling of material back into the mantle. Such curves include the black dashed and solid red curves in which the volume of crust is based on present preserved variation in age and thickness data of continental crust (Artemieva, 2006), Nd isotope ratios in Australian shales (Allègre & Rousseau, 1984), and volumes of rocks with different Nd or Hf crust formation ages (Condie & Aster, 2010). Curves colored blue and green attempt to estimate the volumes of continental crust at different times in Earth history, independent of the relative volumes preserved today. These are based on the proportions of reworked and juvenile crust in the zircon record (Belousova et al., 2010; Dhuime et al., 2012; Roberts & Spencer, 2015), modeled secular evolution of atmospheric argon based on measurements of $^{40}Ar/^{36}Ar$ in fluid inclusions in 3.5 Ga quartz (Pujol et al., 2013), and Nb/U ratio of Archean basalts and komatiites derived from the mantle, along with modeled secular variations (Campbell, 2003). A limitation with all these approaches is that the curves are based on cumulative growth of the crust and sum to unity at the present day, and hence no curve can have a past volume greater than the current volume. The purple curves of Fyfe (1978) and Armstrong (1981) present a set of schematic curves and were amongst the first to highlight that growth not only involved the generation of continental crust through the extraction and crystallization of magma from the mantle, but also its recycling back into the mantle. (b) Selected models for the evolution of mantle potential temperature (T_p) through time. These mantle T_p curves are estimated either from the chemical composition of non-arc basaltic magmas (B. Keller & Schoene, 2018; Ganne & Feng, 2017; Herzberg et al., 2010), or via thermal modeling after extrapolating the present-day Urey ratio back in time (Davies, 2009; Korenaga, 2018a).

are emplaced in one or more pulses over a short duration (1 to <50 Ma) in both oceanic and continental intraplate settings (Figure 6; Ernst, 2014a; Ernst et al., 2021). They are linked to the input of heat associated with mantle plumes (Ernst et al., 2021), but many continental LIPs also displaying variable input from sub-continental lithospheric mantle (Pearce et al., 2021). The mantle plume source for LIPs is commonly linked to large low-shear-velocity provinces at the core mantle boundary (Figure 1; Burke et al., 2008; Koppers et al., 2021). The sub-aerial and high-level crustal components of pre-Mesozoic LIPs have mostly been removed by erosion, with evidence for them based on deep level dyke swarms (e.g., Mackenzie dyke swarm), sill provinces (e.g., Karoo sill province), and large layered intrusions (e.g., Bushveld). LIPs occur at semi-regular intervals throughout Earth history, extending back at least until the Paleoarchean (ca. 3.5 Ga; e.g., Ernst et al., 2021; G. R. Byerly et al., 2019a). The earliest LIPs in the geological record are submarine but subaerial LIPs are first recorded around 3 Ga in the Pilbara and Kaapvaal cratons and then become more widespread across late Archean cratons (Kump & Barley, 2007). LIPs can host major mineral deposits, notably nickel and platinum group elements (e.g., Noril'sk, Bushveld). Kimberlites and carbonatites, which are associated by some with LIPs, can host diamonds and rare-earth deposits, respectively (e.g., kimberlites, southern African; Bayan Obo carbonatite, China; Ernst, 2014b; Ernst & Bell, 2010).

5. Continental Rock Record

Understanding the nature and origin of the rock record is the prime prerequisite for interpreting its significance in unraveling Earth processes. Oceanic lithosphere, which constitutes 60% of the current surface area, is dense, relative to the underlying convecting mantle, resulting in its recycling into the mantle (Cloos, 1993). Apart from minor slivers, preserved as ophiolites, and now emplaced into continents (Coleman, 1971, 1977), the oceanic lithosphere is generally <200 Ma (Granot, 2016; Seton et al., 2020). In contrast, continental lithosphere is more buoyant than the underlying mantle making it difficult to recycle and hence is the long-term archive of Earth history, extending back at least 4 Ga. However, the preserved area of continental crust, and the inferred corresponding volume, decreases with increasing age (Figure 10a). Yet, most estimates of continental volume are considerably greater than the preserved volume for any given time period; for example, the preserved volume of continental crust of Archean age is <15%, whereas the estimated volume present at that time may have been >75% of the present-day volume (Figure 10a). This discrepancy requires extensive recycling of continental lithosphere, and at times this must have been equal to, or greater than, the rate of continental generation (Armstrong, 1991; C. Hawkesworth et al., 2013; Dhuime et al., 2017; Fyfe, 1978; Korenaga, 2018b; McCoy-West et al., 2019). Estimates of current rates of generation and recycling of continental crust suggest recycling may be greater than generation by ~1 km^3/a at least since the Mesozoic and possibly longer (e.g., Cawood & Hawkesworth, 2019; Cawood et al., 2013; Clift et al., 2009; C. R. Stern, 2011), which would equate to a 15% decrease in continental volume since the mid-Neoproterozoic.

The discrepancy between inferred and preserved volumes of continental crust raises concerns over how representative the crustal archive is of the geological processes that have operated through Earth history. In particular, is the preservation of continental lithosphere a random process or is it selective and dependent on the characteristics of the lithosphere (e.g., thickness and density) and/or the processes of crustal generation and recycling (e.g., plate

10.1029/2022RG000789

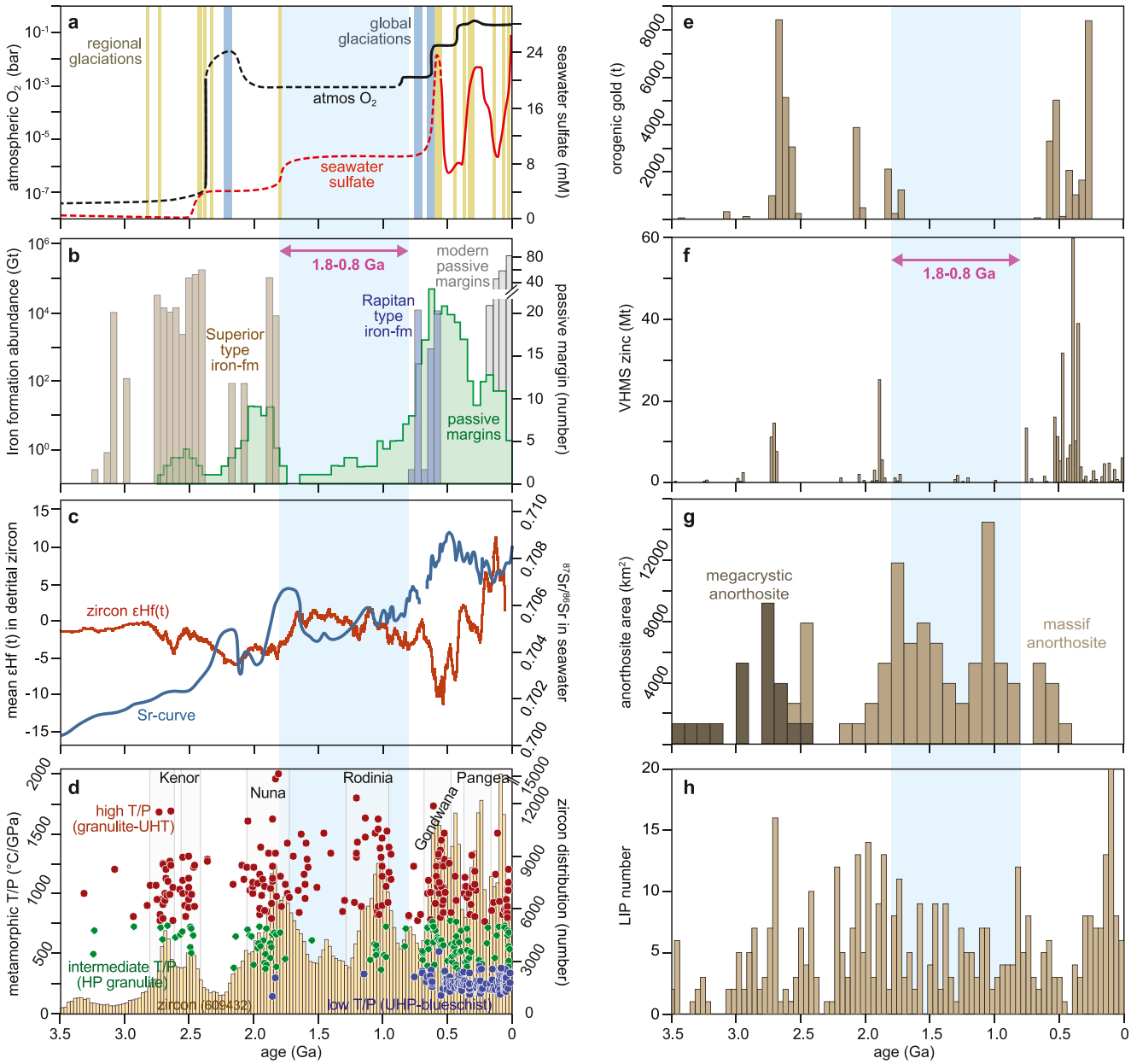

Figure 11. (a) Temporal distribution of glaciations (Bradley, 2011), atmospheric oxygen (Catling & Zahnle, 2020), and seawater sulfate (adapted from Pope and Grotzinger (2003) and Farquhar et al. (2010)). (b) Iron formation abundance (Bekker et al., 2010) and age distribution of ancient and modern passive margins (Bradley, 2008). (c) Normalized seawater $^{87}Sr/^{86}Sr$ curve (X. Chen et al., 2022) and the running mean of initial εHf in ~7,000 detrital zircons from recent sediments (Cawood et al., 2013). (d) Histogram of >600,000 detrital zircon analyses showing several peaks in their U-Pb crystallization ages over course of Earth history (Puetz & Condie, 2019) that are very similar to ages of supercontinent assembly. Also shown is apparent thermal gradient versus age of peak metamorphism for three main types of granulite facies metamorphic belts (Brown, Johnson, et al., 2020); high *T*/*P* (granulite-UHT), intermediate *T*/*P* (HP granulites), and low *T*/*P* (UHP blueschists). (e) Orogenic gold (Huston et al., 2015). (f) Volcanic-hosted massive sulfide (VHMS) deposits (Huston et al., 2015). (g) Anorthosite abundance (Ashwal & Bybee, 2017). (h) Distribution of large igneous provinces (Condie et al., 2015). The timeframe ca. 1.8–0.8 Ga corresponds to Earth's middle age (cf., Cawood & Hawkesworth, 2014).

tectonic vs. non-plate tectonic modes)? Furthermore, the preserved rock record, and the proxies inferred from it, are episodic with a heterogeneous distribution in space and time. The ages of igneous crystallization events, metamorphism, continental margins, and mineralization, as well as changes in seawater and atmospheric composition, are distributed about a series of peaks and troughs or display a secular evolution marked by step changes (Figure 11). From at least the late Archean onwards, these changes correspond with inferred periods of continental assembly (e.g., Campbell & Allen, 2008; Cawood & Hawkesworth, 2015; C. Hawkesworth et al., 2009; Roberts, 2012; Spencer et al., 2015). There has been significant discussion about the drivers for the episodic

record, with end-member models proposing that it represents either a primary or a secondary signal. The former suggests the record represents changes in the rate of magmatic addition to the continental crust (Condie, 1998; Parman, 2015; Puetz & Condie, 2020; Rino et al., 2004), whereas the alternative model argues for enhanced preservation of continental crust during the later stages of continental collision and assembly (Cawood et al., 2013; C. Hawkesworth et al., 2009; Mulder & Cawood, 2022; Roberts, 2012; Spencer, 2020).

We define a primary, generational signal as a direct record of processes or events related to Earth evolution that is preserved in the rock record. This signal may reflect events external to the Earth (meteorite impacts), processes driven by the mantle (bottom-up processes), or surficial processes related to the atmosphere, ocean, and biosphere. A secondary, preservational signal is a record of processes or events modified and/or controlled by tectonic processes, especially those focused at plate margins, including the supercontinent cycle. We consider that some primary processes probably have a secondary component if, for example, the preserved rock archive is itself biased by the supercontinent cycle. Scale is important in impacting whether a record is likely to be biased (C. J. Hawkesworth et al., 2020). Processes or events that homogenize over a short period and on a global scale (e.g., atmosphere and ocean compositions) are likely to preserve a primary record, whereas processes or events that are spatially and temporally heterogeneous (e.g., continental crust), are difficult to produce an overall spatially and temporally representative sample, and are thus more likely to be biased.

The physio-chemical resilience of zircon and its relative ease of age, trace element and isotopic analysis by modern mass spectrometry, has resulted in large databases with a global spatial and temporal range (e.g., Puetz et al., 2021; Voice et al., 2011), which represent the most comprehensive archive of crustal evolution. Consequently, arguments on the nature of the rock record and specifically the rate of igneous crust generation are often centered on the age distribution, isotopic character and trace element composition of zircon (e.g., Balica et al., 2020; Cawood et al., 2013; C. Hawkesworth et al., 2009; Condie et al., 2017; Dhuime et al., 2012; McKenzie et al., 2018; Parman, 2015; Roberts & Spencer, 2015; Tang et al., 2021; Verdel et al., 2021).

We consider the rock record, including inferences from mineral phases such as zircon, to be affected by preservation bias (C. Hawkesworth et al., 2009). Cawood et al. (2013) suggested that data sets based on frequency distribution, such as igneous crystallization ages, ages of metamorphism, or of passive margins (Figure 11), are secondary signals affected by the proportions of rocks and minerals of a specific age preserved by collision processes in the supercontinent cycle. In support of this interpretation, they pointed out that not only the distribution of zircon ages, but a range of other proxies display an episodic temporal distribution. For example, ancient passive margins display peaks in the late Archean, late Paleoproterozoic, and late Neoproterozoic to early Paleozoic (Bradley, 2008), corresponding to times of supercontinent aggregation rather than the time of supercontinent breakup, which would be expected if passive margins were an unbiased record, as breakup marks an increase in area of continental margins. In contrast, for the youngest supercontinent Pangea, the peak in frequency of passive margins post-dates its breakup, conforming to the increased area of passive margins expected during supercontinent dispersal. This discrepancy between Pangea and earlier supercontinent phases may be due to the Pangean record not yet being biased by incorporation into the next cycle of continental amalgamation.

Relationships to the supercontinent cycle may also impact the distribution of certain types of mineral deposits. For example, Phanerozoic orogenic gold and volcanic massive sulphide (VMS) deposits display a relatively continuous temporal distribution and are spatially associated with convergent plate margins of the circum-Pacific (Bierlein et al., 2009; Goldfarb et al., 2001; Huston et al., 2010). The Pacific opened in the Neoproterozoic and is yet to close (Cawood, 2005). Hence, it has not been through a complete Wilson or supercontinent cycle and rock units are yet to experience any resultant preservation bias. Frequency data driven by bottom-up, deep Earth processes may be more independent of secondary controls and tend to display a primary signal. For example, mineral deposits emplaced within intra-plate stable continental interiors and originating from deep mantle driven events (e.g., Ni-Cu-platinum group element deposits) are less likely to have their distribution controlled and modified by plate margin processes associated with the supercontinent cycle (Cawood & Hawkesworth, 2015).

Attempts to establish more rigorous tests to differentiate primary versus secondary signals have focused on the zircon record, due in part to the large data set, its broad spatial and temporal distribution, and the derivation of the bulk of the zircon crystals from magmas of felsic and intermediate composition, and hence a prime component of the continental crust (Rudnick & Gao, 2003; S. R. Taylor & McLennan, 1985). For example, Domeier et al. (2018) showed that the episodic distribution of Phanerozoic igneous and detrital zircons from SW and SE convergent plate margins of the Pacific correlate with fluctuations in the amount of subduction at these margins,

requiring the associated felsic magmatism to be a primary feature. Pulses in the volume of arc magmatism are well established (DeCelles et al., 2009, 2015; Wolfram et al., 2019), but they do not differentiate primary versus secondary signals in the long-term rock archive. This is because pulses in the frequency of arc magmatism are second-order signals of the order of 10s of millions of years, which reflect local events in the arc system and are an order of magnitude smaller than the first-order, 100s of millions of year frequency variations of the global zircon archive and its correlation with the supercontinent cycle (Campbell & Allen, 2008). It is difficult to know how regional variations in magmatism from specific parts of the circum-Pacific, which operate on such 10s or millions of year (or less) duration, will scale to global rates of production of continental crust through time. Furthermore, and as noted above, only after the circum-Pacific has gone through a complete supercontinent cycle will its long-term signal in the rock record be known (Cawood & Hawkesworth, 2015).

Further efforts to test the veracity of the continental record have endeavored to quantify the detrital zircon frequency age peaks with respect to the age of the enclosing sedimentary succession. As clastic sediments sample large regions of continents (e.g., Dhuime et al., 2017), their detrital zircon records provide a broad and time-integrated sampling of the continental crust that was generated and exposed at the surface prior to the deposition of the host sedimentary sequence. Parman (2015) argued that the zircon frequency peaks do not vary with age of the host sedimentary sequence, implying that the age peaks correspond to discrete periods of enhanced crust formation and hence episodic continental growth. In contrast, Spencer (2020) using an updated zircon database and a smaller bin-size to filter the data, showed that zircon frequency peaks decrease in age in younger sedimentary successions. He interpreted this change to reflect continuous zircon growth with peaks modified by ongoing tectonic processes, and hence that the crustal archive is biased. In another study, Spencer et al. (2022) noted secular disparities in the oxygen isotopes of detrital and igneous zircons, including that the $\delta^{18}O$ of detrital zircons is conspicuously higher during periods of supercontinent assembly. They proposed that this discrepancy is due to erosional bias in which high $\delta^{18}O$ zircons are sourced from igneous rocks with a high sedimentary melt component, which are characteristic of collisional orogens (i.e., S-types granites). Recently, Mulder and Cawood (2022) compare a compilation of monazite ages, which preserves a global record of collisional orogenesis, with the zircon archive of continental growth. They demonstrate that the two data sets strongly correlate throughout most of Earth history, with peaks in monazite ages generally younger than peaks in zircon ages by a few tens of millions of years (Figure 12). They interpreted this age offset to represent a link between collisional orogenesis and the record of continental growth inferred from zircon ages. This interpretation is further supported by the correlation of major detrital zircon age peaks with other proxies for collisional tectonics including metamorphic rutile ages, S-type granite zircon ages, and increases in the proportion of reworked sediment in magmas as inferred from the $\delta^{18}O$ systematics of zircon (Figure 12). The correlation between detrital zircon age peaks and multiple proxies for collisional tectonics supports the interpretation that the continental crust represents a preservational, rather than generational, archive of continental growth.

6. Secular Evolution of the Continental Record—A Pulsed Archive

Considering the scale of observation recorded by a data set, whether temporal or spatial, is important in unraveling the processes controlling that record (C. J. Hawkesworth et al., 2020). Scale provides the context for whether evidence is local or global in importance; is the age of an event at one location limited to that region or is it part of a global event of similar character? This can be resolved by comparing local data sets to global compilations of the same type of data. A more challenging task is to integrate different data types into a coherent framework and to determine what, if any, controls exist between different data types and the processes they represent. For example, the time of India-Asia collision is based on a range of criteria including sedimentary facies, geochemical and geochronological data on magmatic activity, and paleomagnetic and geophysical data on plate kinematics and crustal structure. These diverse data types have yielded interpreted ages for the initiation of continent-continent collision that range over 10s of millions of years (ca. 60–30 Ma; Aitchison et al., 2007; D. C. Zhu et al., 2015; Hu et al., 2016; van Hinsbergen et al., 2019). This age range reflects differences in what is recorded by each data type with respect to collision, the time lag between what is preserved and its first appearance in the rock record, and different interpretations of the same data (cf., Cawood, 2020; Cawood et al., 2018). Thus, establishing links between data sets ultimately requires an understanding of the processes involved to validate how they correlate spatially and temporally, and remains a key, yet often unresolved, issue in differentiating cause and effect in the Earth system processes.

10.1029/2022RG000789

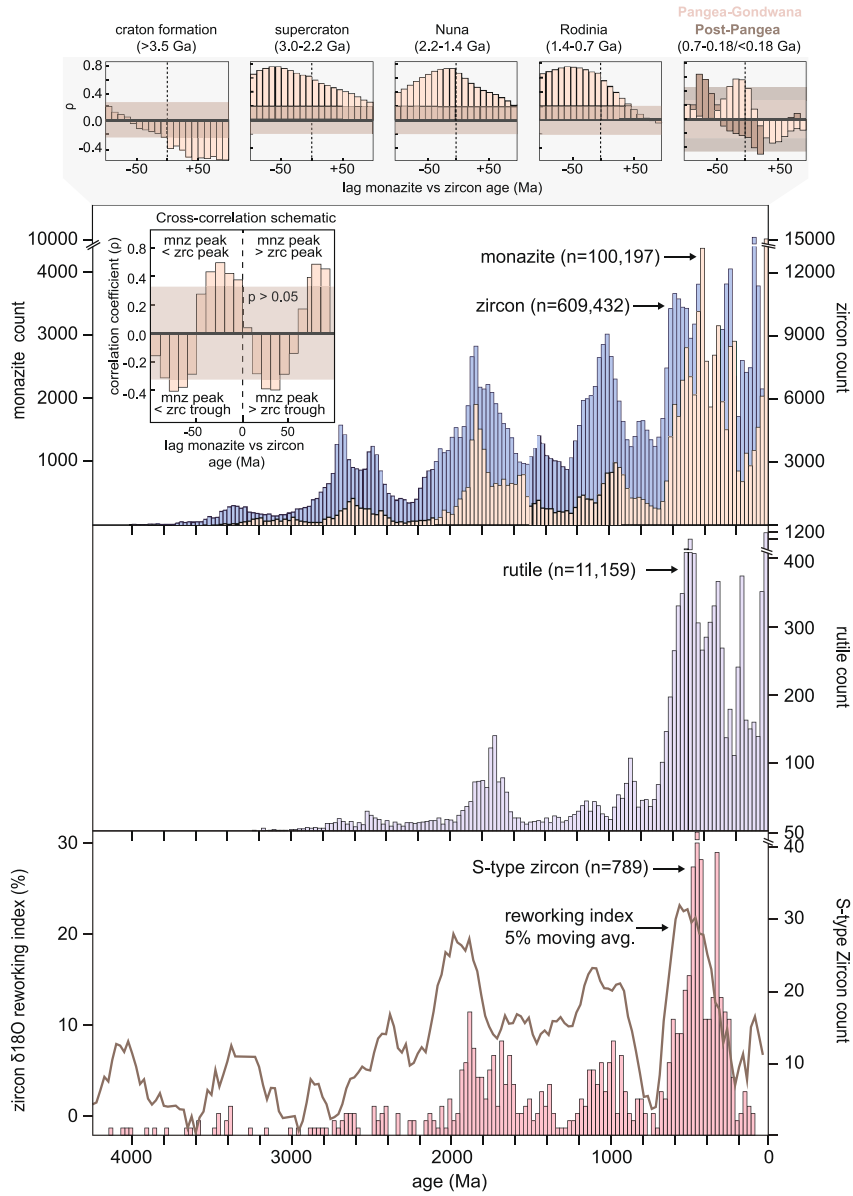

Figure 12. (a) Histograms of global monazite and detrital zircon age distributions from Mulder and Cawood (2022). Bin width is 25 Ma. Top panels summarize the results of cross-correlation analysis. Lag is the difference between the monazite and zircon age frequencies in 10 Ma bins. The transparent brown horizontal field encompasses results that cannot be excluded from the null hypothesis (no correlation) at the $p = 0.05$ significance level. Calculations were performed in R (https://www.r-project.org/). Schematic inset in the main diagram provides a summary of the cross-correlation results. (b) Histograms of global metamorphic rutile U-Pb ages (see Data Set S1 in Supporting Information S1 for references). (c) Histogram of global zircon ages inferred to be derived from S-type granites following Z. Zhu et al. (2020) with additional data compiled from Tang et al. (2021). The brown curve in panel (c) shows the moving average of the sediment reworking index based on the $\delta^{18}O$ systematics of zircon (Spencer et al., 2014).

The continental crust displays a punctuated record of step-changes in the ages of occurrence of mineral phases, rock types, and tectonothermal events. This contrasts with the progressive change in mantle potential temperature through time (e.g., Figure 10). Data sets based on frequency of a rock type or event often show an episodic distribution, at least from the Neoarchean onwards (e.g., zircon ages of magmatic activity, monazite ages of metamorphic events, passive margins, various mineral deposit types, Figures 11 and 12). Data sets based on the mean of a range (or the maximum or minimum value of a range) show trends of broader duration (e.g., the radiogenic Sr composition of seawater and zircon radiogenic Hf isotope compositions, Figure 11).

Based on the frequency and range of available data sets, in part supplemented by knowledge of planetary geology for the unpreserved portion of Earth's early history we propose seven phases in Earth evolution (Figure 1). These are: (a) *Proto-Earth*—initiation and Earth formation (4.57–4.45 Ga); (b) *Primordial Earth*—mafic and initial felsic crust formation ca. 4.45–3.80 Ga; (c) *Primitive Earth*—large-scale craton formation at ca. 3.8–3.2 Ga; (d) *Juvenile Earth*—craton stabilization at 3.2–2.5 Ga; (e) *Youthful Earth*—craton dispersal and initial continental assembly at 2.5–1.8 Ga; (f) *Middle Earth*—apparent global stability of much of the Earth system during Earth's middle age at ca. 1.8–0.8 Ga; and (g) *Contemporary Earth*—establishing the current Earth system since 0.8 Ga. The temporal boundaries between these phases are approximate, and tend to correspond with the first appearance of a key feature of that phase. We informally refer to the pre-Proterozoic (i.e., greater than ca. 2.5 Ga) as the early Earth. The Primitive and Juvenile Earth phases, which approximate the Archean eon, are dominated by the formation and ultimate stabilization of cratons, leading to the long-term preservation of the early continental crust. The data sets for these two phases (as well as for the preceding two) are limited, with the first appearance of a rock association or event often restricted to no more than a few occurrences, perhaps in a single craton. Other cratons may show similar but younger changes. Thus, boundaries between phases may be transitional over 10s or even 100s of millions of years, and likely varied in space and time.

6.1. Proto-Earth: Initiation and Earth Formation—ca. 4.57–4.45 Ga

Gravitational collapse of a molecular cloud into the solar nebula, which then separated over a few million years into the sun, planets, and planetesimals, including the proto-Earth, is dated on the basis of Pb-Pb chronometry of Ca-Al rich inclusions in carbonaceous chondrite meteorites at ca. 4.567 Ga (Connelly et al., 2017). Accretion from the solar nebula also resulted in the formation of the first mineral phases, preserved in chondritic meteorites, which further diversified through partial melting, differentiation and alteration during planet formation (Hazen et al., 2008). Analysis of the compositional character of the Earth-Moon system, notably from short-lived isotopic systems, suggested it formed within ca. 100 Ma of initial accretion of the proto-Earth through impact with the hypothetical planet Theia (e.g., Halliday, 2000; Jacobson et al., 2014). During these initial accretion and impact events, the Earth was largely molten (Elkins-Tanton, 2008), enabling rapid (no more than a few 10s of millions of years) segregation of siderophile elements (e.g., Fe and Ni), refractory metals (e.g., Cr), and some iron soluble elements (e.g., S and Si) into the core (Figure 1; Wood et al., 2006).

6.2. Primordial Earth: Initial Felsic Crust Formation—ca. 4.45–3.80 Ga

Rocks formed between 4.45 and 3.80 Ga have either been largely recycled into the mantle or destroyed during meteorite impacts. Knowledge of this period is derived from analysis of exceptionally rare and spatially restricted (km- to dm-scale) remnants of crust of this age, zircon grains reworked into younger rocks, and isotopic data from younger igneous rocks, which provide information on the nature of an older source. The character of other bodies in the solar system that preserve early crust and mantle not reworked or recycled by later events (e.g., meteorites, Mars, and Moon; Norman, 2019; Smrekar et al., 2019; Yoshizaki & McDonough, 2020, 2021) also provides insights into the nature of the Earth at this time. These data suggest that although the Earth's early crust is now destroyed, significant tracts, or their reworked products, existed until the late Archean (Carlson et al., 2019; Kamber, 2015; Kemp et al., 2010; Mulder et al., 2021; O'Neil & Carlson, 2017).

The early crust is assumed to have solidified from the magma ocean and to have been mafic to ultramafic in composition (e.g., Carlson et al., 2019; Elkins-Tanton, 2008). The presence of Hadean (>4.0 Ga) zircons in younger rocks (Harrison et al., 2017) and outcrops of ca. 4 Ga felsic crust in the Acasta Gneiss Complex (Bowring & Williams, 1999; Reimink et al., 2014), provides direct evidence for the generation of felsic melts on the Primordial Earth. The geochemistry and radiogenic isotope systematics of the only known outcrops of Hadean felsic crust, the Idawhaa Gneiss of the Acasta Gneiss Complex (Reimink et al., 2014, 2016), are consistent with a petrogenesis involving the production of felsic melts by shallow differentiation (Reimink et al., 2014) or re-melting (Johnson et al., 2018) of mafic-ultramafic crust.

Detrital and xenocryst zircon grains in younger rocks extend the record of Hadean felsic magmatism back to ca. 4.4 Ga (Cavosie et al., 2019; Wilde et al., 2001). Hadean zircons have now been identified from most present-day continents (Harrison et al., 2017) with the vast majority (>99%) recovered from the Jack Hills and Mount Narryer regions of the Yilgarn Craton (Cavosie et al., 2019; Dunn et al., 2005; Froude et al., 1983; Holden et al., 2009;

Mulder et al., 2021; Wyche et al., 2019), and additional important caches from the Barberton Greenstone Belt of the Kaapvaal craton (B. L. Byerly et al., 2018) and from the Simlipal volcano-sedimentary complex, Older Metamorphic Tonalitic Gneiss and modern river sediments within the Singhbhum craton (Bhattacharjee et al., 2021; Chaudhuri et al., 2018; Miller et al., 2018). Hadean zircons have been interrogated using a remarkable variety of geochemical and isotopic tracers, the results of which have led to often conflicting interpretations of the nature, volume, and geodynamic setting of their source rocks (e.g., Cavosie et al., 2019; Harrison, 2020; Nebel et al., 2014). One endmember group of models propose that Hadean zircons were derived from felsic melts produced in a subduction zone setting (e.g., Harrison et al., 2005, 2008; Hopkins et al., 2008, 2010; Turner et al., 2020), with the volume of continental crust produced in the Hadean possibly being of comparable magnitude to present day values (Harrison et al., 2005). Alternative interpretations of geochemical and isotopic data favor the formation of Hadean zircons in small felsic melt pockets produced through prolonged crustal re-melting of mafic-ultramafic precursors, possibly associated with meteorite bombardment or magmatic overthickening (Burnham & Berry, 2017; Johnson et al., 2018; Kemp et al., 2010; Laurent et al., 2022; Reimink et al., 2014; Rollinson, 2008). Compilations of zircon La/Yb, Sm/Yb and Eu/Eu*, and whole rock Eu-Eu*, which fluctuate over a limited range during the timeframe of the Primordial Earth (at least after 4.2 Ga), along with experimental data suggest the host felsic rocks crystallized from magma reservoirs formed either at deep crustal levels (>30 km) or at shallow crustal levels (~10 km) depending on the source rock composition and the dominant petrogenetic process (Balica et al., 2020; Borisova et al., 2021, 2022; Tang et al., 2020). Although debate will continue to be driven by novel geochemical and isotopic analyses of these exceptional archives of the Primordial Earth, the formation of Hadean zircons in low-volume felsic melts in an otherwise mafic-ultramafic crust appears to be consistent with thermal and geochemical models of the early Earth (Elkins-Tanton, 2008), lunar analogs (D. J. Taylor et al., 2009; Kemp et al., 2010), and the petrogenesis of preserved Hadean felsic crust in the Acasta Gneiss Complex, northern Canada (Johnson et al., 2018; Reimink et al., 2016).

In addition to formation of the initial mafic proto-crust and at least localized reworking into regions of felsic crust (e.g., Acasta), the period from 4.45–3.80 Ga marks the development of the Earth's initial atmosphere, oceans, and biosphere. The dynamic linked nature of the Earth system also continued to mediate and diversify the mineral species present on Earth (Hazen et al., 2008, 2013). Degassing during solidification of the magma ocean resulted in an early, possibly steam dominated, atmosphere that cooled over millions to tens of millions of years to a water ocean (Elkins-Tanton, 2012) and an anoxic reducing atmosphere rich in CO_2 and N_2 (Catling & Zahnle, 2020). Direct evidence for liquid water early in the Earth's history is provided by O isotopic data from detrital zircons from Jack Hills as old as ca. 4.4 Ga (Valley et al., 2014; Wilde et al., 2001). Life on Earth also likely commenced during this period. The earliest undisputed fossil evidence of life dates from around 3.5–3.4 Ga (Baumgartner et al., 2020; Cavalazzi et al., 2021; Schopf et al., 2018), but sedimentary rocks with inferred but challenged traces of life are dated back to ca. 3.85 Ga (Nutman, Bennett, et al., 2019; Papineau et al., 2010), and modeling of molecular clocks suggest life began prior to ca. 3.9 Ga (Betts et al., 2018; Sleep, 2018b). An older limiting age on the initiation of life is provided by the timing of the Moon-forming impact and solidification of the magma ocean, prior to and during which, the Earth was inhospitable to life. Potential pathways for RNA formation on the early Earth suggest that a major post-Moon forming impact was necessary to provide a suitably reducing atmosphere, which then facilitated rapid RNA formation by ca. 4.36 Ga (Benner et al., 2020).

6.3. Primitive Earth: Large-Scale Craton Formation—ca. 3.8–3.2 Ga

The beginning of this phase (ca. 3.8 Ga) is marked by the preservation of significant rock associations in the geological record (Bleeker, 2003; Kamber, 2015). The Hf isotopic systematics of early Earth zircons also signal an important change in the source of felsic crust formation from ca. 3.80 Ga onwards (Bauer et al., 2020; Mulder et al., 2021). Whereas pre-3.80 Ga zircon grains have almost exclusively sub-chondritic Hf isotopic compositions (Kemp et al., 2010; Mulder et al., 2021), 3.8–3.2 Ga zircon populations from many early Archean cratons define vertical arrays in $\varepsilon Hf_{(t)}$ time-space spanning (supra-)chondritic to sub-chondritic endmembers (Figure 13). The sub-chondritic endmember compositions of these arrays lie along an evolutionary array consistent with continued reworking of the pre-3.8 Ga crust sampled by older zircons (Guitreau et al., 2019; Kemp et al., 2010; Kirkland et al., 2021; Mulder et al., 2021; Naeraa et al., 2012; O'Neil et al., 2013), whereas the chondritic or supra-chondritic endmember requires interaction with a younger and more isotopically juvenile source. Together with the preservation of Hadean crustal Pb and ^{142}Nd isotopic signatures in early Archean mafic rocks (e.g., Kamber, 2015; O'Neil et al., 2008), the Hf isotopic record of early Earth zircons, representing felsic rocks, is

10.1029/2022RG000789

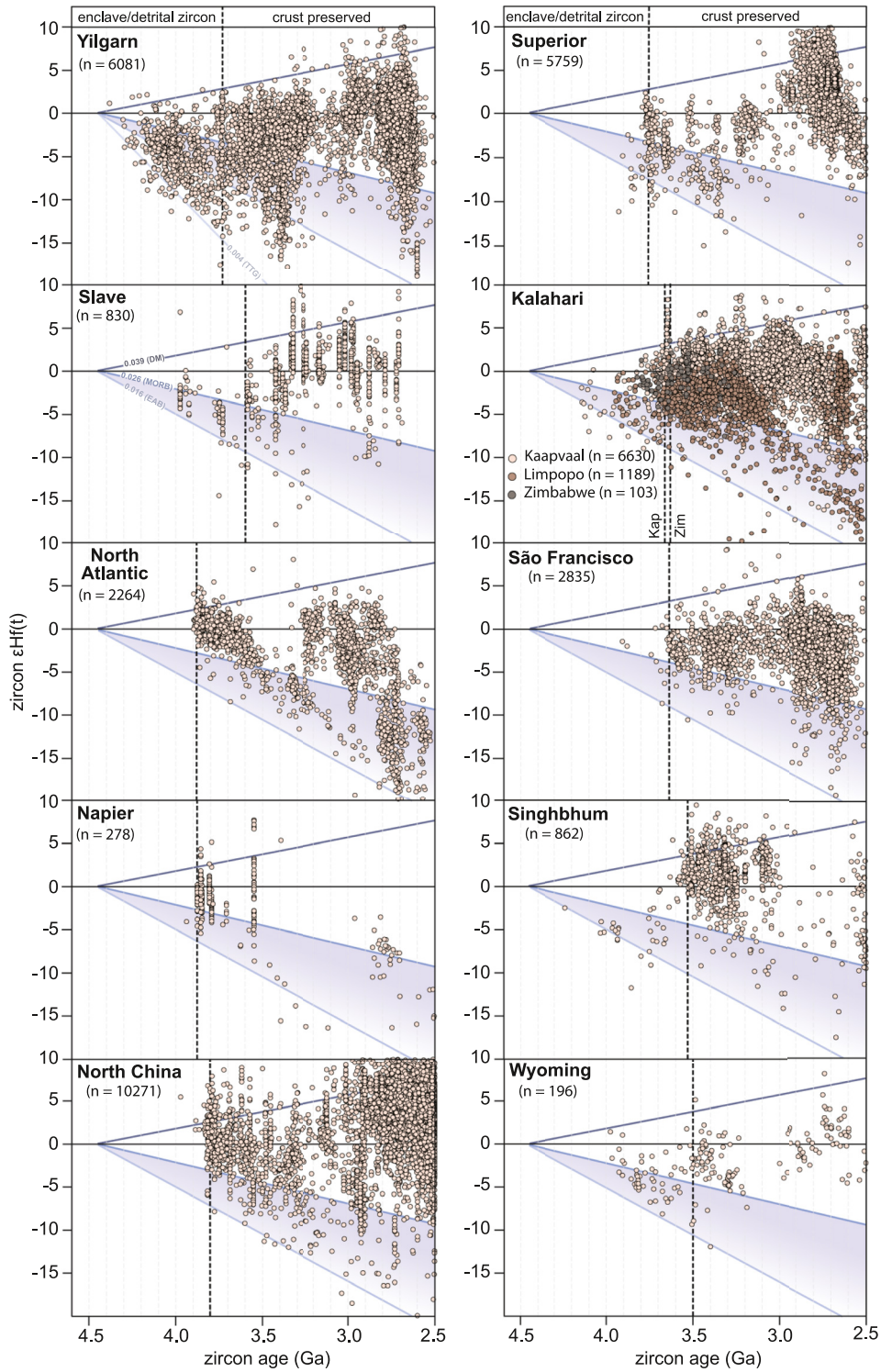

Figure 13. Compilation of initial epsilon Hf composition of zircon grains from Archean cratons that preserve evidence for reworking of Hadean crust in their formation as summarized by Mulder et al. (2021). The purple field encompasses the Hf isotopic evolution of mafic crust extracted from the mantle at ca. 4.45 Ga. The upper bound of the evolutionary array is defined by mafic crust with a Lu/Hf typical of modern mid-ocean ridge basalt (Lu/Hf = 0.026) and the lower bound defined by a representative enriched Archean basalt (Lu/Hf = 0.016; Gardiner et al., 2018). The dashed black vertical lines mark the age of the oldest preserved crust in each craton (Mulder et al., 2021). See Data Set S2 in Supporting Information S1 for references.

consistent with the interpretation that the earliest stable cratons formed through reworking of long-lived Hadean and early Eoarchean (>3.80 Ga) crust by the addition of isotopically juvenile, mantle-derived melts (Drabon et al., 2022; Mulder et al., 2021).

The preserved rock associations comprising early Archean continental crust are dominated by granite—greenstone terranes with a corresponding bimodal distribution of SiO_2 (Figure 5; C. Hawkesworth & Kemp, 2021; C. J. Hawkesworth et al., 2016; Kamber, 2015). The greenstone belts consist of mafic and ultramafic extrusive volcanic rocks and their high-level intrusive equivalents along with interstratified volcaniclastic, clastic, carbonate, and chemical sedimentary rocks. The well-preserved greenstone successions in the Pilbara and Kaapvaal cratons are built up by multiple cycles of igneous activity and sedimentation extending over 100s of millions of years and are up to 1000s of meters thick (G. R. Byerly et al., 2019b; Hickman, 2012; Kemp et al., 2023; Van Kranendonk, Smithies, et al., 2019). The igneous rocks include komatiites, komatiitic basalts, basalts, and basaltic andesites along with variable volumes of dacite and rhyolite (e.g., Van Kranendonk, Smithies, et al., 2019). Rocks of alkaline affinities are absent from greenstone belts (Moyen & Laurent, 2018). Komatiites are a distinctive but volumetrically minor component of the belts. They are characterized by low alkalis and high Mg contents, and have been divided into Al-depleted and Al-undepleted types for a given MgO (or TiO_2) content, with the latter thought to become more common after 3 Ga (Barnes & Arndt, 2019, and references therein; Barnes et al., 2021), although Sossi et al. (2016) did not find any temporal variation in the distribution of the two types. Spinifex textures involving bladed olivine and clinopyroxene within komatiites indicate rapid crystallization from a high temperature magma and have played an important role in constraining the thermal evolution of the Earth's early mantle (Herzberg et al., 2010; Nisbet et al., 1993). Komatiites are rare in the Phanerozoic rock record, which is taken to reflect secular cooling of the mantle (Trela et al., 2017).

On the modern Earth, mafic rocks are separated into arc and non-arc rocks on the basis of trace element patterns (e.g., Th/Yb and Nb/Yb), which correspond to mantle melting under wet and dry conditions, respectively. In contrast, Archean mafic rocks cluster in an intermediate position suggestive of a near-primitive mantle source with moderate amounts of input from crustal material or fluids (Moyen & Laurent, 2018; Pearce, 2008).

The high silica component of the bimodal Archean rock association includes the tonalite–trondhjemite–granodiorite series (TTGs), which contain plagioclase as the main feldspar phase and thus high Na/K (Moyen & Martin, 2012). TTGs are rare in the modern rock record (Moyen & Laurent, 2018) and are characterized by elevated Sr/Y and are generally depleted in HREE, which is indicative of residual garnet in the source (Moyen, 2011). Experimental and petrological data show that TTGs mainly formed through the partial melting of hydrated metabasalts in the lower crust at depths of >25–45 km (Chowdhury, Mulder, et al., 2021; Johnson et al., 2017; Moyen, 2011; Palin et al., 2016; Rapp et al., 2003; S. F. Foley et al., 2003; Smithies et al., 2021), implying deep burial of hydrated surficial crust. Shifts in the $\varepsilon Hf_{(t)}$ isotopic signature of detrital zircons to more juvenile compositions from ca. 3.8 Ga onwards corresponds with the widespread incoming of TTGs in early Archean cratons (Figures 13 and 14). An increase in Sr/Y, La/Yb, and Nb/Ta of TTGs between 3.8 and 3.2 Ga suggests a progressive deepening of the melt source region with time (Johnson et al., 2019; Martin & Moyen, 2002). Through petrogenetic modeling, Chowdhury, Mulder, et al. (2021) confirmed that TTG formation in the Singhbhum craton progressed from ∼33 km at ca. 3.5 Ga to ∼48 km by ca. 3.2 Ga. Empirical estimates of melt formation depth made from Eu/Eu* systematics in zircon also increase through this timeframe from a global average of around 40 km at ca. 3.8 Ga to ∼55 km at ca. 3.2 Ga (Tang et al., 2021).

Eo- to Paleoarchean sedimentary rocks, including clastic, carbonate and chemical sediments, are a relatively minor component within the volcanic succession of the greenstone belts (Fedo et al., 2001; K. A. Eriksson et al., 1994; Kröner & Hofmann, 2019; Mazumder & Chaudhuri, 2021; Nutman, Friend, et al., 2019). Their presence, including shallow marine platformal and lagoonal deposits, implies at least local and transient emergence of the cratons in which they occur and provides evidence for weathering with implications for atmospheric and ocean chemical evolution (Buick et al., 1995; K. A. Eriksson et al., 1994; P. G. Eriksson et al., 2013). Furthermore, these volcanic sedimentary associations provide the first unequivocal evidence for the development of life including possible terrestrial organisms and involved oxygen and methane-producing life forms (Planavsky et al., 2021; Van Kranendonk et al., 2021).

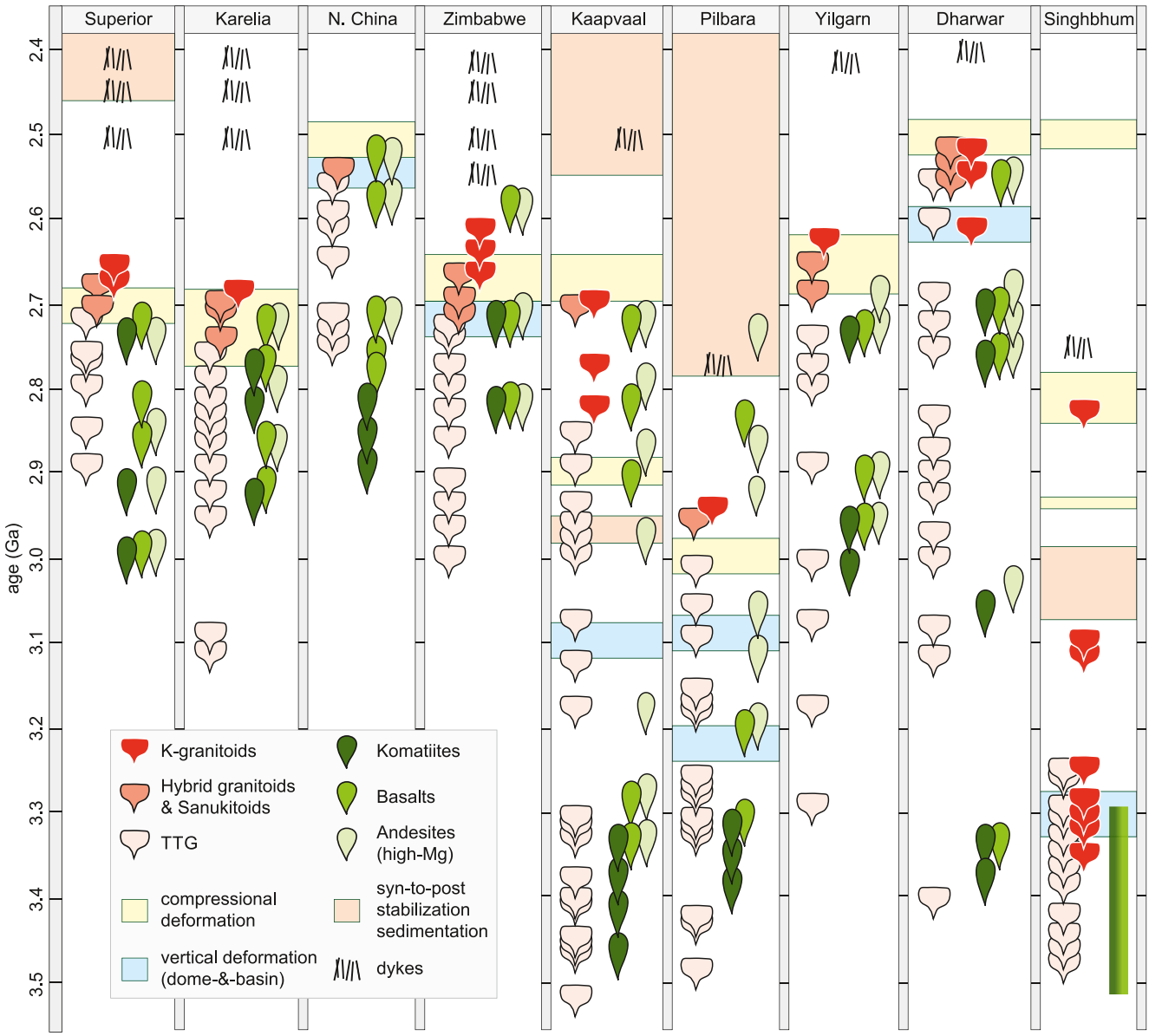

Figure 14. Time-space plot for the Superior, Karelian, Dhawar, North China, Pilbara, Yilgarn, Zimbabwe, and Kaapvaal cratons for the period 3.5–2.4 Ga, showing the time of major felsic and mafic/ultramafic igneous activity, deformational events that are late stage in the orogenic cycle of the craton, mafic dyke emplacement and major late sedimentary basin deposition. Distribution of felsic magmatism adapted from Laurent et al. (2014) and for mafic magmatism from L. Gao et al. (2022b).

6.4. Juvenile Earth: Craton Stabilization—ca. 3.2–2.5 Ga

The granite-greenstone rock association continued into the later part of the Archean, from 3.2 to 2.5 Ga, but there is an overall, and relatively abrupt, change in the composition of felsic magmatism within individual cratons from the Na-rich TTG suite to more potassic magmatic rocks starting around 3 Ga (Figure 14), and is a defining characteristic of this phase. This change is associated with the stabilization and termination of magmatism across the Archean cratons. The timing of this change varies from craton to craton, but all record a similar overall compositional change (Cawood et al., 2018; Laurent et al., 2014). Furthermore, and in contrast to TTG magmatism that extended over many 10s to 100s of millions of years, the late potassic magmatism was generally active for no more than a few 10s of millions of years (Figure 14). The K-granitoids are referred to as high-K or biotite granites (Laurent et al., 2014; cf., Nebel et al., 2018). In addition, this phase of craton magmatism is associated with the emplacement of a minor component of peraluminous (S-type) granites as well as sanukitoids, which are granitoids rich in Mg, Fe, K, Cr, and Ni (Heilimo et al., 2010; Laurent et al., 2014). The compositional character

of K-granitoids requires their formation at shallow depths (<35 km) either via partial melting of pre-existing TTG crust or via fractionation crystallization of TTG melts (Laurent et al., 2014; Moyen, 2011). Low-degree melting (<10%; Johnson et al., 2017) of hydrated metabasalts can also produce K-granitoids but such low melt fractions are unlikely to form extensive batholiths unless huge amount of basalts participate in melting. Thus, the origin of the K-granitoids is suggestive of intracrustal partial melting and consistent with evidence for the occurrence of peraluminous granites at this time, whereas sanukitoids require interaction of TTG with a mantle derived component (Heilimo et al., 2010; Laurent et al., 2014; Nebel et al., 2018; Rapp et al., 2010).

The termination of cratonic magmatism corresponds with regional deformation in many cratons (Figure 14). The associated K-granitoids and sanukitoids are syn- to post-tectonic with respect to regional deformation (Laurent et al., 2014). The structural style of the cratons ranges from those with a well-developed dome and keel structure (e.g., Pilbara, Zimbabwe, Dharwar, and Singhbhum cratons; Choukroune et al., 1997; Collins et al., 1998; Eskola, 1948; MacGregor, 1951), to those dominated by linear structural belts (e.g., Yilgarn and Superior cratons; Czarnota et al., 2010; Percival et al., 2012), but also displaying localized dome formation (Jones et al., 2021; Zibra et al., 2018). The termination of dome and keel structures is often marked by the subsequent development of linear orogenic belts along the margins of, as well as internally within, these cratons and reflects a change from vertical to horizontal tectonic forces. Examples include the development and accretion of the linear West Pilbara terranes with the dome and keel structures of the East Pilbara terrane (Hickman, 2004), the accretion of the Rengali Province to the southwestern margin of the domal Singhbhum craton along the Barakot Shear Zone (Bose et al., 2021), the accretion of the Pietersburg block along the northern margin of the eastern Kaapvaal cratonic nucleus (Laurent et al., 2019), and the overall along strike continuity of belts within the Yilgarn and Superior cratons (Mole et al., 2014; Percival et al., 2012).

Thickening of the cratonic lithosphere resulting from magmatism and deformation led to stabilization and the long-term survival of the cratons, and is associated with overall depletion of lithospheric mantle (Griffin et al., 2009; Jordan, 1978, 1988; Pearson et al., 2021; Priestley et al., 2020). Following the termination of magmatism, the stabilized cratons were exhumed and eroded to variable extent, and then subsided to be unconformably overlain by laterally extensive basinal successions; for example, the Singhbhum Cover Sequence that accumulated across much of the Singhbhum Craton, the Fortescue Supergroup along the southern and eastern margins of the Pilbara Craton, the Pongola, Witwatersrand and Transvaal successions preserved in the central and eastern parts of the Kaapvaal Craton, and the Huronian Supergroup on the southern margin of the Superior Craton (Bennett et al., 1991; Catuneanu & Eriksson, 1999; Chowdhury, Mulder, et al., 2021; Frimmel, 2019; Hickman, 2012; Luskin et al., 2019; P. G. Eriksson et al., 2011; Thorne & Trendall, 2001). Empirical estimates of continental crustal thickness in the period 3.2–2.5 Ga suggest a slight decrease overall, either from ∼55 to ∼50 km (Tang et al., 2021) or from ∼40 to ∼35 km (Balica et al., 2020).

Thickening and stabilization of the cratonic lithosphere in the period 3.2–2.5 Ga would have resulted in the widespread emergence of continental crust, which would in turn affect atmospheric and ocean compositions through weathering and runoff with associated follow-on effects on the biosphere. The early Mesoarchean (ca. 3.1–3.0 Ga) terrestrial-to-shallow marine deposits of vast extent, like those deposited on the stabilized crust of the Singhbhum and Kaapvaal cratons, mark the widespread subaerial emergence of stable continents (Chowdhury, Mulder, et al., 2021). Weathering of emergent cratons, including associated LIPs, likely lead to drawdown of CO_2, and may be expressed through evidence for whiffs of oxygen in the cratonic sedimentary record (Chowdhury, Mulder, et al., 2021; Meixnerová et al., 2021; Ostrander et al., 2021, and references therein; but see Slotznick et al. (2022) for alternative interpretation). Deviation of the normalized seawater $^{87}Sr/^{86}Sr$ curve from the mantle reference line, as well as patterns in other isotopic systems and elemental ratios (e.g., depleted $\delta^{18}O$, $\delta^{66}Zn$, K/La), and the presence of the earliest glacial deposits, provide evidence for weathering of continental crust in the latter half of the Archean (Chowdhury, Mulder, et al., 2021; C. T. Liu & He, 2021; Ostrander et al., 2021; Pons et al., 2013; Shields, 2007; W. Wang et al., 2021a; X. Chen et al., 2022). Direct evidence for the onset of continental emergence on a global scale during the Mesoarchean is provided by ca. 3.0 Ga paleosols in the Kaapvaal (Heard et al., 2021) and Singhbhum (Mukhopadhyay et al., 2014) cratons, 3.2–2.8 Ga shallow marine and terrestrial, quartz-rich clastic sedimentary rocks on most cratons, and the global zircon record (Chowdhury, Mulder, et al., 2021; E. L. Simpson et al., 2012; Fralick & Riding, 2015; Hickman, 2021; K. A. Eriksson & Wilde, 2010; K. A. Eriksson et al., 1994; Mueller et al., 2005; Reimink et al., 2020; Sunder Raju & Mazumder, 2020; Szilas et al., 2014). We do note however, that the inferred general paucity of S-type granitoids throughout the Archean (Figure 12; Z. Zhu et al., 2020) suggests that the supply, burial and melting of sediments within, and along the

margins of, cratons was limited. This in turn could imply that the overall proportion of emergent, actively eroding, and high relief crust was limited relative to later time periods in Earth history, where S-type granites are more prevalent.

The Meso- to Neoarchean timeframe also corresponds with evidence for the extensive recycling of older crust (Dhuime et al., 2012; Kirkland et al., 2021; L. Gao et al., 2022a; X. Wang et al., 2021b). Dhuime et al. (2012; see also Dhuime et al., 2017, 2018) used igneous zircon U-Pb, Hf, and O data to argue for a change in the rate of continental growth at 3 Ga, which they related to increased recycling of crust into the mantle. Recently, X. Wang et al. (2021b) noted an increase in the oxygen isotopic composition of zircon from TTG's in the Kaapvaal craton at ca. 3.2 Ga. They speculate that this increase relates to the onset of recycling of mafic oceanic crust that underwent seawater hydrothermal alteration at low temperature. In contrast, Kirkland et al. (2021) from a study of Hf isotopic data of Archean to Paleoproterozoic detrital zircon from modern stream sediments, West Greenland, augmented by a global Hf data compilation, noted reworking of felsic Hadean-to-Eoarchean crust during subsequent periods of magmatism, and an overall shift to more juvenile Hf values 3.2 to 3.0 billion years ago (see also Figure 13). They suggested this crustal rejuvenation was coincident with an inferred peak in mantle potential temperatures, which resulted in greater degrees of mantle melting and injection of mafic magmas into older felsic crust. Based on whole-rock geochemical data of Archean (3.8–2.5 Ga) basalts from 14 cratons, Gao et al. (2022a) developed a V-Ti proxy of mantle redox conditions (fO_2). Each craton, independent of the age of magmatism, showed an increase in fO_2 values of around 1 log unit indicating progressive oxidation of the underlying mantle. Increases in mantle fO_2 are closely associated with changes in basalt Th/Nb ratios and Nd isotopes that are sensitive to crustal recycling. These increases in mantle oxidation and crustal recycling show similar trends for each of the studied cratons independent of the absolute age range of magmatism and correspond with the progressive stabilization of each craton.

6.5. Youthful Earth: Craton Dispersal and Initial Continental Assembly—ca. 2.5–1.8 Ga

The Archean to the Proterozoic marks a major transition in the evolution of the Earth system. The late Archean corresponds with the final stabilization of the major cratons and the assembly, of at least some, into supercratons/supercontinents (e.g., Bleeker, 2003). This stabilization marks a major change in the type and composition of igneous rocks. Komatiites and TTGs decrease dramatically in abundance across the Archean-Proterozoic transition. This lithologic change is associated with a decrease in MgO, Ni, and Cr, and increasing Na_2O and La/Yb in mafic lithologies, whereas felsic lithologies display decreasing Na_2O/K_2O, La/Yb, Eu/Eu*, and Sr fractionation (C. B. Keller & Schoene, 2012).

Post-craton stabilization LIP activity, marked by dyke swarms and associated volcanic mafic extrusive lavas, is enhanced during the late Archean to early Paleoproterozoic transition (Figure 14; Ernst et al., 2021). The earliest manifestations of this magmatic activity include the 2.78 Ga Black Range dykes that intrude across much of the Pilbara craton and the associated Mount Roe Basalt of the lower Fortescue Group that accumulated on the craton (Arndt et al., 2001; Hickman, 2012; Wingate, 1999), the 2.8–2.76 Ga Newer Dolerite Dyke swarms (Keshargaria and Ghatgaon) that occur throughout the Singhbhum Craton (Srivastava et al., 2019), and similar age magmatism in the Ventersdorp Supergroup within the central Kaapvaal craton (Gumsley et al., 2020). By the end of the Archean and into the Paleoproterozoic, this igneous activity is widespread across numerous cratons, including the 2.57 Ga Great Dyke, Zimbabwe Craton (Oberthür et al., 2002; Söderlund et al., 2010), the 2.46–2.45 Ga event in the Pilbara, Superior, Karelian-Kola and possibly Wyoming cratons, the 2.42–2.40 Ga activity in the Yilgarn, Zimbabwe, Superior, North Atlantic, and Karelian-Kola cratons (Davey et al., 2020; Ernst et al., 2021; Nemchin & Pidgeon, 1998; Pisarevsky et al., 2015), and the ca. 2.22 Ga activity in the Slave, Karelia-Kola, Dharwar, Singhbhum, Superior, North Atlantic, and Pilbara cratons (Ernst et al., 2021; Söderlund et al., 2019). Analysis of atmospheric xenon trapped in samples from the Archean to recent shows a step-change in $\Delta^{129}Xe$ from slightly depleted values prior to 2.6 Ga to modern values by 2.0 Ga, which Marty et al. (2019) argue requires a mantle degassing rate at the end of the Archean at least one order of magnitude higher than today. They propose a burst of mantle activity at the end of the Archean that extended for a few 100 million years, which is perhaps consistent with the extensive late Archean to early Paleoproterozoic LIP events preserved across the cratons. These LIP events indicate that the cratons were stable and rigid, and subjected to broad-scale brittle extension associated with dyke swarm emplacement (Cawood et al., 2018), which is generally related to mantle upwelling (Ernst et al., 2021). However, the distribution of this activity across all major cratons immediately succeeding their

stabilization suggests it is not simply due to the random intersection of plumes and cratonic lithosphere but could reflect an inherent characteristic of the thermal evolution in thick cratonic lithosphere (cf., Coltice et al., 2009).

Lithospheric extension of the Archean cratons associated with the LIP activity led to formation of basinal successions that record rift and thermal subsidence related histories. Taken together, the igneous and sedimentary successions therefore record breakup of larger cratonic masses. The inferred late Archean supercratons, variously termed Superia, Sclavia, Kenor, and Vaalbara, disaggregated into the smaller constituent cratons we recognize today; for example, Pilbara, Kaapvaal, Yilgarn, Zimbabwe, and Superior cratons, the Aldan and Anabar shields in Siberia, and the Archean blocks of Baltica and India (Bleeker, 2003; Bleeker & Ernst, 2006; Cheney, 1996; Davey et al., 2020; Gardiner et al., 2021; Söderlund et al., 2010; Williams et al., 1991).

The margins of the Archean cratons, including onlapping early Paleoproterozoic sedimentary successions, are overprinted and delineated by a series of late Paleoproterozoic orogenic belts (ca. 2.1–1.75 Ga). Together, these lithotectonic assemblages provide a record of initial craton rifting and subsidence followed by their convergence and assembly. Belts of this age are present on most of the present-day continents; North America (Hoffman, 1988), Baltica (Korja et al., 2006), Siberia (Glebovitsky et al., 2008; Kostrovitsky et al., 2016; Rosen et al., 2005), Australia (Cawood & Korsch, 2008), North China (G. Zhao & Cawood, 2012; G. Zhao et al., 2012), and India (Dey et al., 2016; Meert & Pandit, 2015). For example, the Yilgarn and Pilbara cratons have spatially and temporally independent histories of Archean granite-greenstone formation (Figure 14). The now adjoining margins of these two cratons are overlain by late Archean and early Paleoproterozoic basins recording cycles of extension and subsidence, consistent with continental rifting and passive margin thermal subsidence. The two cratons were juxtaposed along the intervening Capricorn Orogen with its record of foreland basin sequences, accreted continental fragments and magmatic arc successions and associated tectonothermal pulses, including the 2 and 1.8 Ga Glenburgh and Capricorn orogenies (Cawood & Tyler, 2004; Jahn et al., 2021; Sheppard et al., 2004). The West Australian and North Australian cratons are also inferred to have undergone assembly at this time (Cawood & Korsch, 2008; L. Zhao et al., 2022). Similarly, the Trans-Hudson Orogen records a history of convergence and subsequent collision between the Churchill composite craton and the Superior craton, which constitute key elements in the assembly of Laurentia during the late Paleoproterozoic (Hoffman, 1988, 1989; St-Onge et al., 2009; Weller et al., 2021).

The early Paleoproterozoic record of sedimentation and LIP-related magmatism on stabilized Archean cratons and their subsequent juxtaposition across major linear late Paleoproterozoic orogenic belts is witness to a series of Wilson cycles of ocean opening and closure. In combination, these events are interpreted to mark the assembly of Earth's first supercontinent, Nuna/Columbia (Hoffman, 1996; Rogers & Santosh, 2002; G. Zhao et al., 2002).

The Archean-Proterozoic transition corresponds with major environmental changes including the Great Oxygenation Event (GOE; Holland, 2002), a linked spike in carbon isotope ratios in marine carbonates (Eguchi et al., 2020; but see also Prave et al., 2021), extensive (possibly global) glaciations (Rasmussen et al., 2013), a change in ocean redox (Poulton et al., 2021), and a greater range of marine authigenic minerals (Hazen et al., 2008). Recent work suggests the GOE may be a protracted transition that extended over 10s to 100s of millions of years (Hodgskiss & Sperling, 2021; Ostrander et al., 2021). Thus, the drivers of the GOE likely commenced in the late Archean and included subaerial exposure of the cratons and widespread mafic magmatism, with associated extensive degassing (including volcanic H_2O, CO_2, N_2, and SO_2) and weathering (Ciborowski & Kerr, 2016; Hodgskiss & Sperling, 2021; Marty et al., 2019; Meixnerová et al., 2021; Zerkle et al., 2021). In turn, these events would have increased nutrient supply to the oceans and enhanced biological activity (Cox et al., 2018; Hao et al., 2020). Increased oxidized weathering of terrestrial rocks as a consequence of the GOE likely accounts for the change from more reduced to more oxidized compositions of biotite and whole rock from Archean to Proterozoic strongly peralkaline granites (Bucholz et al., 2018; Bucholz & Spencer, 2019).

6.6. Middle Earth: Earth's Stable Middle Age—ca. 1.8–0.8 Ga

The period from the late Paleoproterozoic at around 1.8–1.7 Ga to the Neoproterozoic at ca. 0.8–0.75 Ga provides evidence for an extended phase of stability in the Earth system that is marked by apparent limited activity in the preserved records related to the environment, biosphere and lithosphere (Brasier & Lindsay, 1998), and has been variously termed Earth's middle age (Cawood & Hawkesworth, 2014) or the boring billion (Holland, 2006; Roberts, 2013). This time interval is characterized by anomalous distribution of elemental concentrations, mineral

phases, rock types and ore deposits relative to preceding and succeeding time intervals (Figure 11). These include a paucity of passive margins (Bradley, 2008), an absence of glacial deposits (Bradley, 2011) and iron formations (Bekker et al., 2010), low U and Mo concentrations in black shales (C. Scott et al., 2008; Partin et al., 2013), and a scarcity of phosphorite (Cook & McElhinny, 1979; Papineau, 2010). It is also a period of limited orogenic gold, VMS and sediment rock hosted manganese deposits (Bierlein et al., 2009; Frimmel, 2018; Huston et al., 2010; Maynard, 2010). In contrast, during this time interval there is an abundance of massif type anorthosites and related magmatism (AMCG—anorthosite-mangerite-charnockite-granite, rapakivi granite; Ashwal, 2010; Ashwal & Bybee, 2017) and associated Fe-Ti oxide deposits (Barley & Groves, 1992; Groves et al., 2005), and carbonatites and associated REE-bearing ore deposits (C. Liu et al., 2017, 2019). The recently revised Sr isotope paleo-seawater curve displays an initial drop at the start of middle age and then an overall increase with second order peaks and troughs (X. Chen et al., 2022), whereas $\varepsilon Hf_{(t)}$ in detrital zircons maintain an overall constant mean value (Belousova et al., 2010; Roberts & Spencer, 2015). Proxies for crustal thickness, whether based on whole rock Rb/Sr ratios of new crust and La/Yb for average continental crust, or Eu/Eu* in zircon from areas of active continental crust remain relatively constant through this interval (Balica et al., 2020; Dhuime et al., 2015; Tang et al., 2021). Time series analysis of the thermobaric ratio of metamorphic rocks indicates the highest mean *T*/*P* approximates the timeframe of Earth's middle age (ca. 1830–900 Ma; Brown, Kirkland, et al., 2020). Similarly, Liu et al. (2019) noted the enhanced occurrence of high-T minerals (igneous, metamorphic and hydrothermal, which are often enriched in Th, F, Nb, Y, and REE) during this interval (see also Tamblyn et al., 2021).

Earth's middle age is bookended by the assembly of the Nuna supercontinent and the breakup of the succeeding Rodinia supercontinent (Figures 1 and 11). Importantly, core elements of Nuna, including Laurentia, Siberia and Baltica, remained largely unchanged during the transition into Rodinia as evidenced by an apparent paucity of passive margins related to Nuna breakup and the lack of evidence for end Mesoproterozoic orogenesis in and round cratons such as Siberia (Bradley, 2008; Cawood & Hawkesworth, 2014; Evans, 2013; Gladkochub et al., 2010). This contrasts with the well-established major changes in continental configurations during assembly of Nuna and the transition from Rodinia to Gondwana (plus or minus Pannotia; Cawood et al., 2021; Evans, 2013; G. Zhao et al., 2002; Murphy et al., 2020) and has supported the notion of long-term lithospheric stability between 1.80 and 0.8 Ga.

The lack of evidence for breakup and reassembly of the core cratons of Laurentia, Siberia and Baltica during the transition from Nuna to Rodinia, have led to proposals for limited development of thick orogenic crust (at least between these core cratons) with an associated lack of weathering, erosion and run-off of nutrients into the oceans (Tang et al., 2021; Z. Zhu et al., 2022b). However, paleomagnetic and geological data from several major continental blocks suggest that significant relative plate motions and orogenic activity still occurred during Earth's middle age (Pisarevsky, Elming, et al., 2014; Spencer et al., 2021), notably on the margins of the Laurentia-Siberia-Baltica core. For example, the late Paleoproterozoic and Mesoproterozoic records of eastern Australia-Antarctica and western Laurentia provide evidence for a full Wilson Cycle, on a scale comparable those of the Phanerozoic, during the Nuna-Rodinia transition. There is evidence for continent-continent collision between eastern Australia-Antarctica and western Laurentia at ca. 1.60 Ga (Pourteau et al., 2018; Volante et al., 2020), possibly marking the final assembly of Nuna (Pisarevsky, Elming, et al., 2014). Paleomagnetic data imply wide separation of Australia and Laurentia by ca. 1.20 Ga (Elming et al., 2021; Pisarevsky, Wingate, et al., 2014), which may have been achieved through continental rifting associated with regional extension, basin formation, and mafic magmatism, along both continental margins at ca. 1.45–1.30 Ga (Halpin et al., 2014; Morrissey et al., 2019; Mulder et al., 2015; Sears et al., 1998; Yang et al., 2018). Similarly, East Laurentia and southern Baltica provide evidence for widespread Grenville-Sveconorwegian orogenesis during the end Mesoproterozoic and early Neoproterozoic inferred to be related to Amazonia collision (Bingen et al., 2008; Cawood & Pisarevsky, 2017; Hynes & Rivers, 2010) or accretionary margin processes (Roberts & Slagstad, 2015; Slagstad et al., 2013).

6.7. Contemporary Earth: Modern Plate Tectonics—ca. 0.8 Ga to Present Day

The Neoproterozoic marks the appearance in the geologic record of rock associations and events that are considered the archetypal features of our present-day dynamic planet. Thus, many of the distinctive features that characterize Cenozoic plate tectonics first became widespread in the Neoproterozoic (R. J. Stern, 2018, and references therein). These include ophiolites, blueschists and kindred metamorphic assemblages, and ultrahigh pressure (UHP) rocks. Ophiolites are indicators of extension of oceanic lithosphere and form in both non-subduction

(e.g., mid-ocean ridges) and subduction zone settings (e.g., subduction initiation ophiolites and back arc basin ophiolites). They delineate suture zones in Phanerozoic collisional and accretionary orogens (e.g., Bay of Islands ophiolite, Appalachian-Caledonian orogen; Semail, Spontang and Xigaze ophiolites, Alpine-Tethyan orogen; Great Serpentine Belt and western Tasmanian ophiolite, Terra Australis orogen; Dun Mountain ophiolite belt, Gondwanide orogen; Great Valley ophiolite, North American Cordillera). Blueschists, glaucophane-bearing eclogites, lawsonite-bearing metamorphic rocks, and jadeitites are associated with subduction zones at active convergent plate margins. UHP rocks along with the gemstones ruby and sapphire in continental collision zones become common in Neoproterozoic and younger orogenic tracks. However, some of these mineral and rock associations also occur in older successions. Mafic and ultramafic associations, inferred to represent oceanic lithosphere, are reported from the Mesoproterozoic, late Paleoproterozoic and Archean (D. J. Scott et al., 1992; Furnes & Dilek, 2022; Kusky & Li, 2010; Moores, 2002), but alternative interpretations are also possible (e.g., Waterton et al., 2022). Although low *T*/*P* metamorphic assemblages are largely Neoproterozoic and younger, rare late Mesoproterozoic and late Paleoproterozoic occurrences have also been recorded (Brown & Johnson, 2018; Weller & St-Onge, 2017, and references therein).

In addition to the widespread preservation of distinctive metamorphic and igneous rock associations, the transition to the Contemporary Earth is marked by the Neoproterozoic Sturtian and Marinoan global glaciations (e.g., Hoffman et al., 1998). These events are followed by a further rise in atmospheric oxygen to present-day levels (Holland, 2006; Lyons et al., 2014), and the emergence in the Phanerozoic biosphere of complex plant and animal forms (Figure 1; Knoll & Nowak, 2017). In addition, there is the reoccurrence of rock associations that were largely absent in the preceding middle age, for example, gold and VMS deposits (Figure 11; Goldfarb et al., 2001; Huston et al., 2010).

7. Speculations on Tectonic Modes and Earth Evolution

There is an ever growing list of papers discussing when, where, and why the Earth's current tectonic mode, plate tectonics, initiated and the possible precursor modes it may have succeeded (e.g., Bédard, 2020; B. Keller & Schoene, 2018; Brown, Johnson, et al., 2020; Cawood et al., 2018; C. J. Hawkesworth et al., 2016; Dewey et al., 2021; Hamilton, 2011; Korenaga, 2013; Palin & Santosh, 2021; R. J. Stern, 2018; R. Zhu et al., 2021; T. Gerya, 2022; Windley et al., 2021; Zheng & Zhao, 2019). There is general agreement that whatever the tectonic mode operating at a particular time, it occurred within and was influenced by a framework of a secular decrease in mantle potential temperature (Figure 10b). However, our understanding of how the lithosphere responded to this cooling of the mantle, and in particular how mantle melting impacted lithospheric composition and rheology, remain a source of discussion. This has led to the differing interpretations of tectonic mode with suggestions for when plate tectonics initiated, ranging over ~85% of Earth history from the Hadean to the Neoproterozoic. This level of uncertainty for the fundamental process controlling the Earth system is remarkable.

The range of opinions on which tectonic modes operated when, stem from a combination of how we define plate tectonics and alternative modes of operation, and by differing interpretations and selective emphasis on available data (cf., Cawood et al., 2018). The specific tectonic mode operating on the early Earth has become an a priori assumption of many studies, rather than being critically evaluated in the context of the available, yet ambiguous, data. As a result, we are prone to confirmation bias in interpreting the rock record (Chelle-Michou et al., 2022). To move forward and reach consensus we need to countenance data and alternative interpretations that may not conform to our preferred model. Field observations, petrology, geochemistry, geochronology, geophysics, and computational analysis across a range of spatial and temporal scales (cf., C. J. Hawkesworth et al., 2020) have, and will continue to provide, the data needed to evaluate and limit the tectonic modes that may have operated on the Earth.

Furthermore, establishing the tectonic modes that have operated on Earth is fundamental to understanding the evolution of the Earth system, as changes in mode will impact the nature and character of the preserved rock record and the rate and method of cycling between reservoirs. In the following, we discuss possible tectonic modes that operate on planetary bodies and constraints on lithosphere-mantle behavior for the early history of the Earth. We then outline possible links between likely tectonic modes and the evolving Earth system.

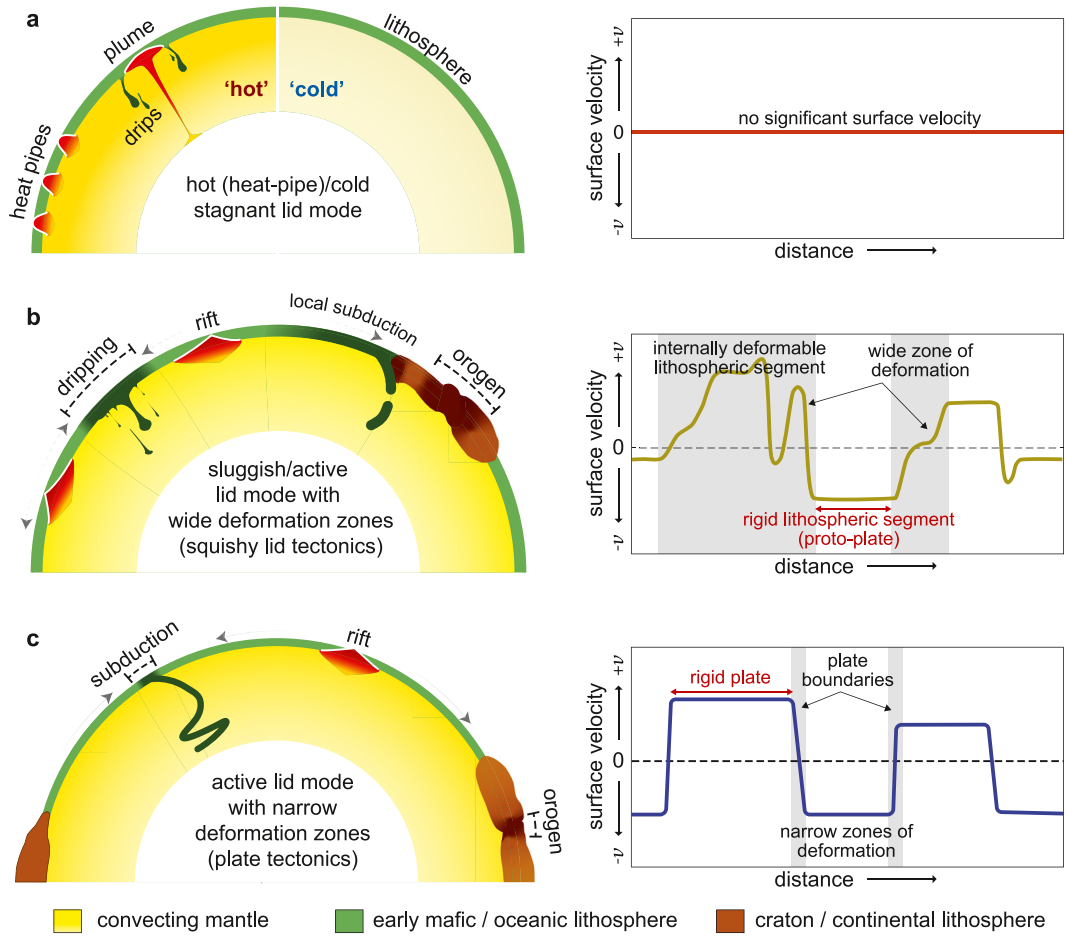

Figure 15. Schematic representation of various planetary tectonic modes postulated based on geodynamic modeling that have implications for early Earth tectonics. The modes are: (a) stagnant lid mode; (b) active lid mode with broad zones of deformation, and (c) active lid mode with narrow zones of deformation, akin to modern plate tectonics. The stagnant-lid mode figure includes two variants: one with a hot interior and volcanically active planetary body (a "hot stagnant lid"; e.g., Venus), and other with a cold interior and volcanically inactive body (a "cold stagnant lid"; e.g., moon). Plots on the right are the surface velocities obtained from 2D numerical models of mantle convection and tectonics for the respective modes (Lenardic, 2018; Richards et al., 2001). Note that the surface velocity profiles for the two variants of the active lid mode. One with wide zones of deformation are characterized by large gradients in horizontal velocity, suggesting internal deformation of the lithosphere. In contrast, the other variant with narrow zones of deformation suggests that deformation is concentrated between two rigid lithospheric segments.

7.1. Tectonic Mode(s)

Tectonic mode encompasses the geological activities (e.g., magmatism, deformation, metamorphism, and sedimentation) that characterize a planetary body at a global scale, and is effectively the means by which the body loses heat (Lenardic, 2018). Depending upon how actively the lithospheric lid participates in mantle convection, the following endmember modes have been suggested: stagnant lid, sluggish lid, and active lid, each with a variety of sub-modes (Lenardic, 2018).

The stagnant lid mode (also known as rigid lid or single-plate mode; Figure 15) excludes any involvement of the lithosphere in mantle convection and is, therefore, characterized by a laterally immobile lid atop the underlying mantle (Moresi & Solomatov, 1998). However, the lithospheric lid experiences variable magmatism and tectonic deformation depending on the planet's thermal state, which gives rise to two sub-modes. A "hot" stagnant lid mode operates when the planet is hot inside, has a convecting mantle and loses heat either via heat-pipe mode of volcanism (e.g., like Jupiter's moon Io) or by plume activity (e.g., like Mars) in addition to conduction (Lenardic, 2018; Moore et al., 2017). Heat-pipes are focused zones of mantle upwelling that brings hot material

directly to the surface of the lithosphere via volcanism and, in the process, advects the pre-existing lithosphere downward. This leads to small scale recycling of the lithosphere through drips. A "cold" stagnant-lid mode operates when the planetary body is volcanically inactive and comprises a lithosphere lying atop a cold, solid, mantle (e.g., the Moon; R. J. Stern, 2018).

In contrast, the active (or mobile) lid tectonic mode involves strong coupling between the lithosphere and the convecting mantle (Figure 15). In this mode, the (negative) buoyancy of the lithosphere exerts a strong control on mantle convection, whether this occurs via intermittent and episodic lithospheric downwelling or ongoing and long-lived subduction. This mode is divisible into a plate tectonic sub-mode with rigid plate interiors and narrow focused zones of deformation at plate boundaries, and a distributed deformation sub-mode consisting of wide zones of deformation (i.e., diffuse plate boundaries) that cover most of the planetary surface (Figure 16; Lenardic, 2018). Consequently, the proportion of rigid plates is lower in the latter case than in the former, plate tectonic mode. These two sub-modes can also be differentiated based on the plate velocity gradients. Sharp changes in the plate velocities occur over a narrow zone in the case of plate tectonics, while in case of distributed deformation mode, the plate velocities change rather gradually over a broad zone (Figure 15).

The sluggish lid mode (Figure 15) is also characterized by a laterally mobile lithosphere but in this case, mobility is generally inferred to be driven by the traction force exerted by convecting mantle along the lithosphere-mantle boundary and not by the buoyancy structure of the lithosphere (Lenardic, 2018). In addition, the numerical models of Sizova et al. (2015) suggest that some lithospheric motion unrelated to drag from the mantle can occur in response to lithospheric drips and delamination. In the sluggish lid mode lithosphere velocities are low and inferred to generally remain lower than those of the convecting mantle, whereas the two are comparable in the active-lid mode (Lenardic, 2018). A variety of sub-modes have been proposed for this mode (Lenardic, 2018). One is the squishy-lid sub-mode, which has been proposed for the early Archean Earth and the present-day Venus (Lourenço et al., 2020; Rozel et al., 2017). This sub-mode includes small, rigid lithospheric segments separated by wide zones of non-rigid, melt-impregnated lithosphere that features surface motion and compressional deformation around the sites of mantle downwelling (Lourenço et al., 2020; Rozel et al., 2017). Thus, this sub-mode can reproduce some of the key geological features of an active-lid (distributed deformation) sub-mode.

Another class of models suggests that a planet can alternate between these endmember modes in time or in space. For example, the numerical models of Rozel et al. (2017) showed temporal switching between stagnant and sluggish lid modes, whereas the models of Capitanio, Nebel, Cawood, Weinberg, and Clos (2019) showed adjoining and contemporaneous occurrence of stagnant and mobile lid modes, which they referred to as lid-and-plate mode. These models show the controls of long-term depletion of the lithospheric mantle on the formation of rigid lithospheric keels (Capitanio et al., 2020), which suppresses mobility, "freezing" tectonics features, such as rifts and lithospheric foundering, now preserved as fossil features in cratons. The intervening of stiffer lithospheric blocks amid a thermal boundary layer is key to the planetary thermal evolution as it reduces the heat released through the Earth's surface (Capitanio et al., 2022; Korenaga, 2006; Lenardic, 1998), while implying a high mobility.

Notably these tectonic modes are largely defined based on the relative motion of lithosphere and the convecting mantle (Figure 16; Lenardic, 2018). As a result, assigning these tectonic modes to different periods of the Earth history has often proved difficult because: (a) we have increasingly little knowledge of this relative motion as we go back in time, particularly of the speed of mantle convection, and (b) different tectonic modes/sub-modes can produce overlapping tectonic environments, leading to the development of similar rock records. For example, both active and sluggish lid modes can account for horizontal mobility of lithosphere leading to the development of extensional (e.g., rift) and compressional (e.g., orogenic) sites, the formation of particular rock assemblages in the Archean (Bédard, 2018; Windley et al., 2021), as well as the evolution of similar *P-T* conditions in the metamorphic and petrogenetic record (Capitanio, Nebel, Cawood, Weinberg, & Chowdhury, 2019; Chowdhury et al., 2020). Additionally, the thermal evolution of the Earth during its early history requires either lower surface velocities, as in a sluggish lid (Korenaga, 2006; Lenardic, 2018), or short episodes of high surface velocity, accounting for inferred short-lived tectonics features (Capitanio et al., 2022; O'Neill et al., 2007), although constraining velocities further has proven difficult.

Therefore, knowledge of lithospheric and mantle velocities is required to distinguish between tectonic modes, which are at best are poorly constrained and in reality largely unknown during the Archean. We suggest that for all practical purposes, these tectonic modes/sub-modes can be simplified into three categories to understand Earth's

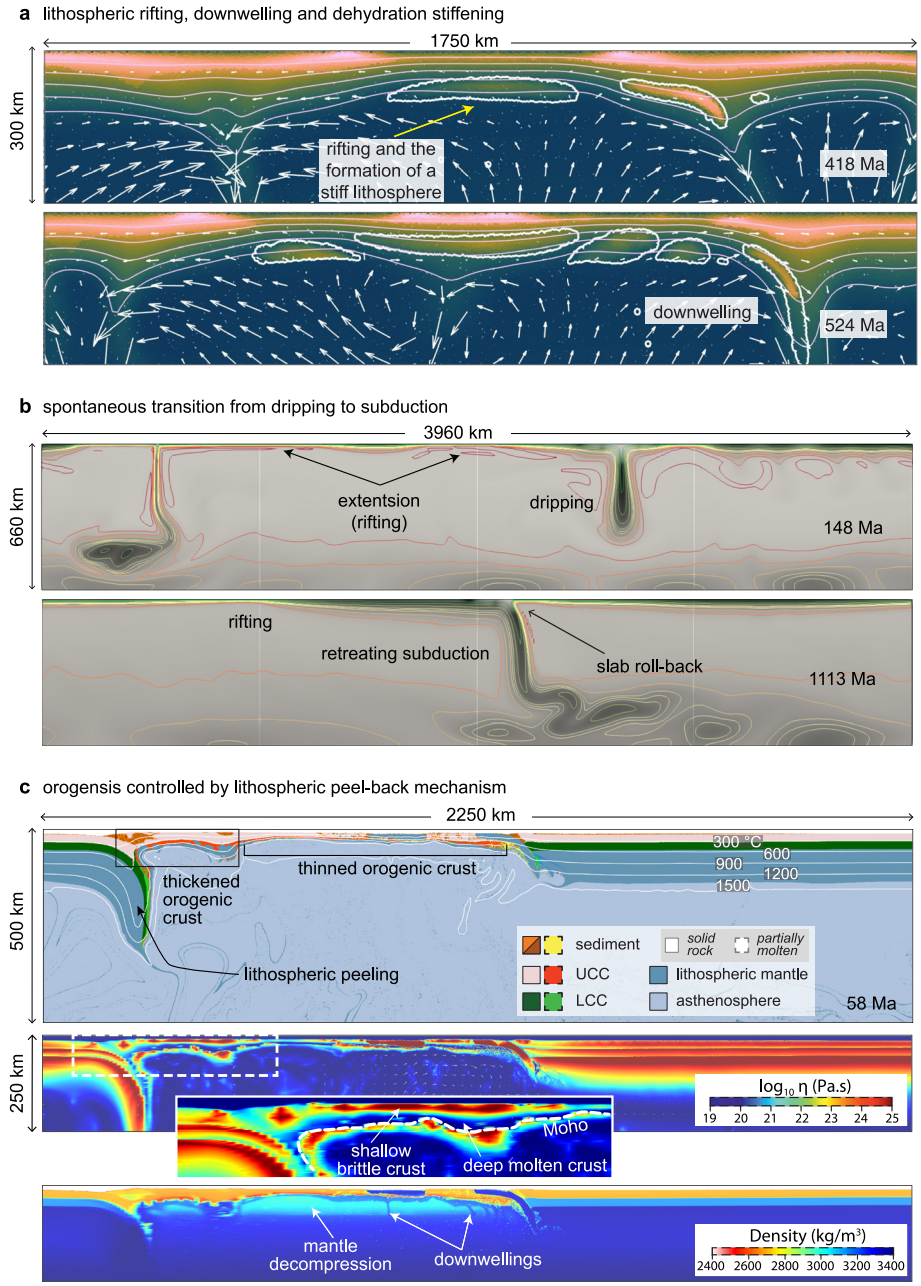

Figure 16. Snapshots of model evolution from different studies investigating the tectonic styles on a hot Earth. (a) Model showing lithosphere stretching and rifting and formation of depleted, stiffer continental lithospheric mantle. The rifting migrates laterally, until large volumes of depleted mantle are embedded in the cold lithosphere and partially entrained in downwellings (modified from Capitanio et al., 2020). (b) Model showing the transition from a dripping-and-rifting regime to a subduction-and-rifting regime (modified after Gunawardana, Chowdhury, Morra and Cawood, unpublished data). The transition from drips to subduction occurs self-consistently within the model as the convecting mantle (T_p) cools down by >150°C (from an initial T_p of ~1600°C). (c) Model showing a lithospheric peel-back driven (collisional) orogenic setting under hotter mantle conditions (initial T_p of 1525°C; modified after Chowdhury et al. (2020)). The viscosity and density distribution are also shown for the upper 250 km. Note the reduced thickness of the orogen due to lithospheric peeling and the mantle upwelling beneath it. The viscosity map shows that the orogenic crust is composed of a brittle upper crust and partially molten lower crust. The orogen is also marked by a laterally extensive, flat Moho surface. This orogenic mode may have operated during late Archean to early Proterozoic conditions when the mantle was hotter and rheologically differentiated continental lithospheres came into existence.

tectonic regime through time: (a) a stagnant-lid mode, (b) a sluggish-to-active lid mode with distributed deformation (squishy-lid tectonics), and (c) an active lid mode featuring narrow zones of deformation (plate tectonics).

7.2. Controls on Early Earth Behavior

The strength and buoyancy of lithosphere played key roles in controlling the type and viability of tectonic modes on early Earth, and both these lithospheric properties are largely controlled by the mantle thermal structure (e.g., Chowdhury et al., 2017, 2020; Herzberg & Rudnick, 2012; Sizova et al., 2010; Sleep & Windley, 1982; van Hunen & van den Berg, 2008). Although we know that mantle potential temperature was higher during the early history of the Earth, the absolute magnitude of the temperature and the rate of cooling are disputed (e.g., Figure 10) and are in part dependent on tectonic mode (e.g., stagnant lid vs. active lid; Lenardic, 2018), which in turn are dependent on inferred mantle temperature; a key conundrum in early Earth research. A hotter mantle has more vigorous convection involving cells of smaller dimension (Bunge et al., 1996; Grigné et al., 2005, 2007; Rolf et al., 2012; Zhong et al., 2007), and results in a warmer lithosphere with a great proportion of impregnated melt (e.g., Sizova et al., 2010). As a result, the lithosphere remains weak with low viscous strength (non-rigid; e.g., van Hunen & van den Berg, 2008; Sizova et al., 2010). In such a scenario, zones of lithospheric extension, whether above upper mantle convection cells or deep mantle plumes, will have limited spatial extent (both along and across strike) and are unlikely to produce linear zones of extension like those found on the modern Earth (e.g., mid-ocean ridges, continental rift zones). Such weak lithospheres will also accommodate compressive stresses largely through internal deformation with limited lateral motion (Sizova et al., 2010). This will hinder the development of subduction zones or orogens like those we observe on the modern Earth (Chowdhury et al., 2017, 2020; Sizova et al., 2010). Local subduction events may occur under hotter mantle conditions (Capitanio et al., 2020; O"Neill et al., 2020; Sizova et al., 2015; T. V. Gerya et al., 2015), but they will be impeded/terminated by shallow slab break-off event(s) since the subducted lithosphere will readily undergo viscous detachment due to its low yield strength that would prevent the development of a continuous "slab-pull" force (van Hunen & van den Berg, 2008), or to rheological stiffening of the mantle wedge following extensive dehydration (Capitanio et al., 2020). Similarly, orogenesis involving hot and weak continental lithospheres will be controlled by lithospheric peel-back (Chowdhury et al., 2017, 2020). Besides providing rheological weakening, a hotter mantle leads to greater degrees of adiabatic decompression melting, producing thicker basaltic crust and a residual harzburgitic lithospheric mantle that has greater buoyancy than modern oceanic lithospheres (Herzberg & Rudnick, 2012; Sleep & Windley, 1982). These factors would have negatively influenced the viability of plate tectonics, at least in its present form, on the early Earth. In contrast, the lithospheres may have experienced intense dripping and delamination (e.g., B. J. Foley, 2018; Chowdhury et al., 2017, 2020; Johnson et al., 2014; Lourenço et al., 2020; Rozel et al., 2017; Sizova et al., 2015).

7.3. Linking Tectonic Modes to the Evolution of the Earth System

7.3.1. Magma Ocean and a Stagnant/Squishy Lid Mode

Figure 17 is our attempt to link the proposed stages in the evolution of the Earth system with a tectonic mode. After formation of the Earth-Moon system and solidification of the magma ocean (phase I, ca. 4.57–4.45 Ga), a lithosphere with thick, mafic primary crust likely prevailed throughout the Primordial Earth stage (ca. 4.4–3.8 Ga; Kramers, 2007). We infer this initial lithosphere behaved as a stagnant lid based on the sub-chondritic Hf isotopic composition of early Earth zircons (Figure 13), which indicates crystallization from felsic melts produced via intra-lithospheric reworking, with little or no juvenile mantle input (Mulder et al., 2021). The lack of evidence for juvenile magmatic additions to the crust argues against overturn and recycling of the initial lithosphere, or the injection within it of significant volumes of mantle-derived magmas, at least in the sources for the preserved detrital zircon record (which are from areas that included relatively thick felsic crust). This implies that although a stagnant-lid mode may have been viable, a "heat-pipe" mode of volcanism (e.g., Moore et al., 2017) was likely not prevalent, at least in the lithospheric portions that have survived. These inferences are also consistent with the results of numerical modeling investigating Hadean geodynamics (e.g., O'Neill & Zhang, 2019). However, given the limited nature of the preserved Hadean record we cannot rule out that heat-pipe tectonics and/or other tectonic modes (like squishy lid tectonics), operated in parts of the globe that are not preserved.

10.1029/2022RG000789

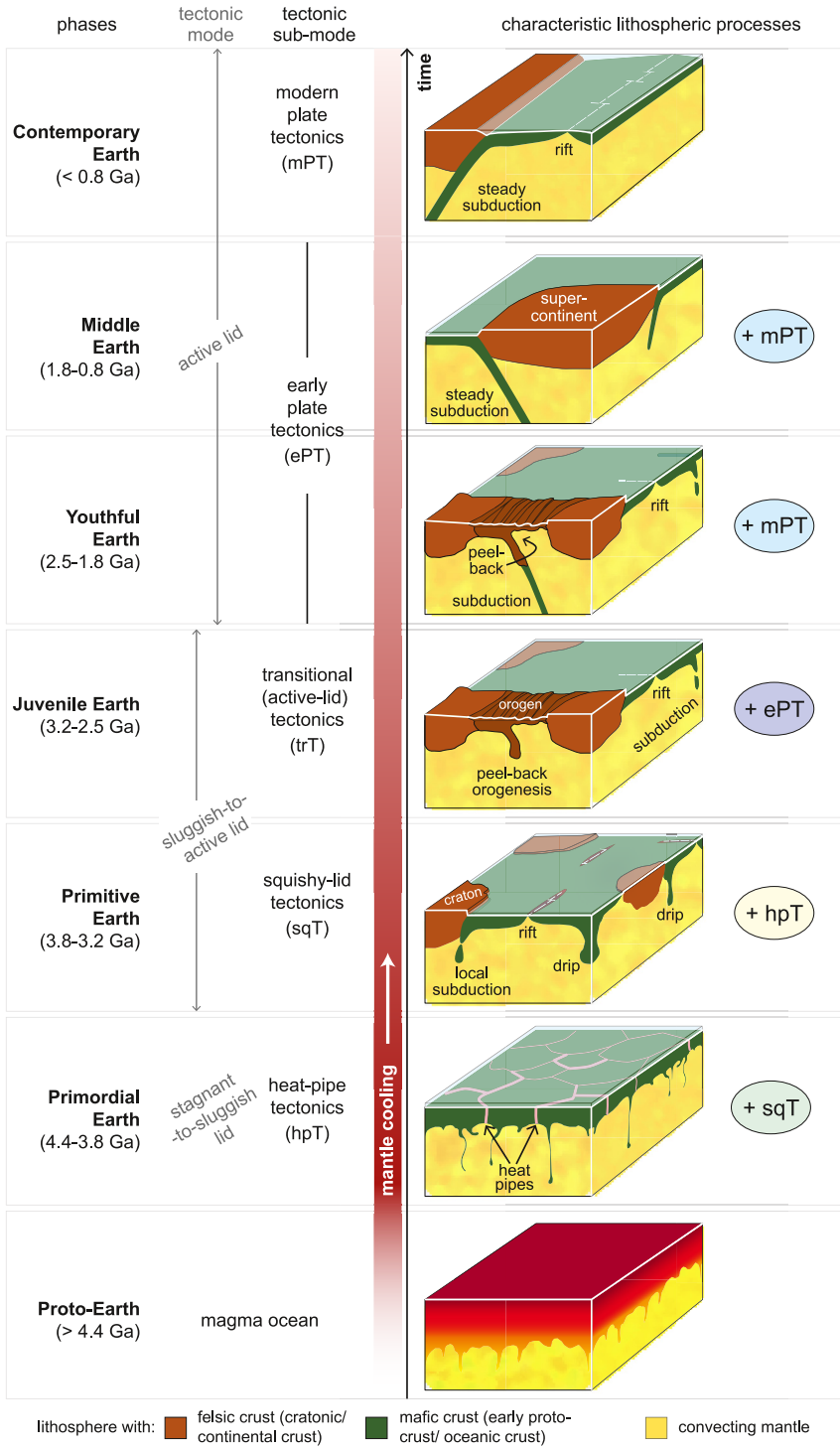

Figure 17. Linking various tectonic styles to different phases of Earth's evolution. The schematic diagrams represent the dominant tectonic style that may have been operating during the different phases. The tectonic styles are classified according to the three main modes and their sub-modes mentioned in this study (see text; cf., Figure 15). The Earth likely started with a magma-ocean conditions and evolved through various sub-modes of stagnant/sluggish lid modes before entering the plate tectonic mode by the end of Archean. The plate tectonic mode also likely evolved from an "early, hot style" to the "modern, cold style" during the Proterozoic and Phanerozoic eons. Coeval with this tectonic change, the secular cooling of Earth's mantle is also shown. Given mantle thermal conditions exert the first order control of tectonics and it may have varied between places at any given point of time, other tectonic modes may have also operated besides the dominant tectonic mode during any evolutionary phase. The acronyms on the right side of the tectonic diagrams represent these subsidiary tectonic modes for each evolutionary phase. For example, modern plate tectonic processes may have occurred sporadically during the Youthful Earth phase (see text for more discussion).

7.3.2. Squishy Lid Mode

The period from ca. 3.8 to 2.5 Ga (i.e., during phases III and IV) marks the formation and stabilization of Earth's cratons. The beginning of this time range is marked by the preservation of granite-greenstone terranes and high-grade gneisses in the rock record, and after 3.2 Ga there was ongoing craton formation and also widespread stabilization of these associations leading to their long-term preservation. Voluminous mafic volcanism during greenstone belt formation and the concomitant production of TTGs with supra-chondritic Hf signature during ca. 3.8–3.2 Ga suggests significant input of mantle-derived, juvenile melts during this time-period (Figure 13; Mulder et al., 2021). These rock types eventually formed the cratonic crust and were shielded from the convecting mantle by a rigid layer of harzburgitic lithospheric mantle (cratonic keel). Formation of this continental lithospheric mantle during juvenile melt extraction was fundamental in ensuring the cratons' long-term preservation (Korenaga, 2006; Pearson et al., 2021). Studies of the cratonic mantle lithosphere reveal internal layering due to variations in the amount of melt depletion (Griffin et al., 2003; Yuan & Romanowicz, 2010). Furthermore, the numerical models of Perchuk et al. (2020) propose that this layering is a complex multistage process that occurs through the juxtaposition of depleted lithospheric mantle by spatially and temporally discrete processes (cf., Z. Wang et al., 2022). Importantly, the formation of these lithospheric keels likely marks the transformation of a lithosphere region undergoing intense plutonism and non-rigid, distributed deformation to a rigid and buoyant lithosphere (cratonic core) that is a prerequisite for plate tectonics. Coincident with increased rigidity is evidence after ca. 3.2 Ga for increased thickening of the lithosphere including geochemical data for increased depth of crustal melting in the production of TTG's, the evolving source of felsic magmatism from melting of mafic lower crust to TTG-like compositions for potassic granites (Moyen & Laurent, 2018; Moyen & Martin, 2012; Nebel et al., 2018), and evidence for continental emergence above sea-level at craton scale (Chowdhury, Mulder, et al., 2021; Reimink et al., 2020; W. Wang et al., 2021a). In addition, data from modeling proportions of juvenile versus evolved global detrital zircon populations as well as orogen specific studies (Dhuime et al., 2018; L. Gao et al., 2022a; S. Gao et al., 2002; X. Wang et al., 2021b) provide evidence for recycling and hence destruction of lithospheric mantle throughout the Archean (<3.8 Ga).

We interpret the rock association and geochemical changes commencing at 3.8 Ga to result from a sluggish/active-lid regime, involving some degree of coupling between the convecting mantle and the lithosphere resulting in lateral mobility of the latter. Direct paleomagnetic evidence for lithospheric mobility is however limited to Meso- and Neoarchean (and younger) rock successions (Brenner et al., 2020; Cawood et al., 2018). Modeling geodynamics and felsic crust production at mantle potential temperatures through this time suggest the lithosphere was not uniformly rigid (Capitanio et al., 2020; Lourenço et al., 2020; Rozel et al., 2017), leading to the formation of small, rigid lithospheric segments (proto-plates) separated by wide zones of hot and weak lithosphere experiencing deformation and plutonism (Figure 16; i.e., squishy lid tectonics involving distributed deformation). Downwelling of lithospheric mantle (±crust) in the form of drips or delamination likely occurred around these weak zones, resulting in lateral surface motion that gradually accentuated toward the downwelling sites. Thus, fast lateral velocities may have existed in the vicinity of dripping/delamination sites triggered by the downwelling lithosphere, while sluggish motion of lithospheric segments lying away from these sites may have resulted from convective traction (Capitanio et al., 2020; Lourenço et al., 2020). Localized subduction may have also occurred in this tectonic regime either triggered by plumes/meteorite impacts (O'Neill et al., 2020; T. V. Gerya et al., 2015), or by mantle convection (Sizova et al., 2015). In addition, the recycling of lithosphere requires compensation through the generation of new lithosphere along zones of extension (rifts), and together imply lithospheric mobility (Capitanio et al., 2020). Modeling studies showed that such extensional zones may have developed at the sites of the convective upwelling of mantle and its decompressive melting. Some models even showed these extensional zones to be the sites where rigid lithospheric mantle, constituting the cratonic cores, may have formed via melt loss (Capitanio et al., 2020).

Proposed evidence for recycling of Archean lithosphere (e.g., Smart et al., 2016), and for geochemical signatures comparable to modern convergent plate margins (e.g., Windley et al., 2021), lies at the heart of many arguments as to the viability of Hadean-to-Archean plate tectonics. However, modeling studies have shown that these signatures are also consistent with non-plate tectonic modes; that is, lithospheric recycling need not be synonymous with subduction. Thus, lithospheric recycling via drips or delamination are characteristic of the active/sluggish lid tectonic modes likely operating during the early-to-mid Archean (Capitanio et al., 2019b, 2020; Johnson et al., 2014; Lourenço et al., 2020; Rozel et al., 2017). These processes are also capable of imparting geochemical signatures based on relatively immobile elements to Archean igneous rocks similar to those found in modern

convergent plate margins (e.g., Chowdhury, Mulder, et al., 2021; Gunawardana et al., 2020; Johnson et al., 2017; Nebel et al., 2018; Smithies et al., 2021). From this, we infer that although variable coupling between mantle and lithosphere during this time-period resulted in simultaneous multi-mode tectonic environments, none of them were akin to the modern day globally linked system of plate boundaries (cf., Capitanio, Nebel, Cawood, Weinberg, & Clos, 2019; Cawood et al., 2018). The regions of lithospheric extension and convergence are likely to taper out and not extend along strike for significant distances, thus inhibiting linked continuous lithospheric boundaries (Figure 17). Furthermore, the reduced strength of Archean lithosphere at predicted mantle potential temperatures results in any lithosphere undergoing recycling disaggregating into lenses via viscous detachments at shallow mantle depths (Fischer & Gerya, 2016; Moyen & van Hunen, 2012; van Hunen & van den Berg, 2008). This prevents the formation of coherent continuous subducting slabs, and hence the development of a slab-pull force, which constitutes a major force driving long-lived/continuous subduction processes at a global scale (Forsyth & Uyeda, 1975).

7.3.3. Transition From Squishy Lid Mode to Plate Tectonics Mode

During the late Archean (ca. 3.2–2.5 Ga), the preserved rock record indicates cratonic stabilization and thickening. We consider that this increasing rigidity of the lithosphere represents a gradual global transition from tectonic modes with distributed deformation (i.e., squishy lid) to an active lid mode involving rigid plates (i.e., plate tectonics). The development of rigid lithospheric blocks and plate margin processes are consistent with the appearance of massive dyke swarms, granulite facies metamorphism, and linear, orogenic (accretionary) belts around the cratonic cores during the late Archean. It has been argued that metamorphic *P*/*T* data can be split into two groups for the Proterozoic and Archean, and that these be regarded as evidence for paired metamorphism (Brown & Johnson, 2018; Brown, Johnson, et al., 2020), and hence for the development of plate tectonics. Like most data from the early Earth, there are spatial and temporal limitations on the distribution of such *P*/*T* groups and the interpretive significance that can be placed on them. For example, the data for paired metamorphic belts are essentially a temporally constrained data set with their relative spatial distribution at the time of formation largely unconstrained, yet spatial controls remain central to any interpretation of tectonic processes (Marimon et al., 2022). Recently, however, B. Huang et al. (2020) argued for a spatially and temporally linked paired metamorphic belt in the Neoarchean of North China.

The development of rigid cratonic cores likely played a significant role in concentrating horizontal stresses along their margins, leading to lithospheric failures and recycling via dripping and incipient subduction, and craton assembly. For example, evidence for block accretion onto the margins of the East Pilbara, Singhbhum and Kaapvaal cratons requires these margins being sites of focused deformation (Bose et al., 2021; Hickman, 2012; Laurent et al., 2019). In addition, the geochemistry of basalts suggests that the mantle underwent significant cooling during this time (e.g., B. Keller & Schoene, 2018; C. B. Keller & Schoene, 2012), allowing the development of long wavelength convective cells and better lithosphere-mantle coupling (Bunge et al., 1996; Grigné et al., 2005; Zhong et al., 2007). Evidence for assembly of cratons with discrete earlier histories (implying spatial separation) into supercratons (Bleeker, 2003; Söderlund et al., 2010), along with limited paleomagnetic data (Brenner et al., 2020; Cawood et al., 2018), provide further evidence for lithospheric mobility. However, the transition to plate tectonics at a global scale happened over a protracted time period and most likely, was not completed until ca. 2.5 Ga (cf., Brown, Johnson, et al., 2020; Cawood et al., 2018). This is based on the diachronous development of geological evidence in favor of plate margin processes in different cratons (e.g., Figure 14). Furthermore, the form of plate tectonic processes that operated during this time remains contentious, as the mantle was still warmer when compared to its modern thermal state (cf., Ganne & Feng, 2017; Herzberg et al., 2010). Modeling shows that accretionary/collisional processes were dominated by lithospheric peeling (Figure 16; Chowdhury et al., 2017, 2020), which is a process that also occurs on modern Earth where weak lithospheres are involved (e.g., Apennines; Magni et al., 2013). Subduction under warmer mantle conditions was likely impeded by slab breakoffs and intense trench roll back leading to mantle decompression and melting (Perchuk et al., 2019; Sizova et al., 2010).

7.3.4. Plate Tectonic Mode

Evidence for widespread dyke emplacement into brittle cratonic crust commenced in the late Archean and dykes become globally distributed through the early Paleoproterozoic (Figure 14; Cawood et al., 2018). These dykes, along with the development of rift and passive margin sedimentation along the edges of a number of cratons, provides evidence for subsidence associated with lithospheric extension. This, together with the development

of linear late Paleoproterozoic collisional orogenic belts, suggests a pattern of oceans opening and closing that we associate with a globally linked pattern of focused plate boundaries. This led to the assembly of the Archean cratons into the first supercontinent Nuna by the late Paleoproterozoic (G. Zhao et al., 2002; Mitchell et al., 2021). Modeling studies show that, although plate tectonics was likely operating under the warm mantle conditions of this time, the nature of the convergent margin processes were likely different (e.g., Chardon et al., 2009) from their modern counterparts. In particular, orogenic processes controlled by lithospheric peeling may have continued to occur (Chowdhury et al., 2017, 2020), while subduction process may have been characterized by faster descent of the slabs along with significant trench roll-back and associated mantle upwelling (Perchuk et al., 2019). Local appearance of high-pressure metamorphic rocks by ca. 1.8 Ga in certain localities (e.g., eclogites in the Trans-Hudson orogen; Weller & St-Onge, 2017) suggests modern type of convergent margin processes may have also appeared during this time period, but possibly limited to areas where the mantle was relatively colder (Brown, Johnson, et al., 2020; Holder et al., 2019).

Commencing in the late Archean, but mainly from the Paleoproterozoic to the present day, the presence for globally distributed passive margins along the edges of pre-existing continental fragments, linear belts of accretionary and collisional orogens with associated tectonothermal events, and paleomagnetic data indicative of relative motion of continental fragments (Bradley, 2008; Cawood et al., 2009; Evans, 2013; G. Zhao et al., 2002; Karlstrom et al., 2001; Wan et al., 2020; Weller et al., 2021) argues for a linked system of divergent and convergent plate margins that formed in an active lid, plate tectonic regime (Cawood et al., 2018; Mitchell et al., 2021). Changes in the distribution of rock associations between 1.8 and 0.8 Ga and from 0.8 Ga to the present day correspond to stages of the plate tectonic driven supercontinent cycle (Cawood & Hawkesworth, 2014).

The Middle Earth phase (ca. 1.8–0.8 Ga) is characterized by the supercontinental cycle involving the formation of Nuna and Rodinia, and the ultimate breakup of the latter (Cawood & Hawkesworth, 2014). What remains unclear is how prominent the supercontinental break-up phase was prior to Rodinia assembly, with direct implications toward the prevailing tectonic style. The prevalence of A-type granitoid magmatism, along with the inferred absence of a complete subduction girdle around the periphery of Nuna, as well as a lack of subduction-related geochemical fingerprints and linked mineral deposits supports a long-lived Nuna-Rodinia supercontinent (cf., Cawood et al., 2016, 2021; Tang et al., 2021). However, a record of well-developed orogens contradicts this interpretation (Spencer et al., 2021). These Mesoproterozoic orogens are further marked by thin crust and unusually high heat flux (causing UHT metamorphism). A long-lived supercontinent may have caused a thermal blanketing effect on the underlying mantle (Gurnis, 1988; Jellinek et al., 2020; Lenardic et al., 2005, 2011), which in turn may have led to warming and weakening the continental lithosphere, limiting the height of mountains that could be supported (Tang et al., 2021). On the contrary, similar features can be generated if the collisional orogens involved weak continental lithospheres and thus deviated from modern orogenic styles (Spencer et al., 2021). The weakening of continental lithospheres may have been caused either by the heat coming from upwelled mantle (due to syn-orogenic lithospheric delamination or shallow slab break-off; Sizova et al., 2014; Spencer et al., 2021), or due to the presence of highly radiogenic crustal lithologies such as pelites or granitoids (McLaren et al., 2003). The preserved continental rock-record is perhaps best reconciled if the effects of a protracted supercontinental cycle and a different orogenic style are considered together. While large tracts of Nuna, notably the core elements of Laurentia, Baltica and Siberia, likely remained largely intact throughout this time-period, marginal blocks disaggregated and re-assembled during the Rodinia assembly via collisional orogenic events that occurred within the overall plate tectonic regime but differed from the modern orogenic style.

The transition to the Contemporary Earth phase (i.e., phase VII) is marked by the widespread appearance of rocks/rock-assemblages that are considered the hallmark of modern-style plate tectonics, particularly of the subduction-collisional settings (e.g., UHP rocks, blueschists, ophiolites, etc.). During this phase, the mantle is inferred to have cooled down to its modern thermal state that kickstarted steady and continuous subduction of the oceanic lithospheres without undergoing shallow break offs (e.g., Fischer & Gerya, 2016; Sizova et al., 2010; van Hunen & van den Berg, 2008). Bending of subducting oceanic lithosphere at the outer rises of trenches results in intense brittle-viscous weakening of the lithosphere and a tendency for slab detachment at elevated temperatures in the mantle (T. V. Gerya et al., 2021). On a hotter early Earth, this tendency would either inhibit subduction or result in punctuated intermittent subduction through frequent slab breakoff. The colder mantle and the increased mechanical integrity of lithospheres on the Contemporary Earth further promoted the coupling between the oceanic and continental lithospheres, which allowed the oceanic lithospheres to pull the attached continental lithospheres deep into the mantle (Chowdhury et al., 2017; Magni et al., 2013; Sizova et al., 2014). These processes

led to the burial of colder crustal material to great depths, leading to their metamorphism along low *T*/*P* thermobaric ratios and forming unique lithologies like blueschists and UHP rocks (Chowdhury et al., 2017; Sizova et al., 2014). A consequence of greater oceanic-continental lithospheric coupling and deep continental burial is that it enhanced the recycling of continental crustal material to mantle depths, a part of which never returns due to slab break-off at great depths (e.g., Figure 9). Chowdhury et al. (2017) determined via modeling that the rate of this break-off-mediated continental recycling varies within ~0.4 to 0.7 km^3/a (which is somewhat higher than the earlier estimates of ~0.3 to 0.4 km^3/a; cf., Scholl and von Huene, 2009). This additional recycling of continental material during this phase may correspond with an inferred on-going decrease in the continental volume since the Neoproterozoic (Cawood & Hawkesworth, 2019; Cawood et al., 2013; Dhuime et al., 2015).

8. Bimodal Hypsometry, Continental Emergence, and Tectonics

The evolution of the continental lithosphere and tectonics through time has direct implications for the surficial morphology of our planet and the Earth system as a whole. The bimodal hypsometry of the modern Earth with the associated 40:60 ratio of continental to oceanic lithosphere (Figure 4; e.g., Cawood & Hawkesworth, 2019) is a direct outcome of plate tectonics in which oceanic lithosphere forms at divergent mid-oceanic ridges whereas continental lithosphere forms at the convergent subduction zone settings. These processes lead to contrasting physical and chemical characteristics of the resultant lithosphere: oceanic lithosphere is thin and dense relative to thicker and less dense continental lithosphere, resulting in the bimodal hypsometry. Most of the other terrestrial planetary bodies, along with the Moon, have a unimodal hypsometry, which is related to an overall, mafic dominated, crust (Aharonson et al., 2001; Criss & Hofmeister, 2020; Stoddard & Jurdy, 2012). Mars, however, has a bimodal hypsometry like the Earth consisting of the northern lowlands with thin and younger crust relative to the southern highlands with thick and older crust. But, unlike the Earth, this hypsometry is not related to plate tectonics (Smrekar et al., 2019).

The timing of development of Earth's bimodal hypsometry and whether it can be uniquely linked to a tectonic mode remain critically unresolved issues in unraveling secular evolution. Petrogenetic models and knowledge of mantle cooling indicate that early mafic crust (prevalent during the Hadean-Archean) was considerably thicker (~20 to 30 km) than the modern oceanic crust (Herzberg et al., 2010; Korenaga, 2013; Sleep & Windley, 1982). Similarly, models of the origin of the felsic component of Archean continental crust require crustal thicknesses of at least 25–35 km for the generation of TTGs (Chowdhury, Mulder, et al., 2021; Johnson et al., 2017; Moyen, 2011). The blurring of the difference between the thickness of the early mafic crust and the continental crust must have impeded the development of bimodal hypsometry. Moreover, the cratonic crust started becoming stable, compositionally mature, and thick (>40–45 km) only since ca. 3.2 Ga (Figure 14; cf., Cawood et al., 2018; Chowdhury, Mulder, et al., 2021). Prior to that its composition was significantly mafic and thus, must have showed limited positive buoyancy compared to the thick, early mafic crust. Owing to these diminished differences in the thickness and bulk composition of the two lithospheres on the early Earth, a distinct bimodal hypsometry is unlikely to have prevailed at that time. Consequently, during its early history, the Earth may have been a water world with no significant amount of stable, emergent landmasses (except for some volcanic islands). This has been corroborated by the variations in the isotopic proxies for seawater through time (e.g., Sr-curve, Zn-in BIF; Pons et al., 2013; X. Chen et al., 2022). Once the stabilized cratons with thick (~40 to 50 km), mature crust came into existence by ca. 3.2–3.0 Ga (marked by the presence of K-granite magmatism within cratonic cores), the bimodal hypsometry started to become prominent. However, these early episodes of continental emergence need not have been controlled by plate tectonic processes. Instead, the formation of thick, felsic crust bearing cratons (like, the Singhbhum, Pilbara and Kaapvaal cratons) at non-plate tectonic settings imparted them a significant isostatic uplift relative to the ambient, mafic crust and eventually pushed them above the sea level, leading to the appearance of stable, continental landmasses by ca. 3.2–3.0 Ga (Chowdhury, Mulder, et al., 2021; Roberts & Santosh, 2018; W. Wang et al., 2021a).

The number of stabilized cratons increased during the Neoarchean and also during this time orogenesis associated with incipient plate tectonic processes appeared. These factors likely resulted in vast continental areas with thick crust, which led to a significant increase in the proportion of emergent continental landmasses by the end of Archean to early Paleoproterozoic (Bindeman et al., 2018; Flament et al., 2008; Reimink et al., 2020). This emergence event is distinctly corroborated by the divergence of the Sr-in-seawater curve from the depleted mantle evolution curve (Shields, 2007; X. Chen et al., 2022), a change in the O-isotope of shales (Bindeman et al., 2018)

and zircons (Spencer et al., 2014, 2019), and an increase in the proportion of subaerial continental LIPs in the geological record (Kump & Barley, 2007). This change in the continental freeboard condition has even been surmised to facilitate the GOE (Campbell & Davies, 2017; Kump & Barley, 2007; Spencer et al., 2019; X. Chen et al., 2022). The amalgamation of Nuna during the late Paleoproterozoic tectonically accentuated the continental crust thickness through global-scale collisional events, thus maintaining the bimodal hypsometry. This tectonic-related crustal thickening facilitated continental uplift and a high freeboard during that time, which led to high weathering fluxes to the oceans (X. Chen et al., 2022; Z. Zhu et al., 2022b).

The middle Proterozoic is inferred to be characterized by thin, orogenic continental crust (Tang et al., 2021), which led to lower continental elevations above sea level. This is corroborated by a decline in the radiogenic Sr composition of the seawater around that time-period, which implies a lower influx of continental detritus into the oceans. The Rodinia amalgamation did not impart a large change in the Sr-isotopic composition, implying either the orogenic events of that time did not lead to thicker crust and enhanced continental weathering, or an increased input of juvenile material (Cawood & Hawkesworth, 2014; Cawood et al., 2013; Spencer et al., 2013; X. Chen et al., 2022). This hypsometric evolution is in accordance with the occurrence of a different style of collisional tectonics (cf., Spencer et al., 2021). The Neoproterozoic era is characterized by the re-appearance of orogenic mountains comprising thickened continental crust, which led to an increase in emergent landmass as well as in the continental elevation (Campbell & Squire, 2010; Tang et al., 2021). An overall increase in the $^{87}Sr/^{86}Sr$ of seawater during this time reflects a gradual increase in the continental weathering rates and the consequent increased supply of nutrients to the oceans (Campbell & Squire, 2010; Shields, 2007; X. Chen et al., 2022; Z. Zhu et al., 2022b). The bimodal hypsometry and the continental freeboard seem to have remained constant subsequently through modern plate tectonics of the Contemporary Earth (e.g., Cawood & Hawkesworth, 2019; Tang et al., 2021).

9. Timescale

Discussions of the geological timescale are largely beyond the remit of this paper but based on our observations of secular changes and the proposal to divide Earth's evolution into seven phases, we would make the following general comments. First order divisions of eon, era and period of the Mesoproterozoic and older divisions of the Precambrian were erected on the basis of changes in episodes of sedimentation, magmatism and orogeny (Plumb, 1991) and are based on approximate ages rounded to the nearest 100 Ma. Subsequent work has highlighted the need to refine the boundaries in terms of new data and better tie them to specific and observable events in the rock archive (Bleeker, 2004; Cloud, 1987; Shields et al., 2021; Strachan et al., 2020). This approach is the foundation for the Phanerozoic timescale, with the events that define eon, era, and period boundaries based on changes in surficial reservoirs (e.g., changes in environment and relationship to species evolution). Although there have been important developments in establishing global biostratigraphic markers for the Precambrian (e.g., Adam et al., 2017; Porter, 2016), the approach of refining the Proterozoic timescale through changes in surficial reservoirs has been hampered by the lack of high precision age constraints on potential global events (e.g., the GOE) and that such events likely occur over a relatively protracted timeframe (millions of years and longer) rather than the relative short, sharp events that divide the Phanerozoic timescale. This scarcity of high-precision age constraints in part reflects the tendency for the best-preserved Proterozoic strata, particularly pre-Neoproterozoic strata, to have formed in intracontinental settings. Although intracontinental basins have high preservation potential, their location distal from plate boundaries results in a general paucity of widespread and frequent syn-sedimentary volcanism (e.g., Cawood et al., 2012), precluding high-precision U-Pb dating of interstratified volcanic units as has been widely applied in refining the Phanerozoic timescale (e.g., Gradstein et al., 2020). In this regard, emerging geochronology techniques such as U-Th-Pb dating of authigenic phosphate minerals (Rasmussen et al., 2001), U-Pb and Lu-Hf dating of carbonates (A. Simpson et al., 2022; Roberts et al., 2020), and Rb/Sr dating of shales (Subarkah et al., 2022) offer a promising way forward by providing a means of absolute dating of sedimentary sequences that lack a well-established biostratigraphy or intercalated volcanic units.

Furthermore, the increasingly fragmented nature of the Precambrian record with increasing age and the fact that any changes in the record largely apply to the solid Earth reservoirs that can vary in timing from craton to craton limit the value of any such changes in their role as possible chronostratigraphic boundaries; for example, the termination of widespread TTG or komatiite magmatism. The two major boundaries of the Precambrian are the Hadean-Archean and Archean-Proterozoic and we make the following observations. The Hadean is informally

defined as the period of Earth history predating the rock record (Cloud, 1972). The boundary with the Archean is generally taken at 4.0 Ga (Shields et al., 2021), which fortuitously corresponds with the age of the Acasta Gneiss, the oldest accepted fragment of continental crust (Bowring & Williams, 1999), although ages >4 Ga have been proposed for parts of the Nuvvuagittuq greenstone belt (O'Neil et al., 2012). Others have suggested the lower boundary of the Hadean should be taken at 3.85 Ga corresponding with the increasing preservation of crust across multiple cratonic fragments (Bleeker, 2004; Kamber, 2015; see also Van Kranendonk, Bennett, & Hoffman, 2019, and references therein). We note that 3.8 Ga corresponds with evidence for input of juvenile igneous rocks (based of Hf in zircon, Figure 13) and may constitute an appropriate boundary, but although this appears to be widespread event recorded in most cratons, its timing on presently available data varies from craton to craton.

The Archean-Proterozoic boundary is taken at 2.5 Ga (Plumb, 1991). Developments of a better geochronological database of events around the boundary have allowed a greater understanding of the time of changes in the rock record. Recent work has suggested placing the boundary at 2.45 or 2.4 Ga on the basis of events such as oxygenation of the atmosphere, and changing proportions of U/Pb, Hf-isotope and trace-element data on zircon, and Re–Os model ages on sulphides (Griffin et al., 2014; Shields et al., 2021). Again, it is not clear whether the timing of these events is synchronous or sufficiently abrupt to be an adequate chronologic division. Furthermore, such changes require significant analytical data sets on suitable samples and are, at the very least, difficult to observe directly in the rock archive.

10. Conclusions

Since accretion from the solar nebula, the composition and character of Earth has continued to evolve. For example, initial differentiation of the solid and surficial reservoirs, including changing compositions and redox state of the oceans, the evolution of the biosphere, cycling between the surficial and solid Earth reservoirs, development and changing mineral and rock associations and resultant evolving mafic and felsic crust compositions, the changing nature of continental lithospheric mantle, the thermal evolution of the mantle and the development of depleted mantle, and crystallization of an inner core.

The evolution of the Earth's solid reservoirs, including cycling with the surficial reservoirs, is largely driven by internal cooling resulting from temperatures generated through gravitational collapse during initial accretion with increasing contributions over time from radioactive decay. Direct effects of solar energy input are limited to the surficial reservoirs. Although there has been continuous and largely secular cooling of the mantle, the preserved continental record displays a punctuated history with periodic, relatively rapid, step changes in rock associations and events. These changes imply that at various times the Earth system reaches a critical point and transitions to a new equilibrium state. Thus, it is possible to divide the geological evolution of the planet into a series of broad phases. What is less clear, and a source of much debate is how, or even if, such phases relate to the tectonic models that are inferred to have operated on Earth. In addition, it is necessary to differentiate such phases against changes such as peaks and troughs in rock ages and events that relate to preservation bias.

Arguments for which tectonic modes may have operated at times thought Earth history are built on geological observations (e.g., Cawood et al., 2006, 2018) and numerical models (e.g., T. Gerya, 2022; van Hunen & Moyen, 2012). These numerical models are particularly useful in exploring possible environments that existed given the incomplete and selective nature of the early Earth record. Such models have their own set of limitations including, at this stage, their largely 2D nature and uncertainties about the values and significance of some early Earth parameters. Integrated geological data and numerical modeling suggest three main tectonic modes may have operated on Earth during its secular evolution: stagnant lid, squishy lid, and plate tectonic modes. We argue on the basis of the limited preserved record that after initial accretion and post-solidification of the magma ocean, the early Earth likely operated in a stagnant lid mode, which entails a rigid, continuous lid above a convecting mantle (i.e., a single plate), and that this mode of behavior probably extended until around 3.8 Ga. However, we recognize that the preserved record is highly limited and selective and at a global scale a squishy lid mode involving some lithospheric mobility and diffuse deformation may be equally plausible, especially on the basis of numerical modeling (Capitanio et al., 2019b, 2020).

By 3.8 Ga, variable coupling between the lithosphere and convecting mantle resulted in lithospheric mobility, with sites of extension and compression. High mantle temperatures and likely widespread impregnation of the

lithosphere with melt resulted in a rheologically weak crust, while leaving a rigid residue in lithospheric mantle roots, and broad scale distributed deformation. Only in the period 3.2–2.5 Ga did the transformation into a rigid whole lithosphere occur, enabling the development of a globally linked system of plate boundaries with the Earth operating under an active lid, plate tectonic mode since at least 2.5 Ga. Zones of focused compressional and extensional deformation are recognized prior to 2.5 Ga, as are geochemical signatures of fluid flux melting. However, the record is insufficient to establish the localized versus global extent of such features and if these represent some form of plate tectonics (i.e., active lid, focused deformation). The later parts of the Archean could have involved regions of lithosphere continuing to undergo squish lid behavior and experiencing distributed deformation but with other segments containing rigid lithosphere with focused zones of deformation. Since 2.5 Ga, a globally linked system of focused convergent and extension boundaries separating internally rigid plates are inferred to have operated, as evidenced from fragmentation of the Archean supercratons and the subsequent assembly of the dispersed cratonic fragments into Nuna, the first supercontinent (Cawood et al., 2018; Wan et al., 2020).

Events at ca. 1.8 and 0.8 Ga, that represent board scale changes in the Earth system and correspond with assembly of Nuna and dispersal of the Rodinia supercontinents, subdivide the overall post-2.5 Ga plate tectonic framework under which the Earth was operating. For the Contemporary Earth, extending from 0.8 Ga to the present day, mantle potential temperatures had cooled sufficiently to enable deep continental subduction at collision zones. Earth's surficial reservoirs continued to evolve and interact with the solid Earth reservoirs through our planet's evolution as expressed in broad-scale changes in composition of the atmosphere, oceans, and biosphere. Although the surficial reservoirs react and homogenize on short timescales with diurnal to millennial periodicity, first order changes within these systems (e.g., oxygenation of the atmosphere, changes in ocean composition, and appearance of major life forms) appear to correspond to phases of lithosphere evolution (e.g., Figure 1) reflecting feedback loops within the system.

The evolution of the individual elements of the Earth system and links between them need to be viewed through the lens of any potential bias in the rock record. Ocean and continental lithosphere have different preservation potential as does thick versus thin continental lithosphere. Similarly, the supercontinent cycle has impacted the preserved rock archive. Thus, for the most part we can expect bias in the long-term continental record. This is a consequence of both the way different tectonic modes impart a discrete signature on the record and are then variably preserved. The resultant continental lithosphere is spatially and temporally heterogeneous (C. J. Hawkesworth et al., 2020). Thus, mixing through convection continually homogenizes the oceans, atmosphere, and mantle (but on different temporal scales) and contrasts with continental lithosphere in which heterogeneities form and are largely locked into the preserved record. This complex multistage and multiscale architecture of the continental lithosphere is now preserved in a record extending back at least 4.4 Ga and contrasts with that of oceanic lithosphere, which is temporally restricted to the last 200 Ma and is much more homogeneous due to its single stage record related to adiabatic decompression melting of the mantle (and magma chamber fractional crystallization).

Although much is made in the Earth Sciences of the concept of uniformitarianism (Hutton, 1788), encapsulated in the phrase “the present is the key to the past,” the pulsed and evolving nature of the continental rock record, likely in response to progressive mantle cooling, suggests that the planet has operated under different tectonic modes through its history and each is likely to have imparted a distinctive and likely non-uniform signature into the rock record.

11. Future Directions (A Way Forward)

Our overview of secular changes in Earth history is based on the rock and mineral archive of the continental crust, integrated with constraints from numerical models that are calibrated for evolving mantle temperatures and consequent lithospheric rheology. From this, we propose seven phases in Earth evolution based on the incoming of, or changes in, distinctive features in the rock record, which from thermal evolution models are related to three broad tectonic modes (e.g., Figure 1). We accept that both the division into phases and the tectonic modes we link to them are open to re-interpretation and indeed rejection by others, especially as additional data are generated in the future. We welcome new data and interpretations and would highlight the following as first order issues to consider.

Continuing study of the other terrestrial planets, especially the potential for sample return missions from the Moon and Mars, along with work on meteorites, will provide much new, albeit statistically limited, data and ideas on the Proto- and Primordial phases of Earth evolution. Ongoing numerical modeling of mantle processes and refinement of mantle potential temperatures, along with an improved understanding of mantle convection (whole vs. layered) will provide a better framework in which to unravel our planet's evolution. Furthermore, a better understanding of the processes of intra- and inter-reservoir cycling, together with additional work on the limited pre-3.8 Ga mineral and rock archive, particularly from novel isotopic systems, has the potential to provide new and better constraints on thermal regimes, melting patterns, and lithospheric character and behavior through Earth history.

Processes of biasing, along with decreasing preservation with increasing age, mean we need approaches to better understanding what is missing (known unknowns) and what implications that might have had for Earth processes, notably for the Hadean and Archean eons (prior to phase V, Figure 1). Thus, for example, can we reverse engineer the preserved rock record, perhaps in conjunction with constraints from experimental data, to better determine mantle thermal structure and its secular evolution? This approach has already been used (e.g., Herzberg et al., 2010) but future work is likely to better constrain the variables involved and improve precision. Similarly, are there new approaches that can be applied to what is preserved to understand how rock units and events interacted with, and were constrained by (and vice versa), those known unknowns that are no longer present?

Our inference of mantle-lithosphere coupling in an overall squishy lid regime requires variable but ongoing movement of lithosphere during the early phases of Earth evolution. Such a regime over this timeframe is based on evidence from numerical modeling, geochemical data for either reworking or recycling of lithosphere, and restricted paleomagnetic data, the latter limited to the Juvenile Earth phase. If lateral motion in a squishy-lid regime is valid, it must also be able to account for the spatially focused greenstone and TTG magmatic records of cratons that temporally extends over 100s of millions of years (Figure 11; e.g., Hickman, 2012; Kemp, 2018). The geochemical and isotopic signature of this magmatism indicates ongoing mantle input as well as crustal melting and reworking (e.g., Figure 13; Mulder et al., 2021). However, it is possible to define and justify a range of tectonic modes based on numerical models. Some of these are known to occur on other planets and planetary bodies (e.g., different types of stagnant lid behavior on the Moon and Venus and heat pipes on Io; Moore et al., 2017; R. J. Stern, 2018) and have thus been invoked for Earth's early history. However, given the large gaps in our record over this early history, the critical evaluation of, and discrimination between, such modes with respect to the available preserved record has yet to reach a consensus, and we suspect this is unlikely to be achieved anytime soon. Thus, can future researchers provide observations from the rock record that can deliver unique criteria to differentiate (or even test) stagnant versus squishy versus rigid lid tectonic models? Data and models presented to date from mesoscopic (outcrop) and regional scales produce similar features and rock associations (often based on the same set of observations) that are interpreted as justification for plate tectonic (rigid lid) and non-plate tectonic (including squishy lid) modes for the same regions.

A plate tectonic framework operating through the Proterozoic and Phanerozoic has achieved a greater consensus among researchers than the range of tectonic modes proposed for the pre-Proterozoic (but see R. J. Stern, 2018, for a discussion of alternative views). This reflects the presence of post-Archean rock associations that are both different from those in the Archean and generally similar to the contemporary Earth, as well as the greater volume of the preserved rock record allowing for a more detailed interrogation across a range of spatial and temporal scales, including global. This has enabled an increasing insight into the development and evolution of the Earth's surficial reservoirs and links to deep Earth processes through this time (Cawood & Hawkesworth, 2014; Lyons et al., 2021). However, better understanding the extent and scale of feedbacks between the solid and surficial Earth, and the potential for time lags between feedbacks (Cawood, 2020) are essential for a deeper understanding of the Earth system, and likely have implications that will enhance our understanding of the pre-Proterozoic Earth.

The use of terms developed for processes and rock associations on the Contemporary Earth and their application to the Earth during its early history are likely to remain an ongoing issue. The beauty of language is the power of words to evolve and adapt as our knowledge grows; for example, what we understand by craton and orogen (née geosyncline) continue to evolve. Thus, it is important to understand the context in which a word is used. What do terms such as subduction, plate tectonics, oceanic lithosphere and continental lithosphere mean when applied to the early Earth (e.g., Chelle-Michou et al., 2022)? On the Contemporary Earth, the concepts of subduction and

convergent plate margin were developed to explain the increasing depth of earthquake foci extending from linear oceanic trenches to depth beneath linear magmatic belts. Without this kinematic context, the terms are applied in the rock record on the basis of field criteria (i.e., magmatic belts) and increasingly geochemical criteria. What is important to note is that geochemical criteria are a proxy for a process (e.g., fluid flux melting), and as such may yield ambiguous results when applied to inferred tectonic modes? Furthermore, numerical models of lithospheric processes that operated during the early history of the Earth suggest that mechanisms of lithospheric recycling other than subduction may have been operative and if so, would likely also result in fluid flux melting in the mantle.

Compilation of large and often multi-proxy data sets (geochemical, isotopic, and geophysical) is playing an increasingly important role in understanding temporal and spatial changes into the age of rocks, timing of processes, the genesis of individual suites of rocks, and the character of the crust, lithosphere and mantle. New proxies may help identifying other aspect of rock genesis, and ever improving precision of existing methods will provide a higher resolution and with this a more profound picture of Earth's past. Ultimately, we as a community need to find practical ways to make use of large data sets with respect to data quality, technique comparison and ways to sensibly bin data. The combination of those aspects will undoubtedly result in a better understanding of system Earth.

Conflict of Interest

The authors declare no conflicts of interest relevant to this study.

Data Availability Statement

Data were not used, nor created for this research.

Acknowledgments
The authors acknowledge support from the Australian Research Council Grant FL160100168, and thank editor Valerio Acocella, and reviewers Taras Gerya, Tim Johnson, and Ming Tang for their constructive feedback. Our knowledge of the early history of the Earth has benefitted from discussions with Bruno Dhuime, Jeff Moyen, and Hugh Smithies and for modern continental crust with Di-Cheng Zhu. Open access publishing facilitated by Monash University, as part of the Wiley - Monash University agreement via the Council of Australian University Librarians.

References

Adam, Z. R., Skidmore, M. L., Mogk, D. W., & Butterfield, N. J. (2017). A Laurentian record of the earliest fossil eukaryotes. *Geology*, *45*(5), 387–390. https://doi.org/10.1130/g38749.1

Aharonson, O., Zuber, M. T., & Rothman, D. H. (2001). Statistics of Mars' topography from the Mars Orbiter Laser Altimeter: Slopes, correlations, and physical models. *Journal of Geophysical Research*, *106*(E10), 23723–23735. https://doi.org/10.1029/2000je001403

Aitchison, J. C., Ali, J. R., & Davis, A. M. (2007). When and where did India and Asia collide? *Journal of Geophysical Research*, *112*(B5), B05423. https://doi.org/10.1029/2006jb004706

Allègre, C. J., & Rousseau, D. (1984). The growth of the continent through geological time studied by Nd isotope analysis of shales. *Earth and Planetary Science Letters*, *67*(1), 19–34. https://doi.org/10.1016/0012-821x(84)90035-9

Amante, C., & Eakins, B. W. (2009). *ETOPO1 1 arc-minute global relief model: Procedures, data sources and analysis* (p. 25). National Ocean and Atmospheric Administration.

Armstrong, R. L. (1981). Radiogenic isotopes: The case for crustal recycling on a near-steady-state no-continental-growth Earth. *Philosophical Transactions of the Royal Society of London. Series A, Mathematical and Physical Sciences*, *301*, 443–472. https://doi.org/10.1098/rsta.1981.0122

Armstrong, R. L. (1991). The persistent myth of crustal growth. *Australian Journal of Earth Sciences*, *38*(5), 613–630. https://doi.org/10.1080/08120099108727995

Arndt, N., Bruzak, G., & Reischmann, T. (2001). The oldest continental and oceanic plateaus: Geochemistry of basalts and komatiites of the Pilbara Craton, Australia. *Special Papers – Geological Society of America*, *352*, 359–387.

Artemieva, I. M. (2006). Global 1° × 1° thermal model TC1 for the continental lithosphere: Implications for lithosphere secular evolution. *Tectonophysics*, *416*(1–4), 245–277. https://doi.org/10.1016/j.tecto.2005.11.022

Artemieva, I. M. (2009). The continental lithosphere: Reconciling thermal, seismic, and petrologic data. *Lithos*, *109*(1–2), 23–46. https://doi.org/10.1016/j.lithos.2008.09.015

Ashwal, L. D. (2010). The temporality of anorthosites. *The Canadian Mineralogist*, *48*(4), 711–728. https://doi.org/10.3749/canmin.48.4.711

Ashwal, L. D., & Bybee, G. M. (2017). Crustal evolution and the temporality of anorthosites. *Earth-Science Reviews*, *173*, 307–330. https://doi.org/10.1016/j.earscirev.2017.09.002

Balica, C., Ducea, M. N., Gehrels, G. E., Kirk, J., Roban, R. D., Luffi, P., et al. (2020). A zircon petrochronologic view on granitoids and continental evolution. *Earth and Planetary Science Letters*, *531*, 116005. https://doi.org/10.1016/j.epsl.2019.116005

Bally, A. W. (1989). Phanerozoic basins of North America. In A. W. Bally & A. R. Palmer (Eds.), *The geology of North America – An overview* (Vol. A, pp. 397–446). Geological Society of America.

Barley, M. E., & Groves, D. I. (1992). Supercontinent cycle and the distribution of metal deposits through time. *Geology*, *20*(4), 291–294. https://doi.org/10.1130/0091-7613(1992)020<0291:scatdo>2.3.co;2

Barnes, S. J., & Arndt, N. T. (2019). Distribution and geochemistry of komatiites and basalts through the Archean. In M. J. Van Kranendonk, V. C. Bennett, & E. Hoffman (Eds.), *Earth's oldest rocks* (pp. 103–132). Elsevier.

Barnes, S. J., Williams, M., Smithies, R. H., Hanski, E., & Lowrey, J. R. (2021). Trace element contents of mantle-derived magmas through time. *Journal of Petrology*, *62*(6), egab024. https://doi.org/10.1093/petrology/egab024

Barrell, J. (1914). The strength of the Earth's crust. *The Journal of Geology*, *22*(8), 729–741. https://doi.org/10.1086/622189

Bauer, A. M., Reimink, J. R., Chacko, T., Foley, B. J., Shirey, S. B., & Pearson, D. G. (2020). Hafnium isotopes in zircons document the gradual onset of mobile-lid tectonics. *Geochemical Perspectives Letters*, *14*, 1–6. https://doi.org/10.7185/geochemlet.2015

Baumgartner, R. J., Van Kranendonk, M. J., Fiorentini, M. L., Pagès, A., Wacey, D., Kong, C., et al. (2020). Formation of micro-spherulitic barite in association with organic matter within sulfidized stromatolites of the 3.48 billion-year-old Dresser Formation, Pilbara Craton. *Geobiology*, *18*(4), 415–425. https://doi.org/10.1111/gbi.12392

Beaumont, C. (1981). Foreland basins. *Geophysical Journal of the Royal Astronomical Society*, *65*(2), 291–329. https://doi.org/10.1111/j.1365-246x.1981.tb02715.x

Bédard, J. H. (2018). Stagnant lids and mantle overturns: Implications for Archaean tectonics, magmagenesis, crustal growth, mantle evolution, and the start of plate tectonics. *Geoscience Frontiers*, *9*(1), 19–49. https://doi.org/10.1016/j.gsf.2017.01.005

Bédard, J. H. (2020). From the LIPS of a serial killer: Endogenic retardation of biological evolution on unstable stagnant-lid planets. *Planetary and Space Science*, *192*, 105068. https://doi.org/10.1016/j.pss.2020.105068

Bekker, A., Slack, J. F., Planavsky, N., Krapež, B., Hofmann, A., Konhauser, K. O., & Rouxel, O. J. (2010). Iron formation: The sedimentary product of a complex interplay among mantle, tectonic, oceanic, and biospheric process. *Economic Geology*, *105*(3), 467–508. https://doi.org/10.2113/gsecongeo.105.3.467

Belousova, E. A., Kostitsyn, Y. A., Griffin, W. L., Begg, G. C., O'Reilly, S. Y., & Pearson, N. J. (2010). The growth of the continental crust: Constraints from zircon Hf-isotope data. *Lithos*, *119*(3–4), 457–466. https://doi.org/10.1016/j.lithos.2010.07.024

Benner, S. A., Bell, E. A., Biondi, E., Brasser, R., Carell, T., Kim, H.-J., et al. (2020). When did life likely emerge on Earth in an RNA-first process? *ChemSystemsChem*, *2*, e1900035. https://doi.org/10.1002/syst.202000009

Bennett, G., Dressler, B. O., & Robertson, J. A. (1991). The Huronian Supergroup. In *Geology of Ontario, special volume 4, part 1* (pp. 549–591). Ontario Geological Survey.

Betts, H. C., Puttick, M. N., Clark, J. W., Williams, T. A., Donoghue, P. C. J., & Pisani, D. (2018). Integrated genomic and fossil evidence illuminates life's early evolution and eukaryote origin. *Nature Ecology & Evolution*, *2*(10), 1556–1562. https://doi.org/10.1038/s41559-018-0644-x

Bhattacharjee, S., Mulder, J. A., Roy, S., Chowdhury, P., Cawood, P. A., & Nebel, O. (2021). Unravelling depositional setting, age and provenance of the Simlipal volcano-sedimentary complex, Singhbhum craton: Evidence for Hadean crust and Mesoarchean marginal marine sedimentation. *Precambrian Research*, *354*, 106038. https://doi.org/10.1016/j.precamres.2020.106038

Bhowmik, S. K., & Chakraborty, S. (2017). Sequential kinetic modelling: A new tool decodes pulsed tectonic patterns in early hot orogens of Earth. *Earth and Planetary Science Letters*, *460*, 171–179. https://doi.org/10.1016/j.epsl.2016.12.018

Bierlein, F. P., Groves, D. I., & Cawood, P. A. (2009). Metallogeny of accretionary orogens – The connection between lithospheric processes and metal endowment. *Ore Geology Reviews*, *36*(4), 282–292. https://doi.org/10.1016/j.oregeorev.2009.04.002

Biggin, A. J., Piispa, E. J., Pesonen, L. J., Holme, R., Paterson, G. A., Veikkolainen, T., & Tauxe, L. (2015). Palaeomagnetic field intensity variations suggest Mesoproterozoic inner-core nucleation. *Nature*, *526*(7572), 245–248. https://doi.org/10.1038/nature15523

Bindeman, I. N., Zakharov, D. O., Palandri, J., Greber, N. D., Dauphas, N., Retallack, G. J., et al. (2018). Rapid emergence of subaerial landmasses and onset of a modern hydrologic cycle 2.5 billion years ago. *Nature*, *557*(7706), 545–548. https://doi.org/10.1038/s41586-018-0131-1

Bingen, B., Nordgulen, Ø., & Viola, G. (2008). A four-phase model for the Sveconorwegian orogeny, SW Scandinavia. *Norwegian Journal of Geology*, *88*, 43–72.

Blackman, D. K., Karson, J. A., Kelley, D. S., Cann, J. R., Früh-Green, G. L., Gee, J. S., et al. (2002). Geology of the Atlantis Massif (Mid-Atlantic Ridge, 30°N): Implications for the evolution of an ultramafic oceanic core complex. *Marine Geophysical Researches*, *23*(5/6), 443–469. https://doi.org/10.1023/b:mari.0000018232.14085.75

Bleeker, W. (2003). The late Archean record: A puzzle in ca. 35 pieces. *Lithos*, *71*(2–4), 99–134. https://doi.org/10.1016/j.lithos.2003.07.003

Bleeker, W. (2004). Towards a 'natural' time scale for the Precambrian – A proposal. *Lethaia*, *37*(2), 219–222. https://doi.org/10.1080/00241160410006456

Bleeker, W., & Ernst, R. E. (2006). Short-lived mantle generated magmatic events and their dike swarms: The key unlocking Earth's paleogeographic record back to 2.6 Ga. In E. Hanski, S. Mertanen, T. Rämö, & J. Vuollo (Eds.), *Dike Swarms: Time markers of crustal evolution* (pp. 3–26). Taylor & Francis/Balkema.

Borisova, A. Y., Nédélec, A., Zagrtdenov, N. R., Toplis, M. J., Bohrson, W. A., Safonov, O. G., et al. (2022). Hadean zircon formed due to hydrated ultramafic protocrust melting. *Geology*, *50*(3), 300–304. https://doi.org/10.1130/g49354.1

Borisova, A. Y., Zagrtdenov, N. R., Toplis, M. J., Bohrson, W. A., Nédélec, A., Safonov, O. G., et al. (2021). Hydrated peridotite – Basaltic melt interaction Part I: Planetary felsic crust formation at shallow depth. *Frontiers of Earth Science*, *9*, 1–20. https://doi.org/10.3389/feart.2021.640464

Bose, S., Ghosh, G., Kawaguchi, K., Das, K., Mondal, A. K., & Banerjee, A. (2021). Zircon and monazite geochronology from the Rengali-Eastern Ghats Province: Implications for the tectonic evolution of the eastern Indian terrane. *Precambrian Research*, *355*, 106080. https://doi.org/10.1016/j.precamres.2020.106080

Bowring, S. A., & Williams, S. I. (1999). Priscoan (4.00–4.03 Ga) orthogneisses from northwestern Canada. *Contributions to Mineralogy and Petrology*, *134*(1), 3–16. https://doi.org/10.1007/s004100050465

Bradley, D. C. (2008). Passive margins through Earth history. *Earth-Science Reviews*, *91*(1–4), 1–26. https://doi.org/10.1016/j.earscirev.2008.08.001

Bradley, D. C. (2011). Secular trends in the geologic record and the supercontinent cycle. *Earth-Science Reviews*, *108*(1–2), 16–33. https://doi.org/10.1016/j.earscirev.2011.05.003

Brasier, M. D., & Lindsay, J. F. (1998). A billion years of environmental stability and the emergence of eukaryotes: New data from northern Australia. *Geology*, *26*(6), 555–558. https://doi.org/10.1130/0091-7613(1998)026<0555:abyoes>2.3.co;2

Brenner, A. R., Fu, R. R., Evans, D. A. D., Smirnov, A. V., Trubko, R., & Rose, I. R. (2020). Paleomagnetic evidence for modern-like plate motion velocities at 3.2 Ga. *Science Advances*, *6*(17), eaaz8670. https://doi.org/10.1126/sciadv.aaz8670

Brown, M., & Johnson, T. (2018). Secular change in metamorphism and the onset of global plate tectonics. *American Mineralogist*, *103*(2), 181–196. https://doi.org/10.2138/am-2018-6166

Brown, M., Johnson, T., & Gardiner, N. J. (2020). Plate tectonics and the Archean Earth. *Annual Review of Earth and Planetary Sciences*, *48*(1), 291–320. https://doi.org/10.1146/annurev-earth-081619-052705

Brown, M., Kirkland, C. L., & Johnson, T. E. (2020). Evolution of geodynamics since the Archean: Significant change at the dawn of the Phanerozoic. *Geology*, *48*(5), 488–492. https://doi.org/10.1130/g47417.1

Bucholz, C. E., & Spencer, C. J. (2019). Strongly peraluminous granites across the Archean–Proterozoic transition. *Journal of Petrology*, *60*(7), 1299–1348. https://doi.org/10.1093/petrology/egz033

Bucholz, C. E., Stolper, E. M., Eiler, J. M., & Breaks, F. W. (2018). A comparison of oxygen Fugacities of strongly peraluminous granites across the Archean–Proterozoic boundary. *Journal of Petrology*, *59*(11), 2123–2156. https://doi.org/10.1093/petrology/egy091

Buick, R., Thornett, J. R., McNaughton, N. J., Smith, J. B., Barley, M. E., & Savage, M. (1995). Record of emergent continental crust ~3.5 billion years ago in the Pilbara craton of Australia. *Nature*, *375*(6532), 574–577. https://doi.org/10.1038/375574a0

Bunge, H.-P., Richards, M. A., & Baumgardner, J. R. (1996). Effect of depth-dependent viscosity on the planform of mantle convection. *Nature*, *379*(6564), 436–438. https://doi.org/10.1038/379436a0

Burke, K., Steinberger, B., Torsvik, T. H., & Smethurst, M. A. (2008). Plume generation zones at the margins of large low shear velocity provinces on the core–mantle boundary. *Earth and Planetary Science Letters*, *265*(1–2), 49–60. https://doi.org/10.1016/j.epsl.2007.09.042

Burnham, A. D., & Berry, A. J. (2017). Formation of Hadean granites by melting of igneous crust. *Nature Geoscience*, *10*(6), 457–461. https://doi.org/10.1038/ngeo2942

Byerly, B. L., Lowe, D. R., Drabon, N., Coble, M. A., Burns, D. H., & Byerly, G. R. (2018). Hadean zircon from a 3.3 Ga sandstone, Barberton greenstone belt, South Africa. *Geology*, *46*(11), 967–970. https://doi.org/10.1130/g45276.1

Byerly, G. R., Lowe, D. R., & Heubeck, C. (2019a). Geologic evolution of the Barberton greenstone belt: A unique record of crustal development, surface processes, and early life 3.55 to 3.20 Ga. In M. J. Van Kranendonk, V. C. Bennett, & E. Hoffman (Eds.), *Earth's oldest rocks* (pp. 569–613). Elsevier.

Byerly, G. R., Lowe, D. R., & Heubeck, C. (2019b). Geologic evolution of the Narberton greenstone belt – A unique record of crustal development, surfaces processes and early life 3.55–3.20 Ga. In M. J. Van Kranendonk, V. C. Bennett, & E. Hoffman (Eds.), *Earth's oldest rocks* (pp. 569–613). Elsevier.

Camiré, G. E., & Burg, J. P. (1993). Late Archaean thrusting in the northwestern Pontiac Subprovince, Canadian shield. *Precambrian Research*, *61*(1–2), 51–66. https://doi.org/10.1016/0301-9268(93)90057-9

Campbell, I. H. (2003). Constraints on continental growth models from Nb/U ratios in the 3.5 Ga Barberton and other Archaean basalt-komatiite suites. *American Journal of Science*, *303*(4), 319–351. https://doi.org/10.2475/ajs.303.4.319

Campbell, I. H., & Allen, C. M. (2008). Formation of supercontinents linked to increases in atmospheric oxygen. *Nature Geoscience*, *1*(8), 554–558. https://doi.org/10.1038/ngeo259

Campbell, I. H., & Davies, D. R. (2017). Raising the continental crust. *Earth and Planetary Science Letters*, *460*, 112–122. https://doi.org/10.1016/j.epsl.2016.12.011

Campbell, I. H., & Squire, R. J. (2010). The mountains that triggered the Late Neoproterozoic increase in oxygen: The Second Great Oxidation Event. *Geochimica et Cosmochimica Acta*, *74*(15), 4187–4206. https://doi.org/10.1016/j.gca.2010.04.064

Capitanio, F. A., Nebel, O., & Cawood, P. A. (2020). Thermochemical lithosphere differentiation and the origin of cratonic mantle. *Nature*, *588*(7836), 89–94. https://doi.org/10.1038/s41586-020-2976-3

Capitanio, F. A., Nebel, O., Cawood, P. A., Weinberg, R. F., & Chowdhury, P. (2019). Reconciling thermal regimes and tectonics of the early Earth. *Geology*, *47*(10), 923–927. https://doi.org/10.1130/g46239.1

Capitanio, F. A., Nebel, O., Cawood, P. A., Weinberg, R. F., & Clos, F. (2019). Lithosphere differentiation in the early Earth controls Archean tectonics. *Earth and Planetary Science Letters*, *525*, 115755. https://doi.org/10.1016/j.epsl.2019.115755

Capitanio, F. A., Nebel, O., Moyen, J.-F., & Cawood, P. A. (2022). Craton Formation in early Earth mantle convection regimes. *Journal of Geophysical Research: Solid Earth*, *127*(4), e2021JB023911. https://doi.org/10.1029/2021jb023911

Carlson, R. W., Garçon, M., O'Neil, J., Reimink, J., & Rizo, H. (2019). The nature of Earth's first crust. *Chemical Geology*, *530*, 119321. https://doi.org/10.1016/j.chemgeo.2019.119321

Castro, A., Vogt, K., & Gerya, T. (2013). Generation of new continental crust by sublithospheric silicic-magma relamination in arcs: A test of Taylor's andesite model. *Gondwana Research*, *23*(4), 1554–1566. https://doi.org/10.1016/j.gr.2012.07.004

Catling, D. C., & Zahnle, K. J. (2020). The Archean atmosphere. *Science Advances*, *6*(9), eaax1420. https://doi.org/10.1126/sciadv.aax1420

Catuneanu, O. (2001). Flexural partitioning of the Late Archaean Witwatersrand foreland system, South Africa. *Sedimentary Geology*, *141–142*, 95–112. https://doi.org/10.1016/s0037-0738(01)00070-7

Catuneanu, O., & Eriksson, P. G. (1999). The sequence stratigraphic concept and the Precambrian rock record: An example from the 2.7–2.1 Ga Transvaal Supergroup, Kaapvaal craton. *Precambrian Research*, *97*(3–4), 215–251. https://doi.org/10.1016/s0301-9268(99)00033-9

Cavalazzi, B., Lemelle, L., Simionovici, A., Cady, S. L., Russell, M. J., Bailo, E., et al. (2021). Cellular remains in a ~3.42-billion-year-old subseafloor hydrothermal environment. *Science Advances*, *7*(29), eabf3963. https://doi.org/10.1126/sciadv.abf3963

Cavosie, A. J., Valley, J. W., & Wilde, S. A. (2019). The oldest terrestrial mineral record: Thirty years of research on Hadean zircons from Jack Hills, Western Australia. In M. J. Van Kranendonk, V. C. Bennett, & E. Hoffman (Eds.), *Earth's oldest rocks* (pp. 225–278). Elsevier.

Cawood, P. A. (2005). Terra Australis Orogen: Rodinia breakup and development of the Pacific and Iapetus margins of Gondwana during the Neoproterozoic and Paleozoic. *Earth-Science Reviews*, *69*(3–4), 249–279. https://doi.org/10.1016/j.earscirev.2004.09.001

Cawood, P. A. (2020). Earth Matters: A tempo to our planet's evolution. *Geology*, *48*(5), 525–526. https://doi.org/10.1130/focus052020.1

Cawood, P. A., & Buchan, C. (2007). Linking accretionary orogenesis with supercontinent assembly. *Earth-Science Reviews*, *82*(3–4), 217–256. https://doi.org/10.1016/j.earscirev.2007.03.003

Cawood, P. A., & Hawkesworth, C. J. (2014). Earth's middle age. *Geology*, *42*(6), 503–506. https://doi.org/10.1130/g35402.1

Cawood, P. A., & Hawkesworth, C. J. (2015). Temporal relations between mineral deposits and global tectonic cycles. In G. R. T. Jenkins, P. A. J. Lusty, I. McDonald, M. P. Smith, A. J. Boyce, & J. J. Wilkinson (Eds.), *Ore deposits in an evolving Earth* (Vol. 393, pp. 9–21). Geological Society, London, Special Publications.

Cawood, P. A., & Hawkesworth, C. J. (2019). Continental crustal volume, thickness and area, and their geodynamic implications. *Gondwana Research*, *66*, 116–125. https://doi.org/10.1016/j.gr.2018.11.001

Cawood, P. A., Hawkesworth, C. J., & Dhuime, B. (2012). Detrital zircon record and tectonic setting. *Geology*, *40*(10), 875–878. https://doi.org/10.1130/g32945.1

Cawood, P. A., Hawkesworth, C. J., & Dhuime, B. (2013). The continental record and the generation of continental crust. *Bulletin of the Geological Society of America*, *125*, 14–32. https://doi.org/10.1130/B30722.1

Cawood, P. A., Hawkesworth, C. J., Pisarevsky, S. A., Dhuime, B., Capitanio, F. A., & Nebel, O. (2018). Geological archive of the onset of plate tectonics. *Philosophical Transactions of the Royal Society A: Mathematical, Physical & Engineering Sciences*, *376*, 20170405.

Cawood, P. A., & Korsch, R. J. (2008). Assembling Australia: Proterozoic building of a continent. *Precambrian Research*, *166*(1–4), 1–35. https://doi.org/10.1016/j.precamres.2008.08.006

Cawood, P. A., Kröner, A., Collins, W. J., Kusky, T. M., Mooney, W. D., & Windley, B. F. (2009). Accretionary orogens through Earth history. *Geological Society Special Publication*, *318*, 1–36. https://doi.org/10.1144/SP318.1

Cawood, P. A., Kröner, A., & Pisarevsky, S. (2006). Precambrian plate tectonics: Criteria and evidence. *Geological Society of America Today*, *16*(7), 4–11. https://doi.org/10.1130/gsat01607.1

Cawood, P. A., Martin, E. L., Murphy, J. B., & Pisarevsky, S. A. (2021). Gondwana's interlinked peripheral orogens. *Earth and Planetary Science Letters*, *568*, 117057. https://doi.org/10.1016/j.epsl.2021.117057

Cawood, P. A., & Pisarevsky, S. A. (2017). Laurentia-Baltica-Amazonia relations during Rodinia assembly. *Precambrian Research*, *292*, 386–397. https://doi.org/10.1016/j.precamres.2017.01.031

Cawood, P. A., Strachan, R. A., Pisarevsky, S. A., Gladkochub, D. P., & Murphy, J. B. (2016). Linking collisional and accretionary orogens during Rodinia assembly and breakup: Implications for models of supercontinent cycles. *Earth and Planetary Science Letters*, *449*, 118–126. https://doi.org/10.1016/j.epsl.2016.05.049

Cawood, P. A., & Tyler, I. M. (2004). Assembling and reactivating the Proterozoic Capricorn Orogen: Lithotectonic elements, orogenies, and significance. *Precambrian Research*, *128*(3–4), 201–218. https://doi.org/10.1016/j.precamres.2003.09.001

Chardon, D., Gapais, D., & Cagnard, F. (2009). Flow of ultra-hot orogens: A view from the Precambrian, clues for the Phanerozoic. *Tectonophysics*, *477*(3–4), 105–118. https://doi.org/10.1016/j.tecto.2009.03.008

Chaudhuri, T., Wan, Y., Mazumder, R., Ma, M., & Liu, D. (2018). Evidence of enriched, Hadean mantle reservoir from 4.2–4.0 Ga zircon xenocrysts from Paleoarchean TTGs of the Singhbhum Craton, Eastern India. *Scientific Reports*, *8*(1), 7069. https://doi.org/10.1038/s41598-018-25494-6

Chelle-Michou, C., McCarthy, A., Moyen, J.-F., Cawood, P. A., & Capitanio, F. A. (2022). Make subductions diverse again. *Earth-Science Reviews*, *226*, 103966. https://doi.org/10.1016/j.earscirev.2022.103966

Chen, K., Rudnick, R. L., Wang, Z., Tang, M., Gaschnig, R. M., Zou, Z., et al. (2020). How mafic was the Archean upper continental crust? Insights from Cu and Ag in ancient glacial diamictites. *Geochimica et Cosmochimica Acta*, *278*, 16–29. https://doi.org/10.1016/j.gca.2019.08.002

Chen, X., Zhou, Y., & Shields, G. A. (2022). Progress towards an improved Precambrian seawater $^{87}Sr/^{86}Sr$ curve. *Earth-Science Reviews*, *224*, 103869. https://doi.org/10.1016/j.earscirev.2021.103869

Cheney, E. S. (1996). Sequence stratigraphy and plate tectonic significance of the Transvaal succession of southern Africa and its equivalent in Western Australia. *Precambrian Research*, *79*(1–2), 3–24. https://doi.org/10.1016/0301-9268(95)00085-2

Choukroune, P., Ludden, J. N., Chardon, D., Calvert, A. J., & Bouhallier, H. (1997). Archaean crustal growth and tectonic processes: A comparison of the Superior province, Canada and the Dharwar Craton, India. *Geological Society, London, Special Publications*, *121*, 63–98. https://doi.org/10.1144/GSL.SP.1997.121.01.04

Chowdhury, P., Chakraborty, S., & Gerya, T. V. (2021). Time will tell: Secular change in metamorphic timescales and the tectonic implications. *Gondwana Research*, *93*, 291–310. https://doi.org/10.1016/j.gr.2021.02.003

Chowdhury, P., Chakraborty, S., Gerya, T. V., Cawood, P. A., & Capitanio, F. A. (2020). Peel-back controlled lithospheric convergence explains the secular transitions in Archean metamorphism and magmatism. *Earth and Planetary Science Letters*, *538*, 116224. https://doi.org/10.1016/j.epsl.2020.116224

Chowdhury, P., Gerya, T., & Chakraborty, S. (2017). Emergence of silicic continents as the lower crust peels off on a hot plate-tectonic Earth. *Nature Geoscience*, *10*(9), 698–703. https://doi.org/10.1038/ngeo3010

Chowdhury, P., Mulder, J. A., Cawood, P. A., Bhattacharjee, S., Roy, S., Wainwright, A. N., et al. (2021). Magmatic thickening of crust in non–plate tectonic settings initiated the subaerial rise of Earth's first continents 3.3 to 3.2 billion years ago. *Proceedings of the National Academy of Sciences*, *118*(46), e2105746118. https://doi.org/10.1073/pnas.2105746118

Ciborowski, T. J. R., & Kerr, A. C. (2016). Did mantle plume magmatism help trigger the Great Oxidation Event? *Lithos*, *246–247*, 128–133. https://doi.org/10.1016/j.lithos.2015.12.017

Clark, C., Taylor, R. J. M., Kylander-Clark, A. R. C., & Hacker, B. R. (2018). Prolonged (>100 Ma) ultrahigh temperature metamorphism in the Napier Complex, East Antarctica: A petrochronological investigation of Earth's hottest crust. *Journal of Metamorphic Geology*, *36*(9), 1117–1139. https://doi.org/10.1111/jmg.12430

Clift, P. D., Vannucchi, P., & Morgan, J. P. (2009). Crustal redistribution, crust–mantle recycling and Phanerozoic evolution of the continental crust. *Earth-Science Reviews*, *97*(1–4), 80–104. https://doi.org/10.1016/j.earscirev.2009.10.003

Cloos, M. (1993). Lithospheric buoyancy and collisional orogenesis: Subduction of oceanic plateaus, continental margins, island arcs, spreading ridges, and seamounts. *The Geological Society of America Bulletin*, *105*(6), 715–737. https://doi.org/10.1130/0016-7606(1993)105<0715:lbacos>2.3.co;2

Cloud, P. (1972). A working model of the primitive Earth. *American Journal of Science*, *272*(6), 537–548. https://doi.org/10.2475/ajs.272.6.537

Cloud, P. (1987). Trends, transitions, and events in cryptozoic history and their calibration: Apropos recommendations by the subcommission on precambrian stratigraphy. *Precambrian Research*, *37*(3), 257–264. https://doi.org/10.1016/0301-9268(87)90070-2

Coleman, R. G. (1971). Plate tectonic emplacement of upper mantle peridotites along continental edges. *Journal of Geophysical Research*, *76*(5), 368–378. https://doi.org/10.1029/jb076i005p01212

Coleman, R. G. (1977). *Ophiolites. Ancient oceanic lithosphere?* (p. 229). Springer Verlag.

Collins, W. J., Van Kranendonk, M. J., & Teyssier, C. (1998). Partial convective overturn of Archaean crust in the east Pilbara Craton, Western Australia: Driving mechanisms and tectonic implications. *Journal of Structural Geology*, *20*(9–10), 1405–1424. https://doi.org/10.1016/s0191-8141(98)00073-x

Coltice, N., Bertrand, H., Rey, P., Jourdan, F., Phillips, B. R., & Ricard, Y. (2009). Global warming of the mantle beneath continents back to the Archaean. *Gondwana Research*, *15*(3–4), 254–266. https://doi.org/10.1016/j.gr.2008.10.001

Condie, K. C. (1998). Episodic continental growth and supercontinents: A mantle avalanche connection? *Earth and Planetary Science Letters*, *163*(1–4), 97–108. https://doi.org/10.1016/s0012-821x(98)00178-2

Condie, K. C., Arndt, N., Davaille, A., & Puetz, S. J. (2017). Zircon age peaks: Production or preservation of continental crust? *Geosphere*, *13*(2), 227–234. https://doi.org/10.1130/ges01361.1

Condie, K. C., & Aster, R. C. (2010). Episodic zircon age spectra of orogenic granitoids: The supercontinent connection and continental growth. *Precambrian Research*, *180*(3–4), 227–236. https://doi.org/10.1016/j.precamres.2010.03.008

Condie, K. C., Davaille, A., Aster, R. C., & Arndt, N. (2015). Upstairs-downstairs: Supercontinents and large igneous provinces, are they related? *International Geology Review*, *57*(11–12), 1341–1348. https://doi.org/10.1080/00206814.2014.963170

Connelly, J. N., Bollard, J., & Bizzarro, M. (2017). Pb–Pb chronometry and the early Solar System. *Geochimica et Cosmochimica Acta*, *201*, 345–363. https://doi.org/10.1016/j.gca.2016.10.044

Conrad, C. P., & Lithgow-Bertelloni, C. (2006). Influence of continental roots and asthenosphere on plate-mantle coupling. *Geophysical Research Letters*, *33*(5), L05312. https://doi.org/10.1029/2005gl025621

Cook, P. J., & McElhinny, M. W. (1979). A reevaluation of the spatial and temporal distribution of sedimentary phosphate deposits in the light of plate tectonics. *Economic Geology*, *74*(2), 315–330. https://doi.org/10.2113/gsecongeo.74.2.315

Cooper, C. M., & Conrad, C. P. (2009). Does the mantle control the maximum thickness of cratons? *Lithosphere*, *1*(2), 67–72. https://doi.org/10.1130/l40.1

Cooper, C. M., Miller, M. S., & Moresi, L. (2017). The structural evolution of the deep continental lithosphere. *Tectonophysics*, *695*, 100–121. https://doi.org/10.1016/j.tecto.2016.12.004

Cox, G. M., Lyons, T. W., Mitchell, R. N., Hasterok, D., & Gard, M. (2018). Linking the rise of atmospheric oxygen to growth in the continental phosphorus inventory. *Earth and Planetary Science Letters*, *489*, 28–36. https://doi.org/10.1016/j.epsl.2018.02.016
Criss, R. E., & Hofmeister, A. M. (2020). Chapter 10 – Thermal history of the terrestrial planets. In A. M. Hofmeister (Ed.), *Heat transport and energetics of the Earth and rocky planets* (pp. 267–297). Elsevier.
Czarnota, K., Champion, D. C., Goscombe, B., Blewett, R. S., Cassidy, K. F., Henson, P. A., & Groenewald, P. B. (2010). Geodynamics of the eastern Yilgarn Craton. *Precambrian Research*, *183*(2), 175–202. https://doi.org/10.1016/j.precamres.2010.08.004
Daly, M. C., Fuck, R. A., Julià, J., Macdonald, D. I. M., & Watts, A. B. (2018). Cratonic basin formation: A case study of the Parnaíba Basin of Brazil. *Geological Society, London, Special Publications*, *472*, 1–15. https://doi.org/10.1144/sp472.20
Daly, R. (1940). *Strength and structure of the Earth* (p. 434). Prentice-Hall.
Davey, S. C., Bleeker, W., Kamo, S. L., Vuollo, J., Ernst, R. E., & Cousens, B. L. (2020). Archean block rotation in Western Karelia: Resolving dyke swarm patterns in metacraton Karelia-Kola for a refined paleogeographic reconstruction of supercraton Superia. *Lithos*, *368–369*, 105553. https://doi.org/10.1016/j.lithos.2020.105553
Davidson, J. P., & Arculus, R. J. (2006). The significance of Phanerozoic arc magmatism in generating continental crust. In M. Brown & T. Rushmer (Eds.), *Evolution and differentiation of the continental crust* (pp. 135–172). Cambridge University Press.
Davies, G. F. (2009). Effect of plate bending on the Urey ratio and the thermal evolution of the mantle. *Earth and Planetary Science Letters*, *287*(3–4), 513–518. https://doi.org/10.1016/j.epsl.2009.08.038
De, S. (2021). Alluvial fan to shallow marine sedimentation record in the ~3.0 Ga Keonjhar Quartzite, Singhbhum Craton, India: An example of Phanerozoic style passive margin sedimentation from the Mesoarchean. *Precambrian Research*, *352*, 105962. https://doi.org/10.1016/j.precamres.2020.105962
DeCelles, P. G., Ducea, M. N., Kapp, P., & Zandt, G. (2009). Cyclicity in Cordilleran orogenic systems. *Nature Geoscience*, *2*(4), 251–257. https://doi.org/10.1038/ngeo469
DeCelles, P. G., & Giles, K. A. (1996). Foreland basin systems. *Basin Research*, *8*(2), 105–123. https://doi.org/10.1046/j.1365-2117.1996.01491.x
DeCelles, P. G., Zandt, G., Beck, S. L., Currie, C. A., Ducea, M. N., Kapp, P., et al. (2015). Cyclical orogenic processes in the Cenozoic central Andes. *Geological Society of America Memoir*, *212*, 459–490.
Dewey, J. F. (1982). Plate tectonics and the evolution of the British Isles. *Journal of the Geological Society of London*, *139*(4), 371–412. https://doi.org/10.1144/gsjgs.139.4.0371
Dewey, J. F. (2005). Orogeny can be very short. *Proceedings of the National Academy of Sciences of the United States of America*, *102*(43), 15286–15293. https://doi.org/10.1073/pnas.0505516102
Dewey, J. F., & Bird, J. M. (1970). Mountain belts and the new global tectonics. *Journal of Geophysical Research*, *75*(14), 2625–2647. https://doi.org/10.1029/jb075i014p02625
Dewey, J. F., Kiseeva, E. S., Pearce, J. A., & Robb, L. J. (2021). Precambrian tectonic evolution of Earth: An outline. *South African Journal of Geology*, *124*(1), 141–162. https://doi.org/10.25131/sajg.124.0019
Dey, A., Mukherjee, S., Sanyal, S., Ibanez-Mejia, M., & Sengupta, P. (2016). Deciphering sedimentary provenance and timing of sedimentation from a suite of metapelites from the Chotanagpur Granite Gneissic Complex, India: Implications for Proterozoic tectonics in the east-central part of the Indian shield. In *Sediment provenance: Influences on compositional change from source to sink* (pp. 453–486). Elsevier.
Dhuime, B., Hawkesworth, C. J., Cawood, P. A., & Storey, C. D. (2012). A change in the geodynamics of continental growth 3 billion years ago. *Science*, *335*(6074), 1334–1336. https://doi.org/10.1126/science.1216066
Dhuime, B., Hawkesworth, C. J., Delavault, H., & Cawood, P. A. (2017). Continental growth seen through the sedimentary record. *Sedimentary Geology*, *357*, 16–32. https://doi.org/10.1016/j.sedgeo.2017.06.001
Dhuime, B., Hawkesworth, C. J., Delavault, H., & Cawood, P. A. (2018). Rates of generation and destruction of the continental crust: Implications for continental growth. *Philosophical Transactions of the Royal Society A: Mathematical, Physical & Engineering Sciences*, *376*(2132), 376. https://doi.org/10.1098/rsta.2017.0403
Dhuime, B., Wuestefeld, A., & Hawkesworth, C. J. (2015). Emergence of modern continental crust about 3 billion years ago. *Nature Geoscience*, *8*(7), 552–555. https://doi.org/10.1038/ngeo2466
Domeier, M., Magni, V., Hounslow, M. W., & Torsvik, T. H. (2018). Episodic zircon age spectra mimic fluctuations in subduction. *Scientific Reports*, *8*(1), 17471. https://doi.org/10.1038/s41598-018-35040-z
Drabon, N., Byerly, B. L., Byerly, G. R., Wooden, J. L., Wiedenbeck, M., Valley, J. W., et al. (2022). Destabilization of Long-Lived Hadean protocrust and the onset of pervasive hydrous melting at 3.8 Ga. *AGU Advances*, *3*(2), e2021AV000520. https://doi.org/10.1029/2021av000520
Dunn, S. J., Nemchin, A. A., Cawood, P. A., & Pidgeon, R. T. (2005). Provenance record of the Jack Hills metasedimentary belt: Source of the Earth's oldest zircons. *Precambrian Research*, *138*(3–4), 235–254. https://doi.org/10.1016/j.precamres.2005.05.001
Eaton, D. W., Darbyshire, F., Evans, R. L., Grütter, H., Jones, A. G., & Yuan, X. (2009). The elusive lithosphere–asthenosphere boundary (LAB) beneath cratons. *Lithos*, *109*(1–2), 1–22. https://doi.org/10.1016/j.lithos.2008.05.009
Eguchi, J., Seales, J., & Dasgupta, R. (2020). Great Oxidation and Lomagundi events linked by deep cycling and enhanced degassing of carbon. *Nature Geoscience*, *13*(1), 71–76. https://doi.org/10.1038/s41561-019-0492-6
Elkins-Tanton, L. T. (2008). Linked magma ocean solidification and atmospheric growth for Earth and Mars. *Earth and Planetary Science Letters*, *271*(1–4), 181–191. https://doi.org/10.1016/j.epsl.2008.03.062
Elkins-Tanton, L. T. (2012). Magma oceans in the inner solar system. *Annual Review of Earth and Planetary Sciences*, *40*(1), 113–139. https://doi.org/10.1146/annurev-earth-042711-105503
Elming, S.-Å., Salminen, J., & Pesonen, L. J. (2021). Chapter 16 – Paleo-Mesoproterozoic Nuna supercycle. In L. J. Pesonen, J. Salminen, S.-Å. Elming, D. A. D. Evans, & T. Veikkolainen (Eds.), *Ancient supercontinents and the paleogeography of Earth* (pp. 499–548). Elsevier.
Eriksson, K. A., Krapez, B., & Fralick, P. W. (1994). Sedimentology of Archean greenstone belts: Signatures of tectonic evolution. *Earth-Science Reviews*, *37*(1–2), 1–88. https://doi.org/10.1016/0012-8252(94)90025-6
Eriksson, K. A., & Wilde, S. A. (2010). Palaeoenvironmental analysis of Archaean siliciclastic sedimentary rocks in the west-central Jack Hills belt, Western Australia with new constraints on ages and correlations. *Journal of the Geological Society*, *167*(4), 827–840. https://doi.org/10.1144/0016-76492008-127
Eriksson, P. G., Banerjee, S., Catuneanu, O., Corcoran, P. L., Eriksson, K. A., Hiatt, E. E., et al. (2013). Secular changes in sedimentation systems and sequence stratigraphy. *Gondwana Research*, *24*(2), 468–489. https://doi.org/10.1016/j.gr.2012.09.008
Eriksson, P. G., Rigby, M. J., Bandopadhyay, P. C., & Steenkamp, N. C. (2011). The Kaapvaal Craton, South Africa: No evidence for a supercontinental affinity prior to 2.0 Ga? *International Geology Review*, *53*(11–12), 1312–1330. https://doi.org/10.1080/00206814.2010.527638
Ernst, R. E. (2014a). *Large igneous provinces* (p. 653). Cambridge University Press.
Ernst, R. E. (2014b). *Large igneous provinces* (pp. 1–653). Cambridge University Press.

Ernst, R. E., & Bell, K. (2010). Large igneous provinces (LIPs) and carbonatites. *Mineralogy and Petrology*, *98*(1–4), 55–76. https://doi.org/10.1007/s00710-009-0074-1

Ernst, R. E., Bond, D. P. G., Zhang, S.-H., Buchan, K. L., Grasby, S. E., Youbi, N., et al. (2021). Large igneous province record through time and implications for secular environmental changes and geological time-scale boundaries. In R. E. Ernst, A. J. Dickson, & A. Bekker, (Eds.), Large Igneous Provinces, 1–26. https://doi.org/10.1002/9781119507444.ch1

Eskola, P. E. (1948). The problem of mantled gneiss domes. *Quarterly Journal of the Geological Society*, *104*(1–4), 461–476. https://doi.org/10.1144/gsl.jgs.1948.104.01-04.21

Evans, D. A. D. (2013). Reconstructing pre-Pangean supercontinents. *The Geological Society of America Bulletin*, *125*(11–12), 1735–1751. https://doi.org/10.1130/b30950.1

Fairbridge, R. W., & Finkl, C. W. (1980). Cratonic erosional unconformities and peneplains. *The Journal of Geology*, *88*(1), 69–86. https://doi.org/10.1086/628474

Farquhar, J., Wu, N., Canfield, D. E., & Oduro, H. (2010). Connections between sulfur cycle evolution, sulfur isotopes, sediments, and base metal sulfide deposits. *Economic Geology*, *105*(3), 509–533. https://doi.org/10.2113/gsecongeo.105.3.509

Fedo, C. M., Myers, J. S., & Appel, P. W. U. (2001). Depositional setting and paleogeographic implications of Earth's oldest supracrustal rocks, the >3.7 Ga Isua Greenstone belt, West Greenland. *Sedimentary Geology*, *141–142*, 61–77. https://doi.org/10.1016/s0037-0738(01)00068-9

Fischer, R., & Gerya, T. (2016). Regimes of subduction and lithospheric dynamics in the Precambrian: 3D thermomechanical modelling. *Gondwana Research*, *37*, 53–70. https://doi.org/10.1016/j.gr.2016.06.002

Flament, N., Coltice, N., & Rey, P. F. (2008). A case for late-Archaean continental emergence from thermal evolution models and hypsometry. *Earth and Planetary Science Letters*, *275*(3–4), 326–336. https://doi.org/10.1016/j.epsl.2008.08.029

Foley, B. J. (2018). The dependence of planetary tectonics on mantle thermal state: Applications to early Earth evolution. *Philosophical Transactions of the Royal Society A: Mathematical, Physical & Engineering Sciences*, *376*(2132), 20170409. https://doi.org/10.1098/rsta.2017.0409

Foley, S. F., Buhre, S., & Jacob, D. E. (2003). Evolution of the Archean crust by shallow subduction and recycling. *Nature*, *421*(6920), 249–252. https://doi.org/10.1038/nature01319

Forsyth, D., & Uyeda, S. (1975). On the relative importance of the driving forces of plate motion. *Geophysical Journal of the Royal Astronomical Society*, *43*(1), 163–200. https://doi.org/10.1111/j.1365-246x.1975.tb00631.x

Fralick, P., & Riding, R. (2015). Steep Rock Lake: Sedimentology and geochemistry of an Archean carbonate platform. *Earth-Science Reviews*, *151*, 132–175. https://doi.org/10.1016/j.earscirev.2015.10.006

Frimmel, H. E. (2018). Episodic concentration of gold to ore grade through Earth's history. *Earth-Science Reviews*, *180*, 148–158. https://doi.org/10.1016/j.earscirev.2018.03.011

Frimmel, H. E. (2019). The Witwatersrand basin and its gold deposits. In A. Kröner & A. Hofmann (Eds.), *The Archaean geology of the Kaapvaal Craton, Southern Africa* (pp. 255–275). Springer International Publishing.

Froude, D. O., Ireland, T. R., Kinny, P. D., Williams, I. S., Compston, W., Williams, I. R., & Myers, J. S. (1983). Ion microprobe identification of 4100—4200 Myr-old terrestrial zircons. *Nature*, *304*(5927), 616–618. https://doi.org/10.1038/304616a0

Furnes, H., & Dilek, Y. (2022). Archean versus Phanerozoic oceanic crust formation and tectonics: Ophiolites through time. *Geosystems and Geoenvironment*, *1*, 100004. https://doi.org/10.1016/j.geogeo.2021.09.004

Furumoto, A. S., Webb, J. P., Odegard, M. E., & Hussong, D. M. (1976). Seismic studies on the Ontong Java Plateau, 1970. *Tectonophysics*, *34*(1–2), 71–90. https://doi.org/10.1016/0040-1951(76)90177-3

Fyfe, W. S. (1978). The evolution of the Earth's crust: Modern plate tectonics to ancient hot spot tectonics? *Chemical Geology*, *23*(1–4), 89–114. https://doi.org/10.1016/0009-2541(78)90068-2

Ganne, J., & Feng, X. (2017). Primary magmas and mantle temperatures through time. *Geochemistry, Geophysics, Geosystems*, *18*(3), 872–888. https://doi.org/10.1002/2016gc006787

Gao, L., Liu, S., Cawood, P. A., Hu, F., Wang, J., Sun, G., & Hu, Y. (2022a). Oxidation of Archean upper mantle caused by crustal recycling. *Nature Communications*, *13*(1), 3283. https://doi.org/10.1038/s41467-022-30886-4

Gao, L., Liu, S. W., Cawood, P. A., Hu, F. Y., Wang, J. T., Sun, G. Z., & Hu, Y. L. (2022b). Oxidation of Archean upper mantle caused by crustal recycling. *Nature Communications*, *13*(1), 1–7. https://doi.org/10.1038/s41467-022-30886-4

Gao, S., Rudnick, R. L., Carlson, R. W., McDonough, W. F., & Liu, Y.-S. (2002). Re–Os evidence for replacement of ancient mantle lithosphere beneath the North China craton. *Earth and Planetary Science Letters*, *198*(3–4), 307–322. https://doi.org/10.1016/s0012-821x(02)00489-2

Gard, M., Hasterok, D., & Halpin, J. A. (2019). Global whole-rock geochemical database compilation. *Earth System Science Data*, *11*(4), 1553–1566. https://doi.org/10.5194/essd-11-1553-2019

Gardiner, N. J., Johnson, T. E., Kirkland, C. L., & Smithies, R. H. (2018). Melting controls on the lutetium–hafnium evolution of Archaean crust. *Precambrian Research*, *305*, 479–488. https://doi.org/10.1016/j.precamres.2017.12.026

Gardiner, N. J., Mulder, J. A., Kirkland, C. L., Johnson, T. E., & Nebel, O. (2021). Palaeoarchaean TTGs of the Pilbara and Kaapvaal cratons compared; an early Vaalbara supercraton evaluated. *South African Journal of Geology*, *124*(1), 37–52. https://doi.org/10.25131/sajg.124.0010

Gerya, T. (2022). Numerical modeling of subduction: State of the art and future direction. *Geosphere*, *18*(2), 503–561. https://doi.org/10.1130/ges02416.1

Gerya, T. V., Bercovici, D., & Becker, T. W. (2021). Dynamic slab segmentation due to brittle–ductile damage in the outer rise. *Nature*, *599*(7884), 245–250. https://doi.org/10.1038/s41586-021-03937-x

Gerya, T. V., Stern, R. J., Baes, M., Sobolev, S. V., & Whattam, S. A. (2015). Plate tectonics on the Earth triggered by plume-induced subduction initiation. *Nature*, *527*(7577), 221–225. https://doi.org/10.1038/nature15752

Gladkochub, D. P., Donskaya, T. V., Wingate, M. T. D., Mazukabzov, A. M., Pisarevsky, S. A., Sklyarov, E. V., & Stanevich, A. M. (2010). A one-billion-year gap in the Precambrian history of the southern Siberian Craton and the problem of the Transproterozoic supercontinent. *American Journal of Science*, *310*(9), 812–825. https://doi.org/10.2475/09.2010.03

Glebovitsky, V. A., Khil'tova, V. Y., & Kozakov, I. K. (2008). Tectonics of the Siberian Craton: Interpretation of geological, geophysical, geochronological, and isotopic geochemical data. *Geotectonics*, *42*(1), 8–20. https://doi.org/10.1134/s0016852108010020

Goldfarb, R. J., Groves, D. I., & Gardoll, S. (2001). Orogenic gold and geologic time: A global synthesis. *Ore Geology Reviews*, *18*(1–2), 1–75. https://doi.org/10.1016/s0169-1368(01)00016-6

Goodwin, A. M. (1996). *Principles of Precambrian geology* (p. 327). Academic Press.

Grad, M., Tiira, T., Behm, M., Belinsky, A. A., Booth, D. C., Brückl, E., et al. (2009). The Moho depth map of the European Plate. *Geophysical Journal International*, *176*(1), 279–292. https://doi.org/10.1111/j.1365-246x.2008.03919.x

Gradstein, F. M., Ogg, J. G., Schmitz, M. D., & Ogg, G. M. (2020). *Geologic time scale 2020* (p. 1357). Elsevier.

Granot, R. (2016). Palaeozoic oceanic crust preserved beneath the eastern Mediterranean. *Nature Geoscience*, *9*, 701–705. https://doi.org/10.1038/ngeo2784

Griffin, W. L., Belousova, E. A., O'Neill, C., O'Reilly, S. Y., Malkovets, V., Pearson, N. J., et al. (2014). The world turns over: Hadean–Archean crust–mantle evolution. *Lithos*, *189*, 2–15. https://doi.org/10.1016/j.lithos.2013.08.018

Griffin, W. L., O'Reilly, S. Y., Abe, N., Aulbach, S., Davies, R. M., Pearson, N. J., et al. (2003). The origin and evolution of Archean lithospheric mantle. *Precambrian Research*, *127*(1–3), 19–41. https://doi.org/10.1016/s0301-9268(03)00180-3

Griffin, W. L., O'Reilly, S. Y., Afonso, J. C., & Begg, G. C. (2009). The composition and evolution of lithospheric mantle: A re-evaluation and its tectonic implications. *Journal of Petrology*, *50*(7), 1185–1204. https://doi.org/10.1093/petrology/egn033

Grigné, C., Labrosse, S., & Tackley, P. J. (2005). Convective heat transfer as a function of wavelength: Implications for the cooling of the Earth. *Journal of Geophysical Research*, *110*(B3), B03409. https://doi.org/10.1029/2004jb003376

Grigné, C., Labrosse, S., & Tackley, P. J. (2007). Convection under a lid of finite conductivity in wide aspect ratio models: Effect of continents on the wavelength of mantle flow. *Journal of Geophysical Research*, *112*(B8), B08403. https://doi.org/10.1029/2006jb004297

Groves, D. I., & Santosh, M. (2020). Craton and thick lithosphere margins: The sites of giant mineral deposits and mineral provinces. *Gondwana Research*, *100*, 195–222. https://doi.org/10.1016/j.gr.2020.06.008

Groves, D. I., Vielreicher, R. M., Goldfarb, R. J., & Condie, K. C. (2005). Controls on the heterogeneous distribution of mineral deposits through time. In I. McDonald, A. J. Boyce, I. B. Butler, R. J. Herrington, & D. A. Polya (Eds.), *Mineral deposits and Earth evolution* (Vol. 248, pp. 71–101). Geological Society, London, Special Publications.

Guitreau, M., Boyet, M., Paquette, J. L., Gannoun, A., Konc, Z., Benbakkar, M., et al. (2019). Hadean protocrust reworking at the origin of the Archean Napier complex (Antarctica). *Geochemical Perspectives Letters*, *12*, 7–11. https://doi.org/10.7185/geochemlet.1927

Gumsley, A., Stamsnijder, J., Larsson, E., Söderlund, U., Naeraa, T., De Kock, M., et al. (2020). Neoarchean large igneous provinces on the Kaapvaal Craton in southern Africa re-define the formation of the Ventersdorp Supergroup and its temporal equivalents. *Bulletin of the Geological Society of America*, *132*(9–10), 1829–1844. https://doi.org/10.1130/b35237.1

Gunawardana, P., Morra, G., Chowdhury, P., & Cawood, P. (2020). Calibrating the yield strength of Archean lithosphere based on the volume of TTG crust. *Frontiers of Earth Science*, *8*, 548724. https://doi.org/10.3389/feart.2020.548724

Gurnis, M. (1988). Large-scale mantle convection and the aggregation and dispersal of supercontinents. *Nature*, *332*(6166), 695–699. https://doi.org/10.1038/332695a0

Hacker, B. R., Kelemen, P. B., & Behn, M. D. (2011). Differentiation of the continental crust by relamination. *Earth and Planetary Science Letters*, *307*(3–4), 501–516. https://doi.org/10.1016/j.epsl.2011.05.024

Hacker, B. R., Kelemen, P. B., & Behn, M. D. (2015). Continental lower crust. *Annual Review of Earth and Planetary Sciences*, *43*(1), 167–205. https://doi.org/10.1146/annurev-earth-050212-124117

Hale, L. D., & Thompson, G. A. (1982). The seismic reflection character of the continental Mohorovicic discontinuity. *Journal of Geophysical Research*, *87*(B6), 4625–4635. https://doi.org/10.1029/jb087ib06p04625

Halliday, A. N. (2000). Terrestrial accretion rates and the origin of the Moon. *Earth and Planetary Science Letters*, *176*(1), 17–30. https://doi.org/10.1016/s0012-821x(99)00317-9

Halpin, J. A., Jensen, T., McGoldrick, P., Meffre, S., Berry, R. F., Everard, J. L., et al. (2014). Authigenic monazite and detrital zircon dating from the Proterozoic Rocky Cape Group, Tasmania: Links to the Belt-Purcell Supergroup, North America. *Precambrian Research*, *250*, 50–67. https://doi.org/10.1016/j.precamres.2014.05.025

Hamblin, W. K., & Christiansen, E. H. (2004). *Earth's dynamic systems*. Prentice Hall, Pearson Education.

Hamilton, W. B. (2011). Plate tectonics began in Neoproterozoic time, and plumes from deep mantle have never operated. *Lithos*, *123*(1–4), 1–20. https://doi.org/10.1016/j.lithos.2010.12.007

Hao, J., Knoll, A. H., Huang, F., Hazen, R. M., & Daniel, I. (2020). Cycling phosphorus on the Archean Earth: Part I. Continental weathering and riverine transport of phosphorus. *Geochimica et Cosmochimica Acta*, *273*, 70–84. https://doi.org/10.1016/j.gca.2020.01.027

Harrison, T. M. (2020). *Hadean Earth* (p. 304). Springer.

Harrison, T. M., Bell, E. A., & Boehnke, P. (2017). Hadean zircon petrochronology. *Reviews in Mineralogy and Geochemistry*, *83*(1), 329–363. https://doi.org/10.2138/rmg.2017.83.11

Harrison, T. M., Blichert-Toft, J., Müller, W., Albarede, F., Holden, P., & Mojzsis, S. J. (2005). Heterogeneous Hadean hafnium: Evidence of continental crust at 4.4 to 4.5 Ga. *Science*, *310*(5756), 1947–1950. https://doi.org/10.1126/science.1117926

Harrison, T. M., Schmitt, A. K., McCulloch, M. T., & Lovera, O. M. (2008). Early (≥4.5 Ga) formation of terrestrial crust: Lu-Hf, $\delta^{18}O$, and Ti thermometry results for Hadean zircons. *Earth and Planetary Science Letters*, *268*(3–4), 476–486. https://doi.org/10.1016/j.epsl.2008.02.011

Hawkesworth, C., Cawood, P., & Dhuime, B. (2013). Continental growth and the crustal record. *Tectonophysics*, *609*, 651–660. https://doi.org/10.1016/j.tecto.2013.08.013

Hawkesworth, C., Cawood, P., Kemp, T., Storey, C., & Dhuime, B. (2009). Geochemistry: A matter of preservation. *Science*, *323*(5910), 49–50. https://doi.org/10.1126/science.1168549

Hawkesworth, C., Dhuime, B., Pietranik, A., Cawood, P., Kemp, T., & Storey, C. (2010). The generation and evolution of the continental crust. *Journal of the Geological Society*, *167*(2), 229–248. https://doi.org/10.1144/0016-76492009-072

Hawkesworth, C., & Jaupart, C. (2021). Heat flow constraints on the mafic character of Archean continental crust. *Earth and Planetary Science Letters*, *571*, 117091. https://doi.org/10.1016/j.epsl.2021.117091

Hawkesworth, C., & Kemp, T. (2021). A Pilbara perspective on the generation of Archaean continental crust. *Chemical Geology*, *578*, 120326. https://doi.org/10.1016/j.chemgeo.2021.120326

Hawkesworth, C. J., Cawood, P. A., & Dhuime, B. (2016). Tectonics and crustal evolution. *Geological Society of America Today*, *26*(09), 4–11. https://doi.org/10.1130/gsatg272a.1

Hawkesworth, C. J., Cawood, P. A., & Dhuime, B. (2020). The evolution of the continental crust and the onset of plate tectonics. *Frontiers of Earth Science*, *8*, 326. https://doi.org/10.3389/feart.2020.00326

Hawkesworth, C. J., Cawood, P. A., Dhuime, B., & Kemp, T. I. S. (2017). Earth's continental lithosphere through time. *Annual Review of Earth and Planetary Sciences*, *45*(1), 169–198. https://doi.org/10.1146/annurev-earth-063016-020525

Hawkesworth, C. J., & Kemp, A. I. S. (2006). Evolution of continental crust. *Nature*, *443*(7113), 811–817. https://doi.org/10.1038/nature05191

Hazen, R. M., Papineau, D., Bleeker, W., Downs, R. T., Ferry, J. M., McCoy, T. J., et al. (2008). Mineral evolution. *American Mineralogist*, *93*(11–12), 1693–1720. https://doi.org/10.2138/am.2008.2955

Hazen, R. M., Sverjensky, D. A., Azzolini, D., Bish, D. L., Elmore, S. C., Hinnov, L., & Milliken, R. E. (2013). Clay mineral evolution. *American Mineralogist*, *98*(11–12), 2007–2029. https://doi.org/10.2138/am.2013.4425

Heard, A. W., Aarons, S. M., Hofmann, A., He, X., Ireland, T., Bekker, A., et al. (2021). Anoxic continental surface weathering recorded by the 2.95 Ga Denny Dalton Paleosol (Pongola Supergroup, South Africa). *Geochimica et Cosmochimica Acta*, *295*, 1–23. https://doi.org/10.1016/j.gca.2020.12.005

Heilimo, E., Halla, J., & Hölttä, P. (2010). Discrimination and origin of the sanukitoid series: Geochemical constraints from the Neoarchean western Karelian Province (Finland). *Lithos*, *115*(1–4), 27–39. https://doi.org/10.1016/j.lithos.2009.11.001
Herzberg, C., Condie, K., & Korenaga, J. (2010). Thermal history of the Earth and its petrological expression. *Earth and Planetary Science Letters*, *292*(1–2), 79–88. https://doi.org/10.1016/j.epsl.2010.01.022
Herzberg, C., & Rudnick, R. (2012). Formation of cratonic lithosphere: An integrated thermal and petrological model. *Lithos*, *149*, 4–15. https://doi.org/10.1016/j.lithos.2012.01.010
Hickman, A. H. (2004). Two contrasting granite−greenstone terranes in the Pilbara Craton, Australia: Evidence for vertical and horizontal tectonic regimes prior to 2900 Ma. *Precambrian Research*, *131*(3–4), 153–172. https://doi.org/10.1016/j.precamres.2003.12.009
Hickman, A. H. (2012). Review of the Pilbara Craton and Fortescue Basin, Western Australia: Crustal evolution providing environments for early life. *Island Arc*, *21*, 1–31. https://doi.org/10.1111/j.1440-1738.2011.00783.x
Hickman, A. H. (2021). *East Pilbara Craton: A record of one billion years in the growth of Archean continental crust* (Report 143, p. 187). Geological Survey of Western Australia, Perth, Western Australia.
Hodgskiss, M. S. W., & Sperling, E. A. (2021). A prolonged, two-step oxygenation of Earth's early atmosphere: Support from confidence intervals. *Geology*, *50*(2), 158–162. https://doi.org/10.1130/G49385.1
Hoffman, P. F. (1988). United plates of America, the birth of a craton: Early Proterozoic assembly and growth of Laurentia. *Annual Review of Earth and Planetary Sciences*, *16*(1), 543–603. https://doi.org/10.1146/annurev.ea.16.050188.002551
Hoffman, P. F. (1989). Speculations on Laurentia's first gigayear (2.0 to 1.0 Ga). *Geology*, *17*(2), 135–138. https://doi.org/10.1130/0091-7613(1989)017<0135:solsfg>2.3.co;2
Hoffman, P. F. (1996). Tectonic genealogy of North America. In B. A. Van der Pluijm & S. Marshak (Eds.), *Earth structure: An introduction to structural geology and tectonics* (pp. 459–464). McGraw-Hill.
Hoffman, P. F., Kaufman, A. J., Halverson, G. P., & Schrag, D. P. (1998). A Neoproterozoic snowball Earth. *Science*, *281*(5381), 1342–1346. https://doi.org/10.1126/science.281.5381.1342
Hofmann, A., Dirks, P. H. G. M., & Jelsma, H. A. (2001). Late Archaean foreland basin deposits, Belingwe greenstone belt, Zimbabwe. *Sedimentary Geology*, *141–142*, 131–168. https://doi.org/10.1016/s0037-0738(01)00072-0
Hoggard, M. J., Czarnota, K., Richards, F. D., Huston, D. L., Jaques, A. L., & Ghelichkhan, S. (2020). Global distribution of sediment-hosted metals controlled by craton edge stability. *Nature Geoscience*, *13*(7), 504–510. https://doi.org/10.1038/s41561-020-0593-2
Holden, P., Lanc, P., Ireland, T. R., Harrison, T. M., Foster, J. J., & Bruce, Z. (2009). Mass-spectrometric mining of Hadean zircons by automated SHRIMP multi-collector and single-collector U/Pb zircon age dating: The first 100,000 grains. *International Journal of Mass Spectrometry*, *286*(2–3), 53–63. https://doi.org/10.1016/j.ijms.2009.06.007
Holder, R. M., Viete, D. R., Brown, M., & Johnson, T. E. (2019). Metamorphism and the evolution of plate tectonics. *Nature*, *572*(7769), 378–381. https://doi.org/10.1038/s41586-019-1462-2
Holland, H. D. (2002). Volcanic gases, black smokers, and the great oxidation event. *Geochimica et Cosmochimica Acta*, *66*(21), 3811–3826. https://doi.org/10.1016/s0016-7037(02)00950-x
Holland, H. D. (2006). The oxygenation of the atmosphere and oceans. *Philosophical Transactions of the Royal Society B: Biological Sciences*, *361*(1470), 903–915. https://doi.org/10.1098/rstb.2006.1838
Holmes, A. (1931). XVIII. Radioactivity and Earth movements. *Transactions of the Geological Society of Glasgow*, *18*(3), 559–606. https://doi.org/10.1144/transglas.18.3.559
Holmes, A. (1965). *Principles of physical geology* (pp. 1288). Nelson.
Hopkins, M., Harrison, T. M., & Manning, C. E. (2008). Low heat flow inferred from >4 Gyr zircons suggests Hadean plate boundary interactions. *Nature*, *456*(7221), 493–496. https://doi.org/10.1038/nature07465
Hopkins, M. D., Harrison, T. M., & Manning, C. E. (2010). Constraints on Hadean geodynamics from mineral inclusions in >4 Ga zircons. *Earth and Planetary Science Letters*, *298*(3–4), 367–376. https://doi.org/10.1016/j.epsl.2010.08.010
Hu, X., Garzanti, E., Wang, J., Huang, W., An, W., & Webb, A. (2016). The timing of India-Asia collision onset – Facts, theories, controversies. *Earth-Science Reviews*, *160*, 264–299. https://doi.org/10.1016/j.earscirev.2016.07.014
Huang, B., Johnson, T. E., Wilde, S. A., Polat, A., Fu, D., & Kusky, T. (2022). Coexisting divergent and convergent plate boundary assemblages indicate plate tectonics in the Neoarchean. *Nature Communications*, *13*(1), 6450. https://doi.org/10.1038/s41467-022-34214-8
Huang, B., Kusky, T. M., Johnson, T. E., Wilde, S. A., Wang, L., Polat, A., & Fu, D. (2020). Paired metamorphism in the Neoarchean: A record of accretionary-to-collisional orogenesis in the North China Craton. *Earth and Planetary Science Letters*, *543*, 116355. https://doi.org/10.1016/j.epsl.2020.116355
Huang, Y., Chubakov, V., Mantovani, F., Rudnick, R. L., & McDonough, W. F. (2013). A reference Earth model for the heat-producing elements and associated geoneutrino flux. *Geochemistry, Geophysics, Geosystems*, *14*(6), 2003–2029. https://doi.org/10.1002/ggge.20129
Huston, D. L., Eglington, B. M., Pehrsson, S., & Piercey, S. J. (2015). The metallogeny of zinc through time: Links to secular changes in the atmosphere, hydrosphere, and the supercontinent cycle. In S. M. Archibald & S. J. Piercey (Eds.), *Current perspectives on zinc deposits* (pp. 1–16). Irish Association for Economic Geology.
Huston, D. L., Pehrsson, S., Eglington, B. M., & Zaw, K. (2010). The geology and metallogeny of volcanic-hosted massive sulfide deposits: Variations through geologic time and with tectonic setting. *Economic Geology*, *105*(3), 571–591. https://doi.org/10.2113/gsecongeo.105.3.571
Hutton, J. (1788). Theory of the Earth; or an investigation of the laws observable in the composition, dissolution, and restoration of land upon the globe. *Transactions of the Royal Society of Edinburgh*, *1*(2), 209–304. https://doi.org/10.1017/s0080456800029227
Hynes, A., & Rivers, T. (2010). Protracted continental collision – Evidence from the Grenville Orogen. *Canadian Journal of Earth Sciences*, *47*(5), 591–620. https://doi.org/10.1139/e10-003
Jackson, J. A. (1997). *Glossary of geology: Alexander* (p. 769). American Geological Institute.
Jacobson, S. A., Morbidelli, A., Raymond, S. N., O'Brien, D. P., Walsh, K. J., & Rubie, D. C. (2014). Highly siderophile elements in Earth's mantle as a clock for the Moon-forming impact. *Nature*, *508*(7494), 84–87. https://doi.org/10.1038/nature13172
Jagoutz, O., & Behn, M. D. (2013). Foundering of lower island-arc crust as an explanation for the origin of the continental Moho. *Nature*, *504*(7478), 131–134. https://doi.org/10.1038/nature12758
Jahn, I., Clark, C., Reddy, S., & Taylor, R. J. M. (2021). Zircon U–Pb geochronology and Hf–O isotope characteristics of granitoids from the Capricorn Orogen, Western Australia. *Journal of Petrology*, *62*(11), egab083. https://doi.org/10.1093/petrology/egab083
Jaupart, C., Mareschal, J.-C., & Iarotsky, L. (2016). Radiogenic heat production in the continental crust. *Lithos*, *262*, 398–427. https://doi.org/10.1016/j.lithos.2016.07.017
Jellinek, A. M., Lenardic, A., & Pierrehumbert, R. T. (2020). Ice, fire, or fizzle: The climate footprint of Earth's supercontinental cycles. *Geochemistry, Geophysics, Geosystems*, *21*(2), e2019GC008464. https://doi.org/10.1029/2019gc008464

Johnson, T. E., Brown, M., Gardiner, N. J., Kirkland, C. L., & Smithies, R. H. (2017). Earth's first stable continents did not form by subduction. *Nature*, *543*(7644), 239–242. https://doi.org/10.1038/nature21383

Johnson, T. E., Brown, M., Kaus, B. J. P., & VanTongeren, J. A. (2014). Delamination and recycling of Archaean crust caused by gravitational instabilities. *Nature Geoscience*, *7*(1), 47–52. https://doi.org/10.1038/ngeo2019

Johnson, T. E., Gardiner, N. J., Miljković, K., Spencer, C. J., Kirkland, C. L., Bland, P. A., & Smithies, H. (2018). An impact melt origin for Earth's oldest known evolved rocks. *Nature Geoscience*, *11*(10), 795–799. https://doi.org/10.1038/s41561-018-0206-5

Johnson, T. E., Kirkland, C. L., Gardiner, N. J., Brown, M., Smithies, R. H., & Santosh, M. (2019). Secular change in TTG compositions: Implications for the evolution of Archaean geodynamics. *Earth and Planetary Science Letters*, *505*, 65–75. https://doi.org/10.1016/j.epsl.2018.10.022

Jones, S. A., Cassidy, K. F., & Davis, B. K. (2021). Unravelling the D1 event: Evidence for early granite-up, greenstone-down tectonics in the Eastern Goldfields, Western Australia. *Australian Journal of Earth Sciences*, *68*, 1–35. https://doi.org/10.1080/08120099.2020.1755364

Jordan, T. H. (1978). Composition and development of the continental tectosphere. *Nature*, *274*(5671), 544–548. https://doi.org/10.1038/274544a0

Jordan, T. H. (1988). Structure and formation of the continental tectosphere. *Journal of Petrology*, *Special_Volume*(1), 11–37. https://doi.org/10.1093/petrology/special_volume.1.11

Kamber, B. S. (2015). The evolving nature of terrestrial crust from the Hadean, through the Archaean, into the Proterozoic. *Precambrian Research*, *258*, 48–82. https://doi.org/10.1016/j.precamres.2014.12.007

Kamber, B. S., Whitehouse, M. J., Bolhar, R., & Moorbath, S. (2005). Volcanic resurfacing and the early terrestrial crust: Zircon U–Pb and REE constraints from the Isua Greenstone Belt, southern West Greenland. *Earth and Planetary Science Letters*, *240*(2), 276–290. https://doi.org/10.1016/j.epsl.2005.09.037

Karlstrom, K. E., Ahall, K.-I., Harlan, S. S., Williams, M. L., McLelland, J., & Geissman, J. W. (2001). Long-lived (1.8–1.0 Ga) convergent orogen in southern Laurentia, its extensions to Australia and Baltica, and implications for refining Rodinia. *Precambrian Research*, *111*(1–4), 5–30. https://doi.org/10.1016/s0301-9268(01)00154-1

Kay, M. (1944). Geosynclines in continental development. *Science*, *99*(2580), 461–462. https://doi.org/10.1126/science.99.2580.461

Kay, M. (1951). North American geosynclines. *Memoirs – Geological Society of America*, *48*, 1–132.

Keller, B., & Schoene, B. (2018). Plate tectonics and continental basaltic geochemistry throughout Earth history. *Earth and Planetary Science Letters*, *481*, 290–304. https://doi.org/10.1016/j.epsl.2017.10.031

Keller, C. B., & Schoene, B. (2012). Statistical geochemistry reveals disruption in secular lithospheric evolution about 2.5 Gyr ago. *Nature*, *485*(7399), 490–493. https://doi.org/10.1038/nature11024

Kemp, A. I. S. (2018). Early Earth geodynamics: Cross examining the geological testimony. *Philosophical Transactions of the Royal Society A: Mathematical, Physical & Engineering Sciences*, *376*(2132), 20180169. https://doi.org/10.1098/rsta.2018.0169

Kemp, A. I. S., Vervoort, J. D., Petersson, A., Hugh Smithies, R., & Lu, Y. (2023). A linked evolution for granite-greenstone terranes of the Pilbara Craton from Nd and Hf isotopes, with implications for Archean continental growth. *Earth and Planetary Science Letters*, *601*, 117895. https://doi.org/10.1016/j.epsl.2022.117895

Kemp, A. I. S., Wilde, S. A., Hawkesworth, C. J., Coath, C. D., Nemchin, A., Pidgeon, R. T., et al. (2010). Hadean crustal evolution revisited: New constraints from Pb–Hf isotope systematics of the Jack Hills zircons. *Earth and Planetary Science Letters*, *296*(1–2), 45–56. https://doi.org/10.1016/j.epsl.2010.04.043

Kerr, A. C. (2003). 3.16 – Oceanic plateaus. In H. D. Holland & K. K. Turekian (Eds.), *Treatise on geochemistry* (pp. 537–565). Pergamon.

Kirkland, C. L., Hartnady, M. I. H., Barham, M., Olierook, H. K. H., Steenfelt, A., & Hollis, J. A. (2021). Widespread reworking of Hadean-to-Eoarchean continents during Earth's thermal peak. *Nature Communications*, *12*(1), 331. https://doi.org/10.1038/s41467-020-20514-4

Knoll, A. H., & Nowak, M. A. (2017). The timetable of evolution. *Science Advances*, *3*(5), e1603076. https://doi.org/10.1126/sciadv.1603076

Kober, L. (1921). *Der Bau der Erde* (p. 324). Gebrüder Borntraeger.

Koppers, A. A. P., Becker, T. W., Jackson, M. G., Konrad, K., Müller, R. D., Romanowicz, B., et al. (2021). Mantle plumes and their role in Earth processes. *Nature Reviews Earth & Environment*, *2*(6), 382–401. https://doi.org/10.1038/s43017-021-00168-6

Korenaga, J. (2006). Archean geodynamics and the thermal evolution of Earth. In K. Benn, J.-C. Mareschal, & K. C. Condie (Eds.), *Archean geodynamics and environments*, *AGU Geophysical Monograph Series* (Vol. *164*, pp. 7–32).

Korenaga, J. (2013). Initiation and evolution of plate tectonics on Earth: Theories and observations. *Annual Review of Earth and Planetary Sciences*, *41*(1), 117–151. https://doi.org/10.1146/annurev-earth-050212-124208

Korenaga, J. (2018a). Crustal evolution and mantle dynamics through Earth history. *Philosophical Transactions of the Royal Society A: Mathematical, Physical & Engineering Sciences*, *376*(2132), 20170408. https://doi.org/10.1098/rsta.2017.0408

Korenaga, J. (2018b). Estimating the formation age distribution of continental crust by unmixing zircon ages. *Earth and Planetary Science Letters*, *482*, 388–395. https://doi.org/10.1016/j.epsl.2017.11.039

Korja, A., Lahtinen, R., & Nironen, M. (2006). The Svecofennian orogen: A collage of microcontinents and island arcs. *Geological Society Memoir*, *32*(1), 561–578. https://doi.org/10.1144/gsl.mem.2006.032.01.34

Kostrovitsky, S. I., Skuzovatov, S. Y., Yakovlev, D. A., Sun, J., Nasdala, L., & Wu, F.-Y. (2016). Age of the Siberian craton crust beneath the northern kimberlite fields: Insights to the craton evolution. *Gondwana Research*, *39*, 365–385. https://doi.org/10.1016/j.gr.2016.01.008

Kramers, J. D. (2007). Hierarchical Earth accretion and the Hadean eon. *Journal of the Geological Society*, *164*(1), 3–17. https://doi.org/10.1144/0016-76492006-028

Kreemer, C., Blewitt, G., & Klein, E. C. (2014). A geodetic plate motion and global strain rate model. *Geochemistry, Geophysics, Geosystems*, *15*(10), 3849–3889. https://doi.org/10.1002/2014gc005407

Kröner, A., & Hofmann, A. (2019). *The Archaean geology of the Kaapvaal Craton, Southern Africa* (p. 312). Springer.

Kump, L. R., & Barley, M. E. (2007). Increased subaerial volcanism and the rise of atmospheric oxygen 2.5 billion years ago. *Nature*, *448*(7157), 1033–1036. https://doi.org/10.1038/nature06058

Kusky, T. M., & Li, J. (2010). Origin and emplacement of Archean ophiolites of the central orogenic belt, North China craton. *Journal of Earth Sciences*, *21*(5), 744–781. https://doi.org/10.1007/s12583-010-0119-8

Laurent, O., Martin, H., Moyen, J. F., & Doucelance, R. (2014). The diversity and evolution of late-Archean granitoids: Evidence for the onset of "modern-style" plate tectonics between 3.0 and 2.5 Ga. *Lithos*, *205*, 208–235. https://doi.org/10.1016/j.lithos.2014.06.012

Laurent, O., Moyen, J.-F., Wotzlaw, J.-F., Björnsen, J., & Bachmann, O. (2022). Early Earth zircons formed in residual granitic melts produced by tonalite differentiation. *Geology*, *50*(4), 437–441. https://doi.org/10.1130/G49232.1

Laurent, O., Zeh, A., Brandl, G., Vezinet, A., & Wilson, A. (2019). Granitoids and greenstone belts of the Pietersburg block—Witnesses of an Archaean accretionary orogen along the northern edge of the Kaapvaal craton. In A. Kröner & A. Hofmann (Eds.), *The Archaean geology of the Kaapvaal Craton, Southern Africa* (pp. 83–107). Springer International Publishing.

Lee, C.-T. A., Luffi, P., & Chin, E. J. (2011). Building and destroying continental mantle. *Annual Review of Earth and Planetary Sciences*, *39*(1), 59–90. https://doi.org/10.1146/annurev-earth-040610-133505

Lenardic, A. (1998). On the partitioning of mantle heat loss below oceans and continents over time and its relationship to the Archaean paradox. *Geophysical Journal International*, *134*(3), 706–720. https://doi.org/10.1046/j.1365-246x.1998.00604.x
Lenardic, A. (2018). The diversity of tectonic modes and thoughts about transitions between them. *Philosophical Transactions of the Royal Society A: Mathematical, Physical & Engineering Sciences*, *376*(2132), 376. https://doi.org/10.1098/rsta.2017.0416
Lenardic, A., Moresi, L., Jellinek, A. M., O'Neill, C. J., Cooper, C. M., & Lee, C. T. (2011). Continents, supercontinents, mantle thermal mixing, and mantle thermal isolation: Theory, numerical simulations, and laboratory experiments. *Geochemistry, Geophysics, Geosystems*, *12*(10), Q10016. https://doi.org/10.1029/2011gc003663
Lenardic, A., Moresi, L. N., Jellinek, A. M., & Manga, M. (2005). Continental insulation, mantle cooling, and the surface area of oceans and continents. *Earth and Planetary Science Letters*, *234*(3–4), 317–333. https://doi.org/10.1016/j.epsl.2005.01.038
Li, Z.-X., Li, X.-H., Wartho, J.-A., Clark, C., Li, W.-X., Zhang, C.-L., & Bao, C. (2010). Magmatic and metamorphic events during the early Paleozoic Wuyi-Yunkai orogeny, southeastern South China: New age constraints and pressure-temperature conditions. *The Geological Society of America Bulletin*, *122*(5–6), 772–793. https://doi.org/10.1130/b30021.1
Liu, C., Knoll, A. H., & Hazen, R. M. (2017). Geochemical and mineralogical evidence that Rodinian assembly was unique. *Nature Communications*, *8*(1), 1950. https://doi.org/10.1038/s41467-017-02095-x
Liu, C., Runyon, S. E., Knoll, A. H., & Hazen, R. M. (2019). The same and not the same: Ore geology, mineralogy and geochemistry of Rodinia assembly versus other supercontinents. *Earth-Science Reviews*, *196*, 102860. https://doi.org/10.1016/j.earscirev.2019.05.004
Liu, C. T., & He, Y. S. (2021). Rise of major subaerial landmasses about 3.0 to 2.7 billion years ago. *Geochemical Perspectives Letters*, *18*, 1–5. https://doi.org/10.7185/geochemlet.2115
Liu, J., Pearson, D. G., Wang, L. H., Mather, K. A., Kjarsgaard, B. A., Schaeffer, A. J., et al. (2021). Plume-driven recratonization of deep continental lithospheric mantle. *Nature*, *592*(7856), 732–736. https://doi.org/10.1038/s41586-021-03395-5
Lourenço, D. L., Rozel, A. B., Ballmer, M. D., & Tackley, P. J. (2020). Plutonic-squishy lid: A new global tectonic Regime generated by intrusive magmatism on Earth-like planets. *Geochemistry, Geophysics, Geosystems*, *21*(4), e2019GC008756. https://doi.org/10.1029/2019gc008756
Luskin, C., Wilson, A., Gold, D., & Hofmann, A. (2019). The Pongola Supergroup: Mesoarchaean deposition following Kaapvaal craton stabilization. In A. Kröner & A. Hofmann (Eds.), *The Archaean geology of the Kaapvaal Craton, Southern Africa* (pp. 225–254). Springer International Publishing.
Lyons, T. W., Diamond, C. W., Planavsky, N. J., Reinhard, C. T., & Li, C. (2021). Oxygenation, life, and the planetary system during Earth's middle history: An overview. *Astrobiology*, *21*(8), 906–923. https://doi.org/10.1089/ast.2020.2418
Lyons, T. W., Reinhard, C. T., & Planavsky, N. J. (2014). The rise of oxygen in Earth's early ocean and atmosphere. *Nature*, *506*(7488), 307–315. https://doi.org/10.1038/nature13068
MacGregor, A. M. (1951). Some milestones in the Precambrian of Southern Rhodesia. *Proceedings of the Geological Society of South Africa*, *54*, 27–71.
MacLeod, C. J., Searle, R. C., Murton, B. J., Casey, J. F., Mallows, C., Unsworth, S. C., et al. (2009). Life cycle of oceanic core complexes. *Earth and Planetary Science Letters*, *287*(3–4), 333–344. https://doi.org/10.1016/j.epsl.2009.08.016
Magni, V., Faccenna, C., van Hunen, J., & Funiciello, F. (2013). Delamination vs. break-off: The fate of continental collision. *Geophysical Research Letters*, *40*(2), 285–289. https://doi.org/10.1002/grl.50090
Marimon, R. S., Hawkesworth, C. J., Trouw, R. A. J., Trouw, C., Dantas, E. L., Ribeiro, A., et al. (2022). Subduction and continental collision in the Neoproterozoic: Sanukitoid-like magmatism and paired metamorphism in SE Brazil. *Precambrian Research*, *383*, 106888. https://doi.org/10.1016/j.precamres.2022.106888
Marschall, H. R., & Schumacher, J. C. (2012). Arc magmas sourced from mélange diapirs in subduction zones. *Nature Geoscience*, *5*(12), 862–867. https://doi.org/10.1038/ngeo1634
Martin, H., & Moyen, J.-F. (2002). Secular changes in tonalite-trondhjemite-granodiorite composition as markers of the progressive cooling of Earth. *Geology*, *30*(4), 319–322. https://doi.org/10.1130/0091-7613(2002)030<0319:scittg>2.0.co;2
Marty, B., Bekaert, D. V., Broadley, M. W., & Jaupart, C. (2019). Geochemical evidence for high volatile fluxes from the mantle at the end of the Archaean. *Nature*, *575*(7783), 485–488. https://doi.org/10.1038/s41586-019-1745-7
Maynard, J. B. (2010). The chemistry of manganese ores through time: A signal of increasing diversity of Earth-surface environments. *Economic Geology*, *105*(3), 535–552. https://doi.org/10.2113/gsecongeo.105.3.535
Mazumder, R., & Chaudhuri, T. (2021). Paleoarchean terrestrial to shallow marine sedimentation on Singhbhum Craton, eastern India (the Western Iron Ore Group). *Precambrian Research*, *354*, 106071. https://doi.org/10.1016/j.precamres.2020.106071
McCoy-West, A. J., Chowdhury, P., Burton, K. W., Sossi, P., Nowell, G. M., Fitton, J. G., et al. (2019). Extensive crustal extraction in Earth's early history inferred from molybdenum isotopes. *Nature Geoscience*, *12*(11), 946–951. https://doi.org/10.1038/s41561-019-0451-2
McKenzie, D., & Priestley, K. (2008). The influence of lithospheric thickness variations on continental evolution. *Lithos*, *102*(1–2), 1–11. https://doi.org/10.1016/j.lithos.2007.05.005
McKenzie, D., & Priestley, K. (2016). Speculations on the formation of cratons and cratonic basins. *Earth and Planetary Science Letters*, *435*, 94–104. https://doi.org/10.1016/j.epsl.2015.12.010
McKenzie, N. R., Smye, A. J., Hegde, V. S., & Stockli, D. F. (2018). Continental growth histories revealed by detrital zircon trace elements: A case study from India. *Geology*, *46*(3), 275–278. https://doi.org/10.1130/g39973.1
McLaren, S., Sandiford, M., Hand, M., Neumann, N., Wyborn, L., & Bastrakova, I. (2003). The hot southern continent: Heat flow and heat production in Australian Proterozoic terranes. In R. R. Hillis & R. D. Müller (Eds.), *Evolution and dynamics of the Australian plate*, *Geological Society of Australia Special Publication 22 and Geological Society of America Special Paper 372* (pp. 157–167).
Meert, J. G., & Pandit, M. K. (2015). Chapter 3 the Archaean and Proterozoic history of Peninsular India: Tectonic framework for Precambrian sedimentary basins in India. *Geological Society, London, Memoirs*, *43*(1), 29–54. https://doi.org/10.1144/m43.3
Meixnerová, J., Blum, J. D., Johnson, M. W., Stüeken, E. E., Kipp, M. A., Anbar, A. D., & Buick, R. (2021). Mercury abundance and isotopic composition indicate subaerial volcanism prior to the end-Archean "whiff" of oxygen. *Proceedings of the National Academy of Sciences*, *118*(33), e2107511118. https://doi.org/10.1073/pnas.2107511118
Mengel, K., & Kern, H. (1992). Evolution of the petrological and seismic Moho-implications for the continental crust-mantle boundary. *Terra Nova*, *4*(1), 109–116. https://doi.org/10.1111/j.1365-3121.1992.tb00455.x
Miller, S. R., Mueller, P. A., Meert, J. G., Kamenov, G. D., Pivarunas, A. F., Sinha, A. K., & Pandit, M. K. (2018). Detrital zircons reveal evidence of Hadean crust in the Singhbhum Craton, India. *The Journal of Geology*, *126*(5), 541–552. https://doi.org/10.1086/698844
Mitchell, R. N., Zhang, N., Salminen, J., Liu, Y., Spencer, C. J., Steinberger, B., et al. (2021). The supercontinent cycle. *Nature Reviews Earth & Environment*, *2*(5), 358–374. https://doi.org/10.1038/s43017-021-00160-0
Mohorovičić, A. (1910). Potres od 8. X 1909. *Godisnje izvjesće Zagrebačkog meteoroloskog opservatorija za godinu*, *9*, 1–56.

Mole, D. R., Fiorentini, M. L., Cassidy, K. F., Kirkland, C. L., Thebaud, N., McCuaig, T. C., et al. (2014). Crustal evolution, intra-cratonic architecture and the metallogeny of an Archaean craton. *Geological Society – Special Publications*, *393*(1), 23–80. https://doi.org/10.1144/sp393.8

Mooney, W. D. (2003). Continental crust. In R. A. Meyers (Ed.), *Encyclopedia of physical science and technology* (3rd ed., pp. 635–647). Academic Press.

Mooney, W. D., & Brocher, T. M. (1987). Coincident seismic reflection/refraction studies of the continental lithosphere; a global review. *Reviews of Geophysics*, *25*(4), 723–742. https://doi.org/10.1029/rg025i004p00723

Moore, W. B., Simon, J. I., & Webb, A. A. G. (2017). Heat-pipe planets. *Earth and Planetary Science Letters*, *474*, 13–19. https://doi.org/10.1016/j.epsl.2017.06.015

Moores, E. M. (2002). Pre–1 Ga (pre-Rodinian) ophiolites: Their tectonic and environmental implications. *The Geological Society of America Bulletin*, *114*(1), 80–95. https://doi.org/10.1130/0016-7606(2002)114<0080:pgprot>2.0.co;2

Moresi, L., & Solomatov, V. (1998). Mantle convection with a brittle lithosphere: Thoughts on the global tectonic styles of the Earth and Venus. *Geophysical Journal International*, *133*(3), 669–682. https://doi.org/10.1046/j.1365-246x.1998.00521.x

Morrissey, L. J., Barovich, K. M., Hand, M., Howard, K. E., & Payne, J. L. (2019). Magmatism and metamorphism at ca. 1.45 Ga in the northern Gawler Craton: The Australian record of rifting within Nuna (Columbia). *Geoscience Frontiers*, *10*(1), 175–194. https://doi.org/10.1016/j.gsf.2018.07.006

Moyen, J. F. (2011). The composite Archaean grey gneisses: Petrological significance, and evidence for a non-unique tectonic setting for Archaean crustal growth. *Lithos*, *123*(1–4), 21–36. https://doi.org/10.1016/j.lithos.2010.09.015

Moyen, J.-F., & Laurent, O. (2018). Archaean tectonic systems: A view from igneous rocks. *Lithos*, *302–303*, 99–125. https://doi.org/10.1016/j.lithos.2017.11.038

Moyen, J.-F., & Martin, H. (2012). Forty years of TTG research. *Lithos*, *148*, 312–336. https://doi.org/10.1016/j.lithos.2012.06.010

Moyen, J.-F., & van Hunen, J. (2012). Short-term episodicity of Archaean plate tectonics. *Geology*, *40*(5), 451–454. https://doi.org/10.1130/g322894.1

Mueller, W. U., Corcoran, P. L., & Pickett, C. (2005). Mesoarchean continental breakup: Evolution and inferences from the >2.8 Ga Slave craton-cover succession, Canada. *The Journal of Geology*, *113*(1), 23–45. https://doi.org/10.1086/425967

Mukhopadhyay, J., Crowley, Q. G., Ghosh, S., Ghosh, G., Chakrabarti, K., Misra, B., et al. (2014). Oxygenation of the Archean atmosphere: New paleosol constraints from eastern India. *Geology*, *42*(10), 923–926. https://doi.org/10.1130/g36091.1

Mulder, J. A., & Cawood, P. A. (2022). Evaluating preservation bias in the continental growth record against the monazite archive. *Geology*, *50*(2), 243–247. https://doi.org/10.1130/G49416.1

Mulder, J. A., Halpin, J. A., & Daczko, N. R. (2015). Mesoproterozoic Tasmania: Witness to the East Antarctica–Laurentia connection within Nuna. *Geology*, *43*(9), 759–762. https://doi.org/10.1130/g36850.1

Mulder, J. A., Nebel, O., Gardiner, N. J., Cawood, P. A., Wainwright, A. N., & Ivanic, T. J. (2021). Crustal rejuvenation stabilised Earth's first cratons. *Nature Communications*, *12*(1), 3535. https://doi.org/10.1038/s41467-021-23805-6

Murphy, J. B., & Nance, R. D. (1991). Supercontinent model for the contrasting character of Late Proterozoic orogenic belts. *Geology*, *19*(5), 469–472. https://doi.org/10.1130/0091-7613(1991)019<0469:smftcc>2.3.co;2

Murphy, J. B., Nance, R. D., Cawood, P. A., Collins, W. J., Dan, W., Doucet, L. S., et al. (2020). Pannotia: In defence of its existence and geodynamic significance. *Geological Society, London, Special Publications*, *503*(1), SP503-2020-96. https://doi.org/10.1144/sp503-2020-96

Naeraa, T., Schersten, A., Rosing, M. T., Kemp, A. I. S., Hoffmann, J. E., Kokfelt, T. F., & Whitehouse, M. J. (2012). Hafnium isotope evidence for a transition in the dynamics of continental growth 3.2 Gyr ago. *Nature*, *485*(7400), 627+–630. https://doi.org/10.1038/nature11140

National Academies of Sciences, Engineering, and Medicine. (2020). *A vision for NSF Earth Sciences 2020–2030: Earth in time* (p. 157). The National Academies Press.

Nebel, O., Capitanio, F. A., Moyen, J. F., Weinberg, R. F., Clos, F., Nebel-Jacobsen, Y. J., & Cawood, P. A. (2018). When crust comes of age: On the chemical evolution of Archaean, felsic continental crust by crustal drip tectonics. *Philosophical Transactions of the Royal Society A: Mathematical, Physical and Engineering Sciences*, *376*(2132), 20180103. https://doi.org/10.1098/rsta.2018.0103

Nebel, O., Rapp, R. P., & Yaxley, G. M. (2014). The role of detrital zircons in Hadean crustal research. *Lithos*, *190–191*, 313–327. https://doi.org/10.1016/j.lithos.2013.12.010

Nemchin, A. A., & Pidgeon, R. T. (1998). Precise conventional and SHRIMP baddeleyite U-Pb age for the Binneringie Dyke, near Narrogin, Western Australia. *Australian Journal of Earth Sciences*, *45*(5), 673–675. https://doi.org/10.1080/08120099808728424

Nisbet, E. G., Cheadle, M. J., Arndt, N. T., & Bickle, M. J. (1993). Constraining the potential temperature of the Archaean mantle: A review of the evidence from komatiites. *Lithos*, *30*(3–4), 291–307. https://doi.org/10.1016/0024-4937(93)90042-b

Norman, M. D. (2019). Origin of the Earth and the late heavy bombarbment. In M. J. Van Kranendonk, V. C. Bennett, & E. Hoffman (Eds.), *Earth's oldest rocks* (pp. 27–47). Elsevier.

Nutman, A. P., Bennett, V. C., Friend, C. R. L., Van Kranendonk, M. J., Rothacker, L., & Chivas, A. R. (2019). Cross-examining Earth's oldest stromatolites: Seeing through the effects of heterogeneous deformation, metamorphism and metasomatism affecting Isua (Greenland) ~3700 Ma sedimentary rocks. *Precambrian Research*, *331*, 105347. https://doi.org/10.1016/j.precamres.2019.105347

Nutman, A. P., Friend, C. R. L., Bennett, V. C., Van Kranendonk, M., & Chivas, A. R. (2019). Reconstruction of a 3700 Ma transgressive marine environment from Isua (Greenland): Sedimentology, stratigraphy and geochemical signatures. *Lithos*, *346–347*, 105164. https://doi.org/10.1016/j.lithos.2019.105164

Oberthür, T., Davis, D. W., Blenkinsop, T. G., & Höhndorf, A. (2002). Precise U–Pb mineral ages, Rb–Sr and Sm–Nd systematics for the Great Dyke, Zimbabwe—Constraints on late Archean events in the Zimbabwe craton and Limpopo belt. *Precambrian Research*, *113*(3–4), 293–305. https://doi.org/10.1016/s0301-9268(01)00215-7

Occhipinti, S., Hocking, R., Lindsay, M., Aitken, A., Copp, I., Jones, J., et al. (2017). Paleoproterozoic basin development on the northern Yilgarn Craton, Western Australia. *Precambrian Research*, *300*, 121–140. https://doi.org/10.1016/j.precamres.2017.08.003

Ohta, K., Kuwayama, Y., Hirose, K., Shimizu, K., & Ohishi, Y. (2016). Experimental determination of the electrical resistivity of iron at Earth's core conditions. *Nature*, *534*(7605), 95–98. https://doi.org/10.1038/nature17957

O'Neil, J., Boyet, M., Carlson, R. W., & Paquette, J.-L. (2013). Half a billion years of reworking of Hadean mafic crust to produce the Nuvvuagittuq Eoarchean felsic crust. *Earth and Planetary Science Letters*, *379*, 13–25. https://doi.org/10.1016/j.epsl.2013.07.030

O'Neil, J., & Carlson, R. W. (2017). Building Archean cratons from Hadean mafic crust. *Science*, *355*(6330), 1199–1202. https://doi.org/10.1126/science.aah3823

O'Neil, J., Carlson, R. W., Francis, D., & Stevenson, R. K. (2008). Neodymium-142 evidence for Hadean mafic crust. *Science*, *321*(5897), 1828–1831. https://doi.org/10.1126/science.1161925

O'Neil, J., Carlson, R. W., Paquette, J. L., & Francis, D. (2012). Formation age and metamorphic history of the Nuvvuagittuq greenstone belt. *Precambrian Research*, *220–221*, 23–44. https://doi.org/10.1016/j.precamres.2012.07.009

O'Neill, C., Lenardic, A., Moresi, L., Torsvik, T. H., & Lee, C. T. A. (2007). Episodic Precambrian subduction. *Earth and Planetary Science Letters*, *262*(3–4), 552–562. https://doi.org/10.1016/j.epsl.2007.04.056

O'Neill, C., Marchi, S., Bottke, W., & Fu, R. (2020). The role of impacts on Archaean tectonics. *Geology*, *48*(2), 174–178. https://doi.org/10.1130/g46533.1

O'Neill, C., & Zhang, S. (2019). Chapter 4 – Modeling early Earth tectonics: The case for stagnant lid behavior. In M. J. Van Kranendonk, V. C. Bennett, & J. E. Hoffmann (Eds.), *Earth's oldest rocks* (2nd ed., pp. 65–80). Elsevier.

O'Reilly, S. Y., & Griffin, W. L. (2013). Moho vs crust–mantle boundary: Evolution of an idea. *Tectonophysics*, *609*, 535–546. https://doi.org/10.1016/j.tecto.2012.12.031

Ostrander, C. M., Johnson, A. C., & Anbar, A. D. (2021). Earth's first redox revolution. *Annual Review of Earth and Planetary Sciences*, *49*(1), 337–366. https://doi.org/10.1146/annurev-earth-072020-055249

Palin, R. M., & Santosh, M. (2021). Plate tectonics: What, where, why, and when? *Gondwana Research*, *100*, 3–24. https://doi.org/10.1016/j.gr.2020.11.001

Palin, R. M., White, R. W., & Green, E. C. R. (2016). Partial melting of metabasic rocks and the generation of tonalitic–trondhjemitic–granodioritic (TTG) crust in the Archaean: Constraints from phase equilibrium modelling. *Precambrian Research*, *287*, 73–90. https://doi.org/10.1016/j.precamres.2016.11.001

Papineau, D. (2010). Global biogeochemical changes at both ends of the Proteorzoic: Insights from phosphorites. *Astrobiology*, *10*(2), 165–181. https://doi.org/10.1089/ast.2009.0360

Papineau, D., De Gregorio, B. T., Cody, G. D., Fries, M. D., Mojzsis, S. J., Steele, A., et al. (2010). Ancient graphite in the Eoarchean quartz-pyroxene rocks from Akilia in southern West Greenland I: Petrographic and spectroscopic characterization. *Geochimica et Cosmochimica Acta*, *74*(20), 5862–5883. https://doi.org/10.1016/j.gca.2010.05.025

Parman, S. W. (2015). Time-lapse zirconography: Imaging punctuated continental evolution. *Geochemical Perspective Letters*, *1*, 43–52. https://doi.org/10.7185/geochemlet.1505

Partin, C. A., Bekker, A., Planavsky, N. J., Scott, C. T., Gill, B. C., Li, C., et al. (2013). Large-scale fluctuations in Precambrian atmospheric and oceanic oxygen levels from the record of U in shales. *Earth and Planetary Science Letters*, *369–370*, 284–293. https://doi.org/10.1016/j.epsl.2013.03.031

Pasyanos, M. E., Masters, T. G., Laske, G., & Ma, Z. (2014). LITHO1.0: An updated crust and lithospheric model of the Earth. *Journal of Geophysical Research: Solid Earth*, *119*(3), 2153–2173. https://doi.org/10.1002/2013jb010626

Pearce, J. A. (2008). Geochemical fingerprinting of oceanic basalts with applications to ophiolite classification and the search for Archean oceanic crust. *Lithos*, *100*(1–4), 14–48. https://doi.org/10.1016/j.lithos.2007.06.016

Pearce, J. A., Ernst, R. E., Peate, D. W., & Rogers, C. (2021). LIP printing: Use of immobile element proxies to characterize Large Igneous Provinces in the geologic record. *Lithos*, *392–393*, 392–393. https://doi.org/10.1016/j.lithos.2021.106068

Pearson, D. G., Carlson, R. W., Shirey, S. B., Boyd, F. R., & Nixon, P. H. (1995). Stabilisation of Archaean lithospheric mantle: A ReOs isotope study of peridotite xenoliths from the Kaapvaal craton. *Earth and Planetary Science Letters*, *134*(3–4), 341–357. https://doi.org/10.1016/0012-821x(95)00125-v

Pearson, D. G., Scott, J. M., Liu, J., Schaeffer, A., Wang, L. H., van Hunen, J., et al. (2021). Deep continental roots and cratons. *Nature*, *596*(7871), 199–210. https://doi.org/10.1038/s41586-021-03600-5

Perchuk, A. L., Gerya, T. V., Zakharov, V. S., & Griffin, W. L. (2020). Building cratonic keels in Precambrian plate tectonics. *Nature*, *586*(7829), 395–401. https://doi.org/10.1038/s41586-020-2806-7

Perchuk, A. L., Safonov, O. G., Smit, C. A., van Reenen, D. D., Zakharov, V. S., & Gerya, T. V. (2018). Precambrian ultra-hot orogenic factory: Making and reworking of continental crust. *Tectonophysics*, *746*, 572–586. https://doi.org/10.1016/j.tecto.2016.11.041

Perchuk, A. L., Zakharov, V. S., Gerya, T. V., & Brown, M. (2019). Hotter mantle but colder subduction in the Precambrian: What are the implications? *Precambrian Research*, *330*, 20–34. https://doi.org/10.1016/j.precamres.2019.04.023

Percival, J. A., Skulski, T., Sanborn-Barrie, M., Stott, G. M., Leclair, A. D., Corkery, M. T., & Boily, M. (2012). Geology and tectonic evolution of the Superior Province, Canada. In J. A. Percival, F. A. Cook, & R. M. Clowes (Eds.), *Tectonic styles in Canada: The Lithoprobe perspective*, *Geological Association of Canada Special Paper* (Vol. *49*, pp. 321–378).

Pisarevsky, S. A., De Waele, B., Jones, S., Söderlund, U., & Ernst, R. E. (2015). Paleomagnetism and U-Pb age of the 2.4Ga Erayinia mafic dykes in the south-western Yilgarn, Western Australia: Paleogeographic and geodynamic implications. *Precambrian Research*, *259*, 222–231. https://doi.org/10.1016/j.precamres.2014.05.023

Pisarevsky, S. A., Elming, S.-Å., Pesonen, L. J., & Li, Z.-X. (2014). Mesoproterozoic paleogeography: Supercontinent and beyond. *Precambrian Research*, *244*, 207–225. https://doi.org/10.1016/j.precamres.2013.05.014

Pisarevsky, S. A., Wingate, M. T. D., Li, Z.-X., Wang, X.-C., Tohver, E., & Kirkland, C. L. (2014). Age and paleomagnetism of the 1210 Ma Gnowangerup–Fraser dyke swarm, Western Australia, and implications for late Mesoproterozoic paleogeography. *Precambrian Research*, *246*, 1–15. https://doi.org/10.1016/j.precamres.2014.02.011

Planavsky, N. J., Crowe, S. A., Fakhraee, M., Beaty, B., Reinhard, C. T., Mills, B. J. W., et al. (2021). Evolution of the structure and impact of Earth's biosphere. *Nature Reviews Earth & Environment*, *2*, 123–139. https://doi.org/10.1038/s43017-020-00116-w

Plumb, K. A. (1991). New Precambrian time scale. *Episodes*, *14*(2), 139–140. https://doi.org/10.18814/epiiugs/1991/v14i2/005

Pons, M. L., Fujii, T., Rosing, M., Quitté, G., Télouk, P., & Albarède, F. (2013). A Zn isotope perspective on the rise of continents. *Geobiology*, *11*(3), 201–214. https://doi.org/10.1111/gbi.12030

Pope, M. C., & Grotzinger, J. P. (2003). Paleoproterozoic Stark formation, Athapuscow basin, Northwest Canada: Record of Cratonic-scale Salinity Crisis. *Journal of Sedimentary Research*, *73*(2), 280–295. https://doi.org/10.1306/091302730280

Porter, S. M. (2016). Tiny vampires in ancient seas: Evidence for predation via perforation in fossils from the 780–740 million-year-old Chuar Group, Grand Canyon, USA. *Proceedings of the Royal Society B: Biological Sciences*, *283*(1831), 20160221. https://doi.org/10.1098/rspb.2016.0221

Poulton, S. W., Bekker, A., Cumming, V. M., Zerkle, A. L., Canfield, D. E., & Johnston, D. T. (2021). A 200-million-year delay in permanent atmospheric oxygenation. *Nature*, *592*(7853), 232–236. https://doi.org/10.1038/s41586-021-03393-7

Pourteau, A., Smit, M. A., Li, Z.-X., Collins, W. J., Nordsvan, A. R., Volante, S., & Li, J. (2018). 1.6 Ga crustal thickening along the final Nuna suture. *Geology*, *46*(11), 959–962. https://doi.org/10.1130/g45198.1

Prave, A. R., Kirsimäe, K., Lepland, A., Fallick, A. E., Kreitsmann, T., Deines, Y. E., et al. (2021). The grandest of them all: The Lomagundi–Jatuli event and Earth's oxygenation. *Journal of the Geological Society*, *179*(1), jgs2021–036. https://doi.org/10.1144/jgs2021-036

Priestley, K., Ho, T., & McKenzie, D. (2020). The formation of continental roots. *Geology*, *49*(2), 190–194. https://doi.org/10.1130/g47696.1

Priestley, K., James, J., & McKenzie, D. (2008). Lithospheric structure and deep earthquakes beneath India, the Himalaya and southern Tibet. *Geophysical Journal International*, *172*(1), 345–362. https://doi.org/10.1111/j.1365-246x.2007.03636.x

Priestley, K., McKenzie, D., & Ho, T. (2018). A lithosphere–asthenosphere boundary—A global model derived from multimode surface-wave tomography and petrology. In H.-L. Yuan & B. Romanowicz (Eds.), *Lithospheric discontinuities*, *Volume Geophysical Monograph 239* (pp. 111–123). American Geophysical Union, John Wiley and Sons, Inc.

Puetz, S. J., & Condie, K. C. (2019). Time series analysis of mantle cycles Part I: Periodicities and correlations among seven global isotopic databases. *Geoscience Frontiers*, *10*(4), 1305–1326. https://doi.org/10.1016/j.gsf.2019.04.002

Puetz, S. J., & Condie, K. C. (2020). Applying Popperian falsifiability to geodynamic hypotheses: Empirical testing of the episodic crustal/zircon production hypothesis and selective preservation hypothesis. *International Geology Review*, *63*(15), 1–31. https://doi.org/10.1080/00206814.2020.1818143

Puetz, S. J., Spencer, C. J., & Ganade, C. E. (2021). Analyses from a validated global UPb detrital zircon database: Enhanced methods for filtering discordant UPb zircon analyses and optimizing crystallization age estimates. *Earth-Science Reviews*, *220*, 103745. https://doi.org/10.1016/j.earscirev.2021.103745

Pujol, M., Marty, B., Burgess, R., Turner, G., & Philippot, P. (2013). Argon isotopic composition of Archaean atmosphere probes early Earth geodynamics. *Nature*, *498*(7452), 87–90. https://doi.org/10.1038/nature12152

Raimondo, T., Hand, M., & Collins, W. J. (2014). Compressional intracontinental orogens: Ancient and modern perspectives. *Earth-Science Reviews*, *130*, 128–153. https://doi.org/10.1016/j.earscirev.2013.11.009

Rapp, R. P., Norman, M. D., Laporte, D., Yaxley, G. M., Martin, H., & Foley, S. F. (2010). Continent formation in the Archean and chemical evolution of the cratonic lithosphere: Melt-rock reaction experiments at 3–4 GPa and petrogenesis of Archean Mg-diorites (Sanukitoids). *Journal of Petrology*, *51*(6), 1237–1266. https://doi.org/10.1093/petrology/egq017

Rapp, R. P., Shimizu, N., & Norman, M. D. (2003). Growth of early continental crust by partial melting of eclogite. *Nature*, *425*(6958), 605–609. https://doi.org/10.1038/nature02031

Rasmussen, B., Bekker, A., & Fletcher, I. R. (2013). Correlation of Paleoproterozoic glaciations based on U–Pb zircon ages for tuff beds in the Transvaal and Huronian Supergroups. *Earth and Planetary Science Letters*, *382*, 173–180. https://doi.org/10.1016/j.epsl.2013.08.037

Rasmussen, B., Fletcher, I. R., & McNaughton, N. J. (2001). Dating low-grade metamorphic events by SHRIMP U-Pb analysis of monazite in shales. *Geology*, *29*(10), 963–966. https://doi.org/10.1130/0091-7613(2001)029<0963:dlgmeb>2.0.co;2

Reimink, J. R., Chacko, T., Stern, R. A., & Heaman, L. M. (2014). Earth's earliest evolved crust generated in an Iceland-like setting. *Nature Geoscience*, *7*, 529–533. https://doi.org/10.1038/ngeo2170

Reimink, J. R., Davies, J. H. F. L., Chacko, T., Stern, R. A., Heaman, L. M., Sarkar, C., et al. (2016). No evidence for Hadean continental crust within Earth/'s oldest evolved rock unit. *Nature Geoscience*, *9*(10), 777–780. https://doi.org/10.1038/ngeo2786

Reimink, J. R., Davies, J. H. F. L., & Ielpi, A. (2020). Global zircon analysis records a gradual rise of continental crust throughout the Neoarchean. *Earth and Planetary Science Letters*, *554*, 116654. https://doi.org/10.1016/j.epsl.2020.116654

Richards, M. A., Yang, W.-S., Baumgardner, J. R., & Bunge, H.-P. (2001). Role of a low-viscosity zone in stabilizing plate tectonics: Implications for comparative terrestrial planetology. *Geochemistry, Geophysics, Geosystems*, *2*(8), 1026. https://doi.org/10.1029/2000gc000115

Rino, S., Komiya, T., Windley, B. F., Katayama, I., Motoki, A., & Hirata, T. (2004). Major episodic increases of continental crustal growth determined from zircon ages of river sands; implications for mantle overturns in the Early Precambrian. *Physics of the Earth and Planetary Interiors*, *146*(1–2), 369–394. https://doi.org/10.1016/j.pepi.2003.09.024

Rivers, T. (2009). The Grenville Province as a large hot long-duration collisional orogen – Insights from the spatial and thermal evolution of its orogenic fronts. *Geological Society, London, Special Publications*, *327*(1), 405–444. https://doi.org/10.1144/sp327.17

Roberts, N. M. W. (2012). Increased loss of continental crust during supercontinent amalgamation. *Gondwana Research*, *21*(4), 994–1000. https://doi.org/10.1016/j.gr.2011.08.001

Roberts, N. M. W. (2013). The boring billion? – Lid tectonics, continental growth and environmental change associated with the Columbia supercontinent. *Geoscience Frontiers*, *4*(6), 681–691. https://doi.org/10.1016/j.gsf.2013.05.004

Roberts, N. M. W., Drost, K., Horstwood, M. S. A., Condon, D. J., Chew, D., Drake, H., et al. (2020). Laser ablation inductively coupled plasma mass spectrometry (LA-ICP-MS) U–Pb carbonate geochronology: Strategies, progress, and limitations. *Geochronology*, *2*(1), 33–61. https://doi.org/10.5194/gchron-2-33-2020

Roberts, N. M. W., & Santosh, M. (2018). Capturing the Mesoarchean emergence of continental crust in the Coorg block, Southern India. *Geophysical Research Letters*, *45*(15), 7444–7453. https://doi.org/10.1029/2018gl078114

Roberts, N. M. W., & Slagstad, T. (2015). Continental growth and reworking on the edge of the Columbia and Rodinia supercontinents; 1.86–0.9 Ga accretionary orogeny in southwest Fennoscandia. *International Geology Review*, *57*(11–12), 1582–1606. https://doi.org/10.1080/00206814.2014.958579

Roberts, N. M. W., & Spencer, C. J. (2015). The zircon archive of continent formation through time. *Geological Society, London, Special Publications*, *389*(1), 197–225. https://doi.org/10.1144/sp389.14

Rogers, J. J. W., & Santosh, M. (2002). Configuration of Columbia, a mesoproterozoic supercontinent. *Gondwana Research*, *5*(1), 5–22. https://doi.org/10.1016/s1342-937x(05)70883-2

Rolf, T., Coltice, N., & Tackley, P. J. (2012). Linking continental drift, plate tectonics and the thermal state of the Earth's mantle. *Earth and Planetary Science Letters*, *351–352*, 134–146. https://doi.org/10.1016/j.epsl.2012.07.011

Rollinson, H. (2008). Ophiolitic trondhjemites: A possible analogue for Hadean felsic 'crust'. *Terra Nova*, *20*(5), 364–369. https://doi.org/10.1111/j.1365-3121.2008.00829.x

Rosen, O. M., Manakov, A. V., & Serenko, V. P. (2005). Paleoproterozoic collisional system and diamondiferous lithospheric keel of the Yakutian kimberlite province. *Russian Geology and Geophysics*, *26*, 1259–1272.

Rozel, A. B., Golabek, G. J., Jain, C., Tackley, P. J., & Gerya, T. (2017). Continental crust formation on early Earth controlled by intrusive magmatism. *Nature*, *545*(7654), 332–335. https://doi.org/10.1038/nature22042

Rudnick, R. L., & Fountain, D. M. (1995). Nature and composition of the continental crust: A lower crustal perspective. *Reviews of Geophysics*, *33*(3), 267–309. https://doi.org/10.1029/95rg01302

Rudnick, R. L., & Gao, S. (2003). Composition of the continental crust. In R. L. Rudnick (Ed.), *Treatise on geochemistry, vol. 3, the crust* (p. 64). Elsevier.

Rudnick, R. L., & Gao, S. (2014). Composition of the continental crust. In R. L. Rudnick (Ed.), *Treatise on geochemistry* (2nd ed., Vol. *4*, pp. 1–51).

Sandiford, M., Hand, M., & McLaren, S. (2001). Tectonic feedback, intraplate orogeny and the geochemical structure of the crust: A central Australian perspective. In J. A. Miller, R. E. Holdsworth, I. S. Buick, & M. Hand (Eds.), *Continental reactivation and reworking, volume special publication no. 184* (pp. 195–218). The Geological Society.

Scholl, D. W., & von Huene, R. (2009). Implications of estimated magmatic additions and recycling losses at the subduction zones of accretionary (non-collisional) and collisional (suturing) orogens. In P. A. Cawood & A. Kröner (Eds.), *Earth accretionary systems in space and time* (Vol. 318, pp. 105–125). Geological Society, London, Special Publication.

Schopf, J. W., Kitajima, K., Spicuzza, M. J., Kudryavtsev, A. B., & Valley, J. W. (2018). SIMS analyses of the oldest known assemblage of microfossils document their taxon-correlated carbon isotope compositions. *Proceedings of the National Academy of Sciences*, *115*(1), 53–58. https://doi.org/10.1073/pnas.1718063115

Scott, C., Lyons, T. W., Bekker, A., Shen, Y., Poulton, S. W., Chu, X., & Anbar, A. D. (2008). Tracing the stepwise oxygenation of the Proterozoic ocean. *Nature*, *452*(7186), 456–459. https://doi.org/10.1038/nature06811

Scott, D. J., Helmstaadt, H., & Bickle, M. J. (1992). Purtuniq ophiolite, Cape Smith belt, northern Quebec, Canada: A reconstructed section of Early Proterozoic oceanic crust. *Geology*, *20*(2), 173–176. https://doi.org/10.1130/0091-7613(1992)020<0173:pocsbn>2.3.co;2

Sears, J. W., Chamberlain, K. R., & Buckley, S. N. (1998). Structural and U-Pb geochronological evidence for 1.47 Ga rifting in the Belt basin, western Montana. *Canadian Journal of Earth Sciences*, *35*(4), 467–475. https://doi.org/10.1139/e97-121

Şengör, A. M. C., Lom, N., & Polat, A. (2021). The nature and origin of cratons constrained by their surface geology. *GSA Bulletin*, *134*(5–6), 1485–1505. https://doi.org/10.1130/b36079.1

Seton, M., Müller, R. D., Zahirovic, S., Williams, S., Wright, N. M., Cannon, J., et al. (2020). A global data set of present-day oceanic crustal age and seafloor spreading parameters. *Geochemistry, Geophysics, Geosystems*, *21*(10), e2020GC009214. https://doi.org/10.1029/2020gc009214

Sheppard, S., Occhipinti, S. A., & Tyler, I. M. (2004). A 2005–1970 Ma Andean-type batholith in the southern Gascoyne complex, Western Australia. *Precambrian Research*, *128*(3–4), 257–277. https://doi.org/10.1016/j.precamres.2003.09.003

Shields, G. A. (2007). A normalised seawater strontium isotope curve: Possible implications for Neoproterozoic-Cambrian weathering rates and the further oxygenation of the Earth. *EEarth*, *2*, 35–42. https://doi.org/10.5194/ee-2-35-2007

Shields, G. A., Strachan, R. A., Porter, S. M., Halverson, G. P., Macdonald, F. A., Plumb, K. A., et al. (2021). A template for an improved rock-based subdivision of the pre-Cryogenian timescale. *Journal of the Geological Society*, *179*(1), jgs2020–222. https://doi.org/10.1144/jgs2020-222

Shu, L., Wang, B., Cawood, P. A., Santosh, M., & Xu, Z. (2015). Early Paleozoic and Early Mesozoic intraplate tectonic and magmatic events in the Cathaysia Block, South China. *Tectonics*, *34*(8), 1600–1621. https://doi.org/10.1002/2015tc003835

Simpson, A., Glorie, S., Hand, M., Spandler, C., Gilbert, S., & Cave, B. (2022). In-situ Lu–Hf geochronology of calcite. *Geochronology*, *2022*, 1–18. https://doi.org/10.5194/gchron-4-353-2022

Simpson, E. L., Eriksson, K. A., & Mueller, W. U. (2012). 3.2 Ga eolian deposits from the Moodies group, Barberton greenstone belt, South Africa: Implications for the origin of first-cycle quartz sandstones. *Precambrian Research*, *214–215*, 185–191. https://doi.org/10.1016/j.precamres.2012.01.019

Sizova, E., Gerya, T., & Brown, M. (2014). Contrasting styles of Phanerozoic and Precambrian continental collision. *Gondwana Research*, *25*(2), 522–545. https://doi.org/10.1016/j.gr.2012.12.011

Sizova, E., Gerya, T., Brown, M., & Perchuk, L. L. (2010). Subduction styles in the Precambrian: Insight from numerical experiments. *Lithos*, *116*(3–4), 209–229. https://doi.org/10.1016/j.lithos.2009.05.028

Sizova, E., Gerya, T., Stüwe, K., & Brown, M. (2015). Generation of felsic crust in the Archean: A geodynamic modeling perspective. *Precambrian Research*, *271*, 198–224. https://doi.org/10.1016/j.precamres.2015.10.005

Slagstad, T., Roberts, N. M. W., Marker, M., Røhr, T. S., & Schiellerup, H. (2013). A non-collisional, accretionary Sveconorwegian orogen. *Terra Nova*, *25*(1), 30–37. https://doi.org/10.1111/ter.12001

Sleep, N. H. (2005). Evolution of the continental lithosphere. *Annual Review of Earth and Planetary Sciences*, *33*(1), 369–393. https://doi.org/10.1146/annurev.earth.33.092203.122643

Sleep, N. H. (2018a). Cratonic basins with reference to the Michigan basin. *Geological Society, London, Special Publications*, *472*(1), 17–35. https://doi.org/10.1144/sp472.1

Sleep, N. H. (2018b). Geological and geochemical constraints on the origin and evolution of life. *Astrobiology*, *18*(9), 1199–1219. https://doi.org/10.1089/ast.2017.1778

Sleep, N. H., & Windley, B. F. (1982). Archean plate tectonics: Constraints and inferences. *The Journal of Geology*, *90*(4), 363–379. https://doi.org/10.1086/628691

Sloss, L. L. (1963). Sequences in the cratonic interior of North America. *GSA Bulletin*, *74*(2), 93–114. https://doi.org/10.1130/0016-7606(1963)74[93:sitcio]2.0.co;2

Sloss, L. L. (1988a). Introduction. In L. L. Sloss (Ed.), *Sedimentary cover—North American craton*. Geological Society of America.

Sloss, L. L. (1988b). Tectonic evolution of the craton in Phanerozoic time. In L. L. Sloss (Ed.), *Sedimentary cover—North American craton*. Geological Society of America.

Slotznick, S. P., Johnson, J. E., Rasmussen, B., Raub, T. D., Webb, S. M., Zi, J.-W., et al. (2022). Reexamination of 2.5-Ga "whiff" of oxygen interval points to anoxic ocean before GOE. *Science Advances*, *8*(1), eabj7190. https://doi.org/10.1126/sciadv.abj7190

Smart, K. A., Tappe, S., Stern, R. A., Webb, S. J., & Ashwal, L. D. (2016). Early Archaean tectonics and mantle redox recorded in Witwatersrand diamonds. *Nature Geoscience*, *9*(3), 255–259. https://doi.org/10.1038/ngeo2628

Smit, M. A., & Mezger, K. (2017). Earth's early O_2 cycle suppressed by primitive continents. *Nature Geoscience*, *10*, 788–792. https://doi.org/10.1038/ngeo3030

Smithies, R. H., Lu, Y., Kirkland, C. L., Johnson, T. E., Mole, D. R., Champion, D. C., et al. (2021). Oxygen isotopes trace the origins of Earth's earliest continental crust. *Nature*, *592*(7852), 70–75. https://doi.org/10.1038/s41586-021-03337-1

Smrekar, S. E., Lognonné, P., Spohn, T., Banerdt, W. B., Breuer, D., Christensen, U., et al. (2019). Pre-mission InSights on the interior of Mars. *Space Science Reviews*, *215*(1), 1–72. https://doi.org/10.1007/s11214-018-0563-9

Snyder, D. B., Humphreys, E., & Pearson, D. G. (2017). Construction and destruction of some North American cratons. *Tectonophysics*, *694*, 464–485. https://doi.org/10.1016/j.tecto.2016.11.032

Söderlund, U., Bleeker, W., Demirer, K., Srivastava, R. K., Hamilton, M., Nilsson, M., et al. (2019). Emplacement ages of Paleoproterozoic mafic dyke swarms in eastern Dharwar craton, India: Implications for paleoreconstructions and support for a ~30° change in dyke trends from south to north. *Precambrian Research*, *329*, 26–43. https://doi.org/10.1016/j.precamres.2018.12.017

Söderlund, U., Hofmann, A., Klausen, M. B., Olsson, J. R., Ernst, R. E., & Persson, P.-O. (2010). Towards a complete magmatic barcode for the Zimbabwe craton: Baddeleyite U–Pb dating of regional dolerite dyke swarms and sill complexes. *Precambrian Research*, *183*(3), 388–398. https://doi.org/10.1016/j.precamres.2009.11.001

Sossi, P. A., Eggins, S. M., Nesbitt, R. W., Nebel, O., Hergt, J. M., Campbell, I. H., et al. (2016). Petrogenesis and geochemistry of Archean komatiites. *Journal of Petrology*, *57*(1), 147–184. https://doi.org/10.1093/petrology/egw004

Spencer, C. J. (2020). Continuous continental growth as constrained by the sedimentary record. *American Journal of Science*, *320*(4), 373–401. https://doi.org/10.2475/04.2020.02

Spencer, C. J., Cavosie, A. J., Morrell, T. R., Lu, G. M., Liebmann, J., & Roberts, N. M. W. (2022). Disparities in oxygen isotopes of detrital and igneous zircon identify erosional bias in crustal rock record. *Earth and Planetary Science Letters*, *577*, 117248. https://doi.org/10.1016/j.epsl.2021.117248

Spencer, C. J., Cawood, P. A., Hawkesworth, C. J., Prave, A. R., Roberts, N. M. W., Horstwood, M. S. A., & Whitehouse, M. J. (2015). Generation and preservation of continental crust in the Grenville Orogeny. *Geoscience Frontiers*, *6*(3), 357–372. https://doi.org/10.1016/j.gsf.2014.12.001

Spencer, C. J., Cawood, P. A., Hawkesworth, C. J., Raub, T. D., Prave, A. R., & Roberts, N. M. W. (2014). Proterozoic onset of crustal reworking and collisional tectonics: Reappraisal of the zircon oxygen isotope record. *Geology*, *42*(5), 451–454. https://doi.org/10.1130/g35363.1

Spencer, C. J., Hawkesworth, C., Cawood, P. A., & Dhuime, B. (2013). Not all supercontinents are created equal: Gondwana-Rodinia case study. *Geology*, *41*(7), 795–798. https://doi.org/10.1130/g34520.1

Spencer, C. J., Mitchell, R. N., & Brown, M. (2021). Enigmatic mid-Proterozoic Orogens: Hot, thin, and low. *Geophysical Research Letters*, *48*(16), e2021GL093312. https://doi.org/10.1029/2021gl093312

Spencer, C. J., Partin, C. A., Kirkland, C. L., Raub, T. D., Liebmann, J., & Stern, R. A. (2019). Paleoproterozoic increase in zircon $\delta^{18}O$ driven by rapid emergence of continental crust. *Geochimica et Cosmochimica Acta*, *257*, 16–25. https://doi.org/10.1016/j.gca.2019.04.016

Srivastava, R. K., Söderlund, U., Ernst, R. E., Mondal, S. K., & Samal, A. K. (2019). Precambrian mafic dyke swarms in the Singhbhum craton (eastern India) and their links with dyke swarms of the eastern Dharwar craton (southern India). *Precambrian Research*, *329*, 5–17. https://doi.org/10.1016/j.precamres.2018.08.001

Stern, C. R. (2011). Subduction erosion: Rates, mechanisms, and its role in arc magmatism and the evolution of the continental crust and mantle. *Gondwana Research*, *20*(2–3), 284–308. https://doi.org/10.1016/j.gr.2011.03.006

Stern, R. J. (2018). The evolution of plate tectonics. *Philosophical Transactions of the Royal Society A: Mathematical, Physical & Engineering Sciences*, *376*(2132), 20170406. https://doi.org/10.1098/rsta.2017.0406

Stille, H. (1936). Tektonische Beziehungen zwischen Nordamerika und Europa. *Comptes Rendus International Geological Congress, Report of the XVI Session, United States of America*, *2*, 829–838.

Stoddard, P. R., & Jurdy, D. M. (2012). Topographic comparisons of uplift features on Venus and Earth: Implications for Venus tectonics. *Icarus*, *217*(2), 524–533. https://doi.org/10.1016/j.icarus.2011.09.003

St-Onge, M. R., Van Gool, J. A. M., Garde, A. A., & Scott, D. J. (2009). Correlation of Archaean and Palaeoproterozoic units between northeastern Canada and western Greenland: Constraining the pre-collisional upper plate accretionary history of the Trans-Hudson orogen. In P. A. Cawood & A. Kröner (Eds.), *Earth accretionary systems in space and time* (Vol. 318, pp. 193–235). Geological Society, London, Special Publication.

Strachan, R., Murphy, J. B., Darling, J., Storey, C., & Shields, G. (2020). Chapter 16 – Precambrian (4.56–1 Ga). In F. M. Gradstein, J. G. Ogg, M. D. Schmitz, & G. M. Ogg (Eds.), *Geologic time scale 2020* (pp. 481–493). Elsevier.

Subarkah, D., Blades, M. L., Collins, A. S., Farkaš, J., Gilbert, S., Löhr, S. C., et al. (2022). Unraveling the histories of Proterozoic shales through in situ Rb-Sr dating and trace element laser ablation analysis. *Geology*, *50*(1), 66–70. https://doi.org/10.1130/g49187.1

Sunder Raju, P. V., & Mazumder, R. (2020). Archean sedimentation on Dharwar Craton, India and its implications. *Earth-Science Reviews*, *202*, 102999. https://doi.org/10.1016/j.earscirev.2019.102999

Szilas, K., van Gool, J. A. M., Scherstén, A., & Frei, R. (2014). The Neoarchaean Storø Supracrustal Belt, Nuuk region, southern West Greenland: An arc-related basin with continent-derived sedimentation. *Precambrian Research*, *247*, 208–222. https://doi.org/10.1016/j.precamres.2014.04.010

Tamblyn, R., Hasterok, D., Hand, M., & Gard, M. (2021). Mantle heating at ca. 2 Ga by continental insulation: Evidence from granites and eclogites. *Geology*, *50*(1), 91–95. https://doi.org/10.1130/G49288.1

Tang, M., Chen, K., & Rudnick, R. L. (2016). Archean upper crust transition from mafic to felsic marks the onset of plate tectonics. *Science*, *351*(6271), 372–375. https://doi.org/10.1126/science.aad5513

Tang, M., Chu, X., Hao, J., & Shen, B. (2021). Orogenic quiescence in Earth's middle age. *Science*, *371*(6530), 728–731. https://doi.org/10.1126/science.abf1876

Tang, M., Ji, W.-Q., Chu, X., Wu, A., & Chen, C. (2020). Reconstructing crustal thickness evolution from europium anomalies in detrital zircons. *Geology*, *49*(1), 76–80. https://doi.org/10.1130/g47745.1

Taylor, D. J., McKeegan, K. D., & Harrison, T. M. (2009). Lu–Hf zircon evidence for rapid lunar differentiation. *Earth and Planetary Science Letters*, *279*(3–4), 157–164. https://doi.org/10.1016/j.epsl.2008.12.030

Taylor, S. R. (1967). The origin and growth of continents. *Tectonophysics*, *4*(1), 17–34. https://doi.org/10.1016/0040-1951(67)90056-x

Taylor, S. R., & McLennan, S. M. (1985). *The continental crust: Its composition and evolution* (p. 312). Blackwell Scientific Publications.

Thorne, A. M., & Trendall, A. F. (2001). Geology of the Fortescue Group, Pilbara Craton, Western Australia. *Geological Survey of Western Australia*, *144*, 249.

Trela, J., Gazel, E., Sobolev, A. V., Moore, L., Bizimis, M., Jicha, B., & Batanova, V. G. (2017). The hottest lavas of the Phanerozoic and the survival of deep Archaean reservoirs. *Nature Geoscience*, *10*(6), 451–456. https://doi.org/10.1038/ngeo2954

Turner, S., Wilde, S., Wörner, G., Schaefer, B., & Lai, Y.-J. (2020). An andesitic source for Jack Hills zircon supports onset of plate tectonics in the Hadean. *Nature Communications*, *11*(1), 1241. https://doi.org/10.1038/s41467-020-14857-1

Valley, J. W., Cavosie, A. J., Ushikubo, T., Reinhard, D. A., Lawrence, D. F., Larson, D. J., et al. (2014). Hadean age for a post-magma-ocean zircon confirmed by atom-probe tomography. *Nature Geoscience*, *7*(3), 219–223. https://doi.org/10.1038/ngeo2075

van Hinsbergen, D. J. J., Lippert, P. C., Li, S., Huang, W., Advokaat, E. L., & Spakman, W. (2019). Reconstructing Greater India: Paleogeographic, kinematic, and geodynamic perspectives. *Tectonophysics*, *760*, 69–94. https://doi.org/10.1016/j.tecto.2018.04.006

van Hinsbergen, D. J. J., Steinberger, B., Guilmette, C., Maffione, M., Gürer, D., Peters, K., et al. (2021). A record of plume-induced plate rotation triggering subduction initiation. *Nature Geoscience*, *14*(8), 626–630. https://doi.org/10.1038/s41561-021-00780-7

van Hunen, J., & Moyen, J.-F. (2012). Archean subduction: Fact or fiction? *Annual Review of Earth and Planetary Sciences*, *40*(1), 195–219. https://doi.org/10.1146/annurev-earth-042711-105255

van Hunen, J., & van den Berg, A. P. (2008). Plate tectonics on the early Earth: Limitations imposed by strength and buoyancy of subducted lithosphere. *Lithos*, *103*(1–2), 217–235. https://doi.org/10.1016/j.lithos.2007.09.016

Van Kranendonk, M. J., Baumgartner, R., Djokic, T., Ota, T., Steller, L., Garbe, U., & Nakamura, E. (2021). Elements for the origin of life on land: A deep-time perspective from the Pilbara Craton of Western Australia. *Astrobiology*, *21*(1), 39–59. https://doi.org/10.1089/ast.2019.2107

Van Kranendonk, M. J., Bennett, V. C., & Hoffman, E. (2019). *Earth's oldest rocks* (pp. 1112). Elsevier.

Van Kranendonk, M. J., Smithies, R. H., & Champion, D. C. (2019). Paleoarchean development of a continental nucleus: The East Plbara terrane of the Pilbara craton, Western Australia. In M. J. Van Kranendonk, V. C. Bennett, & E. Hoffman (Eds.), *Earth's oldest rocks* (pp. 437–462). Elsevier.

Verdel, C., Campbell, M. J., & Allen, C. M. (2021). Detrital zircon petrochronology of central Australia, and implications for the secular record of zircon trace element composition. *Geosphere*, *17*(2), 538–560. https://doi.org/10.1130/ges02300.1
Voice, P. J., Kowalewski, M., & Eriksson, K. A. (2011). Quantifying the timing and rate of crustal evolution: Global compilation of radiometrically dated detrital zircon grains. *The Journal of Geology*, *119*(2), 109–126. https://doi.org/10.1086/658295
Volante, S., Pourteau, A., Collins, W. J., Blereau, E., Li, Z.-X., Smit, M., et al. (2020). Multiple P–T–d–t paths reveal the evolution of the final Nuna assembly in northeast Australia. *Journal of Metamorphic Geology*, *38*(6), 593–627. https://doi.org/10.1111/jmg.12532
Wan, B., Yang, X., Tian, X., Yuan, H., Kirscher, U., & Mitchell, R. N. (2020). Seismological evidence for the earliest global subduction network at 2 Ga ago. *Science Advances*, *6*(32), eabc5491. https://doi.org/10.1126/sciadv.abc5491
Wang, Q., Bagdassarov, N., & Ji, S. (2013). The Moho as a transition zone: A revisit from seismic and electrical properties of minerals and rocks. *Tectonophysics*, *609*, 395–422. https://doi.org/10.1016/j.tecto.2013.08.041
Wang, W., Cawood, P. A., Spencer, C. J., Pandit, M. K., Zhao, J.-H., Xia, X.-P., et al. (2021). Global-scale emergence of continental crust during the Mesoarchean–early Neoarchean. *Geology*, *50*(2), 184–188. https://doi.org/10.1130/g49418.1
Wang, X., Tang, M., Moyen, J., Wang, D., Kröner, A., Hawkesworth, C., et al. (2021). The onset of deep recycling of supracrustal materials at the Paleo-Mesoarchean boundary. *National Science Review*, *9*(3), nwab136. https://doi.org/10.1093/nsr/nwab136
Wang, Z., Capitanio, F. A., Wang, Z., & Kusky, T. M. (2022). Accretion of the cratonic mantle lithosphere via massive regional relamination. *Proceedings of the National Academy of Sciences*, *119*(39), e2201226119. https://doi.org/10.1073/pnas.2201226119
Waterton, P., Guotana, J. M., Nishio, I., Morishita, T., Tani, K., Woodland, S., et al. (2022). No mantle residues in the Isua supracrustal belt. *Earth and Planetary Science Letters*, *579*, 117348. https://doi.org/10.1016/j.epsl.2021.117348
Weller, O. M., Mottram, C. M., St-Onge, M. R., Möller, C., Strachan, R., Rivers, T., & Copley, A. (2021). The metamorphic and magmatic record of collisional orogens. *Nature Reviews Earth & Environment*, *2*(11), 781–799. https://doi.org/10.1038/s43017-021-00218-z
Weller, O. M., & St-Onge, M. R. (2017). Record of modern-style plate tectonics in the Palaeoproterozoic Trans-Hudson orogen. *Nature Geoscience*, *10*(4), 305–311. https://doi.org/10.1038/ngeo2904
Wilde, S. A., Valley, J. W., Peck, W. H., & Graham, C. M. (2001). Evidence from detrital zircons for the existence of continental crust and oceans on the Earth 4.4 Gyr ago. *Nature*, *409*(6817), 175–178. https://doi.org/10.1038/35051550
Williams, H., Hoffman, P. F., Lewry, J. F., Monger, J. W. H., & Rivers, T. (1991). Anatomy of North America: Thematic geologic portrayals of the continent. *Tectonophysics*, *187*(1–3), 117–134. https://doi.org/10.1016/0040-1951(91)90416-p
Wilson, J. T. (1966). Did the Atlantic close and then re-open? *Nature*, *211*(5050), 676–681. https://doi.org/10.1038/211676a0
Windley, B. F., Kusky, T., & Polat, A. (2021). Onset of plate tectonics by the Eoarchean. *Precambrian Research*, *352*, 105980. https://doi.org/10.1016/j.precamres.2020.105980
Wingate, M. T. D. (1999). Ion microprobe baddeleyite and zircon ages for Late Archaean mafic dykes of the Pilbara Craton, Western Australia. *Australian Journal of Earth Sciences*, *46*(4), 493–500. https://doi.org/10.1046/j.1440-0952.1999.00726.x
Wolfram, L. C., Weinberg, R. F., Nebel, O., Hamza, K., Hasalová, P., Míková, J., & Becchio, R. (2019). A 60-Myr record of continental back-arc differentiation through cyclic melting. *Nature Geoscience*, *12*(3), 215–219. https://doi.org/10.1038/s41561-019-0298-6
Wood, B. J., Walter, M. J., & Wade, J. (2006). Accretion of the Earth and segregation of its core. *Nature*, *441*(7095), 825–833. https://doi.org/10.1038/nature04763
Wyche, S., Lu, Y., & Wingate, M. T. D. (2019). Evidence of Hadean to Paleoarchean crust in the Youanmi and South West terranes, and Eastern Goldfields Superterrane of the Yilgarn Craton, Western Australia. In M. J. Van Kranendonk, V. C. Bennett, & E. Hoffman (Eds.), *Earth's oldest rocks* (pp. 279–292). Elsevier.
Xu, Y., Cawood, P. A., & Du, Y.-S. (2016). Intraplate orogenesis in response to Gondwana assembly: Kwangsian orogeny, South China. *American Journal of Science*, *316*(4), 329–362. https://doi.org/10.2475/04.2016.02
Yang, B., Smith, T. M., Collins, A. S., Munson, T. J., Schoemaker, B., Nicholls, D., et al. (2018). Spatial and temporal variation in detrital zircon age provenance of the hydrocarbon-bearing upper Roper Group, Beetaloo Sub-basin, Northern Territory, Australia. *Precambrian Research*, *304*, 140–155. https://doi.org/10.1016/j.precamres.2017.10.025
Yoshida, M., & Yoshizawa, K. (2021). Continental drift with deep Cratonic roots. *Annual Review of Earth and Planetary Sciences*, *49*(1), 117–139. https://doi.org/10.1146/annurev-earth-091620-113028
Yoshizaki, T., & McDonough, W. F. (2020). The composition of Mars. *Geochimica et Cosmochimica Acta*, *273*, 137–162. https://doi.org/10.1016/j.gca.2020.01.011
Yoshizaki, T., & McDonough, W. F. (2021). Earth and Mars – Distinct inner solar system products. *Geochemistry*, *81*(2), 125746. https://doi.org/10.1016/j.chemer.2021.125746
Yuan, H., & Romanowicz, B. (2010). Lithospheric layering in the North American craton. *Nature*, *466*(7310), 1063–1068. https://doi.org/10.1038/nature09332
Zerkle, A. L., Claire, M. W., Rocco, T. D., Grassineau, N. V., Nisbet, E. G., Sun, R., & Yin, R. (2021). Sulfur and mercury MIF suggest volcanic contributions to Earth's atmosphere at 2.7 Ga. *Geochemical Perspectives Letters*, *18*, 48–52. https://doi.org/10.7185/geochemlet.2124
Zhang, X., Teng, J., Sun, R., Romanelli, F., Zhang, Z., & Panza, G. F. (2014a). Structural model of the lithosphere–asthenosphere system beneath the Qinghai–Tibet Plateau and its adjacent areas. *Tectonophysics*, *634*, 208–226. https://doi.org/10.1016/j.tecto.2014.08.017
Zhang, Y., Hou, M., Liu, G., Zhang, C., Prakapenka, V. B., Greenberg, E., et al. (2020). Reconciliation of experiments and theory on transport properties of iron and the geodynamo. *Physical Review Letters*, *125*(7), 078501. https://doi.org/10.1103/physrevlett.125.078501
Zhang, Z., Yuan, X., Chen, Y., Tian, X., Kind, R., Li, X., & Teng, J. (2010). Seismic signature of the collision between the east Tibetan escape flow and the Sichuan Basin. *Earth and Planetary Science Letters*, *292*(3–4), 254–264. https://doi.org/10.1016/j.epsl.2010.01.046
Zhao, G., & Cawood, P. A. (2012). Precambrian geology of China. *Precambrian Research*, *222–223*, 13–54. https://doi.org/10.1016/j.precamres.2012.09.017
Zhao, G., Cawood, P. A., Li, S., Wilde, S. A., Sun, M., Zhang, J., et al. (2012). Amalgamation of the North China Craton: Key issues and discussion. *Precambrian Research*, *222–223*, 55–76. https://doi.org/10.1016/j.precamres.2012.09.016
Zhao, G., Cawood, P. A., Wilde, S. A., & Sun, M. (2002). Review of global 2.1–1.8 Ga orogens: Implications for a pre-Rodinia supercontinent. *Earth-Science Reviews*, *59*(1–4), 125–162. https://doi.org/10.1016/s0012-8252(02)00073-9
Zhao, L., Tyler, I. M., Gorczyk, W., Murdie, R. E., Gessner, K., Lu, Y., et al. (2022). Seismic evidence of two cryptic sutures in Northwestern Australia: Implications for the style of subduction during the Paleoproterozoic assembly of Columbia. *Earth and Planetary Science Letters*, *579*, 117342. https://doi.org/10.1016/j.epsl.2021.117342
Zheng, Y.-F., & Zhao, G. (2019). Two styles of plate tectonics in Earth's history. *Science Bulletin*, *65*(4), 329–334. https://doi.org/10.1016/j.scib.2018.12.029
Zhong, S., Zhang, N., Li, Z.-X., & Roberts, J. H. (2007). Supercontinent cycles, true polar wander, and very long-wavelength mantle convection. *Earth and Planetary Science Letters*, *261*(3–4), 551–564. https://doi.org/10.1016/j.epsl.2007.07.049

Zhu, D. C., Wang, Q., Weinberg, R. F., Cawood, P. A., Chung, S. L., Zheng, Y. F., et al. (2022). Interplay between oceanic subduction and continental collision in building continental crust. *Nature Communications*, *13*(1), 7141. https://doi.org/10.1038/s41467-022-34826-0

Zhu, D. C., Wang, Q., Zhao, Z. D., Chung, S. L., Cawood, P. A., Niu, Y., et al. (2015). Magmatic record of India-Asia collision. *Scientific Reports*, *5*(1), 14289. https://doi.org/10.1038/srep14289

Zhu, R., Zhao, G., Xiao, W., Chen, L., & Tang, Y. (2021). Origin, accretion, and reworking of continents. *Reviews of Geophysics*, *59*(3), e2019RG000689. https://doi.org/10.1029/2019rg000689

Zhu, Z., Campbell, I. H., Allen, C. M., Brocks, J. J., & Chen, B. (2022). The temporal distribution of Earth's supermountains and their potential link to the rise of atmospheric oxygen and biological evolution. *Earth and Planetary Science Letters*, *580*, 117391. https://doi.org/10.1016/j.epsl.2022.117391

Zhu, Z., Campbell, I. H., Allen, C. M., & Burnham, A. D. (2020). S-type granites: Their origin and distribution through time as determined from detrital zircons. *Earth and Planetary Science Letters*, *536*, 116140. https://doi.org/10.1016/j.epsl.2020.116140

Zibra, I., Peternell, M., Schiller, M., Wingate, M. T. D., Lu, Y., & Clos, F. (2018). Tectono-magmatic evolution of the Neoarchean Yalgoo Dome (Yilgarn Craton): Diapirism in a pre-orogenic setting: Peth, Western Australia. *Geological Survey of Western Australia, Report 176*, 47.

References From the Supporting Information

Abbo, A., Avigad, D., & Gerdes, A. (2020). Crustal evolution of peri-Gondwana crust into present day Europe: The Serbo-Macedonian and Rhodope massifs as a case study. *Lithos*, *356–357*, 105295. https://doi.org/10.1016/j.lithos.2019.105295

Agangi, A., Hofmann, A., & Elburg, M. A. (2018). A review of Palaeoarchaean felsic volcanism in the eastern Kaapvaal craton: Linking plutonic and volcanic records. *Geoscience Frontiers*, *9*(3), 667–688. https://doi.org/10.1016/j.gsf.2017.08.003

Agangi, A., Plavsa, D., Reddy, S. M., Olierook, H., & Kylander-Clark, A. (2020). Compositional modification and trace element decoupling in rutile: Insight from the Capricorn Orogen, Western Australia. *Precambrian Research*, *345*, 105772. https://doi.org/10.1016/j.precamres.2020.105772

Albert, C., Farina, F., Lana, C., Stevens, G., Craig, S., Gerdes, A., & Dopico, C. M. (2016). Archean crustal evolution in the Southern São Francisco craton, Brazil: Constraints from U-Pb, Lu-Hf and O isotope analyses. *Lithos*, *266–267*, 64–86. https://doi.org/10.1016/j.lithos.2016.09.029

Andersen, T., Elburg, M. A., & Van Niekerk, H. S. (2019). Detrital zircon in sandstones from the Palaeoproterozoic Waterberg and Nylstroom basins, South Africa: Provenance and recycling. *South African Journal of Geology*, *122*(1), 79–96. https://doi.org/10.25131/sajg.122.0008

Apen, F. E., Rudnick, R. L., Cottle, J. M., Kylander-Clark, A. R. C., Blondes, M. S., Piccoli, P. M., & Seward, G. (2020). Four-dimensional thermal evolution of the East African Orogen: Accessory phase petrochronology of crustal profiles through the Tanzanian Craton and Mozambique Belt, northeastern Tanzania. *Contributions to Mineralogy and Petrology*, *175*(11), 97. https://doi.org/10.1007/s00410-020-01737-6

Augland, L. E., & David, J. (2015). Protocrustal evolution of the Nuvvuagittuq Supracrustal Belt as determined by high precision zircon Lu–Hf and U–Pb isotope data. *Earth and Planetary Science Letters*, *428*, 162–171. https://doi.org/10.1016/j.epsl.2015.07.039

Avigad, D., Morag, N., Abbo, A., & Gerdes, A. (2017). Detrital rutile U-Pb perspective on the origin of the great Cambro-Ordovician sandstone of North Gondwana and its linkage to orogeny. *Gondwana Research*, *51*, 17–29. https://doi.org/10.1016/j.gr.2017.07.001

Axelsson, E., Mezger, K., & Ewing, T. (2020). The Kuunga Orogeny in the Eastern Ghats Belt: Evidence from geochronology of biotite, amphibole and rutile, and implications for the assembly of Gondwana. *Precambrian Research*, *347*, 105805. https://doi.org/10.1016/j.precamres.2020.105805

Bai, W., Dong, C., Song, Z., Nutman, A. P., Zie, H., Wang, S., et al. (2020). Late Neoarchean granites in the Qixingtai region, western Shandong: Further evidence for the recycling of early Neoarchean juvenile crust in the North China Craton. *Geological Journal*, *55*(9), 6462–6486. https://doi.org/10.1002/gj.3824

Bai, X., Liu, S., Guo, R., & Wang, W. (2015). Zircon U–Pb–Hf isotopes and geochemistry of two contrasting Neoarchean charnockitic rock series in Eastern Hebei, North China Craton: Implications for petrogenesis and tectonic setting. *Precambrian Research*, *267*, 72–93. https://doi.org/10.1016/j.precamres.2015.06.004

Bai, X., Liu, S., Guo, R., & Wang, W. (2016). A Neoarchean arc–back-arc system in Eastern Hebei, North China Craton: Constraints from zircon U–Pb–Hf isotopes and geochemistry of dioritic–tonalitic–trondhjemitic–granodioritic (DTTG) gneisses and felsic paragneisses. *Precambrian Research*, *273*, 90–111. https://doi.org/10.1016/j.precamres.2015.12.003

Bai, X., Liu, S., Guo, R., Zhang, L., & Wang, W. (2014). Zircon U–Pb–Hf isotopes and geochemistry of Neoarchean dioritic–trondhjemitic gneisses, Eastern Hebei, North China Craton: Constraints on petrogenesis and tectonic implications. *Precambrian Research*, *251*, 1–20. https://doi.org/10.1016/j.precamres.2014.05.027

Bao, H., Liu, S., Wan, Y., Wang, M., Sun, G., Gao, L., et al. (2022). Neoarchean granitoids and tectonic regime of lateral growth in northeastern North China Craton. *Gondwana Research*, *107*, 176–200. https://doi.org/10.1016/j.gr.2022.02.015

Barber, D. E., Stockli, D. F., & Galster, F. (2019). The Proto-Zagros foreland basin in Lorestan, western Iran: Insights from multimineral detrital geothermochronometric and trace elemental provenance analysis. *Geochemistry, Geophysics, Geosystems*, *20*(6), 2657–2680. https://doi.org/10.1029/2019GC008185

Bauer, A. M., Fisher, C. M., Vervoort, J. D., & Bowring, S. A. (2017). Coupled zircon Lu–Hf and U–Pb isotopic analyses of the oldest terrestrial crust, the >4.03 Ga Acasta Gneiss Complex. *Earth and Planetary Science Letters*, *458*, 37–48. https://doi.org/10.1016/j.epsl.2016.10.036

Be'eri-Shlevin, Y., Avigad, D., & Gerdes, A. (2018). The White Nile as a source for Nile sediments: Assessment using U-Pb geochronology of detrital rutile and monazite. *Journal of African Earth Sciences*, *140*, 1–8. https://doi.org/10.1016/j.jafrearsci.2017.12.032

Bell, E. A., Harrison, T. M., Kohl, I. E., & Young, E. D. (2014). Eoarchean crustal evolution of the Jack Hills zircon source and loss of Hadean crust. *Geochimica et Cosmochimica Acta*, *146*, 27–42. https://doi.org/10.1016/j.gca.2014.09.028

Bjorkman, K. E. (2017). *40 Crust-mantle evolution of the western Superior Craton: Implications for Archaean granite-greenstone petrogenesis and geodynamics* (Doctoral thesis). The University of Western Australia. https://doi.org/10.4225/23/5a39c88a2f559

Bolhar, R., Hofmann, A., Kemp, A. I. S., Whitehouse, M. J., Wind, S., & Kamber, B. S. (2017). Juvenile crust formation in the Zimbabwe Craton deduced from the O-Hf isotopic record of 3.8–3.1Ga detrital zircons. *Geochimica et Cosmochimica Acta*, *215*, 432–446. https://doi.org/10.1016/j.gca.2017.07.008

Bracciali, L., Najman, Y., Parrish, R. R., Akhter, S. H., & Millar, I. (2015). The Brahmaputra tale of tectonics and erosion: Early Miocene river capture in the Eastern Himalaya. *Earth and Planetary Science Letters*, *415*, 25–37. https://doi.org/10.1016/j.epsl.2015.01.022

Bracciali, L., Parrish, R. R., Horstwood, M. S. A., Condon, D. J., & Najman, Y. (2013). UPb LA-(MC)-ICP-MS dating of rutile: New reference materials and applications to sedimentary provenance. *Chemical Geology*, *347*, 82–101. https://doi.org/10.1016/j.chemgeo.2013.03.013

Bracciali, L., Parrish, R. R., Najman, Y., Smye, A., Carter, A., & Wijbrans, J. R. (2016). Plio-Pleistocene exhumation of the eastern Himalayan syntaxis and its domal 'pop-up'. *Earth-Science Reviews*, *160*, 350–385. https://doi.org/10.1016/j.earscirev.2016.07.010

Brown, D. A., Martin, H., Morrissey, L. J., & Goodge, J. W. (2020). Cambrian eclogite-facies metamorphism in the central Transantarctic Mountains, East Antarctica: Extending the record of early Palaeozoic high-pressure metamorphism along the eastern Gondwanan margin. *Lithos*, *366–367*, 105571. https://doi.org/10.1016/j.lithos.2020.105571

Bruguier, O., Bosch, D., Renaud, C., Vitale-Brovarone, A., Fernandez, L., Hammor, D., et al. (2017). Age of UHP metamorphism in the Western Mediterranean: Insight from rutile and minute zircon inclusions in a diamond-bearing garnet megacryst (Edough Massif, NE Algeria). *Earth and Planetary Science Letters*, *474*, 215–225. https://doi.org/10.1016/j.epsl.2017.06.043

Bruno, H., Heilbron, M., Strachan, R., Fowler, M., de Morisson Valeriano, C., Bersan, S., et al. (2021). Earth's new tectonic regime at the dawn of the Paleoproterozoic: Hf isotope evidence for efficient crustal growth and reworking in the São Francisco craton, Brazil. *Geology*, *49*(10), 1214–1219. https://doi.org/10.1130/G49024.1

Butler, J. P., Jamieson, R. A., Dunning, G. R., Pecha, M. E., Robinson, P., & Steenkamp, H. M. (2018). Timing of metamorphism and exhumation in the Nordøyane ultra-high-pressure domain, Western Gneiss Region, Norway: New constraints from complementary CA-ID-TIMS and LA-MC-ICP-MS geochronology. *Lithos*, *310–311*, 153–170. https://doi.org/10.1016/j.lithos.2018.04.006

Cabral, A. R., Otto, E., Brauns, M., Lehmann, B., Rösel, D., Zack, T., et al. (2013). Direct dating of gold by radiogenic helium: Testing the method on gold from Diamantina, Minas Gerais, Brazil. *Geology*, *21*(2), 163–166. https://doi.org/10.1130/G33751.1

Cerva-Alves, T., Hartmann, L. A., Remus, M. V. D., & Lana, C. (2020). Integrated ophiolite and arc evolution, southern Brasiliano Orogen. *Precambrian Research*, *341*, 105648. https://doi.org/10.1016/j.precamres.2020.105648

Çetinkaplan, M., Pourteau, A., Candan, O., Ersin Koralay, O., Oberhansli, R., Okay, A. I., et al. (2016). P–T–t evolution of eclogite/blueschist facies metamorphism in Alanya Massif: Time and space relations with HP event in Bitlis Massif, Turkey. *International Journal of Earth Sciences*, *105*(1), 247–281. https://doi.org/10.1007/s00531-014-1092-8

Chen, N. H.-C., Zhao, G., Jahn, B.-M., Sun, M., & Zhou, H. (2017). U-Pb zircon ages and Hf isotopes of ~2.5 Ga granitoids from the Yinshan Block, North China Craton: Implications for crustal growth. *Precambrian Research*, *303*, 171–182. https://doi.org/10.1016/j.precamres.2017.03.016

Chen, Y., Zhang, J., Liu, J., Han, Y., Yin, C., Qian, J., & Liu, X. (2020). Crustal growth and reworking of the eastern North China Craton: Constraints from the age and geochemistry of the Neoarchean Taishan TTG gneisses. *Precambrian Research*, *343*, 105706. https://doi.org/10.1016/j.precamres.2020.10570

Chew, D. M., Pedemonte, G., & Corbett, E. (2016). Proto-Andean evolution of the Eastern Cordillera of Peru. *Gondwana Research*, *35*, 59–78. https://doi.org/10.1016/j.gr.2016.03.016

Chowdhury, P., Mulder, J. A., Cawood, P. A., Bhattacharjee, S., Roy, S., Wainwright, A. N., et al. (2021). Magmatic thickening of crust in non-plate tectonic settings initiated the subaerial rise of Earth's first continents 3.3 to 3.2 billion years ago. *Proceedings of the National Academy of Sciences*, *118*, 46. https://doi.org/10.1073/pnas.2105746118

Chowdhury, W., Trail, D., Guitreau, M., Bell, E. A., Buettner, J., & Mojzsis, S. J. (2020). Geochemical and textural investigations of the Eoarchean Ukaliq supracrustals, Northern Québec (Canada). *Lithos*, *372–373*, 105673. https://doi.org/10.1016/j.lithos.2020.105673

Corfu, F., Polteau, S., Planke, S., Faleide, J., Svensen, H., Zayoncheck, A., & Stolbov, N. (2013). U-Pb geochronology of Cretaceous magmatism on Svalbard and Fran Josef Land, Barents Sea large igneous province. *Geological Magazine*, *150*(6), 1127–1135. https://doi.org/10.1017/S0016756813000162

Cutts, J. A., Smit, M. A., Kooijman, E., & Schmitt, M. (2019). Two-stage cooling and exhumation of deeply subducted continents. *Tectonics*, *38*(3), 863–877. https://doi.org/10.1029/2018TC005292

Davis, D. W., Amelin, Y., Nowell, G. M., & Parrish, R. R. (2005). Hf isotopes in zircon from the western Superior province, Canada: Implications for Archean crustal development and evolution of the depleted mantle reservoir. *Precambrian Research*, *140*(3–4), 132–156. https://doi.org/10.1016/j.precamres.2005.07.005

De, S., Rosiere, C. A., & Mukhopadhyay, J. (2022). Detrital zircon LA-ICPMS U-Pb and Lu-Hf signature from the Mesoarchean Keonjhar Quartzite: Implications for the nature of Archean continental crust and geodynamics. *Geosystems and Geoenvironment*, *1*(4), 100057. https://doi.org/10.1016/j.geogeo.2022.100057

de Assis Barros, R., de Andrade Caxito, F., Egydio-Silva, M., Dantas, E. L., Pinheiro, M. A. P., Rodrigues, J. B., et al. (2020). Archean and Paleoproterozoic crustal evolution and evidence for cryptic Paleoarchean-Hadean sources of the NW São Francisco Craton, Brazil: Lithochemistry, geochronology, and isotope systematics of the Cristalândia do Piauí Block. *Gondwana Research*, *88*, 268–295. https://doi.org/10.1016/j.gr.2020.07.004

de Camargo Moreira, I., Oliveira, E. P., & de Sousa, D. F. M. (2022). Evolution of the 3.65–2.58 Ga Mairi Gneiss Complex, Brazil: Implications for growth of the continental crust in the São Francisco Craton. *Geoscience Frontiers*, *13*(5), 101366. https://doi.org/10.1016/j.gsf.2022.101366

de Morisson Valeriano, C., Turbay, C. V. G., Bruno, H., Simonetti, A., Heilbron, M., Moreira Bersan, S., & Strachan, R. (2022). Paleo- and Mesoarchean TTG-sanukitoid to high-K granite cycles in the southern São Francisco craton, SE Brazil. *Geoscience Frontiers*, *13*(5), 101372. https://doi.org/10.1016/j.gsf.2022.101372

Deng, B., Chew, D., Jiang, L., Mark, C., Cogné, N., Wang, Z., & Liu, S. (2018). Heavy mineral analysis and detrital U-Pb ages of the intracontinental Paleo-Yangzte basin: Implications for a transcontinental source-to-sink system during Late Cretaceous time. *The Geological Society of America Bulletin*, *130*(11–12), 2087–2109. https://doi.org/10.1130/B32037.1

Deng, H., Kusky, T., Polat, A., Fu, H., Wang, L., Wang, J., et al. (2020). A Neoarchean arc-backarc pair in the Linshan Massif, southern North China Craton. *Precambrian Research*, *341*, 105649. https://doi.org/10.1016/j.precamres.2020.105649

de Sousa, D. F. M., Oliveira, E. P., Amaral, W. S., & Baldim, M. R. (2020). The Itabuna-Salvador-Curaçá Orogen revisited, São Francisco Craton, Brazil: New zircon U–Pb ages and Hf data support evolution from Archean continental arc to Paleoproterozoic crustal reworking during block collision. *Journal of South American Earth Sciences*, *104*, 102826. https://doi.org/10.1016/j.jsames.2020.102826

Dey, S., Nayak, S. K., Mitra, A., Zong, K., & Liu, Y. (2020). Mechanism of Paleoarchaean continental crust formation as archived in granitoids from northern part of Singhbhum craton, eastern India. *Geological Society of London Special Publicatoin*, *489*, 189–214. https://doi.org/10.1144/SP484-2019-202

Dey, S., Topno, A., Liu, Y., & Zong, K. (2017). Generation and evolution of Palaeoarchaean continental crust in the central part of the Singhbhum craton, eastern India. *Precambrian Research*, *298*, 268–291. https://doi.org/10.1016/j.precamres.2017.06.009

Diwu, C., Sun, Y., Yuan, H., Wang, H., Zhong, X., & Liu, X. (2008). U-Pb ages and Hf isotopes for detrital zircons from quartzite in the Paleoproterozoic Songshan Group on the southwestern margin of the North China Craton. *Chinese Science Bulletin*, *53*(18), 2828–2839. https://doi.org/10.1007/s11434-008-0342-1

Diwu, C., Wang, T., & Yan, J. (2020). New evidence for Neoarchean (ca. 2.7 Ga) crustal growth in the North China Craton. *Precambrian Research*, *350*, 105921. https://doi.org/10.1016/j.precamres.2020.105921

Dong, C., Wan, Y., Xie, H., Nutman, A. P., Xie, S., Liu, S., et al. (2017). The Mesoarchean Tiejiashan-Gongchangling potassic granite in the Anshan-Benxi area, North China Craton: Origin by recycling of Paleo- to Eoarchean crust from U-Pb-Nd-Hf-O isotopic studies. *Lithos*, *290–291*, 116–135. https://doi.org/10.1016/j.lithos.2017.08.009

Dong, Y., Ge, W.-C., Yang, H., Liu, X.-W., Bi, J.-H., Zheng, J., & Xu, W.-L. (2019). Geochemical and SIMS U-Pb rutile and LA–ICP–MS U-Pb zircon geochronological evidence of the tectonic evolution of the Mudanjiang Ocean from amphibolites of the Heilongjiang Complex, NE China. *Gondwana Research*, *69*, 25–44. https://doi.org/10.1016/j.gr.2018.11.012

Dopico, C. I. M., Lana, C., Moreira, H. S., Cassino, L. F., & Alkmim, F. F. (2017). U–Pb ages and Hf-isotope data of detrital zircons from the late Neoarchean-Paleoproterozoic Minas Basin, SE Brazil. *Precambrian Research*, *291*, 143–161. https://doi.org/10.1016/j.precamres.2017.01.026

dos Santos, C., Zincone, S. A., Queiroga, G. N., Bersan, S. M., Lana, C. C., & Oliveira, E. P. (2022). Evidence for change in crust formation process during the Paleoarchean in the São Francisco Craton (Gavião Block): Coupled zircon Lu-Hf and U-Pb isotopic analyses and tectonic implications. *Precambrian Research*, *368*, 106472. https://doi.org/10.1016/j.precamres.2021.106472

Doyle, M. G., Fletcher, I. R., Foster, J., Large, R. R., Mathur, R., McNaughton, N. J., et al. (2015). Geochronological Constraints on the Tropicana Gold deposit and Albany-Fraser Orogen, Western Australia. *Economic Geology*, *110*(2), 355–386. https://doi.org/10.2113/econgeo.110.2.355

Du, L., Yang, C., Wang, W., Ren, L., Wan, Y., Song, H., et al. (2012). Provenance of the Paleoproterozoic Hutuo Group basal conglomerates and Neoarchean crustal growth in the Wutai Mountains, North China Craton: Evidence from granite and quartzite pebble zircon U-Pb ages and Hf isotopes. *Science China Earth Sciences*, *55*(11), 1796–1814. https://doi.org/10.1007/s11430-012-4407-2

Du, L., Yang, C., Wyman, D. A., Nutman, A. P., Lu, Z., Song, H., et al. (2016). Age and depositional setting of the Paleoproterozoic Gantaohe Group in Zanhuang Complex: Constraints from zircon U–Pb ages and Hf isotopes of sandstones and dacite. *Precambrian Research*, *286*, 59–100. https://doi.org/10.1016/j.precamres.2016.09.027

Dunn, S. C., von der Heyden, B. P., Bracciali, L., & StPierre, B. (2020). Geology and U–Pb geochronology of the Amani Region, southwestern Tanzania. *Journal of African Earth Sciences*, *162*, 103729. https://doi.org/10.1016/j.jafrearsci.2019.103729

Elburg, M. A., & Poujol, M. (2020). Lu-Hf analyses of zircon from the Makoppa Dome and Amalia-Kraaipan area: Implications for evolution of the Kimberley and Pietersburg blocks of the Kaapvaal Craton. *South African Journal of Geology*, *123*(3), 369–380. https://doi.org/10.25131/sajg.123.0025

Engvik, A. K., Corfu, F., Solli, A., & Austrheim, H. (2017). Sequence and timing of mineral replacement reactions during albitisation in the high-grade Bamble lithotectonic domain, S-Norway. *Precambrian Research*, *291*, 1–16. https://doi.org/10.1016/j.precamres.2017.01.010

Engvik, A. K., Mezger, K., Wortelkamp, S., Bast, R., Corfu, F., Korneliussen, A., et al. (2010). Metasomatism of gabbro–mineral replacement and element mobilization during the Sveconorwegian metamorphic event. *Journal of Metamorphic Geology*, *29*(4), 399–423. https://doi.org/10.1111/j.1525-1314.2010.00922.x

Ewing, T. A., Rubatto, D., Beltrando, M., & Hermann, J. (2015). Constraints on the thermal evolution of the Adriatic margin during Jurassic continental break-up: U–Pb dating of rutile from the Ivrea–Verbano Zone, Italy. *Contributions to Mineralogy and Petrology*, *169*(4), 44. https://doi.org/10.1007/s00410-015-1135-6

Fisher, C. M., & Vervoort, J. D. (2018). Using the magmatic record to constrain the growth of continental crust—The Eoarchean zircon Hf record of Greenland. *Earth and Planetary Science Letters*, *488*, 79–91. https://doi.org/10.1016/j.epsl.2018.01.031

Frieman, B. M., Kelly, N. M., Kuiper, Y. D., Monecke, T., Kylander-Clark, A., & Guitreau, M. (2021). Insight into Archean crustal growth and mantle evolution from multi-isotope U-Pb and Lu-Hf analysis of detrital zircon grains from the Abitibi and Pontiac subprovinces, Canada. *Precambrian Research*, *357*, 106136. https://doi.org/10.1016/j.precamres.2021.106136

Frost, C. D., McLaughlin, J. F., Frost, B. R., Fanning, C. M., Swapp, S. M., Kruckenberg, S. C., & Gonzalez, J. (2017). Hadean origins of Paleoarchean continental crust in the central Wyoming Province. *The Geological Society of America Bulletin*, *129*(3–4), 259–280. https://doi.org/10.1130/B31555.1

Fu, J., Liu, S., Chen, X., Bai, X., Guo, R., & Wang, W. (2016). Petrogenesis of taxitic dioritic–tonalitic gneisses and Neoarchean crustal growth in Eastern Hebei, North China Craton. *Precambrian Research*, *284*, 64–87. https://doi.org/10.1016/j.precamres.2016.08.002

Fu, J., Liu, S., Wang, M., Chen, X., Guo, B., & Hu, F. (2017). Late Neoarchean monzogranitic–syenogranitic gneisses in the Eastern Hebei–Western Liaoning Province, North China Craton: Petrogenesis and implications for tectonic setting. *Precambrian Research*, *303*, 392–413. https://doi.org/10.1016/j.precamres.2017.05.002

Fu, J., Liu, S., Zhang, B., Guo, R., & Wang, M. (2019). A Neoarchean K-rich granitoid belt in the northern North China Craton. *Precambrian Research*, *328*, 193–216. https://doi.org/10.1016/j.precamres.2019.04.021

Gao, L., Liu, S., Hu, Y., Sun, G., Guo, R., & Bao, H. (2020). Late Neoarchean geodynamic evolution: Evidence from the metavolcanic rocks of the Western Shandong Terrane, North China Craton. *Gondwana Research*, *80*, 303–320. https://doi.org/10.1016/j.gr.2019.10.017

Gao, L., Liu, S., Sun, G., Guo, R., Hu, Y., Fu, J., et al. (2018). Petrogenesis of late Neoarchean high-K granitoids in the Western Shandong terrane, North China Craton, and their implications for crust-mantle interactions. *Precambrian Research*, *315*, 138–161. https://doi.org/10.1016/j.precamres.2018.07.006

Gao, L., Liu, S., Sun, G., Hu, Y., Guo, R., Fu, J., et al. (2019). Neoarchean crust-mantle interactions in the Yishui Terrane, south-eastern margin of the North China Craton: Constraints from geochemistry and zircon U-Pb-Hf isotopes of metavolcanic rocks and high-K granitoids. *Gondwana Research*, *65*, 97–124. https://doi.org/10.1016/j.gr.2018.10.002

Gao, M., Zhang, Z.-J., Cheng, Q.-M., & Grujic, D. (2021). Zircon U-Pb and Lu-Hf isotopes of Huai'an complex granites, North China Craton: Implications for crustal growth, reworking and tectonic evolution. *Gondwana Research*, *90*, 118–134. https://doi.org/10.1016/j.gr.2020.10.015

Gao, X.-Y., Zheng, Y.-F., Xia, X.-P., & Chen, Y.-X. (2014). U–Pb ages and trace elements of metamorphic rutile from ultrahigh-pressure quartzite in the Sulu orogen. *Geochimica et Cosmochimica Acta*, *143*, 87–114. https://doi.org/10.1016/j.gca.2014.04.032

Gardiner, N. J., Kirkland, C. L., Hollis, J., Szilas, K., Steenfelt, A., Yakymchuk, C., & Heide-Jorgensen, H. (2019). Building Mesoarchaean crust upon Eoarchaean roots: The Akia Terrane, West Greenland. *Contributions to Mineralogy and Petrology*, *174*(3), 20. https://doi.org/10.1007/s00410-019-1554-x

Gaschnig, R. M. (2019). Benefits of a multiproxy approach to detrital mineral provenance analysis: An example from the Merrimack River, New England, USA. *Geochemistry, Geophysics, Geosystems*, *20*(3), 1557–1573. https://doi.org/10.1029/2018GC008005

Gaschnig, R. M., Horan, M. F., Rudnick, R. L., Vervoort, J. D., & Fisher, C. M. (2022). History of crustal growth in Africa and the Americas from detrital zircon and Nd isotopes in glacial diamictites. *Precambrian Research*, *373*, 106641. https://doi.org/10.1016/j.precamres.2022.106641

Gasser, D., Jeřábek, P., Faber, C., Stünitz, H., Menegon, L., Corfu, F., et al. (2015). Behaviour of geochronometers and timing of metamorphic reactions during deformation at lower crustal conditions: Phase equilibrium modelling and U–Pb dating of zircon, monazite, rutile and titanite from the Kalak Nappe Complex, northern Norway. *Journal of Metamorphic Geology*, *33*(5), 513–534. https://doi.org/10.1111/jmg.12131

Geng, Y., Du, L., & Ren, L. (2012). Growth and reworking of the early Precambrian continental crust in the North China Craton: Constraints from zircon Hf isotopes. *Gondwana Research*, *21*(2–3), 517–529. https://doi.org/10.1016/j.gr.2011.07.006

Gifford, J. N., Malone, S. J., & Mueller, P. A. (2020). The medicine hat block and the early Paleoproterozoic assembly of western Laurentia. *Geosciences*, *10*(7), 271. https://doi.org/10.3390/geosciences10070271

Godet, A., Guilmette, C., Labrousse, L., Smit, M. A., Davis, D. W., Raimondo, T., et al. (2020). Contrasting P-T-t paths reveal a metamorphic discontinuity in the New Quebec Orogen: Insights into Paleoproterozoic orogenic processes. *Precambrian Research*, *342*, 105675. https://doi.org/10.1016/j.precamres.2020.105675

Gonçalves, G. O., Lana, C., Buick, I. S., Alkmim, F. F., Scholz, R., & Queiroga, G. (2019). Twenty million years of post-orogenic fluid production and hydrothermal mineralization across the external Araçuaí orogen and adjacent São Francisco craton, SE Brazil. *Lithos*, *342–343*, 557–572. https://doi.org/10.1016/j.lithos.2019.04.022

Guitreau, M., Blichert-Toft, J., Martin, H., Mojzsis, S. J., & Albarède, F. (2012). Hafnium isotope evidence from Archean granitic rocks for deep-mantle origin of continental crust. *Earth and Planetary Science Letters*, *337–338*, 211–223. https://doi.org/10.1016/j.epsl.2012.05.029

Guo, B., Liu, S., Santosh, M., & Wang, W. (2017). Neoarchean arc magmatism and crustal growth in the north-eastern North China Craton: Evidence from granitoid gneisses in the Southern Jilin Province. *Precambrian Research*, *303*, 30–53. https://doi.org/10.1016/j.precamres.2016.12.009

Guo, B., Liu, S., Zhang, J., Wang, W., Fu, J., & Wang, M. (2016). Neoarchean Andean-type active continental margin in the northeastern North China Craton: Geochemical and geochronological evidence from metavolcanic rocks in the Jiapigou granite-greenstone belt. *Southern Jilin Province, Precambrian Research*, *285*, 147–169. https://doi.org/10.1016/j.precamres.2016.09.025

Guo, B., Liu, S., Zhang, J., & Yan, M. (2015). Zircon U–Pb–Hf isotope systematics and geochemistry of Helong granite-greenstone belt in Southern Jilin Province, China: Implications for Neoarchean crustal evolution of the northeastern margin of North China Craton. *Precambrian Research*, *271*, 254–277. https://doi.org/10.1016/j.precamres.2015.10.009

Guo, R., Hu, X., Garzanti, E., Wen, L., Yan, B., & Mark, C. (2020). How faithfully do the geochronological and geochemical signatures of detrital zircon, titanite, rutile and monazite record magmatic and metamorphic events? A case study from the Himalaya and Tibet. *Earth-Science Reviews*, *201*, 103082. https://doi.org/10.1016/j.earscirev.2020.103082

Guo, R., Liu, S., Gong, E., Wang, W., Wang, M., Fu, J., & Qin, T. (2017). Arc-generated metavolcanic rocks in the Anshan–Benxi greenstone belt, North China Craton: Constraints from geochemistry and zircon U–Pb–Hf isotopic systematics. *Precambrian Research*, *303*, 228–250. https://doi.org/10.1016/j.precamres.2017.03.028

Guo, R., Liu, S., Santosh, M., Li, Q., Bai, X., & Wang, W. (2013). Geochemistry, zircon U–Pb geochronology and Lu–Hf isotopes of metavolcanics from eastern Hebei reveal Neoarchean subduction tectonics in the North China Craton. *Gondwana Research*, *24*(2), 664–686. https://doi.org/10.1016/j.gr.2012.12.025

Guo, R., Liu, S., Wyman, D., Bai, X., Wang, W., Yan, M., & Li, Q. (2015). Neoarchean subduction: A case study of arc volcanic rocks in Qinglong-Zhuzhangzi area of the Eastern Hebei Province, North China Craton. *Precambrian Research*, *264*, 36–62. https://doi.org/10.1016/j.precamres.2015.04.007

Halpin, J. A., Gerakiteys, C. L., Clarke, G. L., Belousova, E. A., & Griffin, W. L. (2005). In-situ U–Pb geochronology and Hf isotope analyses of the Rayner Complex, east Antarctica. *Contributions to Mineralogy and Petrology*, *148*(6), 689–706. https://doi.org/10.1007/s00410-004-0627-6

Hartlaub, R. P., Heaman, L. M., Simonetti, A., & Böhm, C. O. (2006). Relicts of Earth's earliest crust: U-Pb, Lu-Hf, and morphological characteristics of >3.7 Ga detrital zircon of the western Canadian Shield. *Processes on the Early Earth*. https://doi.org/10.1130/2006.2405(05)

Hässig, M., Rolland, Y., Melis, R., Sosson, M., Galoyan, G., & Bruguier, O. (2019). P-T-T history of the Amasia and Stepanavan sub-ophiolitic metamorphic units (NW Armenia, Lesser Caucasus): Implications for metamorphic sole development and for the obduction process. *Ofioliti*, *44*, 43–70. https://doi.org/10.4454/ofioliti.v44i1.516

He, X., Wang, W., Santosh, M., Yao, J., Gao, K., Zhang, Y., et al. (2021). Late Neoarchean crustal growth under paired continental arc-back arc system in the North China Craton. *Geoscience Frontiers*, *12*(3), 101120. https://doi.org/10.1016/j.gsf.2020.12.003

Hicks, N., Elburg, M., & Andersen, T. (2015). U-Pb and Hf isotope constraints for emplacement of the Nkandla Granite, southeastern Kaapvaal Craton, South Africa. *South African Journal of Geology*, *118*(2), 119–128. https://doi.org/10.2113/gssajg.118.2.119

Hoffmann, J. E., Kröner, A., Hegner, E., Viehmann, S., Xie, H., Iaccheri, L. M., et al. (2016). Axel Hofmann, Jean Wong, Hongyan Geng, Jinhui Yang, Source composition, fractional crystallization and magma mixing processes in the 3.48–3.43Ga Tsawela tonalite suite (Ancient Gneiss Complex, Swaziland) – Implications for Palaeoarchaean geodynamics. *Precambrian Research*, *276*, 43–66. https://doi.org/10.1016/j.precamres.2016.01.026

Hoffmann, J. E., Musese, E., Kröner, A., Schneider, K. P., Wong, J., Hofmann, A., et al. (2020). Hafnium-Neodymium isotope, trace element and U-Pb zircon age constraints on the petrogenesis of the 3.44–3.46 Ga Dwalile greenstone remnant, Ancient gneiss Complex. *Swaziland, Precambrian Research*, *351*, 105970. https://doi.org/10.1016/j.precamres.2020.105970

Hofmann, A., Kröner, A., Iaccheri, L. M., Wong, J., Geng, H., & Xie, H. (2022). 3.63 Ga grey gneisses reveal the Eoarchaean history of the Zimbabwe craton. *South African Journal of Geology*, *124*, 1–12. https://doi.org/10.25131/sajg.125.0005

Hou, Z., Xiao, Y., Shen, J., & Yu, C. (2020). In situ rutile U-Pb dating based on zircon calibration using LA-ICP-MS, geological applications in the Dabie orogen, China. *Journal of Asian Earth Sciences*, *192*, 104261. https://doi.org/10.1016/j.jseaes.2020.104261

Iizuka, T., Komiya, T., Johnson, S. P., Kon, Y., Maruyama, S., & Hirata, T. (2009). Reworking of Hadean crust in the Acasta gneisses, northwestern Canada: Evidence from in-situ Lu–Hf isotope analysis of zircon. *Chemical Geology*, *259*(3–4), 230–239. https://doi.org/10.1016/j.chemgeo.2008.11.007

Janoušek, V., Holub, F. V., Verner, K., Čopjaková, R., Gerdes, A., Hora, J. M., et al. (2019). Two-pyroxene syenitoids from the Moldanubian Zone of the Bohemian Massif: Peculiar magmas derived from a strongly enriched lithospheric mantle source. *Lithos*, *342–343*, 239–262. https://doi.org/10.1016/j.lithos.2019.05.028

Jia, X., Zhai, M., Xiao, W., Li, L., Ratheesh-Kumar, R. T., Wu, J., & Liu, Y. (2020). Mesoarchean to Paleoproterozoic crustal evolution of the Taihua Complex in the southern North China Craton. *Precambrian Research*, *337*, 105451. https://doi.org/10.1016/j.precamres.2019.105451

Jia, X., Zhu, X., Zhai, M., Zhao, Y., Zhang, H., Wu, J., & Liu, T. (2016). Late Mesoarchean crust growth event: Evidence from the ca. 2.8 Ga granodioritic gneisses of the Xiaoqinling area, southern North China Craton. *Science Bulletin*, *61*(12), 974–990. https://doi.org/10.1007/s11434-016-1094-y

Jia, X.-L., Zhai, M.-G., Xiao, W.-J., Sun, Y., Ratheesh-Kumar, R. T., Yang, H., et al. (2019). Late Neoarchean to early Paleoproterozoic tectonic evolution of the southern North China Craton: Evidence from geochemistry, zircon geochronology and Hf isotopes of felsic gneisses from the Taihua complex. *Precambrian Research*, *326*, 222–239. https://doi.org/10.1016/j.precamres.2017.11.013

Jodder, J., Hofmann, A., & Ueckermann, H. (2021). 3.51 Ga old felsic volcanic rocks and carbonaceous cherts from the Gorumahisani Greenstone Belt – Insights into the Palaeoarchaean record of the Singhbhum Craton, India. *Precambrian Research*, *357*, 106109. https://doi.org/10.1016/j.precamres.2021.106109

Joe, H., & Bennett, V. C. (2016). Chondritic Lu/Hf in the early crust–mantle system as recorded by zircon populations from the oldest Eoarchean rocks of Yilgarn Craton, West Australia and Enderby Land, Antarctica. *Chemical Geology*, *427*, 125–143. https://doi.org/10.1016/j.chemgeo.2016.02.011

Kellett, D. A., Weller, O. M., Zagorevski, A., & Regis, D. (2018). A petrochronological approach for the detrital record: Tracking mm-sized eclogite clasts in the northern Canadian Cordillera. *Earth and Planetary Science Letters*, *494*, 23–31. https://doi.org/10.1016/j.epsl.2018.04.036

Kemp, A. I. S., Whitehouse, M. J., & Vervoort, J. D. (2019). Deciphering the zircon Hf isotope systematics of Eoarchean gneisses from Greenland: Implications for ancient crust-mantle differentiation and Pb isotope controversies. *Geochimica et Cosmochimica Acta*, *250*, 76–97. https://doi.org/10.1016/j.gca.2019.01.041

Koglin, N., Zeh, A., Cabral, A. R., Gomes, A. A. S., Neto, A. V. C., Brunetto, W. J., & Galbiatti, H. (2014). Depositional age and sediment source of the auriferous Moeda Formation, Quadrilátero Ferrífero of Minas Gerais, Brazil: New constraints from U–Pb–Hf isotopes in zircon and xenotime. *Precambrian Research*, *255*, 96–108. https://doi.org/10.1016/j.precamres.2014.09.010

Koglin, N., Zeh, A., Frimmel, H. E., & Gerdes, A. (2010). New constraints on the auriferous Witwatersrand sediment provenance from combined detrital zircon U–Pb and Lu–Hf isotope data for the Eldorado Reef (Central Rand Group, South Africa). *Precambrian Research*, *183*(4), 817–824. https://doi.org/10.1016/j.precamres.2010.09.009

Kooijman, E., Smit, M. A., Ratschbacher, L., & Kylander-Clark, A. R. C. (2017). A view into crustal evolution at mantle depths. *Earth and Planetary Science Letters*, *465*, 59–69. https://doi.org/10.1016/j.epsl.2017.02.032

Krabbendam, M., Bonsor, H., Horstwood, M. S. A., & Rivers, T. (2017). Tracking the evolution of the Grenvillian foreland basin: Constraints from sedimentology and detrital zircon and rutile in the Sleat and Torridon groups. *Scotland, Precambrian Research*, *295*, 67–89. https://doi.org/10.1016/j.precamres.2017.04.027

Kröner, A., Anhaeusser, C. R., Hoffmann, J. E., Wong, J., Geng, H., Hegner, E., et al. (2016). Chronology of the oldest supracrustal sequences in the Palaeoarchaean Barberton Greenstone Belt, South Africa and Swaziland. *Precambrian Research*, *279*, 123–143. https://doi.org/10.1016/j.precamres.2016.04.007

Kröner, A., Hoffmann, J. E., Xie, H., Münker, C., Hegner, E., Wan, Y., et al. (2014). Generation of early Archaean grey gneisses through melting of older crust in the eastern Kaapvaal craton, southern Africa. *Precambrian Research*, *255*, 823–846. https://doi.org/10.1016/j.precamres.2014.07.017

Kröner, A., Hoffmann, J. E., Xie, H., Wu, F., Münker, C., Hegner, E., et al. (2013). Generation of early Archaean felsic greenstone volcanic rocks through crustal melting in the Kaapvaal, craton, southern Africa. *Earth and Planetary Science Letters*, *381*, 188–197. https://doi.org/10.1016/j.epsl.2013.08.029

Kröner, A., Wong, J., & Xie, H. (2018). The oldest granite clast in the Moodies conglomerate, Barberton greenstone belt, South Africa, and its likely origin. *South African Journal of Geology*, *121*(1), 43–50. https://doi.org/10.25131/sajg.121.0001

Kuribara, Y., Tsunogae, T., Santosh, M., Takamura, Y., Costa, A. G., & Rosière, C. A. (2019). Eoarchean to Neoproterozoic crustal evolution of the Mantiqueira and the Juiz de Fora Complexes, SE Brazil: Petrology, geochemistry, zircon U-Pb geochronology and Lu-Hf isotopes. *Precambrian Research*, *323*, 82–101. https://doi.org/10.1016/j.precamres.2019.01.008

Kusiak, M. A., Dunkley, D. J., Wilde, S. A., Whitehouse, M. J., & Kemp, A. I. S. (2021). Eoarchean crust in East Antarctica: Extension from Enderby Land into Kemp Land. *Gondwana Research*, *93*, 227–241. https://doi.org/10.1016/j.gr.2020.12.031

Larson, K. P., Graziani, R., Cottle, J. M., Apen, F., Corthouts, T., & Lageson, D. (2020). The structural evolution of the Qomolangma formation, Mount Everest, Nepal. *Journal of Structural Geology*, *138*, 104123. https://doi.org/10.1016/j.jsg.2020.104123

Laurent, O., Björnsen, J., Wotzlaw, J. F., Bretscher, S., Pimenta Silva, M., Moyen, J.-F., et al. (2020). Earth's earliest granitoids are crystal-rich magma reservoirs tapped by silicic eruptions. *Nature Geoscience*, *13*(2), 163–169. https://doi.org/10.1038/s41561-019-0520-6

Laurent, O., & Zeh, A. (2015). A linear Hf isotope-age array despite different granitoid sources and complex Archean geodynamics: Example from the Pietersburg block (South Africa). *Earth and Planetary Science Letters*, *430*, 326–338. https://doi.org/10.1016/j.epsl.2015.08.028

Li, D., Hollings, P., Chen, H., Sun, X., Tan, C., & Shannon, Z. (2020). Zircon U–Pb and Lu–Hf systematics of the major terranes of the Western Superior Craton, Canada: Mantle-crust interaction and mechanism(s) of craton formation. *Gondwana Research*, *78*, 261–277. https://doi.org/10.1016/j.gr.2019.09.006

Li, X., Hu, R., Rusk, B., Xiao, R., Wang, C., & Yang, F. (2013). U–Pb and Ar–Ar geochronology of the Fujiawu porphyry Cu–Mo deposit, Dexing district, Southeast China: Implications for magmatism, hydrothermal alteration, and mineralization. *Journal of Asian Earth Sciences*, *74*, 330–342. https://doi.org/10.1016/j.jseaes.2013.04.012

Li, X.-Y., Li, S., Wang, T.-S., Dong, Y., Liu, X.-G., Zhao, S.-J., et al. (2020). Geochemistry and detrital zircon records of the Ruyang-Luoyu groups, southern North China Craton: Provenance, crustal evolution and Paleo–Mesoproterozoic tectonic implications. *Geoscience Frontiers*, *11*(2), 679–696. https://doi.org/10.1016/j.gsf.2019.08.003

Li, Y., Zheng, J., Xiao, W., Wang, G., & Brouwer, F. M. (2019). Circa 2.5 Ga granitoids in the eastern North China craton: Melting from ca. 2.7 Ga accretionary crust. *The Geological Society of America Bulletin*, *132*(3–4), 817–834. https://doi.org/10.1130/B35091.1

Li, Z., Wei, C., Chen, B., Fu, B., & Gong, M. (2020). Late Neoarchean reworking of the Mesoarchean crustal remnant in northern Liaoning, North China Craton: A U–Pb–Hf–O–Nd perspective. *Gondwana Research*, *80*, 350–369. https://doi.org/10.1016/j.gr.2019.10.020

Li, Z., Wei, C., Chen, B., Zhang, W., & Yang, F. (2021). U–Pb–Hf–O–Nd isotopic and geochemical constraints on the origin of Archean TTG gneisses from the North China Craton: Implications for crustal growth. *Precambrian Research*, *354*, 106078. https://doi.org/10.1016/j.precamres.2020.106078

Lie, X., fu, B., Li, Q., Zhao, Y., Liu, J., & Chen, H. (2020). The impact of Pan-African-aged tectonothermal event on high-grade rocks at Mount Brown, East Antarctica. *Antarctic Science*, *32*(1), 45–57. https://doi.org/10.1017/S0954102019000518

Liou, P., Cui, X., Guo, J., & Zhai, M. (2020). Possible link between the oldest supracrustal unit and the oldest rock unit of China. *Precambrian Research*, *342*, 105672. https://doi.org/10.1016/j.precamres.2020.105672

Liou, P., & Guo, J. (2019). Deciphering the Mesoarchean to Neoarchean history of crustal growth and recycling in the Caochang region of the Eastern Hebei Province, North China Craton using combined zircon U–Pb and Lu-Hf isotope analysis. *Lithos*, *334–335*, 281–294. https://doi.org/10.1016/j.lithos.2019.03.013

Liou, P., Guo, J., Mitchell, R. N., Spencer, C. J., Li, X., Zhai, M., et al. (2022). Zircons underestimate mantle depletion of early Earth. *Geochimica et Cosmochimica Acta*, *317*, 538–551. https://doi.org/10.1016/j.gca.2021.11.015

Liu, B., Han, B.-F., Zhao, X., Ren, R., Zhang, J.-R., Zhou, J., et al. (2016). The Cambrian initiation of intra-oceanic subduction in the southern Paleo-Asian Ocean: Further evidence from the Barleik subduction-related metamorphic complex in the West Junggar region, NW China. *Journal of Asian Earth Sciences*, *123*, 1–21. https://doi.org/10.1016/j.jseaes.2016.03.015

Liu, C., Zhao, G., Liu, F., & Shi, J. (2014). Geochronological and geochemical constraints on the Lüliang Group in the Lüliang Complex: Implications for the tectonic evolution of the Trans-North China Orogen. *Lithos*, *198–199*, 298–315. https://doi.org/10.1016/j.lithos.2014.04.003

Liu, C., Zhao, G., Sun, M., Zhang, J., & Yin, C. (2012). U–Pb geochronology and Hf isotope geochemistry of detrital zircons from the Zhongtiao Complex: Constraints on the tectonic evolution of the Trans-North China Orogen. *Precambrian Research*, *222–223*, 159–172. https://doi.org/10.1016/j.precamres.2011.08.007

Liu, D., Wilde, S. A., Wan, Y., Wu, J., Zhou, H., Dong, C., & Yin, X. (2008). New U-Pb and Hf isotopic data confirm Anshan as the oldest preserved segment of the North China Craton. *American Journal of Science*, *308*(3), 200–231. https://doi.org/10.2475/03.2008.02

Liu, H., Wang, W., Cawood, P. A., Mu, Y., Yao, J., Li, J., & Guo, L. (2020). Synchronous late Neoarchean Na- and K-rich granitoid magmatism at an active continental margin in the Eastern Liaoning Province of North China Craton. *Lithos*, *376–377*, 105770. https://doi.org/10.1016/j.lithos.2020.105770

Liu, J., Liu, F., Ding, Z., Liu, C., Yang, H., Liu, P., et al. (2013). The growth, reworking and metamorphism of early Precambrian crust in the Jiaobei terrane, the North China Craton: Constraints from U–Th–Pb and Lu–Hf isotopic systematics, and REE concentrations of zircon from Archean granitoid gneisses. *Precambrian Research*, *224*, 287–303. https://doi.org/10.1016/j.precamres.2012.10.003

Liu, L., Yang, X., Santosh, M., & Aulbach, S. (2015). Neoarchean to Paleoproterozoic continental growth in the southeastern margin of the North China Craton: Geochemical, zircon U–Pb and Hf isotope evidence from the Huoqiu complex. *Gondwana Research*, *28*(3), 1002–1018. https://doi.org/10.1016/j.gr.2014.08.011

Liu, L., Yang, X., Santosh, M., Zhao, G., & Aulbach, S. (2016). U–Pb age and Hf isotopes of detrital zircons from the Southeastern North China Craton: Meso- to Neoarchean episodic crustal growth in a shifting tectonic regime. *Gondwana Research*, *35*, 1–14. https://doi.org/10.1016/j.gr.2016.03.017

Liu, S., Wang, M., Wan, Y., Guo, R., Wang, W., Wang, K., et al. (2017). A reworked ~3.45 Ga continental microblock of the North China Craton: Constraints from zircon U-Pb-Lu-Hf isotopic systematics of the Archean Beitai-Waitoushan migmatite-syenogranite complex. *Precambrian Research*, *303*, 332–354. https://doi.org/10.1016/j.precamres.2017.04.003

Lu, Y., Wingate, M. T. D., Romano, S. S., Mole, D. R., Kirkland, C. L., Kemp, A. I. S., et al. (2021). Zircon Lutetium-hafnium isotope map of Western Australia, digital data layer. Retrieved from www.dmirs.wa.gov.au/geoview

Lv, B., Zhai, M., Li, T., & Peng, P. (2012). Zircon U–Pb ages and geochemistry of the Qinglong volcano-sedimentary rock series in Eastern Hebei: Implication for ~2500 Ma intra-continental rifting in the North China Craton. *Precambrian Research*, *208–211*, 145–160. https://doi.org/10.1016/j.precamres.2012.04.002

Ma, Q., Xu, Y.-G., Huang, X.-L., Zheng, J.-P., Ping, X., & Xia, X.-P. (2020). Eoarchean to Paleoproterozoic crustal evolution in the North China Craton: Evidence from U-Pb and Hf-O isotopes of zircons from deep-crustal xenoliths. *Geochimica et Cosmochimica Acta*, *278*, 94–109. https://doi.org/10.1016/j.gca.2019.09.009

Madlakana, N., Stevens, G., & Bracciali, L. (2020). Paleoproterozoic amphibolite facies retrogression and exhumation of Archean metapelitic granulites in the Southern Marginal Zone of the Limpopo Belt, South Africa. *Precambrian Research*, *337*, 105532. https://doi.org/10.1016/j.precamres.2019.105532

Mark, C., Cogné, N., & Chew, D. (2016). Tracking exhumation and drainage divide migration of the Western Alps: A test of the apatite U-Pb thermochronometer as a detrital provenance tool. *The Geological Society of America Bulletin*, *128*(9–10), 1439–1460. https://doi.org/10.1130/B31351.1

Martins, L., Lana, C., Mazoz, A., & Novo, T. (2022). Chemical-abrasion U-Pb zircon geochronology reveals 150 Myr of partial melting events in the Archean crust of the São Francisco Craton. *Geoscience Frontiers*, *13*(5), 101289. https://doi.org/10.1016/j.gsf.2021.101289

McIntyre, T., Waterton, P., Vezinet, A., Szilas, K., & Pearson, D. G. (2021). Extent and age of Mesoarchean components in the Nagssugtoqidian orogen, West Greenland: Implications for tectonic environments and crust building in cratonic orogenic belts. *Lithos*, *396–397*, 106182. https://doi.org/10.1016/j.lithos.2021.106182

Medaris, L. G., Brueckner, H. K., Cai, Y., Griffin, W. L., & Janák, M. (2018). Eclogites in peridotite massifs in the Western Gneiss Region, Scandinavian Caledonides: Petrogenesis and comparison with those in the Variscan Moldanubian Zone. *Lithos*, *322*, 325–346. https://doi.org/10.1016/j.lithos.2018.10.013

Meinhold, G., Morton, A. C., Fanning, C. M., & Whitham, A. G. (2011). U-Pb SHRIMP ages of detrital granulite-facies rutiles: Further constraints on provenance of Jurassic sandstone on the Norwegian margin. *Geological Magazine*, *148*(3), 473–480. https://doi.org/10.1017/S0016756810000877

Meng, E., Liu, F.-L., Cui, Y., & Jia, C. (2013). Zircon U–Pb and Lu–Hf isotopic and whole-rock geochemical constraints on the protolith and tectonic history of the Changhai metamorphic supracrustal sequence in the Jiao–Liao–Ji Belt, southeast Liaoning Province, northeast China. *Precambrian Research*, *233*, 297–315. https://doi.org/10.1016/j.precamres.2013.05.004

Meng, E., Liu, F.-L., Liu, J.-H., Liu, P.-H., Cui, Y., Liu, C.-H., et al. (2013). Zircon U–Pb and Lu–Hf isotopic constraints on Archean crustal evolution in the Liaonan Complex of northeast China. *Lithos*, *177*, 164–183. https://doi.org/10.1016/j.lithos.2013.06.020

Meng, F., Tian, Y., Kerr, A. C., Wang, Q., Chen, Y., Zhou, Y., & Yang, F. (2022). Neoarchean reworking of Mesoarchean and Paleoarchean crust (3.4 ~ 3.0 Ga) within the North China Craton: Constraints from zircon U-Pb geochronology and Lu-Hf isotopes from the basement of the Bohai Bay Basin. *Precambrian Research*, *369*, 106497. https://doi.org/10.1016/j.precamres.2021.106497

Meng, X., Richards, J., Mao, J., Ye, H., DuFrane, S. A., Creaser, R., et al. (2020). The Tongkuangyu Cu deposit, trans-north china orogen: A metamorphosed Paleoproterozoic porphyry Cu deposit. *Economic Geology*, *115*(1), 51–77. https://doi.org/10.5382/econgeo.4693

Mitra, A., Dey, S., Zong, K., Liu, Y., & Mitra, A. (2019). Building the core of a Paleoarchean continent: Evidence from granitoids of Singhbhum Craton, eastern India. *Precambrian Research*, *335*, 105436. https://doi.org/10.1016/j.precamres.2019.105436

Moghadam, H. S., Corfu, F., Stern, R. J., & Lotfi Bakhsh, A. (2019). The Eastern Khoy metamorphic complex of NW Iran: A Jurassic ophiolite or continuation of the Sanandaj–Sirjan Zone? *Journal of the Geological Society*, *176*(3), 517–529. https://doi.org/10.1144/jgs2018-081

Mole, D. R., Kirkland, C. L., Fiorentini, M. L., Barnes, S. J., Cassidy, K. F., Isaac, C., et al. (2019). Time-space evolution of an Archean craton: A Hf-isotope window into continent formation. *Earth-Science Reviews*, *196*, 102831. https://doi.org/10.1016/j.earscirev.2019.04.003

Mole, D. R., Thurston, P. C., Marsh, J. H., Stern, R. A., Ayer, J. A., Martin, L. A. J., & Lu, Y. J. (2021). The formation of Neoarchean continental crust in the south-east Superior Craton by two distinct geodynamic processes. *Precambrian Research*, *356*, 106104. https://doi.org/10.1016/j.precamres.2021.106104

Moore, J., Beinlich, A., Porter, J. K., Talavera, C., Berndt, J., Piazolo, S., et al. (2020). Microstructurally controlled trace element (Zr, U–Pb) concentrations in metamorphic rutile: An example from the amphibolites of the Bergen Arcs. *Journal of Metamorphic Geology*, *38*(1), 103–127. https://doi.org/10.1111/jmg.12514

Moreira, H., Cassino, L., Lana, C., Storey, C., & Albert, C. (2019). Insights into orogenic processes from drab schists and minor intrusions: Southern São Francisco Craton, Brazil. *Lithos*, *346–347*, 105146. https://doi.org/10.1016/j.lithos.2019.07.013

Moreira, H., Lana, C., & Nalini, H. A. (2016). The detrital zircon record of an Archaean convergent basin in the Southern São Francisco Craton, Brazil. *Precambrian Research*, *275*, 84–99. https://doi.org/10.1016/j.precamres.2015.12.015

Moreira Santos, M., Lana, C., Scholz, R., Buick, I. S., Kamo, S. L., Corfu, F., & Queiroga, G. (2020). LA-ICP-MS U–Pb dating of rutiles associated with hydrothermal mineralization along the southern Araçuaí Belt, SE Brazil. *Journal of South American Earth Sciences*, *99*, 102502. https://doi.org/10.1016/j.jsames.2020.102502

Moyen, J. F., Zeh, A., Cuney, M., Dziggel, A., & Carrouée, S. (2021). The multiple ways of recycling Archaean crust: A case study from the ca. 3.1 Ga granitoids from the Barberton Greenstone Belt, South Africa. *Precambrian Research*, *353*, 105998. https://doi.org/10.1016/j.precamres.2020.105998

Mueller, P. A., & Wooden, J. L. (2012). Trace element and Lu-Hf systematics in Hadean-Archean detrital zircons: Implications for crustal evolution. *The Journal of Geology*, *120*(1), 15–29. https://doi.org/10.1086/662719

Müller, S., Dziggel, A., Sindern, S., Kokfelt, T. F., Gerdes, A., & Kolb, J. (2018). Age and temperature-time evolution of retrogressed eclogite-facies rocks in the Paleoproterozoic Nagssugtoqidian Orogen, South-East Greenland: Constrained from U-Pb dating of zircon, monazite, titanite and rutile. *Precambrian Research*, *314*, 468–486. https://doi.org/10.1016/j.precamres.2018.07.002

Najman, Y., Mark, C., Barfod, D. N., Carter, A., Parrish, R., Chew, D., & Gemignani, L. (2019). Spatial and temporal trends in exhumation of the Eastern Himalaya and syntaxis as determined from a multitechnique detrital thermochronological study of the Bengal Fan. *The Geological Society of America Bulletin*, *131*(9–10), 1607–1622. https://doi.org/10.1130/B35031.1

Næraa, T., Scherstén, A., Rosing, M., Kemp, A. I. S., Hoffmann, J. E., Kokfelt, T. F., & Whitehouse, M. J. (2012). Hafnium isotope evidence for a transition in the dynamics of continental growth 3.2 Gyr ago. *Nature*, *485*(7400), 627–630. https://doi.org/10.1038/nature11140

Nebel-Jacobsen, Y., Münker, C., Nebel, O., Gerdes, A., Mezger, K., & Nelson, D. R. (2010). Reworking of Earth's first crust: Constraints from Hf isotopes in Archean zircons from Mt. Narryer, Australia. *Precambrian Research*, *182*(3), 175–186. https://doi.org/10.1016/j.precamres.2010.07.002

Nutman, A. P., Bennett, V. C., Friend, C. R. L., Yi, K., & Lee, S. R. (2015). Mesoarchaean collision of Kapisilik terrane 3070 Ma juvenile arc rocks and >3600 Ma Isukasia terrane continental crust (Greenland). *Precambrian Research*, *258*, 146–160. https://doi.org/10.1016/j.precamres.2014.12.013

Odlum, M. L., Stockli, D. F., Capaldi, T. N., Thomson, K. D., Clark, J., Puigdefàbregas, C., & Fildani, A. (2019). Tectonic and sediment provenance evolution of the South Eastern Pyrenean foreland basins during rift margin inversion and orogenic uplift. *Tectonophysics*, *765*, 226–248. https://doi.org/10.1016/j.tecto.2019.05.008

Okay, N., Zack, T., Okay, A. I., & Barth, M. (2011). Sinistral transport along the Trans-European Suture Zone: Detrital Zircon-Rutile Geochronology and Sanstone Petrography from Carboniferous flysch of the Pontides. *Geological Magazine*, *148*(3), 380–403. https://doi.org/10.1017/S0016756810000804

Olierook, H. K. H., Agangi, A., Plavsa, D., Reddy, S. M., Yao, W., Clark, C., et al. (2019). Neoproterozoic hydrothermal activity in the West Australian Craton related to Rodinia assembly or breakup? *Gondwana Research*, *68*, 1–12. https://doi.org/10.1016/j.gr.2018.10.019

Olierook, H. K. H., Clark, C., Reddy, S. M., Mazumder, R., Jourdan, F., & Evans, N. J. (2019). Evolution of the Singhbhum Craton and supracrustal provinces from age, isotopic and chemical constraints. *Earth-Science Reviews*, *193*, 237–259. https://doi.org/10.1016/j.earscirev.2019.04.020

Oliveira, E. P., McNaughton, N. J., Zincone, S. A., & Talavera, C. (2020). Birthplace of the São Francisco Craton, Brazil: Evidence from 3.60 to 3.64 Ga Gneisses of the Mairi Gneiss Complex. *Terra Nova*, *32*(4), 281–289. https://doi.org/10.1111/ter.12460

Oliveira, E. P., Talavera, C., Windley, B. F., Zhao, L., Semprich, J. J., McNaughton, N. J., et al. (2019). Mesoarchaean (2820 Ma) high-pressure mafic granulite at Uauá, São Francisco Craton, Brazil, and its potential significance for the assembly of Archaean supercratons. *Precambrian Research*, *331*, 105366. https://doi.org/10.1016/j.precamres.2019.105366

O'Sullivan, G. J., Chew, D. M., & Samson, S. D. (2016). Detecting magma-poor orogens in the detrital record. *Geology*, *44*(10), 871–874. https://doi.org/10.1130/G38245.1

Pandey, O. P., Mezger, K., Ranjan, S., Upadhyay, D., Villa, I. M., Nägler, T. F., & Vollstaedt, H. (2019). Genesis of the Singhbhum Craton, eastern India; implications for Archean crust-mantle evolution of the Earth. *Chemical Geology*, *512*, 85–106. https://doi.org/10.1016/j.chemgeo.2019.02.040

Pe-Piper, G., Nagle, J., Piper, D. J. W., & McFarlane, C. R. M. (2019). Geochronology and trace element mobility in rutile from a Carboniferous syenite pegmatite and the role of halogens. *American Mineralogist*, *104*(4), 501–513. https://doi.org/10.2138/am-2019-6668

Pereira, I., Storey, C., Darling, J., Lana, C., & Alkmim, A. R. (2019). Two billion years of evolution enclosed in hydrothermal rutile: Recycling of the São Francisco Craton Crust and constraints on gold remobilisation processes. *Gondwana Research*, *68*, 69–92. https://doi.org/10.1016/j.gr.2018.11.008

Pereira, I., Storey, C. D., Strachan, R. A., dos Santos, T. B., & Darling, J. R. (2020). Detrital rutile ages can deduce the tectonic setting of sedimentary basins. *Earth and Planetary Science Letters*, *537*, 116193. https://doi.org/10.1016/j.epsl.2020.116193

Pi, Q., Hu, R., Xiong, B., Li, Q., & Zhong, R. (2017). In situ SIMS U-Pb dating of hydrothermal rutile: Reliable age for the Zhesang Carlin-type gold deposit in the golden triangle region, SW China. *Mineralium Deposita*, *52*(8), 1179–1190. https://doi.org/10.1007/s00126-017-0715-y

Picazo, S. M., Ewing, T. A., & Müntener, O. (2019). Paleocene metamorphism along the Pennine–Austroalpine suture constrained by U–Pb dating of titanite and rutile (Malenco, Alps). *Swiss Journal of Geosciences*, *112*(2–3), 517–542. https://doi.org/10.1007/s00015-019-00346-1

Pietranik, A. B., Hawkesworth, C. J., Storey, C. D., Kemp, A. I. S., Sircombe, K. N., Whitehouse, M. J., & Bleeker, W. (2008). Episodic, mafic crust formation from 4.5 to 2.8 Ga: New evidence from detrital zircons, Slave craton, Canada. *Geology*, *36*(11), 875–878. https://doi.org/10.1130/G24861A.1

Ping, X., Zheng, J., Tang, H., Ma, Q., Griffin, W. L., Xiong, Q., & Su, Y. (2018). Hadean continental crust in the southern North China Craton: Evidence from the Xinyang felsic granulite xenoliths. *Precambrian Research*, *307*, 155–174. https://doi.org/10.1016/j.precamres.2017.10.011

Polat, A., Frei, R., Deng, H., Yang, X.-M., & Sotiriou, P. (2022). Anatomy of a Neoarchean continental arc-backarc system in the Cross Lake-Pipestone Lake region, northwestern Superior Province, Canada. *Precambrian Research*, *370*, 106556. https://doi.org/10.1016/j.precamres.2021.106556

Ragozin, A. L., Zedgenizov, D. A., Shatskii, V. S., Orihashi, Y., Agashev, A. M., & KAgi, H. (2014). U-Pb age of rutile from the eclogite xenolith of the Udachnaya kimberlite pipe. *Doklady Earth Sciences*, *457*(1), 861–864. https://doi.org/10.1134/S1028334X14070162

Ranjan, S., Upadhyay, D., Pruseth, K. L., & Nanda, J. K. (2020). Detrital zircon evidence for change in geodynamic regime of continental crust formation 3.7–3.6 billion years ago. *Earth and Planetary Science Letters*, *538*, 116206. https://doi.org/10.1016/j.epsl.2020.116206

Reimink, J. R., Pearson, D. G., Shirey, S. B., Carlson, R. W., & Ketchum, J. W. F. (2019). Onset of new, progressive crustal growth in the central Slave craton at 3.55 Ga. *Geochemical Perspectives Letters*, *10*, 8–13. https://doi.org/10.7185/geochemlet.1907

Reinhardt, J., Elburg, M. A., & Andersen, T. (2015). Zircon U-PB age data and HF isotopic signature of Kaapvaal basement granitoids from the Archaean White Mfolozi Inlier, northern KwaZulu-Natal. *South African Journal of Geology*, *118*(4), 473–488. https://doi.org/10.2113/gssajg.118.4.473

Roberts, N. M. W., Thomas, R. J., & Jacobs, J. (2016). Geochronological constraints on the metamorphic sole of the Semail ophiolite in the United Arab Emirates. *Geoscience Frontiers*, *7*(4), 609–619. https://doi.org/10.1016/j.gsf.2015.12.003

Rösel, D., David Boger, S., Möller, A., Gaitzsch, B., Barth, M., Oalmann, J., & Zack, T. (2014). Indo-Antarctic derived detritus on the northern margin of Gondwana: Evidence for continental-scale sediment transport. *Terra Nova*, *26*(1), 64–71. https://doi.org/10.1111/ter.12070

Rösel, D., Zack, T., & Boger, S. D. (2014). LA-ICP-MS U–Pb dating of detrital rutile and zircon from the Reynolds Range: A window into the Palaeoproterozoic tectonosedimentary evolution of the North Australian Craton. *Precambrian Research*, *255*, 381–400. https://doi.org/10.1016/j.precamres.2014.10.006

Rösel, D., Zack, T., & Möller, A. (2019). Interpretation and significance of combined trace element and U–Pb isotopic data of detrital rutile: A case study from late Ordovician sedimentary rocks of Saxo-Thuringia, Germany. *International Journal of Earth Sciences*, *108*, 1–25. https://doi.org/10.1007/s00531-018-1643-5

Satkoski, A. M., Bickford, M. E., Samson, S. D., Bauer, R. L., Mueller, P. A., & Kamenov, G. D. (2013). Geochemical and Hf–Nd isotopic constraints on the crustal evolution of Archean rocks from the Minnesota River Valley, USA. *Precambrian Research*, *224*, 36–50. https://doi.org/10.1016/j.precamres.2012.09.003

Schmitt, A. K., Zack, T., Kooijman, E., Logvinova, A. M., & Sobolev, N. V. (2019). U–Pb ages of rare rutile inclusions in diamond indicate entrapment synchronous with kimberlite formation. *Lithos*, *350–351*, 105251. https://doi.org/10.1016/j.lithos.2019.105251

Shaanan, U., Avigad, D., Morag, N., Güngör, T., & Gerdes, A. (2020). Drainage response to Arabia–Eurasia collision: Insights from provenance examination of the Cyprian Kythrea flysch (Eastern Mediterranean Basin). *Basin Research*, *33*(1), 26–47. https://doi.org/10.1111/bre.12452

Shi, G., Li, X., Li, Q., Chen, Z., Deng, J., Liu, Y., et al. (2012). Ion microprobe U-Pb age and Zr-in-rutile thermometry of rutiles from the Daixian rutile deposit in the Hengshan Mountains, Shanxi Province, China. *Economic Geology*, *107*(3), 525–535. https://doi.org/10.2113/econgeo.107.3.525

Skublov, S. G., Zack, T., Berezin, A. V., Mel'nik, A. E., & Rizvanova, N. G. (2013). In situ LA-ICP-MS investigation of the geochemistry and U-Pb age of rutile from the rocks of the Belomorian mobile belt. *Geochemistry International*, *51*(2), 164–171. https://doi.org/10.1134/S0016702912120051

Small, D., Parrish, R. R., Austin, W. E. N., Cawood, P. A., & Rinterknecht, V. (2013). Provenance of North Atlantic ice-rafted debris during the last deglaciation—A new application of U-Pb rutile and zircon geochronology. *Geology*, *41*(2), 155–158. https://doi.org/10.1130/G33594.1

Smit, M. A., Ratschbacher, L., Kooijman, E., & Stearns, M. A. (2014). Early evolution of the Pamir deep crust from Lu-Hf and U-Pb geochronology and garnet thermometry. *Geology*, *42*(12), 1047–1050. https://doi.org/10.1130/G35878.1

Smye, A. J., Lavier, L. L., Zack, T., & Stockli, D. F. (2019). Episodic heating of continental lower crust during extension: A thermal modeling investigation of the Ivrea-Verbano Zone. *Earth and Planetary Science Letters*, *521*, 158–168. https://doi.org/10.1016/j.epsl.2019.06.015

Smye, A. J., Marsh, J. H., Vermeesch, P., Garber, J. M., & Stockli, D. F. (2018). Applications and limitations of U-Pb thermochronology to middle and lower crustal thermal histories. *Chemical Geology*, *494*, 1–18. https://doi.org/10.1016/j.chemgeo.2018.07.003

Smye, A. J., & Stockli, D. F. (2014). Rutile U–Pb age depth profiling: A continuous record of lithospheric thermal evolution. *Earth and Planetary Science Letters*, *408*, 171–182. https://doi.org/10.1016/j.epsl.2014.10.013

Soares, M. B., Neto, A. V. C., & Fabricio-Silva, W. (2020). The development of a Meso- to Neoarchean rifting-convergence-collision-collapse cycle over an ancient thickened protocontinent in the south São Francisco craton, Brazil. *Gondwana Research*, *77*, 40–66. https://doi.org/10.1016/j.gr.2019.06.017

Sorokina, E. S., Rösel, D., Häger, T., Mertz-Kraus, R., & Saul, J. M. (2017). LA-ICP-MS U–Pb dating of rutile inclusions within corundum (ruby and sapphire): New constraints on the formation of corundum deposits along the Mozambique belt. *Mineralium Deposita*, *52*(5), 641–649. https://doi.org/10.1007/s00126-017-0732-x

Sreenivas, B., Dey, S., Bhaskar Rao, Y. J., Kumar, T. V., Babu, E., & Williams, I. S. (2019). A new cache of Eoarchaean detrital zircons from the Singhbhum craton, eastern India and constraints on early Earth geodynamics. *Geoscience Frontiers*, *10*(4), 1359–1370. https://doi.org/10.1016/j.gsf.2019.02.001

Strong, J. W. D., Cawood, P. A., Cruden, A. R., Nebel, O., Mulder, J., & Dickin, A. P. (2022). Forging isotopically juvenile metamorphic zircon from and within Archean TTG gneiss: Whole-rock Sr-Nd-Pb and zircon U-Pb-Hf-REE constraints. *Chemical Geology*, *590*, 120710. https://doi.org/10.1016/j.chemgeo.2022.120710

Sukhanov, M. K., Mitrofanov, F. P., Bayanova, T. B., & Chistyakov, A. V. (2016). U-Pb isotopic study of the gabbronorite–anorthosite drusite (coronite) body of Vorony Island (Kandalaksha Archipelago, the White Sea). *Petrology*, *24*(1), 75–83. https://doi.org/10.1134/S0869591116010069

Sun, D., Li, Q., Liu, S., Chen, X., Wang, Z., Chen, Y., et al. (2019). Neoarchean-Paleoproterozoic magmatic arc evolution in the Wutai-Hengshan-Fuping area, North China Craton: New perspectives from zircon U–Pb ages and Hf isotopic data. *Precambrian Research*, *331*, 105368. https://doi.org/10.1016/j.precamres.2019.105368

Sun, J.-F., Yang, J.-H., Wu, F.-Y., & Wilde, S. A. (2012). Precambrian crustal evolution of the eastern North China Craton as revealed by U–Pb ages and Hf isotopes of detrital zircons from the Proterozoic Jing'eryu Formation. *Precambrian Research*, *200–203*, 184–208. https://doi.org/10.1016/j.precamres.2012.01.018

Sun, Q., Zhou, Y., Zhao, T., & Wang, W. (2017). Geochronology and geochemistry of the Paleoproterozoic Yinyugou Group in the southern North China Craton: Implications for provenance and tectonic evolution. *Precambrian Research*, *296*, 120–147. https://doi.org/10.1016/j.precamres.2017.04.012

Tamblyn, R., Zack, T., Schmitt, A. K., Hand, M., Kelsey, D., Morrissey, L., et al. (2019). Blueschist from the Mariana forearc records long-lived residence of material in the subduction channel. *Earth and Planetary Science Letters*, *519*, 171–181. https://doi.org/10.1016/j.epsl.2019.05.013

Tang, L., Santosh, M., Tsunogae, T., & Teng, X.-M. (2016b). Late Neoarchean arc magmatism and crustal growth associated with microblock amalgamation in the North China Craton: Evidence from the Fuping Complex. *Lithos*, *248–251*, 324–338. https://doi.org/10.1016/j.lithos.2016.01.022

Tappe, S., Kjarsgaard, B. A., Kurszlaukis, S., Nowell, G. M., & Phillips, D. (2014). Petrology and Nd–Hf isotope geochemistry of the Neoproterozoic Amon kimberlite sills, Baffin Island (Canada): Evidence for deep mantle magmatic activity linked to supercontinent cycles. *Journal of Petrology*, *55*(10), 2003–2042. https://doi.org/10.1093/petrology/egu048

Taylor, J., Zeh, A., & Gerdes, A. (2016). U–Pb–Hf isotope systematics of detrital zircons in high-grade paragneisses of the Ancient Gneiss Complex, Swaziland: Evidence for two periods of juvenile crust formation, Paleo- and Mesoarchaean sediment deposition, and 3.23 Ga terrane accretion. *Precambrian Research*, *280*, 205–220. https://doi.org/10.1016/j.precamres.2016.05.012

Teles, G., Chemale, F., & de Oliveira, C. G. (2015). Paleoarchean record of the detrital pyrite-bearing, Jacobina Au–U deposits, Bahia, Brazil. *Precambrian Research*, *256*, 289–313. https://doi.org/10.1016/j.precamres.2014.11.004

Teles, G. S., Chemale, F., Ávila, J. N., & Ireland, T. R. (2022). The Paleoarchean Northern Mundo Novo Greenstone Belt, São Francisco Craton: Geochemistry, U–Pb–Hf–O in zircon and pyrite δ34S-Δ33S-Δ36S signatures. *Geoscience Frontiers*, *13*(5), 101252. https://doi.org/10.1016/j.gsf.2021.101252

Tong, X., Wang, C., Peng, Z., Huang, H., Zhang, L., & Zhai, M. (2019). Geochemistry of meta-sedimentary rocks associated with the Neoarchean Dagushan BIF in the Anshan-Benxi area, North China Craton: Implications for their provenance and tectonic setting. *Precambrian Research*, *325*, 172–191. https://doi.org/10.1016/j.precamres.2019.02.022

Triantafyllou, J. B., Baele, J.-M., Bruguier, O., Diot, H., Ennih, N., Monnier, C., et al. (2018). Intra-oceanic arc growth driven by magmatic and tectonic processes recorded in the Neoproterozoic Bougmane arc complex (Anti-Atlas, Morocco). *Precambrian Research*, *304*, 39–63. https://doi.org/10.1016/j.precamres.2017.10.022

Újvári, G., Klötzli, U., Kiraly, F., & Ntaflos, T. (2013). Towards identifying the origin of metamorphic components in Austrian loess: Insights from detrital rutile chemistry, thermometry and U–Pb geochronology. *Quaternary Science Reviews*, *75*, 132–142. https://doi.org/10.1016/j.quascirev.2013.06.002

Upadhyay, D., Chattopadhyay, S., & Mezger, K. (2019). Formation of Paleoarchean-Mesoarchean Na-rich (TTG) and K-rich granitoid crust of the Singhbhum craton, eastern India: Constraints from major and trace element geochemistry and Sr-Nd-Hf isotope composition. *Precambrian Research*, *327*, 255–272. https://doi.org/10.1016/j.precamres.2019.04.009

Uzel, J., Lagabrielle, Y., Fourcade, S., Chopin, C., Monchoux, P., Clerc, C., & Poujol, M. (2020). The sapphirine-bearing rocks in contact with the Lherz peridotite body: New mineralogical data, age and interpretation. *BSGF – Earth Science Bulletin*, *191*, 28. https://doi.org/10.1051/bsgf/2019015

Van Kranendonk, M. J., Kröner, A., Hoffmann, J. E., Nagel, T., & Anhaeusser, C. R. (2014). Just another drip: Re-analysis of a proposed Mesoarchean suture from the Barberton Mountain Land, South Africa. *Precambrian Research*, *254*, 19–35. https://doi.org/10.1016/j.precamres.2014.07.022

van Schijndel, V., Stevens, G., Lana, C., Zack, T., & Frei, D. (2021). De Kraalen and Witrivier Greenstone Belts, Kaapvaal Craton, South Africa: Characterisation of the Palaeo-Mesoarchaean evolution by rutile and zircon U-Pb geochronology combined with Hf isotopes. *South African Journal of Geology*, *124*(1), 17–36. https://doi.org/10.25131/sajg.124.0011

van Schijndel, V., Stevens, G., Zeh, A., Frei, D., & Lana, C. (2017). Zircon geochronology and Hf isotopes of the Dwalile Supracrustal Suite, Ancient Gneiss Complex, Swaziland: Insights into the diversity of Palaeoarchaean source rocks, depositional and metamorphic ages. *Precambrian Research*, *295*, 48–66. https://doi.org/10.1016/j.precamres.2017.04.025

Vezinet, A., Pearson, D. G., Heaman, L. M., Sarkar, C., & Stern, R. A. (2020). Early crustal evolution of the Superior craton – A U–Pb, Hf and O isotope study of zircon from the Assean lake complex and a comparison to early crust in other cratons. *Lithos*, *368–369*, 105600. https://doi.org/10.1016/j.lithos.2020.105600

Vezinet, A., Pearson, D. G., Thomassot, E., Stern, R. A., Sarkar, C., Luo, Y., & Fisher, C. M. (2018). Hydrothermally-altered mafic crust as source for early Earth TTG: Pb/Hf/O isotope and trace element evidence in zircon from TTG of the Eoarchean Saglek Block, N. Labrador. *Earth and Planetary Science Letters*, *503*, 95–107. https://doi.org/10.1016/j.epsl.2018.09.015

Walsh, A. K., Raimondo, T., Kelsey, D. E., Hand, M., Pfitzner, H. L., & Clark, C. (2013). Duration of high-pressure metamorphism and cooling during the intraplate Petermann Orogeny. *Gondwana Research*, *24*(3–4), 969–983. https://doi.org/10.1016/j.gr.2012.09.006

Wan, Y., Dong, C., Wang, S., Kröner, A., Xie, H., Ma, M., et al. (2014). Middle Neoarchean magmatism in western Shandong, North China Craton: SHRIMP zircon dating and LA-ICP-MS Hf isotope analysis. *Precambrian Research*, *255*, 865–884. https://doi.org/10.1016/j.precamres.2014.07.016

Wan, Y., Xie, S., Yang, C., Kröner, A., Ma, M., Dong, C., et al. (2014). Early Neoarchean (~2.7 Ga) tectono-thermal events in the North China Craton: A synthesis. *Precambrian Research*, *247*, 45–63. https://doi.org/10.1016/j.precamres.2014.03.01

Wang, A.-D., Liu, Y.-C., Gu, X.-F., Hou, Z.-H., & Song, B. (2012). Late-Neoarchean magmatism and metamorphism at the southeastern margin of the North China Craton and their tectonic implications. *Precambrian Research*, *220–221*, 65–79. https://doi.org/10.1016/j.precamres.2012.07.011

Wang, C., Huang, H., Tong, X., Zheng, M., Peng, Z., Nan, J., et al. (2016). Changing provenance of late Neoarchean metasedimentary rocks in the Anshan-Benxi area, North China Craton: Implications for the tectonic setting of the world-class Dataigou banded iron formation. *Gondwana Research*, *40*, 107–123. https://doi.org/10.1016/j.gr.2016.08.010

Wang, C., Lai, Y.-J., Foley, S. F., Liu, Y., Belousova, E., Zong, K., & Hu, Z. (2020). Rutile records for the cooling history of the Trans-North China orogen from assembly to break-up of the Columbia supercontinent. *Precambrian Research*, *346*, 105763. https://doi.org/10.1016/j.precamres.2020.105763

Wang, C., Peng, Z., Tong, Z., Huan, H., Zheng, M., Zhang, L., & Zhai, M. (2017). Late Neoarchean supracrustal rocks from the Anshan-Benxi terrane, North China Craton: New geodynamic implications from the geochemical record. *American Journal of Science*, *317*(10), 1095–1148. https://doi.org/10.2475/10.2017.02

Wang, C.-Y., Meng, E., Lin, S., & Li, Y.-G. (2021). Late Neoarchean metavolcanic rocks from the Tonghua area, Southern Jilin Province, China: Constraints on the formation and evolution of the northeastern North China Craton. *Precambrian Research*, *362*, 106266. https://doi.org/10.1016/j.precamres.2021.106266

Wang, C.-Y., Meng, E., Yang, H., Liu, C.-H., Cai, J., Ji, L., & Li, Y.-G. (2018). Geochronological and petrogenetic constraints on the regional tectonic evolution of the Guanghua Group in northeastern Jiao-Liao-Ji Belt, China. *Precambrian Research*, *305*, 427–443. https://doi.org/10.1016/j.precamres.2017.10.012

Wang, D., Guo, J., Huang, G., & Scheltens, M. (2015). The Neoarchean ultramafic–mafic complex in the Yinshan Block, North China Craton: Magmatic monitor of development of Archean lithospheric mantle. *Precambrian Research*, *270*, 80–99. https://doi.org/10.1016/j.precamres.2015.09.002

Wang, H., Yang, J.-H., Zhu, Y.-S., Huang, C., Xu, L., Wu, S.-T., & Liu, Y. (2022). Archean crustal growth and reworking revealed by combined U-Pb-Hf-O isotope and trace element data of detrital zircons from ancient and modern river sediments of the eastern Kaapvaal Craton. *Geochimica et Cosmochimica Acta*, *320*, 79–104. https://doi.org/10.1016/j.gca.2021.12.025

Wang, J.-M., Rubatto, D., & Zhang, J.-J. (2015). Timing of partial melting and cooling across the Greater Himalayan Crystalline Complex (Nyalam, Central Himalaya): In-sequence Thrusting and its implications. *Journal of Petrology*, *56*(9), 1677–1702. https://doi.org/10.1093/petrology/egv050

Wang, K., Liu, S., Wang, M., & Yan, M. (2017). Geochemistry and zircon U-Pb-Hf isotopes of the late Neoarchean granodiorite-monzogranite-quartz syenite intrusions in the Northern Liaoning Block, North China Craton: Petrogenesis and implications for geodynamic processes. *Precambrian Research*, *295*, 151–171. https://doi.org/10.1016/j.precamres.2017.04.021

Wang, M., Liu, S., Fu, J., Wang, K., Guo, R., & Guo, B. (2017). Neoarchean DTTG gneisses in southern Liaoning Province and their constraints on crustal growth and the nature of the Liao-Ji Belt in the Eastern Block. *Precambrian Research*, *303*, 183–207. https://doi.org/10.1016/j.precamres.2017.03.017

Wang, M., Liu, S., Wang, W., Wang, K., Yan, M., Guo, B., et al. (2016). Petrogenesis and tectonic implications of the Neoarchean North Liaoning tonalitic-trondhjemitic gneisses of the North China Craton, North China. *Journal of Asian Earth Sciences*, *131*, 12–39. https://doi.org/10.1016/j.jseaes.2016.09.012

Wang, Q., & Wilde, S. A. (2018). New constraints on the Hadean to Proterozoic history of the Jack Hills belt, Western Australia. *Gondwana Research*, *55*, 74–91. https://doi.org/10.1016/j.gr.2017.11.008

Wang, Q., Zheng, J., Pan, Y., Dong, Y., Liao, F., Zhang, Y., et al. (2014). Archean crustal evolution in the southeastern North China Craton: New data from the Huoqiu Complex. *Precambrian Research*, *255*, 294–315. https://doi.org/10.1016/j.precamres.2014.10.005

Wang, W., Liu, S., Cawood, P. A., Bai, X., Guo, R., Guo, B., & Wang, K. (2016). Late Neoarchean subduction-related crustal growth in the Northern Liaoning region of the North China Craton: Evidence from ~2.55 to 2.50 Ga granitoid gneisses. *Precambrian Research*, *281*, 200–223. https://doi.org/10.1016/j.precamres.2016.05.018

Wang, W., Liu, S., Cawood, P. A., Guo, R., Bai, X., & Guo, B. (2017). Late Neoarchean crust-mantle geodynamics: Evidence from Pingquan Complex of the Northern Hebei Province, North China Craton. *Precambrian Research*, *303*, 470–493. https://doi.org/10.1016/j.precamres.2017.06.007

Wang, W., Liu, S., Santosh, M., Bai, X., Li, Q., Yang, P., & Guo, R. (2013). Zircon U–Pb–Hf isotopes and whole-rock geochemistry of granitoid gneisses in the Jianping gneissic terrane, Western Liaoning Province: Constraints on the Neoarchean crustal evolution of the North China Craton. *Precambrian Research*, *224*, 184–221. https://doi.org/10.1016/j.precamres.2012.09.019

Wang, W., Liu, S., Santosh, M., Wang, G., Bai, X., & Guo, R. (2015). Neoarchean intra-oceanic arc system in the Western Liaoning Province: Implications for Early Precambrian crustal evolution in the Eastern Block of the North China Craton. *Earth-Science Reviews*, *150*, 329–364. https://doi.org/10.1016/j.earscirev.2015.08.00

Wang, W., Zhai, M., Wang, S., Santosh, M., Du, L., Xie, H., et al. (2013). Crustal reworking in the North China Craton at ~2.5 Ga: Evidence from zircon U–Pb age, Hf isotope and whole rock geochemistry of the felsic volcano-sedimentary rocks from the western Shandong Province. *Geological Journal*, *48*(5), 406–428. https://doi.org/10.1002/gj.2493

Wang, X., Huang, X.-L., & Fan, Y. (2019). Revisiting the Lushan-Taihua Complex: New perspectives on the Late Mesoarchean-Early Neoarchean crustal evolution of the southern North China Craton. *Precambrian Research*, *325*, 132–149. https://doi.org/10.1016/j.precamres.2019.02.020

Wang, X., Zheng, Y.-F., & Zhu, W.-B. (2019). Geochemical constraints on the origin of Neoarchean magmatic rocks in the Lüliang Complex, North China Craton: Tectonic implications. *Precambrian Research*, *327*, 212–231. https://doi.org/10.1016/j.precamres.2019.04.006

Wang, X., Zheng, Y.-F., & Zhu, W.-B. (2019). Geochemical evidence for reworking of the juvenile crust in the Neoarchean for felsic magmatism in the Yunzhongshan area, the North China Craton. *Precambrian Research*, *335*, 105493. https://doi.org/10.1016/j.precamres.2019.105493

Wang, Y.-F., Li, X.-H., Jin, W., Zeng, L., & Zhang, J.-H. (2020). Generation and maturation of Mesoarchean continental crust in the Anshan Complex, North China Craton. *Precambrian Research*, *341*, 105651. https://doi.org/10.1016/j.precamres.2020.105651

Wang, Y.-F., Li, X.-H., Jin, W., & Zhang, J.-H. (2015). Eoarchean ultra-depleted mantle domains inferred from ca. 3.81 Ga Anshan trondhjemitic gneisses, North China Craton. *Precambrian Research*, *263*, 88–107. https://doi.org/10.1016/j.precamres.2015.03.005

Warren, C. J., Grujic, D., Cottle, J. M., & Rogers, N. W. (2012). Constraining cooling histories: Rutile and titanite chronology and diffusion modelling in NW Bhutan. *Journal of Metamorphic Geology*, *30*(2), 113–130. https://doi.org/10.1111/j.1525-1314.2011.00958.x

Wasilewski, B., O'Neil, J., Rizo, H., Paquette, J.-L., & Gannoun, A.-M. (2021). Over one billion years of Archean crust evolution revealed by zircon U-Pb and Hf isotopes from the Saglek-Hebron complex. *Precambrian Research*, *359*, 106092. https://doi.org/10.1016/j.precamres.2021.106092

Wawrzenitz, N., Krohe, A., Baziotis, I., Mposkos, E., Kylander-Clark, A. R. C., & Romer, R. L. (2015). LASS U–Th–Pb monazite and rutile geochronology of felsic high-pressure granulites (Rhodope, N Greece): Effects of fluid, deformation and metamorphic reactions in local subsystems. *Lithos*, *232*, 266–285. https://doi.org/10.1016/j.lithos.2015.06.029

Will, T. M., Schmädicke, E., Ling, X.-X., Li, X.-H., & Li, Q.-L. (2018). New evidence for an old idea: Geochronological constraints for a paired metamorphic belt in the central European Variscides. *Lithos*, *302–303*, 278–297. https://doi.org/10.1016/j.lithos.2018.01.008

Wilson, A. H., & Zeh, A. (2018). U-Pb and Hf isotopes of detrital zircons from the Pongola Supergroup: Constraints on deposition ages, provenance and Archean evolution of the Kaapvaal craton. *Precambrian Research*, *305*, 177–196. https://doi.org/10.1016/j.precamres.2017.12.02

Wu, F.-Y., Zhang, Y.-B., Yang, J.-H., Xie, L.-W., & Yang, Y.-H. (2008). Zircon U–Pb and Hf isotopic constraints on the Early Archean crustal evolution in Anshan of the North China Craton. *Precambrian Research*, *167*(3–4), 339–362. https://doi.org/10.1016/j.precamres.2008.10.002

Wu, M., Lin, S., Wan, Y., & Gao, J.-F. (2016). Crustal evolution of the Eastern Block in the North China craton: Constraints from zircon U–Pb geochronology and Lu–Hf isotopes of the Northern Liaoning complex. *Precambrian Research*, *275*, 35–47. https://doi.org/10.1016/j.precamres.2015.12.013

Wu, M., Lin, S., Wan, Y., Gao, J.-F., & Stern, R. A. (2021). Episodic Archean crustal accretion in the North China Craton: Insights from integrated zircon U-Pb-Hf-O isotopes of the Southern Jilin Complex, northeast China. *Precambrian Research*, *358*, 106150. https://doi.org/10.1016/j.precamres.2021.106150

Wu, M., Zhao, G., Sun, M., Li, S., Bao, Z., Tam, P. Y., et al. (2014). Eizenhöefer, Yanhong He, Zircon U–Pb geochronology and Hf isotopes of major lithologies from the Jiaodong Terrane: Implications for the crustal evolution of the Eastern Block of the North China Craton. *Lithos*, *190–191*, 71–84. https://doi.org/10.1016/j.lithos.2013.12.004

Wu, M., Zhao, G., Sun, M., Li, S., He, Y., & Bao, Z. (2013). Zircon UPb geochronology and Hf isotopes of major lithologies from the Yishui Terrane: Implications for the crustal evolution of the Eastern Block, North China Craton. *Lithos*, *170–171*, 164–178. https://doi.org/10.1016/j.lithos.2013.03.005

Xie, H., Wan, Y., Dong, C., Kröner, A., Xie, S., Liu, S., et al. (2019). Late Neoarchean synchronous TTG gneisses and potassic granitoids in southwestern Liaoning Province, North China Craton: Zircon U-Pb-Hf isotopes, geochemistry and tectonic implications. *Gondwana Research*, *70*, 171–200. https://doi.org/10.1016/j.gr.2018.11.016

Xie, S., Xie, H., Wang, S., Kröner, A., Liu, S., Zhou, H., et al. (2014). Ca. 2.9Ga granitoid magmatism in eastern Shandong, North China Craton: Zircon dating, Hf-in-zircon isotopic analysis and whole-rock geochemistry. *Precambrian Research*, *255*, 538–562. https://doi.org/10.1016/j.precamres.2014.09.006

Xiong, B. Q., Xu, W. L., Li, Q. L., Yang, D. B., & Zhou, Q. J. (2015). SIMS U-Pb dating of rutile within eclogitic xenoliths in the Early Cretaceous adakitic rocks of the Xuzhou-Huaibei area, China: Constraints on the timing of crustal thickening of the eastern North China Craton. *Science China Earth Sciences*, *58*(7), 1100–1106. https://doi.org/10.1007/s11430-014-5043-9

Yang, L., Hou, G., Gao, L., & Liu, S. (2020). Neoarchaean subduction tectonics in Western Shandong Province, China: Evidence from geochemistry and zircon U–Pb–Hf isotopes of metabasalts. *Geological Journal*, *55*(5), 3575–3600. https://doi.org/10.1002/gj.3605

Yang, Q.-Y., & Santosh, M. (2017). The building of an Archean microcontinent: Evidence from the North China Craton. *Gondwana Research*, *50*, 3–37. https://doi.org/10.1016/j.gr.2017.01.003

Yang, Q.-Y., Santosh, M., Collins, A. S., & Teng, X.-M. (2016). Microblock amalgamation in the North China Craton: Evidence from Neoarchaean magmatic suite in the western margin of the Jiaoliao Block. *Gondwana Research*, *31*, 96–123. https://doi.org/10.1016/j.gr.2015.04.002

Yang, Q.-Y., Santosh, M., & Kim, S. W. (2019). Continental outbuilding along the margin of an Archean cratonic nucleus in the North China Craton. *Precambrian Research*, *326*, 35–57. https://doi.org/10.1016/j.precamres.2017.11.010

Yao, J., Wang, W., Liu, S., Cawood, P. A., Niu, P., Lu, D., & Guo, L. (2020). Crust-mantle geodynamic origin of ~2.7 Ga granitoid diversification in the Jiaobei terrane, North China Craton. *Precambrian Research*, *346*, 105821. https://doi.org/10.1016/j.precamres.2020.105821

Yi, K., Bennett, V. C., Nutman, A. P., & Lee, S. R. (2014). Tracing Archaean terranes under Greenland's Icecap: U–Th–Pb–Hf isotopic study of zircons from melt-water rivers in the Isua area. *Precambrian Research*, *255*, 900–921. https://doi.org/10.1016/j.precamres.2014.04.006

Zack, T., Stockli, D. F., Luvizotto, G. L., Barth, M. G., Belousova, E., Wolfe, M. R., & Hinton, R. W. (2011). In situ U–Pb rutile dating by LA-ICP-MS: 208Pb correction and prospects for geological applications. *Contributions to Mineralogy and Petrology*, *162*(3), 515–530. https://doi.org/10.1007/s00410-011-0609-4

Zeh, A., Gerdes, A., Barton, J., & Klemd, R. (2010). U–Th–Pb and Lu–Hf systematics of zircon from TTG's, leucosomes, meta-anorthosites and quartzites of the Limpopo Belt (South Africa): Constraints for the formation, recycling and metamorphism of Palaeoarchaean crust. *Precambrian Research*, *179*(1–4), 50–68. https://doi.org/10.1016/j.precamres.2010.02.012

Zeh, A., Gerdes, A., & Barton, J. M., Jr. (2009). Archean accretion and crustal evolution of the Kalahari Craton—The zircon age and Hf isotope record of granitic rocks from Barberton/Swaziland to the Francistown Arc. *Journal of Petrology*, *50*(5), 933–966. https://doi.org/10.1093/petrology/egp027

Zeh, A., Gerdes, A., & Heubeck, C. (2013). U–Pb and Hf isotope data of detrital zircons from the Barberton Greenstone Belt: Constraints on provenance and Archaean crustal evolution. *Journal of the Geological Society*, *170*(1), 215–223. https://doi.org/10.1144/jgs2011-162

Zeh, A., Gerdes, A., & Leo, M. (2011). Hafnium isotope record of the Ancient Gneiss Complex, Swaziland, southern Africa: Evidence for Archaean crust–mantle formation and crust reworking between 3.66 and 2.73 Ga. *Journal of the Geological Society*, *168*(4), 953–964. https://doi.org/10.1144/0016-76492010-117

Zeh, A., Jaguin, J., Poujol, M., Boulvais, P., Block, S., & Paquette, J.-L. (2013). Juvenile crust formation in the northeastern Kaapvaal Craton at 2.97 Ga—Implications for Archean terrane accretion, and the source of the Pietersburg gold. *Precambrian Research*, *233*, 20–43. https://doi.org/10.1016/j.precamres.2013.04.013

Zeh, A., & Kirchenbaur, M. (2022). Zircon U-Pb-Hf isotope systematics of Limpopo Belt quartzites and igneous rocks, implications for Kaapvaal – Zimbabwe Craton accretion. *Precambrian Research*, *373*, 106631. https://doi.org/10.1016/j.precamres.2022.106631

Zeh, A., Stern, R. A., & Gerdes, A. (2014). The oldest zircons of Africa—Their U–Pb–Hf–O isotope and trace element systematics, and implications for Hadean to Archean crust–mantle evolution. *Precambrian Research*, *241*, 203–230. https://doi.org/10.1016/j.precamres.2013.11.006

Zeh, A., & Wilson, A. H. (2022). U-Pb-Hf isotopes and shape parameters of zircon from the Mozaan Group (South Africa) with implications for depositional ages, provenance and Witwatersrand – Pongola Supergroup correlations. *Precambrian Research*, *368*, 106500. https://doi.org/10.1016/j.precamres.2021.106500

Zeh, A., Wilson, A. H., & Gerdes, A. (2020). Zircon U-Pb-Hf isotope systematics of Transvaal Supergroup – Constraints for the geodynamic evolution of the Kaapvaal Craton and its hinterland between 2.65 and 2.06 Ga. *Precambrian Research*, *345*, 105760. https://doi.org/10.1016/j.precamres.2020.105760

Zeh, A., Wilson, A. H., & Ovtcharova, M. (2016). Source and age of upper Transvaal Supergroup, South Africa: Age-Hf isotope record of zircons in Magaliesberg quartzite and Dullstroom lava, and implications for Paleoproterozoic (2.5–2.0Ga) continent reconstruction. *Precambrian Research*, *278*, 1–21. https://doi.org/10.1016/j.precamres.2016.03.017

Zhang, G., Zhang, L., Christy, A. G., Song, S., & Li, Q. (2014). Differential exhumation and cooling history of North Qaidam UHP metamorphic rocks, NW China: Constraints from zircon and rutile thermometry and U–Pb geochronology. *Lithos*, *205*, 15–27. https://doi.org/10.1016/j.lithos.2014.06.018

Zhang, H.-F., Wang, J.-L., Zhou, D.-W., Yang, Y.-H., Zhang, G.-W., Santosh, M., et al. (2014). Hadean to Neoarchean episodic crustal growth: Detrital zircon records in Paleoproterozoic quartzites from the southern North China Craton. *Precambrian Research*, *254*, 245–257. https://doi.org/10.1016/j.precamres.2014.09.003

Zhang, H.-F., Zhang, J., Zhang, G.-W., Santosh, M., Yu, H., Yang, Y.-H., & Wang, J.-L. (2016). Detrital zircon U–Pb, Lu–Hf, and O isotopes of the Wufoshan Group: Implications for episodic crustal growth and reworking of the southern North China craton. *Precambrian Research*, *273*, 112–128. https://doi.org/10.1016/j.precamres.2015.12.004

Zhang, J., Gong, J., Yu, S., Li, H., & Hou, K. (2013). Neoarchean–Paleoproterozoic multiple tectonothermal events in the western Alxa block, North China Craton and their geological implication: Evidence from zircon U–Pb ages and Hf isotopic composition. *Precambrian Research*, *235*, 36–57. https://doi.org/10.1016/j.precamres.2013.05.002

Zhang, J. X., Mattinson, C. G., Yu, S. Y., & Li, Y. S. (2014). Combined rutile–zircon thermometry and U–Pb geochronology: New constraints on Early Paleozoic HP/UHT granulite in the south Altyn Tagh, north Tibet, China. *Lithos*, *200–201*, 241–257. https://doi.org/10.1016/j.lithos.2014.05.006

Zhang, P., Najman, Y., Mei, L., Millar, I., Sobel, E. R., Carter, A., et al. (2019). Palaeodrainage evolution of the large rivers of East Asia, and Himalayan-Tibet tectonics. *Earth-Science Reviews*, *192*, 601–630. https://doi.org/10.1016/j.earscirev.2019.02.00

Zhang, Q.-Q., Zhang, S.-H., Zhao, Y., & Hu, G.-H. (2021). Geochronology, geochemistry and petrogenesis of the Neoarchean magmatism in the Jiefangyingzi area, northern North China Craton: Implications for crustal growth and tectonic affinity. *Precambrian Research*, *357*, 106144. https://doi.org/10.1016/j.precamres.2021.106144

Zhang, S.-B., Tang, J., & Zheng, Y.-F. (2014). Contrasting Lu–Hf isotopes in zircon from Precambrian metamorphic rocks in the Jiaodong Peninsula: Constraints on the tectonic suture between North China and South China. *Precambrian Research*, *245*, 29–50. https://doi.org/10.1016/j.precamres.2014.01.006

Zhang, X.-Z., Wang, Q., Dong, Y.-S., Zhang, C., Li, Q.-Y., Xia, X.-P., & Xu, Q. (2017). High-pressure granulite facies overprinting during the exhumation of eclogites in the Bangong-Nujiang suture zone, central Tibet: Link to flat-slab subduction. *Tectonics*, *36*(12), 2918–2935. https://doi.org/10.1002/2017TC004774

Zhou, T., Li, Q., Klemd, R., Shi, Y., Tang, X., Li, C., & Liu, Y. (2020). Multi-system geochronology of North Dabie eclogite: Ineffective garnet 'shielding' on rutile inclusions under multi-thermal conditions. *Lithos*, *368–369*, 105573. https://doi.org/10.1016/j.lithos.2020.105573

Zhou, Y., Sun, Q., Zheng, Y., Zhao, T., & Zhai, M. (2021). Delineation of the early Neoarchean (2.75 to 2.70 Ga) crustal growth and reworking processes in the southeast base of Taihang Mountain, North China Craton. *Lithos*, *380–381*, 105829. https://doi.org/10.1016/j.lithos.2020.105829

Zhu, X., Zhai, M., Chen, F., Lyu, B., Wang, W., Peng, P., & Hu, B. (2013). ~2.7-Ga crustal growth in the North China craton: Evidence from zircon U-Pb ages and Hf isotopes of the Sushui complex in the Zhongtiao terrane. *The Journal of Geology*, *121*(3), 239–254. https://doi.org/10.1086/669977

Zincone, S. A., Oliveira, E. P., Laurent, O., Zhang, H., & Zhai, M. (2016). 3.30 Ga high-silica intraplate volcanic–plutonic system of the Gavião Block, São Francisco Craton, Brazil: Evidence of an intracontinental rift following the creation of insulating continental crust. *Lithos*, *266–267*, 414–434. https://doi.org/10.1016/j.lithos.2016.10.011